# BEHAVIOR OF CFRP CONFINED CONCRETE SPECIMENS UNDER TEMPERATURE CYCLES AND SUSTAINED LOADS

A THESIS SUBMITTED TO
THE GRADUATE SCHOOL OF NATURAL AND APPLIED SCIENCES
OF
MIDDLE EAST TECHNICAL UNIVERSITY

BY

BARIŞ ERDİL

IN PARTIAL FULFILLMENT OF THE REQUIREMENTS
FOR
THE DEGREE OF DOCTOR OF PHILOSOPHY
IN
CIVIL ENGINEERING

FEBRUARY 2012

Approval of the thesis:

**BEHAVIOR OF CFRP CONFINED CONCRETE SPECIMENS UNDER TEMPERATURE CYCLES AND SUSTAINED LOADS**

submitted by **BARIŞ ERDİL** in partial fulfillment of the requirements for the degree of **Doctor of Philosophy in Civil Engineering Department, Middle East Technical University** by,

Prof. Dr. Canan Özgen _____
Dean, Graduate School of **Natural and Applied Sciences**

Prof. Dr. Güney Özcebe _____
Head of Department, **Civil Engineering**

Prof. Dr. Uğurhan Akyüz
Supervisor, **Civil Engineering Dept., METU** _____

Assoc. Prof. Dr. İsmail Özgür Yaman
Co-Supervisor, **Civil Engineering Dept., METU** _____

**Examining Committee Members:**

Prof. Dr. Mustafa Tokyay _____
Civil Engineering Dept., METU

Prof. Dr. Uğurhan Akyüz _____
Civil Engineering Dept., METU

Assoc. Prof. Dr. Erdem Canbay _____
Civil Engineering Dept., METU

Assoc. Prof. Dr. Özgür Anıl _____
Civil Engineering Dept., Gazi University

Assist. Prof. Dr. Sinan Turhan Erdoğan _____
Civil Engineering Dept., METU

**Date:** 03.02.2012

**I hereby declare that all information in this document has been obtained and presented in accordance with academic rules and ethical conduct. I also declare that, as required by these rules and conduct, I have fully cited and referenced all material and results that are not original to this work.**

Name, Last Name: Barış Erdil

Signature :

# ABSTRACT

## BEHAVIOR OF CFRP CONFINED CONCRETE SPECIMENS UNDER TEMPERATURE CYCLES AND SUSTAINED LOADS

Erdil, Barış
Ph.D., Department of Civil Engineering
Supervisor : Prof. Dr. Uğurhan Akyüz
Co-Supervisor : Assoc. Prof. Dr. İsmail Özgür Yaman

February 2012, 264 pages

The application of carbon fiber reinforced polymers (CFRP) is one of the effective retrofitting and strengthening methods that is used worldwide and is starting to be used in Turkey as well because they have high strength and high modulus in the fiber direction, have very low coefficient of thermal expansion when compared to concrete and steel and are known not to corrode. Since FRPs are lightweight, their mass can be neglected when compared to concrete and steel.

However, before proposing this material as an alternative for strengthening and retrofitting applications their long-term behavior should be understood because they are applied on to concrete by several layers of epoxy-based adhesives, which can be affected by change in humidity, temperature and load. Therefore, behavior of CFRP-strengthened structures in varying temperature and humidity conditions must be investigated.

In this dissertation, behavior of CFRP confined cylindrical and prismatic concrete specimens having square cross-section were investigated under sustained compressive loads, dry and wet heating-cooling cycles, and outdoor exposures under direct sunlight, to determine the possible changes in their mechanical properties. Sustained loads were applied as the 40% and 50% of their confined axial load capacity. In addition to the sustained loads, specimens were subjected to 200 heating-cooling cycles between -10°C to 50°C. In order to understand the change in behavior of CFRP confined concrete specimens better, they were divided in six groups. A single effect was investigated in each group. After aging tests mechanical properties of the specimens were recorded via monotonic uniaxial loading. It was observed that temperature cycles had little effect on behavior but sustained loads changed the shape of the axial stress-strain diagram and resulted in a dramatic decrease in ultimate strain. Based on the test results and also using the data of similar studies available in the literature, strength and strain models considering the exposures as independent parameters were established and finally axial stress-strain curve was tried to be predicted.

**Keywords:** CFRP-confined concrete, heating-cooling, sustained loading, axial stress-strain curve

# ÖZ

## KARBON LİFLİ POLİMER İLE GÜÇLENDİRİLMİŞ BETON NUMUNELERİN ISI ÇEVRİMLERİ VE KALICI YÜKLER ALTINDA DAVRANIŞI

Erdil, Barış
Doktora, İnşaat Mühendisliği Bölümü
Tez Yöneticisi : Prof. Dr. Uğurhan Akyüz
Ortak Tez Yöneticisi : Doç. Dr. İsmail Özgür Yaman

Şubat 2012, 264 sayfa

Karbon takviyeli polimerler (CFRP) ile yapılan uygulamalar dünyada geçmişten beri kullanılan ve ülkemizde de gittikçe kullanımı yaygınlaşan etkili onarım ve güçlendirme yöntemlerinden biridir. CFRP'ler fiber doğrultusunda yüksek dayanım ve yüksek elastik modül değerlerine sahip olup ısıl genleşme katsayıları çok düşüktür ve korozyona uğrayabilen bir malzeme değildir. Hafif olduklarından beton ve çelik ile kıyaslandıklarında ağırlıkları ihmal edilebilir.

Fakat, bu malzemeleri onarım ve güçlendirme uygulamalarında önerebilmek için uzun süreli davranışlarının bilinmesi gerekmektedir çünkü uygulama, nem, sıcaklık ve yükten etkilenebilen, çeşitli kademeler halinde uygulanan epoksi tabanlı yapıştırıcılar ile yapılmaktadır. Bu yüzden CFRP ile güçlendirilmiş yapıların değişken sıcaklık ve nem durumlarından nasıl etkilendikleri araştırılmalıdır.

Bu doktora tezinde, CFRP ile sarılmış silindirik ve kare kesitli prizmatik beton numunelerin davranışı kalıcı eksenel yük, kuru ve ıslak ısıtma ve soğutma şeklinde uygulanan sıcaklık çevrimleri ve direk güneş ışığına maruz bir şekilde dış çevre koşulları altında incelenmiş ve mekanik özelliklerindeki olası değişimler belirlenmeye çalışılmıştır. Uzun süreli sabit yük, numunenin eksenel sargılı eksenel yük kapasitelerinin %40'ı ve %50'si şeklinde uygulanmıştır. Uzun süreli sabit yüklere ilaveten, numuneler -10 ile 50°C arasında uygulanan 200 ısıtma-soğutma çevrimlerine maruz bırakılmıştır. CFRP ile sarılmış beton numunelerin davranışlarındaki değişimleri daha iyi anlayabilmek için numuneler altı gruba ayrılmıştır. Her grupta tek bir etki incelenmeye çalışılmıştır. Yaşlandırma testlerinden sonra numunelerin mekanik özellikleri monotonik yükleme ile kaydedilmiştir. Sonuçlardan, sıcaklık çevrimlerinin davranışa çok az etki ettiği gözlendi fakat kalıcı yüklerin hem eksenel gerilme-birim şekil değiştirme grafiğini değiştirdiği hem de nihai birim şekil değiştirme değerini olumsuz yönde etkilediği görüldü. Deney sonuçları temel alınıp, literatürde yer alan benzer çalışmaların dataları kullanılarak bu doktora tezinde incelenen yaşlandırma etkilerinin de ayrı birer parametre olarak yer aldığı dayanım ve şekil değiştirme modelleri oluşturulmuş ve sonuç olarak eksenel gerilme-birim şekil değiştirme eğrisi tahmin edilmeye çalışılmıştır.

**Anahtar Kelimeler:** CFRP sargılı beton, ısıtma-soğutma, uzun süreli sabit yük, eksenel gerilme-şekil değiştirme eğrisi

*To My Family*

## ACKNOWLEDGMENTS

I am deeply grateful to my supervisor, Prof. Dr. Uğurhan Akyüz, for his guidance throughout this study. He was always helpful and encouraging. It was great pleasure working with him.

I am also grateful to my co-supervisor, Assoc. Prof. Dr. İsmail Özgür Yaman. His comments and informative feedbacks are highly appreciated.

I would like to convey my sincere thanks to Prof. Dr. Mustafa Tokyay and Assoc. Prof. Dr. Özgür Anıl for their constructive contributions during thesis progress. I would like to thank to Asst. Prof. Dr. Ayhan İrfanoğlu for his comments on analytical studies when I was at Purdue University, USA.

I would like to express my sincere thanks to my friends, Dr. Dilek Okuyucu, Dr. Ramazan Özçelik, Dr. Bora Acun, Tuba Eroğlu, Salim Azak, Dr. Emre Akın, Dr. Yasemin Didem Aktaş Erdem, Dr. Seval Pınarbaşı, Dr. Gökhan Özdemir, Dr. Beyhan Bayhan, Altan Zervent and Bahadır Keskin. Their friendship are always valuable.

I am grateful to my family for their continuous support. Special thanks go to my brother Güven Erdil.

I would like to thank to METU-Structural Engineering Laboratory staff; especially to Hasan Metin. I also would like to extend my thanks to METU-Materials of Construction Laboratory staff; especially to Cuma Yıldırım.

I would like to express my sincere appreciation to the Scientific and Technological Research Council of Turkey TÜBİTAK (Project No: ICTAG I599) and METU (BAP-08-11-DPT-2002K120510) for their financial support.

**TABLE OF CONTENTS**

**ABSTRACT** ..... **iv**

**ÖZ** ..... **vi**

**ACKNOWLEDGMENTS** ..... **ix**

**TABLE OF CONTENTS** ..... **x**

**LIST OF TABLES** ..... **xv**

**LIST OF FIGURES** ..... **xxii**

**LIST OF SYMBOLS** ..... **xxxvi**

**ABBREVIATIONS** ..... **xxxviii**

**CHAPTERS**

**1. INTRODUCTION** ..... **1**

1.1 GENERAL ..... 1

1.2 AIM OF THE DISSERTATION ..... 2

1.3 SCOPE ..... 3

1.4 ORGANIZATION OF THE DISSERTATION ..... 5

**2. LITERATURE REVIEW** ..... **7**

2.1 INTRODUCTION ..... 7

2.2 STUDIES ON FRP CONFINEMENT ..... 7

2.3 STUDIES ON CREEP OF FRP-CONFINED CONCRETE ..... 13

2.4 STUDIES ON DURABILITY OF FRP-CONFINED CONCRETE 17

2.5 STUDIES OF SIMULTANEOUS EXPOSURE OF ENVIRONMENTAL EFFECTS AND SL ON FRP-CONFINED CONCRETE ..... 25

**3. EXPERIMENTAL PROGRAM ..... 28**

3.1 INTRODUCTION ..... 28

3.2 MATERIAL PROPERTIES ..... 29

3.2.1. Concrete ..... 29

3.2.2. Carbon Fiber Reinforced Polymer (CFRP) ..... 34

3.2.3. Primer, Putty and Epoxy ..... 37

3.2.4. CFRP Wrapping and Specimen Preparation ..... 39

3.3 TEST PROCEDURE ..... 41

3.3.1 Heating-Cooling Tests ..... 44

3.3.2 Outdoor-Exposure Tests ..... 50

3.3.3 Sustained Loading Tests ..... 52

3.3.4 Uniaxial Compression Tests ..... 57

**4. TEST RESULTS ..... 63**

4.1 INTRODUCTION ..... 63

4.2 MECHANICAL PROPERTIES OF CFRP-CONFINED CONCRETE COLUMNS ..... 63

4.3 CONCRETE SPECIMENS HAVING 10 MPa STRENGTH ..... 65

4.3.1 Cylindrical Specimens ..... 65

4.3.1.1 SET 1 – Specimens with 6% overlap length ..... 67

4.3.1.1.1 Group-1: Reference Specimens ..... 67

4.3.1.1.2 Group-2: Specimens exposed to H-C Cycles ..... 71

4.3.1.1.3 Group-3: Specimens Exposed to H-C Cycles and SL. 73

4.3.1.2 SET 2 – Specimens with 11% overlap length ..... 76

4.3.1.2.1 Group-1: Reference Specimens ..... 76
4.3.1.2.2 Group-2: Specimens exposed to H-C Cycles..... 79
4.3.1.2.3 Group-3: Specimens Exposed to H-C Cycles and SL. 81
4.3.1.2.4 Group-4: Specimens Subjected to SL ..... 83
4.3.1.2.5 Group-6: Specimens Subjected to Outdoor Exposure . 85
4.3.2 Prismatic Specimens..... 87
4.3.2.1. SET 3: Prismatic Specimens with r = 25 mm ..... 91
4.3.2.1.1. Group-1: Reference Specimens ..... 91
4.3.2.1.2. Group-2: Specimens exposed to H-C Cycles ..... 98
4.3.2.1.3. Group-3: Specimens Exposed to H-C Cycles and SL . 104
4.3.2.1.4. Group-4: Specimens Subjected to SL..... 111
4.3.2.1.5. Group-6: Specimens Subjected to Outdoor Exposure . 113
4.3.2.2. SET 4: Prismatic Specimens with r = 37.5 mm ..... 117
4.3.2.2.1. Group-1: Reference Specimens ..... 117
4.3.2.2.2. Group-2: Specimens Exposed to H-C Cycles..... 120
4.3.2.2.3. Group-3: Specimens Exposed to H-C Cycles and SL . 121
4.3.2.2.4. Group-4: Specimens Subjected to SL..... 125
4.3.2.2.5. Group-5: Specimens kept in water and exposed to H-C Cycles ..... 129
4.3.2.2.6. Group-6: Specimens Subjected to Outdoor Exposure . 131
4.4 CONCRETE SPECIMENS HAVING 15 MPa STRENGTH ..... 133
4.4.1. Group-1: Reference Specimens..... 134
4.4.2. Group-2: Specimens exposed to H-C Cycles..... 138
4.4.3. Group-3: Specimens Exposed to H-C Cycles and SL..... 141
4.4.4. Group-4: Specimens Subjected to SL ..... 144

4.4.5. Group-5: Specimens kept in water and exposed to H-C Cycles . 147
4.4.6. Group-6: Specimens subjected to outdoor exposure..... 149

4.5 CONCRETE SPECIMENS HAVING 20 MPa STRENGTH ..... 151
4.5.1. Cylindrical Specimens ..... 151
4.5.1.1 Group-1: Reference Specimens..... 152
4.5.1.2. Group-2: Specimens Exposed to H-C Cycles ..... 155
4.5.1.3. Group-3: Specimens Exposed to H-C Cycles and SL..... 158
4.5.2. Prismatic Specimens ..... 161
4.5.2.1 Group-1: Reference Specimens..... 162
4.5.2.2 Group-2: Specimens Exposed to H-C Cycles ..... 165
4.5.2.3 Group-3: Specimens Exposed to H-C Cycles and SL..... 167

**5. DISCUSSION OF THE TEST RESULTS ..... 171**

5.1 INTRODUCTION ..... 171

5.2 EFFECT OF CFRP CONFINEMENT ON BEHAVIOR OF CONCRETE COLUMNS ..... 171

5.3 EFFECT OF HEATING-COOLING (H-C) CYCLES ON BEHAVIOR OF CFRP-CONFINED CONCRETE COLUMNS ..... 179
5.3.1 Effect of H-C cycles on axial stress-strain diagram ..... 181
5.3.2 Effect of H-C cycles on ultimate strength ($f_{cc}$) ..... 187
5.3.3 Effect of H-C cycles on ultimate strain ($\varepsilon_{cc}$) ..... 190

5.4 EFFECT OF OUTDOOR EXPOSURE ON BEHAVIOR OF CFRP-CONFINED CONCRETE COLUMNS ..... 192
5.4.1 Effect of outdoor exposure on axial stress-strain diagram ..... 193
5.4.2 Effect of outdoor exposure on ultimate strength ($f_{cc}$) ..... 195
5.4.3 Effect of outdoor exposure on ultimate strain ($\varepsilon_{cc}$) ..... 197

5.5 EFFECT OF SUSTAINED LOADING ON BEHAVIOR OF CFRP-CONFINED CONCRETE COLUMNS ..... 199

5.5.1 Effect of SL on axial stress-strain diagram ..... 199
5.5.2 Effect of SL on transition stress ($f_{ct}$)..... 206
5.5.3 Effect of SL on ultimate strength ($f_{cc}$) ..... 209
5.5.4 Effect of SL on ultimate strain ($\varepsilon_{cc}$)..... 211
5.5.4 Effect of different SL levels on behavior of CFRP-confined prismatic specimens ..... 214

**6. ANALYTICAL STUDIES ..... 218**

6.1 INTRODUCTION ..... 218

6.2 BEHAVIOR OF FRP-CONFINED CONCRETE ..... 219
6.2.1. Parameters affecting the strength and strain capacities of cylindrical specimens ..... 219
6.2.2. Parameters affecting the ultimate strength and strain of square-section prismatic specimens ..... 223
6.2.3. Behavior under axial compression ..... 226

6.3 FRP-CONFINED CONCRETE MODEL INCLUDING CREEP AND TEMPERATURE EFFECTS ..... 228
6.3.1. Point 1, Initial BP ..... 229
6.3.2. Point 2, Transition BP ..... 229
6.3.3. Point 3, Final BP ..... 230
6.3.3.1. Ultimate axial strength estimation ..... 230
6.3.3.2. Ultimate axial strain estimation ..... 234
6.3.4. Axial stress-strain model ..... 237

6.4 MODEL VERIFICATION..... 238

**7. CONCLUSIONS ..... 241**

**REFERENCES ..... 246**

**CURRICULUM VITAE ..... 264**

# LIST OF TABLES

TABLES

Table 1. 1 Description of the test groups ..... 5

Table 2.1 Studies related to the cylindrical concrete columns confined with FRP.... 11

Table 2.2 Studies related to the prismatic concrete columns confined with FRP..... 12

Table 3.1 Description of the test groups ..... 29

Table 3.2 Physical properties of aggregates..... 30

Table 3.3 Concrete mix proportions..... 32

Table 3.4 Specimen shapes used in the dissertation ..... 33

Table 3.5 Mechanical and Physical Properties of the CFRP (MBrace C1-30)..... 35

Table 3.6 Coupon test results for specimens coated with epoxy ..... 37

Table 3.7 Material properties of the primer ..... 38

Table 3.8 Material Properties of the putty ..... 38

Table 3.9 Material Properties of the epoxy ..... 39

Table 3.10 Test matrix for Phase 1-Exposure Test ..... 43

Table 3.11 Coding scheme for the specimens..... 44

Table 3.12 Coding scheme for the groups ..... 44

Table 3.13 Freeze-thaw cycles for different regions considering the period of 2000-2006..... 47

Table 3.14 Sustained load level on specimens..... 55

Table 4.1 Summary of the 10 MPa cylindrical specimens..... 66

Table 4.2. The limits to identify the quality control of concrete ..... 67

Table 4.3. Mechanical properties of unconfined cylindrical specimens in Group-1 (SET1 - $f_{co}$=10 MPa) ..... 68

Table 4.4. Mechanical properties of CFRP-confined cylindrical specimens in Group-1 (SET1-$f_{co}$=10 MPa) ..... 70

Table 4.5. Mechanical properties of unconfined cylindrical specimens in Group-2 (SET1 - $f_{co}$=10 MPa) ..... 72

Table 4.6. Mechanical properties of CFRP-confined cylindrical specimens in Group-2 (SET 1 - $f_{co}$=10 MPa) ..... 73

Table 4.7. Mechanical properties of unconfined cylindrical specimens in Group-3 ( SET 1 - $f_{co}$=10 MPa) ..... 74

Table 4.8. Mechanical properties of unconfined cylindrical specimens in Group-1 (SET2 - $f_{co}$=10 MPa) ..... 77

Table 4.9. Mechanical properties of CFRP-confined cylindrical specimens in Group-1 (SET 2 - $f_{co}$=10 MPa) ..... 79

Table 4.10. Mechanical properties of CFRP-confined cylindrical specimens in Group-2 (SET 2 - $f_{co}$=10 MPa)..... 81

Table 4.11. Mechanical properties of CFRP-confined cylindrical specimens in Group-3 (SET 2 - $f_{co}$=10 MPa)..... 83

Table 4.12. Mechanical properties of CFRP-confined cylindrical specimens in Group-4 (SET 2 - $f_{co}$=10 MPa)..... 85

Table 4.13. Mechanical properties of CFRP-confined cylindrical specimens in Group-6 (SET 2 - $f_{co}$=10 MPa)..... 86

Table 4.14. Relationship between corner radius, specimen width and the MCR ..... 89

Table 4.15 Summary of the 10 MPa prismatic specimens with r=25 mm ..... 90

Table 4.16 Summary of the 10 MPa prismatic specimens with r=37.5 mm ..... 91

Table 4.17. Mechanical properties of unconfined prismatic specimens in Group-1 (SET 3 - $f_{co}$=10 MPa and r=25 mm) ..... 93

Table 4.18 Mechanical properties of CFRP-confined prismatic specimens in Group-1 (SET 3 - $f_{co}$=10 MPa and r=25 mm) ..... 95

Table 4.19. Mechanical properties of unconfined prismatic specimens in Group-2 (SET 3 - $f_{co}$=10 MPa and r=25 mm) ..... 99

Table 4.20. Mechanical properties of CFRP-confined prismatic specimens in Group-2 (SET 3 - $f_{co}$=10 MPa and r=25 mm) ..... 102

Table 4.21. Mechanical properties of unconfined prismatic specimens in Group-3 (SET 3 - $f_{co}$=10 MPa and r=25 mm) ..... 105

Table 4.22. Mechanical properties of CFRP-confined prismatic specimens in Group-3 (SET 3 - $f_{co}$=10 MPa, r=25 mm and SL=0.4$f_{cc}$) ..... 107

Table 4.23. Mechanical properties of CFRP-confined prismatic specimens in Group-3 (SET 3 - $f_{co}$=10 MPa, r=25 mm and SL=0.55$f_{cc}$) ..... 108

Table 4.24. Mechanical properties of CFRP-confined prismatic specimens in Group-4 (SET 3 - $f_{co}$=10 MPa, r=25 mm and SL=0.4$f_{cc}$) ..... 113

Table 4.25. Mechanical properties of CFRP-confined prismatic specimens in Group-6 (SET 3 - $f_{co}$=10 MPa, r=25 mm) ..... 115

Table 4.26. Mechanical properties of unconfined prismatic specimens in Group-1 (SET 4 - $f_{co}$=10 MPa and r=37.5 mm) ..... 118

Table 4.27. Mechanical properties of CFRP-confined prismatic specimens in Group-1 (SET 4 - $f_{co}$=10 MPa and r=37.5 mm) ..... 119

Table 4.28. Mechanical properties of CFRP-confined prismatic specimen in Group-2 (SET 4 - $f_{co}$=10 MPa, r=37.5 mm and SL=0.5$f_{cc}$) ..... 120

Table 4.29. Mechanical properties of CFRP-confined prismatic specimens in Group-3 (SET 4 - $f_{co}$=10 MPa, r=37.5 mm and SL=0.5$f_{cc}$) ..... 123

Table 4.30. Mechanical properties of CFRP-confined prismatic specimens in Group-3 (SET 4 - $f_{co}$=10 MPa, r=37.5 mm and SL=0.4$f_{cc}$) ..... 123

Table 4.31. Mechanical properties of CFRP-confined prismatic specimens in Group-4 (SET 4 - $f_{co}$=10 MPa, r=37.5 mm and SL=0.5$f_{cc}$) ..... 127

Table 4.32. Mechanical properties of CFRP-confined prismatic specimens in Group-5 (SET 4 - $f_{co}$=10 MPa and r=37.5 mm)..... 130

Table 4.33. Mechanical properties of CFRP-confined prismatic specimens in Group-6 (SET 4 - $f_{co}$=10 MPa, r=37.5 mm and SL=0.5$f_{cc}$) ..... 133

Table 4.34 Summary of the 15 MPa prismatic specimens..... 134

Table 4.35. Mechanical properties of unconfined prismatic specimens in Group-1 ($f_{co}$=15 MPa and r=37.5 mm) ..... 136

Table 4.36. Mechanical properties of CFRP-confined prismatic specimens in Group-1 ($f_{co}$=15 MPa and r=37.5 mm) ..... 138

Table 4.37. Mechanical properties of unconfined prismatic specimens in Group-2 ($f_{co}$=15 MPa and r=37.5 mm) ..... 139

Table 4.38. Mechanical properties of CFRP-confined prismatic specimens in Group-2 ($f_{co}$=15 MPa and r=37.5 mm) ..... 141

Table 4.39. Mechanical properties of unconfined prismatic specimens in Group-3 ($f_{co}$=15 MPa and r=37.5 mm) ..... 141

Table 4.40. Mechanical properties of CFRP-confined prismatic specimens in Group-3 ($f_{co}$=15 MPa and r=37.5 mm) ..... 144

Table 4.41. Mechanical properties of CFRP-confined prismatic specimens in Group-4 ($f_{co}$=15 MPa and r=37.5 mm) ..... 145

Table 4.42. Mechanical properties of CFRP-confined prismatic specimens in Group-5 ($f_{co}$=15 MPa and r=37.5 mm) ..... 149

Table 4.43. Mechanical properties of CFRP-confined prismatic specimens in Group-6 ($f_{co}$=15 MPa and r=37.5 mm) ..... 150

Table 4.44 Summary of the 20 MPa cylindrical specimens ..... 152

Table 4.45. Mechanical properties of unconfined cylindrical specimens in Group-1 ($f_{co}$=20 MPa) ..... 153

Table 4.46. Mechanical properties of CFRP-confined cylindrical specimens in Group-1 ($f_{co}$=20 MPa) ..... 155

Table 4.47. Mechanical properties of unconfined cylindrical specimens in Group-2 ($f_{co}$=20 MPa) ..... 156

Table 4.48. Mechanical properties of CFRP-confined cylindrical specimens in Group-2 ($f_{co}$=20 MPa) ..... 158

Table 4.49. Mechanical properties of CFRP-confined cylindrical specimens in Group-3 ($f_{co}$=20 MPa) ..... 161

Table 4.50 Summary of the 20 MPa prismatic specimens ..... 162

Table 4.50. Mechanical properties of unconfined prismatic specimens in Group-1 ($f_{co}$=20 MPa) ..... 163

Table 4.51. Mechanical properties of CFRP-confined prismatic specimens in Group-1 ($f_{co}$=20 MPa) ..... 164

Table 4.52. Mechanical properties of CFRP-confined prismatic specimens in Group-2 ($f_{co}$=20 MPa) ..... 166

Table 4.53. Mechanical properties of CFRP-confined prismatic specimens in Group-3 ($f_{co}$=20 MPa) ..... 168

Table 5. 1 Effect of CFRP confinement on mechanical properties of concrete columns ..... 178

Table 5.2. Effect of workmanship on mechanical properties of CFRP-confined cylinders ..... 179

Table 5.3 Effect of dry H-C cycles on stiffness properties of CFRP-confined cylindrical specimens ..... 182

Table 5.4 Effect of dry H-C cycles on stiffness properties of CFRP-confined prismatic specimens ..... 185

Table 5.5 Effect of wet H-C cycles on stiffness properties of CFRP-confined prismatic specimens ..... 186

Table 5.6 Effect of dry H-C cycles on ultimate strength of CFRP-confined cylindrical specimens ..... 187

Table 5.7 Effect of H-C cycles on ultimate strength of CFRP-confined prismatic specimens ..... 189

Table 5.8 Effect of dry H-C cycles on ultimate strain of CFRP-confined cylindrical specimens ..... 190

Table 5.9 Effect of H-C cycles on ultimate strain of CFRP-confined prismatic specimens ..... 192

Table 5.10 Effect of outdoor exposure on stiffness properties of CFRP-confined concrete ..... 195

Table 5.11 Effect of outdoor exposure on ultimate strength of CFRP-confined specimens ..... 196

Table 5.12 Effect of outdoor exposure on ultimate strain of CFRP-confined specimens ..... 198

Table 5.13 Effect of H-C cycles and SL on stiffness properties of CFRP-confined cylindrical specimens ..... 201

Table 5.14 Effect of H-C cycles and SL on stiffness properties of CFRP-confined prismatic specimens ..... 204

Table 5.15 Effect of only SL on mechanical properties of CFRP-confined prismatic specimens ..... 205

Table 5.16 Effect of H-C cycles and SL on transition stress ($f_{ct}$) of CFRP-confined cylindrical specimens ..... 207

Table 5.17 Effect of H-C cycles and SL on transition stress ($f_{ct}$) of CFRP-confined prismatic specimens ..... 208

Table 5.18 Effect of SL on ultimate strength of CFRP-confined cylindrical specimens ..... 209

Table 5.19 Effect of SL on ultimate strength of CFRP-confined prismatic specimens ..... 210

Table 5.20 Effect of SL on ultimate strain of CFRP-confined cylindrical specimens ..... 212

Table 5.21 Effect of SL on ultimate strain of CFRP-confined prismatic specimens213

Table 5.22 Effect of SL level on mechanical properties of CFRP-confined prismatic specimens ..... 216

## LIST OF FIGURES

FIGURES

Figure 3.1 Sieve analysis results of the aggregates ..... 30

Figure 3.2 Preparation of the cylindrical concrete specimens; ..... 31

Figure 3.3 Moulds for prismatic specimens ..... 34

Figure 3.4 Specimens for coupon tests; a) CFRP, b) CFRP with epoxy ..... 35

Figure 3.5 Tensile test machine and coupon test specimen ..... 36

Figure 3.6 Failure types of coupon test specimens ..... 36

Figure 3.7 CFRP wrapping process; a) Primer layer, b) Putty layer c) Epoxy coated CFRP application, d) Schematic view of the wrapping sequence ..... 41

Figure 3.8 a) Environmental Test Chamber, b) Terminal outside the chamber, c) Terminal inside the chamber, d) Heating equipment ..... 46

Figure 3.9 Yearly maximum and minimum temperature values between 1975-2005 for 200 data points in Turkey ..... 48

Figure 3.10 Maximum temperature differences between 1975-2005 for 200 data points in Turkey ..... 48

Figure 3.11 Typical H-C cycles and relative humidity in the ETC ..... 49

Figure 3.12 Typical temperature variations in a specimen under H-C cycles ..... 50

Figure 3.13 Recorded temperature values during the exposure tests ..... 51

Figure 3.14 Recorded average relative humidity values during the exposure tests ... 51

Figure 3.15 Specially designed loading frame ..... 53

Figure 3.16 Loading Frames in the ETC ..... 53

Figure 3.17 Applied sustained stress level ..... 54

Figure 3.18 Relaxation and an attempt to increase the sustained load ..... 56

Figure 3.19 Sustained load was almost constant after 10 days ..... 56

Figure 3.20 a) ELE Autotest compression testing machine b) Data Acquisition system connected to the testing machine ..... 57

Figure 3.21 The compressometer used to test cylindrical specimens ..... 59

Figure 3.22 Working principle of the compressometer used to test cylindrical specimens ..... 59

Figure 3.23 The compressometer used to test prismatic specimens ..... 61

Figure 3.24 Working principle of the compressometer used to test prismatic specimens ..... 61

Figure 3.25 Schematic view of the strain gage locations ..... 62

Figure 4.1. Axial stress-strain diagram and mechanical properties of CFRP-confined concrete ..... 64

Figure 4.2. Axial stress-strain diagrams of unconfined cylindrical specimens in Group-1 (SET1 - $f_{co}$=10 MPa) ..... 68

Figure 4.3. Failure types of CFRP-confined cylindrical specimens in Group-1 (SET1 - $f_{co}$=10 MPa) ..... 69

Figure 4.4. Axial stress-strain diagrams of CFRP-confined cylindrical specimens in Group-1 (SET 1 - $f_{co}$=10 MPa) ..... 70

Figure 4.5. Axial stress-strain diagrams of unconfined cylindrical specimens in Group-2 (SET1 - $f_{co}$=10 MPa) ..... 71

Figure 4.6. Failure types of CFRP-confined cylindrical specimens in Group-2 (SET1 - $f_{co}$=10 MPa)..... 72

Figure 4.7. Axial stress-strain diagrams of CFRP-confined cylindrical specimens in Group-2 (SET1 - $f_{co}$=10 MPa)..... 73

Figure 4.8. Axial stress-strain diagrams of unconfined cylindrical specimens in Group-3 (SET 1 - $f_{co}$=10 MPa)..... 74

Figure 4.9. The moment at which CFRP-confined specimens failed under sustained loading..... 75

Figure 4.10. Failure of CFRP-confined specimens due to delamination..... 76

Figure 4.11. Axial stress-strain diagrams of unconfined cylindrical specimens in Group-1 (SET 2 - $f_{co}$=10 MPa)..... 77

Figure 4.12. Failure types of CFRP-confined cylindrical specimens in Group-1 (SET 2 - $f_{co}$=10 MPa)..... 78

Figure 4.13. Axial stress-strain diagrams of CFRP-confined cylindrical specimens in Group-1 ( SET 2 - $f_{co}$=10 MPa)..... 78

Figure 4.14. Failure types of CFRP-confined cylindrical specimens in Group-2 (SET 2 - $f_{co}$=10 MPa)..... 80

Figure 4.15. Axial stress-strain diagrams of CFRP-confined cylindrical specimens in Group-2 (SET 2 - $f_{co}$=10 MPa)..... 80

Figure 4.16. Failure types of CFRP-confined cylindrical specimens in Group-3 (SET 2 - $f_{co}$=10 MPa)..... 82

Figure 4.17. Axial stress-strain diagrams of CFRP-confined cylindrical specimens in Group-3 (SET 2 - $f_{co}$=10 MPa)..... 82

Figure 4.18. Failure types of CFRP-confined cylindrical specimens in Group-4 (SET 2 - $f_{co}$=10 MPa)..... 84

Figure 4.19. Axial stress-strain diagrams of CFRP-confined cylindrical specimens in Group-4 (SET 2 - $f_{co}$=10 MPa) ..... 84

Figure 4.20. Failure types of CFRP-confined cylindrical specimens in Group-6 (SET 2 - $f_{co}$=10 MPa) ..... 86

Figure 4.21. Axial stress-strain diagrams of CFRP-confined cylindrical specimens in Group-6 (SET 2 - $f_{co}$=10 MPa) ..... 86

Figure 4.22 The effectiveness of the FRP in concrete ..... 87

Figure 4.23. Failure types of unconfined prismatic specimens in Group-1 (SET 3 – $f_{co}$=10 MPa and r=25mm) ..... 92

Figure 4.24. Axial stress-strain diagrams of unconfined prismatic specimens in Group-1 (SET 3 - $f_{co}$=10 MPa and r=25 mm) ..... 93

Figure 4.25. Failure types of CFRP-confined prismatic specimens in Group-1 (SET 3 - $f_{co}$=10 MPa and r=25mm) ..... 94

Figure 4.26. Axial stress-strain diagrams of CFRP-confined prismatic specimens in Group-1 (SET 3 - $f_{co}$=10 MPa and r=25 mm) ..... 94

Figure 4.27 Schematic view of the gages used in C10-S300-25-103 ..... 96

Figure 4.28 Failure of C10-S300-25-103 (a, b and c) and confining stresses (d) ..... 97

Figure 4.29 Axial and lateral strain distributions in C10-S300-25-103 ..... 97

Figure 4.30 Stress-strain behavior of C10-S300-25-103 ..... 98

Figure 4.31. Failure types of unconfined prismatic specimens in Group-2 (SET 3 - $f_{co}$=10 MPa and r=25mm) ..... 99

Figure 4.32. Axial stress-strain diagrams of unconfined prismatic specimens in Group-2 (SET 3 - $f_{co}$=10 MPa and r=25 mm) ..... 100

Figure 4.33. Failure types of CFRP-confined prismatic specimens in Group-2 (SET 3 - $f_{co}$=10 MPa and r=25mm) ..... 101

Figure 4.34. Axial stress-strain diagrams of CFRP-confined prismatic specimens in Group-2 (SET 3 - $f_{co}$=10 MPa and r=25 mm) ..... 101

Figure 4.35 Schematic view of the gages used in C10-S300-25-204 ..... 103

Figure 4.36 Stress-strain behavior of C10-S300-25-204 ..... 103

Figure 4.37 Axial and lateral strain distributions in C10-S300-25-204..... 103

Figure 4.38. Failure types of unconfined prismatic specimens in Group-3 (SET 3 - $f_{co}$=10 MPa and r=25mm)..... 104

Figure 4.39. Axial stress-strain diagrams of unconfined prismatic specimens in Group-3 (SET 3 - $f_{co}$=10 MPa and r=25 mm) ..... 105

Figure 4.40. Failure types of CFRP-confined prismatic specimens in Group-3 (SET 3 - $f_{co}$=10 MPa, r=25mm and SL=0.4$f_{cc}$) ..... 106

Figure 4.41. Axial stress-strain diagrams of CFRP-confined prismatic specimens in Group-3 (SET 3 - $f_{co}$=10 MPa, r=25mm and SL=0.4$f_{cc}$)..... 107

Figure 4.42. Failure types of CFRP-confined prismatic specimens in Group-3 (SET 3 - $f_{co}$=10 MPa, r=25mm and SL=0.55$f_{cc}$) ..... 108

Figure 4.43. Axial stress-strain diagrams of CFRP-confined prismatic specimens in Group-3 (SET 3 - $f_{co}$=10 MPa, r=25mm and SL=0.55$f_{cc}$)..... 109

Figure 4.44 Schematic view of the gages used in C10-S300-25-305 ..... 110

Figure 4.45 Stress-strain behavior of C10-S300-25-305 ..... 110

Figure 4.46 Axial and lateral strain distributions in C10-S300-25-305..... 111

Figure 4.47. Failure types of CFRP-confined prismatic specimens in Group-4 (SET 3 - $f_{co}$=10 MPa, r=25mm and SL=0.4$f_{cc}$) ..... 112

Figure 4. 48. Axial stress-strain diagrams of CFRP-confined prismatic specimens in Group-4 (SET 3 - $f_{co}$=10 MPa, r=25mm and SL=0.4$f_{cc}$)..... 112

Figure 4.49. Failure types of CFRP-confined prismatic specimens in Group-6 (SET 3 - $f_{co}$=10 MPa, r=25mm) ..... 114

Figure 4.50. Axial stress-strain diagrams of CFRP-confined prismatic specimens in Group-6 (SET 3 - $f_{co}$=10 MPa, r=25mm) ..... 114

Figure 4.51 Schematic view of the gages used in C10-S300-25-601 ..... 115

Figure 4.52 Axial and lateral strain distributions in C10-S300-25-601 ..... 116

Figure 4.53 Axial stress-axial strain and axial stress-lateral strain behavior of C10-S300-25-601 ..... 116

Figure 4.54. Axial stress-strain diagrams of unconfined prismatic specimens in Group-1 (SET 4 - $f_{co}$=10 MPa and r=37.5mm) ..... 117

Figure 4.55. Failure types of CFRP-confined prismatic specimens in Group-1 (SET 4 - $f_{co}$=10 MPa and r=37.5mm) ..... 119

Figure 4.56. Axial stress-strain diagrams of CFRP-confined prismatic specimens in Group-1 (SET 4 - $f_{co}$=10 MPa and r=37.5mm) ..... 119

Figure 4.57. Axial stress-strain diagram of CFRP-confined prismatic specimen in Group-2 (SET 4 - $f_{co}$=10 MPa and r=37.5mm) ..... 120

Figure 4.58. Failure types of CFRP-confined prismatic specimens in Group-3 (SET 4 - $f_{co}$=10 MPa and r=37.5mm) ..... 122

Figure 4.59. Failure of C10-S300-37.5-302 ..... 122

Figure 4.60. Axial stress-strain diagrams of CFRP-confined prismatic specimens in Group-3 (SET 4 - $f_{co}$=10 MPa and r=37.5mm) ..... 123

Figure 4.61 Schematic view of the gages used in C10-S300-37.5-303 ..... 124

Figure 4.62 Axial and lateral strain distributions in C10-S300-37.5-303 ..... 124

Figure 4.63 Stress-strain behavior of C10-S300-37.5-303 ..... 125

Figure 4.64. Failure types of CFRP-confined prismatic specimens in Group-4 (SET 4 - $f_{co}$ =10 MPa and r=37.5mm) ..... 126

Figure 4.65. Axial stress-strain diagrams of CFRP-confined prismatic specimens in Group-4 (SET 4 - $f_{co}$=10 MPa and r=37.5mm) ..... 126

Figure 4.66 Schematic view of the gages used in C10-S300-37.5-403 ..... 128

Figure 4.67 Stress-strain behavior of C10-S300-37.5-403 ..... 128

Figure 4.68 Axial and lateral strain distributions in C10-S300-37.5-403..... 128

Figure 4.69. Failure types of CFRP-confined prismatic specimens in Group-5 (SET 4 - $f_{co}$=10 MPa and r=37.5mm) ..... 130

Figure 4.70. Axial stress-strain diagrams of CFRP-confined prismatic specimens in Group-5 (SET 4 - $f_{co}$=10 MPa and r=37.5mm) ..... 131

Figure 4.71. Failure types of CFRP-confined prismatic specimens in Group-6 (SET 4 - $f_{co}$=10 MPa and r=37.5mm) ..... 132

Figure 4.72. Axial stress-strain diagrams of CFRP-confined prismatic specimens in Group-6 (SET 4 - $f_{co}$=10 MPa and r=37.5mm) ..... 132

Figure 4.73. Failure types of unconfined prismatic specimens in Group-1 ($f_{co}$=15 MPa and r=37.5mm) ..... 135

Figure 4.74. Axial stress-strain diagrams of unconfined prismatic specimens in Group-1 ($f_{co}$=15 MPa and r=37.5mm) ..... 135

Figure 4.75. Failure types of CFRP-confined prismatic specimens in Group-1 ($f_{co}$=15 MPa and r=37.5mm) ..... 137

Figure 4.76. Axial stress-strain diagrams of CFRP-confined prismatic specimens in Group-1 ($f_{co}$=15 MPa and r=37.5mm) ..... 137

Figure 4.77. Failure types of unconfined prismatic specimens in Group-2 ($f_{co}$=15 MPa and r=37.5mm) ..... 138

Figure 4.78. Axial stress-strain diagrams of unconfined prismatic specimens in Group-2 ($f_{co}$=15 MPa and r=37.5mm) ..... 139

Figure 4.79. Failure types of CFRP-confined prismatic specimens in Group-2 ($f_{co}$=15 MPa and r=37.5mm) ..... 140

Figure 4.80. Axial stress-strain diagrams of CFRP-confined prismatic specimens in Group-2 ($f_{co}$=15 MPa and r=37.5mm) ..... 140

Figure 4.81. Failure types of unconfined prismatic specimens in Group-3 ($f_{co}$=15 MPa and r=37.5mm) ..... 142

Figure 4.82. Axial stress-strain diagrams of unconfined prismatic specimens in Group-3 ($f_{co}$=15 MPa and r=37.5mm) ..... 142

Figure 4.83. Failure types of CFRP-confined prismatic specimens in Group-3 ($f_{co}$=15 MPa and r=37.5mm) ..... 143

Figure 4.84. Axial stress-strain diagrams of CFRP-confined prismatic specimens in Group-3 ($f_{co}$=15 MPa and r=37.5mm) ..... 143

Figure 4.85. Failure types of CFRP-Confined prismatic specimens in Group-4 ($f_{co}$=15 MPa and r=37.5mm) ..... 145

Figure 4.86. Axial stress-strain diagrams of CFRP-Confined prismatic specimens in Group-4 ($f_{co}$=15 MPa and r=37.5mm) ..... 145

Figure 4.87 Schematic view of the gages used in C15-S300-37.5-401 ..... 146

Figure 4.88 Stress-strain behavior of C15-S300-37.5-401 ..... 146

Figure 4.89 Axial and lateral strain distributions in C15-S300-37.5-401..... 147

Figure 4.90. Failure types of CFRP-Confined prismatic specimens in Group-5 ($f_{co}$=15 MPa and r=37.5mm) ..... 148

Figure 4.91. Axial stress-strain diagrams of CFRP-Confined prismatic specimens in Group-5 ($f_{co}$=15 MPa and r=37.5mm) ..... 148

Figure 4.92. Failure types of CFRP-confined prismatic specimens in Group-6 ($f_{co}$=15 MPa and r=37.5mm) ..... 150

Figure 4.93. Axial stress-strain diagrams of CFRP-confined prismatic specimens in Group-6 ($f_{co}$=15 MPa and r=37.5mm) ..... 150

Figure 4.94. Axial stress-strain diagrams of unconfined cylindrical specimens in Group-1 ($f_{co}$=20 MPa) ..... 153

Figure 4.95. Failure types of CFRP-confined cylindrical specimens in Group-1 ($f_{co}$=20 MPa) ..... 154

Figure 4.96. Axial stress-strain diagrams of CFRP-confined cylindrical specimens in Group-1 ($f_{co}$=20 MPa) ..... 155

Figure 4.97. Axial stress-strain diagrams of unconfined cylindrical specimens in Group-2 ($f_{co}$=20 MPa) ..... 156

Figure 4.98. Failure types of CFRP-confined cylindrical specimens in Group-2 ($f_{co}$=20 MPa) ..... 157

Figure 4.99. Axial stress-strain diagrams of CFRP-confined cylindrical specimens in Group-2 ($f_{co}$=20 MPa) ..... 157

Figure 4.100. Undesired failure types of CFRP-confined cylindrical specimens in Group-3 ($f_{co}$=20 MPa) ..... 159

Figure 4.101. Effect of undesired failure types on the axial stress-axial strain diagrams ..... 159

Figure 4.102. Desired failure types of CFRP-confined cylindrical specimens in Group-3 ($f_{co}$=20 MPa) ..... 160

Figure 4.103. Axial stress-strain diagrams of CFRP-confined cylindrical specimens in Group-3 ($f_{co}$=20 MPa) ..... 160

Figure 4.104. Axial stress-strain diagrams of unconfined prismatic specimens in Group-1 ($f_{co}$=20 MPa) ..... 163

Figure 4.105. Failure types of CFRP-confined prismatic specimens in Group-1 ($f_{co}$=20 MPa) ..... 164

Figure 4.106. Axial stress-strain diagrams of CFRP-confined prismatic specimens in Group-1 ($f_{co}$=20 MPa) ..... 165

Figure 4.107. Failure types of CFRP-confined prismatic specimens in Group-2 ($f_{co}$=20 MPa) ..... 166

Figure 4.108. Axial stress-strain diagrams of CFRP-confined prismatic specimens in Group-2 ($f_{co}$=20 MPa) ..... 166

Figure 4.109. Failure types of CFRP-confined prismatic specimens in Group-3 ($f_{co}$=20 MPa) ..... 167

Figure 4.110. Axial stress-strain diagrams of CFRP-confined prismatic specimens in Group-3 ($f_{co}$=20 MPa) ..... 168

Figure 4.111 Schematic view of the gages used in C20-S300-37.5-303 ..... 169

Figure 4.113 Axial and lateral strain distributions in C20-S300-37.5-303 ..... 169

Figure 4.112 Stress-strain behavior of C20-S300-37.5-303 ..... 170

Figure 5.1 Strain distribution around the circumference of cylindrical [82] and prismatic specimens ..... 173

Figure 5.2. Behavior of unconfined and CFRP-confined specimens under compression ..... 175

Figure 5.3. Effect of CFRP confinement on behavior of concrete columns a) 10 MPa cylinder, b) 20 MPa cylinder, c) 10 MPa prismatic r=25 mm, d) 10 MPa prismatic r=37.5 mm, e) 15 MPa prismatic r=37.5 mm, f) 20 MPa prismatic r=37.5 mm..... 176

Figure 5.4. Effect of corner radius on the mechanical properties of CFRP-confined specimens a) Effect on strength, b) Effect on strain ..... 177

Figure 5.5. Effect of workmanship on the failure types of CFRP-confined cylinders ..... 179

Figure 5.6. Effect of dry H-C cycles on behavior of CFRP-confined cylindrical specimens a) 10 MPa, b) 20 MPa ..... 181

Figure 5.7. Effect of dry H-C cycles on CFRP-confined cylindrical specimens a) Effect on $E_1$, b) Effect on $E_2$ ..... 183

Figure 5.8. Effect of H-C cycles on behavior of CFRP-confined prismatic specimens, a) 10 MPa with r=25 mm, b) 10 MPa with r=37.5 mm, c) 15 MPa with r=37.5 mm, d) 20 MPa with r=37.5 mm ..... 184

Figure 5.9. Effect of dry H-C cycles on CFRP-confined prismatic specimens a) Effect on $E_1$, b) Effect on $E_2$ ..... 185

Figure 5.10. Comparison of dry and wet H-C cycles a) $E_1$, b) $E_2$ ..... 186

Figure 5.11. Effect of dry H-C cycles on ultimate strength of CFRP-confined cylindrical specimens ..... 188

Figure 5.12. Change in ultimate strength of CFRP-confined prismatic specimens with a) Dry H-C cycles, b) Wet H-C cycles ..... 189

Figure 5.13. Effect of dry H-C cycles on ultimate strain of CFRP-confined cylindrical specimens ..... 190

Figure 5.14. Change in ultimate strain of CFRP-confined prismatic specimens with a) Dry H-C cycles, b) Wet H-C cycles ..... 191

Figure 5.15. Effect of outdoor exposure on behavior of CFRP-confined specimens a) 10 MPa cylinder, b) 10 MPa prismatic r=25 mm, c) 10 MPa prismatic r=37.5 mm, d) 15 MPa prismatic r=37.5 mm, ..... 194

Figure 5.16. Comparative presentation of the behaviors of CFRP-confined specimens subjected to outdoor exposure ..... 194

Figure 5.17. Effect of outdoor exposure on a) $E_1$, b) $E_2$ ..... 195

Figure 5.18. Effect of outdoor exposure on ultimate strength of CFRP-confined specimens ..... 197

Figure 5.19. Effect of outdoor exposure on ultimate strain of CFRP-confined specimens ..... 198

Figure 5.20. Effect of SL on behavior of CFRP-confined cylindrical specimens a) 10 MPa, b) 20 MPa ..... 200

Figure 5.21. Effect of H-C cycles and SL on stiffness properties of CFRP-confined cylindrical specimens a) Effect on $E_1$, b) Effect on $E_2$ ..... 202

Figure 5.22. Effect of SL on behavior of CFRP-confined prismatic specimens a) 10 MPa prismatic r=25 mm, b) 10 MPa prismatic r=37.5 mm, c) 15 MPa prismatic r=37.5 mm, d) 20 MPa prismatic r=37.5 mm ..... 203

Figure 5.23. Effect of H-C cycles and SL on stiffness properties of CFRP-confined prismatic specimens a) Effect on $E_1$, b) Effect on $E_2$..... 204

Figure 5.24. Effect of H-C cycles and SL on strain distribution along the perimeter ..... 206

Figure 5.25. Effect of simultaneous exposure of H-C cycles and SL on $f_{ct}$ a) Change with corner radius b) Change with $f_{co}$ ..... 208

Figure 5.26. Effect of SL on ultimate strength of CFRP-confined specimens a) Change with corner radius, b) Change with $f_{co}$ ..... 211

Figure 5.27. Effect of SL on ultimate strain of CFRP-confined specimens a) Change with corner radius, b) Change with $f_{co}$ ..... 214

Figure 5.28. Effect of SL level on behavior of CFRP-confined prismatic specimens ..... 216

Figure 5.29. Effect of SL level on a) $f_{cc}$ b) $\varepsilon_{cc}$ c) $f_{ct}$..... 217

Figure 6.1. Effect of $f_{co}$ on a) $f_{cc}$, b) $\varepsilon_{cc}$..... 220

Figure 6.2. Effect of FRP thickness ($t_{FRP}$) on a) $f_{cc}$, b) $\varepsilon_{cc}$ ..... 220

Figure 6.3. Effect of overlap length on a) $f_{cc}$, b) $\varepsilon_{cc}$ ..... 221

Figure 6.4. Effect of SL on a) $f_{cc}$ and b) $\varepsilon_{cc}$..... 222

Figure 6.5. Effect of H-C cycles on a) $f_{cc}$, b) $\varepsilon_{cc}$ ..... 222

Figure 6.6. Effect of Outdoor Exposure on a) $f_{cc}$, b) $\varepsilon_{cc}$..... 223

Figure 6.7. Effect of [$2r/(D.f_{co})$] on a) $f_{cc}$, b) $\varepsilon_{cc}$..... 224

Figure 6.8. Effect of SL level on a) $f_{cc}$, b) $\varepsilon_{cc}$..... 225

Figure 6.9. Effect of H-C cycles on a) $f_{cc}$, b) $\varepsilon_{cc}$ ..... 226

Figure 6.10. Effect of outdoor exposure on a) $f_{cc}$, b) $\varepsilon_{cc}$ ..... 226

Figure 6.11. Axial stress-strain behavior of unconfined and FRP-confined concrete under compression ..... 227

Figure 6.12. Effect of SL level on FRP-reinforced concrete ..... 228

Figure 6.13. Transition stress estimation of FRP-reinforced concrete a) Cylindrical specimens b) Prismatic specimens ..... 230

Figure 6.14. Strength estimation of FRP-confined cylindrical specimens a) All data b) Data from this dissertation ..... 233

Figure 6.15. Strength estimation of FRP-confined prismatic specimens a) All data b) Data from this dissertation ..... 233

Figure 6.16. RMS errors for the strength estimation a) Cylindrical specimens b) Prismatic specimens..... 234

Figure 6.17. Strain estimation of FRP-confined cylindrical specimens a) All data b) Data from this dissertation ..... 235

Figure 6.18. Strain estimation of FRP-confined prismatic specimens a) All data b) Data from this dissertation ..... 236

Figure 6.19. RMS errors for the strain estimation a) Cylindrical specimens b) Prismatic specimens ..... 236

Figure 6.20. Behavior of FRP-reinforced concrete and the assumptions for the model ..... 237

Figure 6.21. Axial stress-strain diagrams of a) 10 MPa cylindrical specimens b) 20 MPa cylindrical specimens ..... 239

Figure 6.22. Axial stress-strain diagram of a) 11 MPa prismatic specimens b) 15 MPa prismatic specimens ..... 240

Figure 6.23. Axial stress-strain diagram of a) 16 MPa prismatic specimens b) 28 MPa prismatic specimens ..... 240

## LIST OF SYMBOLS

| | |
|---|---|
| $A_c$ | : Gross area of the specimen |
| $b$ | : Specimen width |
| $C$ | : Correction factor for creep effect |
| $c$ | : Power function for the confinement effect |
| $D$ | : Diameter of cylinder or side width of the square section |
| $d$ | : Displacement due to specimen deformation |
| $d_1$ | : Displacement measured by the left gage |
| $d_2$ | : Displacement measured by the right gage |
| $E_1$ | : Secant Modulus of Elasticity calculated at $0.4f_{co}$ |
| $E_2$ | : Slope of the linear part of axial stress-strain diagram of FRP-confined concrete |
| $E_{FRP}$ | : Modulus of Elasticity of FRP |
| $e_g$ | : Perpendicular distance from the gage to the vertical plane passing through the two support points of the rotating yokes |
| $e_r$ | : Perpendicular distance from the pivot rod to the vertical plane passing through the two support points of the rotating yokes |
| $f_c$ | : Stress corresponding to $\varepsilon$ |
| $f_{cc}$ | : Confined concrete strength |
| $f_{ccr}$ | : Strength of the confined reference specimen |
| $f_{co}$ | : Cylinder strength of unconfined concrete |
| $f_{conf}$ | : Confinement pressure |
| $f_{cop}$ | : Strength of unconfined prismatic specimen |
| $f_{ct}$ | : Transition stress |
| $f_{FRP}$ | : Tensile strength of FRP |

| | |
|---|---|
| $f_l$ | : Confinement effectiveness |
| $g$ | : Gage reading |
| $h$ | : Distance between upper and lower yokes |
| $H$ | : Height of the specimen |
| $k_1$ | : Strength coefficient |
| $k_2$ | : Strain factor |
| $l_{overlap}$ | : Overlap length of final wrapping |
| $n$ | : Number of FP layers |
| $n_d$ | : Number of data points |
| $P$ | : Perimeter of the specimen |
| $P_{confined}$ | : Axial load capacity of the confined specimen |
| $P_{unconfined}$ | : Axial load capacity of the unconfined specimen |
| $r$ | : Corner radius |
| $T$ | : Correction factor for temperature effect |
| $t_{eff}$ | : Effective thickness of FRP |
| $t_{FRP}$ | : Thickness of FRP |
| $T_g$ | : Glass transition temperature |
| $x_a$ | : Analytical data |
| $x_e$ | : Experimental data |
| $\Delta T$ | : Temperature difference |
| $\alpha$ | : Coefficient of thermal expansion |
| $\varepsilon$ | : Strain in concrete |
| $\varepsilon_{cc}$ | : Ultimate strain of FRP-confined concrete strain |
| $\varepsilon_{co}$ | : Unconfined concrete strain at $f_{co}$ |
| $\varepsilon_d$ | : Strain at the midpoint of the specimen |
| $\varepsilon_{FRP}$ | : Ultimate strain of FRP |
| $\varepsilon_g$ | : Strain at gage point |

## ABBREVIATIONS

| | |
|---|---|
| AFRP | : Aramid Fiber Reinforced Polymer |
| ASTM | : American Society for Testing and Materials |
| BP | : Boundary Point |
| CFFT | : Concrete Filled FRP Tube |
| CFRP | : Carbon Fiber Reinforced Polymer |
| COV | : Coefficient of variation |
| ETC | : Environmental Test Chamber |
| FRP | : Fiber Reinforced Polymer |
| FWCC | : FRP Wrapped Concrete Column |
| G1 | : Group 1 |
| G2 | : Group 2 |
| G3 | : Group 3 |
| G4 | : Group 4 |
| G5 | : Group 5 |
| G6 | : Group 6 |
| GFRP | : Glass Fiber Reinforced Polymer |
| H-C | : Heating-Cooling |
| KFRP | : Kevlar Fiber Reinforced Polymer |
| MCR | : Modified Confinement Ratio |
| RC | : Reinforced Concrete |
| RH | : Relative Humidity |
| RMS | : Root Mean Square |
| SL | : Sustained Loading |
| TEC | : Turkish Earthquake Code |
| UV | : Ultraviolet |

# CHAPTER 1

# INTRODUCTION

## 1.1 GENERAL

Reinforced concrete (RC) structures are being retrofitted because of deteriorations and material loss due to environmental effects. They are also being strengthened to withstand higher loads or to regain the load carrying capacities. In either procedure, the conventional techniques are to use the concrete and steel materials. Both materials are heavy, need special equipments and consume a considerable amount of space in the end product. Although the first investment costs of these techniques are relatively cheap, their maintenance costs are high [1].

Fiber reinforced polymers (FRPs) are introduced as alternative strengthening and retrofitting materials for reinforced concrete structures. They are composite materials, which are a combination of fibers and resin. The main load carrying material of this composite is the fibers, which have high strength in fiber direction. The resin enables load transfer between fibers.

FRPs have high strength and high modulus in the fiber direction and they have very low coefficient of thermal expansion when compared to concrete and steel. Besides their high mechanical properties, they are known not to corrode [2]. Since FRPs are lightweight, their mass can be neglected when compared to concrete and steel. They are easy to handle and do not need any special equipment for the application.

Although their initial costs are high, their maintenance costs are low when compared to other materials [2-6].

The advantages of FRPs made them popular in the concrete researches. They were used to increase the strength and strain capacity of a concrete column, or the moment and shear capacity of a beam or the lateral load carrying capacity of an RC frame by applying on an infill wall [2, 7].

Several studies were performed to investigate the strength and strain capacities of cylindrical and rectangular concrete columns with various strength levels wrapped with several layers of CFRP. In these studies, it was found out that the use of CFRP wrapping increases the strength of concrete columns depending on the number of CFRP plies applied, concrete grade, type of CFRP and the properties of the matrix material. Most of the experiments were conducted under room temperature and did not take into account the effects of environmental conditions.

Questioning the long-term behaviors of FRP-confined specimens, researchers conducted series of long-term exposure tests. However, in this time, the experiments considering freezing-thawing and/or sustained loading were performed on concrete grades above 20 MPa and the specimens were mainly in cylindrical form. It is known that reinforced concrete structures that are being retrofitted may have concrete grades much lower than that [8] and those structures include rectangular columns as well.

## 1.2 AIM OF THE DISSERTATION

This dissertation tries to fill the gap between the short-term and long-term behavior of FRP-confined concrete specimens. Therefore the main aim of this dissertation is

- To understand the effect of simultaneous exposure of heating-cooling cycles and sustained loading on the mechanical properties of concrete columns wrapped with one-layer of CFRP

- To establish a reliable model to predict the strength and strain capacities and stress-strain relationship of FRP-confined concrete under the experimentally studied exposures

In order to achieve the main aims given above, the following secondary parameters were investigated

- To understand the effectiveness of the confinement in different concrete strengths. The concrete strengths were chosen to be 10 MPa (the common concrete strength in Turkey [8]) representing very low concrete grade, 15 MPa (intermediate strength) and 20 MPa denoting the minimum concrete grade as given in Turkish Earthquake Code-2007[7].
- To understand the effectiveness of the confinement in different cross-sections. Concrete specimens were either in cylindrical or prismatic form.
- Effect of heating-cooling cycles, performed either in dry or wet conditions, on the mechanical properties of FRP-confined concrete
- Effect of outdoor exposures on the mechanical properties of FRP-confined concrete
- Effect of different sustained loading levels on mechanical properties of FRP-confined concrete

## 1.3 SCOPE

In this dissertation, both unconfined and CFRP-confined cylindrical and prismatic concrete specimens were utilized. Reinforcements were not provided in the specimens. Cylindrical specimens were prepared with 150x300 mm in dimension. As for the prismatic specimens having square-section, they were cast to have 150 mm side dimensions and 300 mm height. Corners of the prismatic specimens were rounded to increase the confinement effectiveness. Three different concrete grades were aimed: 10 MPa, 15 MPa and 20 MPa.

All specimens were tested in two phases. In Phase 1, they were subjected to aging tests and in the second phase (Phase 2), they were loaded monotonically up to failure to determine their mechanical properties.

Aging tests (Phase 1) were performed in six groups as shown in Table 1.1. In the first group, specimens were not subjected to any exposures, i.e. they were used as control specimens. In the second group, they were exposed to heating-cooling cycles (H-C) in a specially designed Environmental Test Chamber (ETC) under approximately 40% of relative humidity (RH). Specimens in the third group were subjected to simultaneous exposure of H-C cycles and sustained loading (SL), which was applied as the 40% of the ultimate axial load capacity. Some specimens were also loaded to 50% of their axial load capacity. In the fourth group, specimens were subjected to SL only. Wet H-C cycles were performed in Group 5 and specimens were subjected to outdoor exposures while being under direct sunlight in Group 6.

After the aging tests, specimens were loaded uniaxially until failure (Phase 2). No intentional eccentricity was allowed during the compression tests. During these tests, stress-strain behaviors were recorded. From the recorded data, strength, strain and modulus characteristics of all specimens were calculated to understand the change in their mechanical properties.

From the experimental results, an analytical axial stress-strain model including temperature changes and sustained loading level was established. The model was constructed using the data from three boundary points (BPs) which were also included the effect of the exposures studied in this dissertation.

**Table 1. 1 Definition of the test groups**

| Test Group | Definition of the test group |
|---|---|
| Group 1 | Control specimens |
| Group 2 | H-C cycles under approximately 40% of RH |
| Group 3 | Simultaneous exposure of SL and H-C cycles under approximately 40% of RH |
| Group 4 | Sustained loading |
| Group 5 | H-C cycles in water |
| Group 6 | Outdoor environment under direct sunlight |

## 1.4 ORGANIZATION OF THE DISSERTATION

The dissertation starts with a brief introduction concerning the strengthening of RC structures and use of FRP as an alternative technique (Chapter 1). Following this discussion, the aim and scope were outlined.

The available literature were reviewed and summarized in Chapter 2. First, studies conducted on FRP-confined concrete in ambient lab environment were presented. The effect of sustained loading, i.e., creep, on FRP-confined concrete were explained in terms of material point of view and then the effect on global structure were written. Durability of concrete and FRP was discussed later and then durability of FRP-confined concrete was presented. Finally, limited researches conducted on simultaneous exposure of environmental effect and sustained loading on specimens were reviewed.

Chapter 3 explains the experimental test program in detail. In this chapter, material properties were presented. Test procedures and the special equipments designed for the specific tests were discussed.

In Chapter 4, experimental test results were provided. The chapter was divided into three parts based on the concrete strength. In the first part test results of 10 MPa concretes, both cylindrical and prismatic forms were explained. Second part contains the results of 15 MPa prismatic specimens. Cylindrical specimens were not utilized in this part. As for the last part, experimental test results of 20 MPa cylindrical and prismatic specimens were presented.

Tests results given in Chapter 4 were discussed in Chapter 5. The discussions were given separately for each aging tests. First, effect of the confinement on the mechanical properties of concrete was given. Following this part, the change in mechanical properties of CFRP-confined concrete under H-C cycles was discussed. Discussion of the effect of outdoor exposure on mechanical properties of CFRP-confined concrete was provided in the next section. Finally, the effect of sustained loading with or without H-C cycles was presented.

The analytical studies were performed in Chapter 6. Parameters affecting the strength and strain capacities of FRP-confined concrete were discussed and a model was developed to predict the axial stress-strain behavior of FRP-confined concrete in either cylindrical or prismatic form. Sustained load level and temperature effects are included in the model. The model was verified with the tests results and it was found to be in good agreement with the experimental data.

The conclusions and recommendations for future studies were presented in Chapter 7.

# CHAPTER 2

# LITERATURE REVIEW

## 2.1 INTRODUCTION

Fiber Reinforced Polymers (FRPs) are known to be one of the effective confining materials in strengthening and retrofitting of concrete structures. They have high modulus and high strength. Since they are easy to apply and durable, they reduce the application time and maintenance cost [3]. Being lightweight, they will not contribute to the total weight of structures.

Besides their unique mechanical and material properties, their reliability was verified via experimental tests. Researchers performed tests considering several aspects of the material and its interaction with the concrete.

Summary of the literature review related to FRP-confined concretes and their long-term behavior was given below. The studies in material point of view were also presented.

## 2.2 STUDIES ON FRP CONFINEMENT

Columns are the most important load carrying members in a structure. Any loss in strength may push the whole structure to total collapse. Therefore, their strength should always be above a certain point. Because of their important, column strengthening and retrofitting was studied more.

One of the first attempts to use FRP as a confining material was made by Fardis and Khalili [3]. They tested short cylindrical concrete specimens strengthened with GFRP under uniaxial compression and under environmental effects such as weathering and fire. The columns had 31-34 MPa strength. After the tests, they reported that the strength and ductility characteristics of FRP-encased columns were excellent. Either the strength equation proposed by Richart [9] or Newman and Newman [10] were stated to be used to predict the strength of FRP-confined concrete. Besides strength estimation, the authors proposed a strain equation for the strengthened columns. The conclusions drawn by the authors were as follows:

- With the use of FRP, since the cross-sectional dimensions would reduce, dead loads and the material costs would reduce also.
- FRP serving as a formwork would reduce the formwork cost
- Since FRP is durable and non-corrosive, the maintenance cost would reduce.
- With the help of resin stabilizers or gel coats, FRP was found to be resistant to weathering

Saadatmanesh et al. [11] defined FRP confinement as a new technique for seismic strengthening. Their aim was to strengthen the bridge columns, which had deficiencies associated with design principles. They analytically studied the effectiveness of FRP confinement. The equation proposed by Mander et al [12] was taken as the base equation and it was modified with additional parameters to account with the FRP-confinement. Parametric studies were conducted to understand the axial force-moment interaction of the columns. They concluded that:

- The increase in axial load capacity is higher than the increase in moment capacity
- With increase in concrete strength, the rate of increase in axial load capacity, ductility and moment capacity reduces.
- If the thickness of the wrap increases, ductility would increase

Karbhari and Gao [13] tested cylindrical concrete specimens confined with CFRP considering several wrapping schemes. Since their aim was to establish a reliable model to predict the strength and ultimate strain, they did not use only a single orientation instead they changed the orientation of the main axis of CFRP. The main axis was either parallel to the hoop, or perpendicular, or made an angle with the hoop. Based on their test data they proposed two equations, one of which is empirical. Comparing their models with the available ones, they stated that in FRP wrapped systems, constant confinement assumption was not reliable. In addition, having bilinear response, FRP confinement differs from that of steel spiral reinforcement.

Early attempts to use FRP confinement in concrete columns were focused on the strengthening or retrofitting cylindrical bridge columns. Getting reasonable results, researchers extended the area of FRP usage and they tried to implement this technique in regular buildings having rectangular load carrying members. Rochette [14,15], tested rectangular short columns wrapped with CFRP and AFRP considering various corner radii. Strength of the specimens ranged from 35 to 43 MPa. As a conclusion, they stated that:

- The efficiency of the FRP confinement depends on the shape of the specimen. In circular specimens, the efficiency factor is the highest
- Corners of a rectangular specimen should be sufficiently rounded in order to prevent the premature failure of FRP
- In order to avoid sudden and destructive compression failure, specimens should not be highly confined.

Mirmiran et al. [16] made similar studies on rectangular short columns. They used 40 MPa square specimens and confined them with GFRP tubes with 6, 10 and 14 plies. A single corner radius of 6.35 mm was used in the tubes. Corners of the concrete specimens were not rounded. Based on the test results of their study and the results of Rochette [15]’s tests, they proposed an equation called Modified Confinement

Ratio (MCR). This equation could be used to estimate how much corner radius was necessary to achieve a specific confinement. They stated that:

- For a given confinement and corner radius if MCR was lower than 0.15, the specimen would not to be properly confined. In other words, the confinement would be inadequate if MCR was less than 0.15.
- Other than MCR factors, they stated that strength and ductility were not affected significantly by length to diameter ratios within the range of 2:1 and 5:1.

There are various studies experimentally investigating the strength and strain capacities of cylindrical and rectangular concrete columns with various strength levels wrapped with several layers of FRP. Table 2.1 summarizes some of the studies which were investigated the effect of FRP thickness on the behavior of cylindrical concrete columns. The concrete strengths ($f_{co}$) in the table varied from 6 MPa to 107 MPa and the number of FRP layers changed from 1 to 15. Considering all these studies, main findings can be listed as follows:

- Strength and strain capacities of confined concrete increase with increase in FRP thickness
- The strength and modulus of FRP play an important role on the effectiveness of the confinement
- The rate of increase in strength and strain reduces with increasing concrete strength
- Hoop strain capacity of FRP is lower than its strain capacity obtained from flat coupon test

**Table 2.1 Studies related to the cylindrical concrete columns confined with FRP**

| Author | Dimensions | $f_{co}$, MPa | FRP Type | Number of plies |
|---|---|---|---|---|
| Samaan et al. [17] | 150x300 | 30 | GFRP | 6,10,14 |
| Shahawy et al. [18] | 150x300 | 20 and 41 | CFRP | 1 to 5 |
| Ilki et al. [19] | 150x300 | 6 | CFRP | 1 to 6 |
| Li et al. [20] | 100x200<br>120x240<br>150x300 | 17-20-27 | CFRP | 1,2,3 |
| Lam and Teng [21] | 150x300 | 35 | CFRP<br>GFRP | 1,2,3 |
| Xia and Wu [22] | 150x300 | 33 to 63 | CFRP<br>GFRP | 1 to 4 |
| Harries and Kharel [23] | 150x300 | 36 to 60 | CFRP<br>GFRP | 1 to15 |
| Tamuzs et al. [24] | 150x300 | 20 to 60 | CFRP | 1,2,3 |
| Almusallam [25] | 150x300 | 50 to 100 | GFRP | 1,3 |

As for tests on rectangular specimens, authors studied the effect of corner radius (*r*) and the aspect ratio in addition to the FRP type, FRP thickness and concrete grade (Table 2.2). The most important observations were stated as:

- FRP is an effective confinement material in rectangular concrete columns. It can increase both strength and strain capacities.
- Corner radius and the properties of FRP directly affect the confinement effectiveness. FRP confinement is not effective in specimens having sharp corners.
- Failure of rectangular specimens confined with FRP occurs at the corners where stress concentrations are high.
- With increasing concrete strength, the required corner radius to achieve an adequate confinement increases

- Aspect ratio affects the strength and strain enhancement. As the aspect ratio increases, the enhancement reduces.

**Table 2.2 Studies related to the prismatic concrete columns confined with FRP**

| Author | Dimensions | r , mm | $f_{co}$, MPa | FRP Type | Number of plies |
|---|---|---|---|---|---|
| Parvin and Wang [26] | 108x108x305 | 8 | 21 | CFRP | 1,2 |
| Chaallal et al. [27] | 133x133x305<br>108x165x305<br>95x190x305 | 25 | 20-40 | CFRP | 1 to 4 |
| Lam and Teng [28] | 150x150x600 | 15-25 | 24-33-41 | CFRP | 1 to 5 |
| Masia et al. [29] | 100x100x300<br>125x125x375<br>150x150x450 | 25 | 25 | CFRP | 2 |
| Al-Salloum [30] | 150x150x500 | 5 to 50 | 30 | CFRP | 1 |
| Rousakis and Karabinis [31] | 200x200x320 | 30 | 33-40 | CFRP<br>GFRP | 1 to 6 |
| Benzaid et al. [32] | 100x100x300 | 0-8-16 | 55 | GFRP | 1,2 |
| Wang and Wu [33] | 150x150x300 | 0 to 60 | 30-50 | CFRP | 2 |
| Wu and Wei [34] | 150x150x300<br>188x150x300<br>225x150x300<br>263x150x300<br>300x150x300 | 30 | 30 | CFRP | 1,2 |

## 2.3 STUDIES ON CREEP OF FRP-CONFINED CONCRETE

***a) Concrete***

Concrete columns experience time-dependent increase in deformation due to the sustained loading (SL), which is called as creep. Creep occurs due to either bond-breakage between aggregates and cement paste or seepage of gel water flow, or viscous flow of cement paste or delayed elasticity or combination of all [35]. It is affected by several factors such as [36]:

- The composition of the concrete
- Age of concrete
- Humidity and temperature
- Level of sustained loading etc.

Creep increases with increase in water-cement ratio, sustained loading, temperature and humidity level but it decreases with the age of concrete [35]. Concrete creeps even under small SLs. The maximum value of the SL that can be applied on a concrete column was found to be approximately 80% of the axial load capacity [37].

Since several authors performed creep tests at constant temperature and relative humidity (RH), Vandewalle [38] tried to understand the creep of concrete under variable temperature and humidity. They uniaxially loaded the cylindrical concrete specimens cast from three different mixes and kept them under heating-cooling cycles and RH based on the temperature variations in Belgium. From their experiments, they observed that:

- Concrete mix has little effect on the creep and shrinkage behavior of concrete
- The variation in basic and total creep during one year exposure to RH cycles is not well pronounced
- Creep is affected by the concrete casting season

***b) Fiber Reinforced Polymer***

FRP is totally a different material as compared to concrete. It is orthotropic and can be regarded as elastic up to failure. Being an elastic material, its creep performance is questioned by Raghavan and Meshii [39, 40]. They performed tests on CFRP composites with different orientations to understand the creep behavior and finally they proposed a model to predict the creep of polymer composites. They stated that stress, temperature and time play an important role in the creep of composite. All these factors increase the creep. In addition, they found that the fibers in the composite cannot prevent composite from creeping but they reduce the creep and creep rate of the epoxy matrix.

***c) FRP-Confined Concrete***

Since both concrete and FRP creep under SL and their creep performances are affected by similar factors, same behavior can be expected from FRP-confined concrete.

Naguib and Mirmiran [41] studied the time-dependent behavior of ‘‘concrete filled FRP tube (CFFT)’’ and ‘‘FRP wrapped concrete column (FWCC)’’. The concrete strengths in their studies were 38 MPa for CFFT and 29 MPa for FWCC. The sustained loading level was chosen to be minimum 9 % and maximum 33% of axial load capacity. After 3 or 6 months from loading, they concluded that;

- Since concrete is stressed multiaxially upon confining with FRP, it experiences relatively less creep
- Stress redistribution takes place between concrete and FRP which results in a stress relief in the concrete. This phenomenon leads to a decrease in creep
- Since FRP shell prevents moisture to escape, it creates sealing effect and results in a reduction in shrinkage and creep.

Based on their study, Naguib and Mirmiran[42] proposed a model to estimate the time-dependent behavior of FRP-confined concrete. From the model, they tried to predict the creep rupture life and with this study they stated that:

- If the FRP-wrapped concrete column (FWCC) is loaded to its 70% of the axial load capacity, the creep rupture life will not be less than 100 years for $D/t_{FRP}$ ratios greater than 40, where D is the diameter of the concrete core and t is the thickness of the FRP used in the confinement.
- As for CFFTs with $D/t_{FRP}$ ratios above 40, the creep rupture life will be 75 years for a sustained loading level of 70% of the axial load capacity

Theriault et al. [43] performed static, short-term (three days) and long-term (150 days) creep tests on CFRP-wrapped cylindrical concrete columns having 24.5 and 29 MPa strength. CFRP was applied as one, two and three layers to correlate the FRP thickness with creep performance. The other parameter of the study was the level of SL. They investigated the creep limit associated with the SL level. Therefore, SL level was applied as the $0.4f_{cc}$ through $0.9f_{cc}$. High level of SL was utilized in short-term loading. They reported that:

- Creep resistance and SL level are inversely proportional
- Creep resistance will increase with increase in the confinement level

Al-Chami [44] in his dissertation prepared a set of experiments to test creep performance of cylindrical short columns, beams and CFRP. 28-day concrete strength changed from 24 to 34 MPa. The parameters were the CFRP thickness (one, two and three layers were used) and SL level. In columns and CFRP experiments, he performed static, short-term creep and long-term creep tests whereas in beams, only static and long-term tests were conducted. Static tests denoted for the tests in which specimens loaded to failure in a short period of time. Short-term creep tests were performed by applying higher SL to make the specimen fail in a few hours or days. As for the long-term tests, specimens were loaded to a sustained loading level such that they could survive 416 days. The results he stated after the tests are as follows:

- CFRP sheets exhibited more creep than CFRP laminates
- The creep performance of CFRPs is quite good because they survived until the end of the tests

- Reserve strength of CFRP-confined concrete columns increased due to the SL
- Despite the strength increase, columns experienced a decrease in the ductility, i.e., ultimate axial strains seem to reduce
- The transition in the stress-strain curve changes with SL and it becomes apparent for higher levels of SL
- A slight decrease was observed in the modulus of elasticity of specimens subjected to SL
- Creep results in an increase in the confining pressure. The increase in the confining pressure was observed to reduce with increase in the number of CFRP layers
- Confinement enhances the creep performance of the concrete
- SL level of 70% of the confined concrete strength can be taken as the creep limit for CFRP-confined concrete columns. This limit was advised to be the minimum of 100% of the unconfined concrete strength and 70% of the confined concrete strength.

Wang and Zhang [45] used cylindrical specimens and Zhang et al. [46] tested prismatic specimens having 47.3 and 51.1 MPa strengths. Both cylindrical and prismatic specimens were wrapped with two layers of AFRP. They were subjected to a sustained load level of 30% of the measured 28-day strength. Some cylindrical specimens were prepared with internal steel reinforcements. After 312 days under sustained loading, the authors observed that;

- The pattern of the stress-strain curve of FRP-confined concrete was not affected by the plastic strains resulted from creep. After subjecting sustained loading, the confined concrete still had a bilinear behavior.
- Although modulus of elasticity increased with creep, a slight decrease was observed in the strength
- Creep resulted in a reduction in the ultimate strain capacity, which directly affected the deformability of the concrete.

## 2.4 STUDIES ON DURABILITY OF FRP-CONFINED CONCRETE

***a) Concrete***

Concrete structures are often exposed to various environmental exposures such as temperature changes, humidity, sulfate attack, ultraviolet light and alkalines. All these exposures create various deterioration mechanisms depending on the durability of the concrete [47]. "Durability of Portland cement concrete is defined as the ability to resist weathering action, chemical attack, abrasion, or any other process of deterioration [48]".

Freezing-thawing is found to be one of the unfavorable effects on hardened concrete. Powers [49] tried to explain the mechanism of frost in the concrete. He stated that water expands almost 9% upon freezing and this freezing forces the free water to migrate, which creates hydraulic pressure due to the resistance of concrete to this migration. If the hydraulic pressure is greater enough it causes cracks in the concrete. Air-entrained admixtures may be the solution to the durability of concrete under freezing and thawing action. Using air-entrained admixtures, however, results in a strength reduction because increasing the air content for 1% was found to decrease the strength about 5% [50].

Wong et al. [51] studied the effect of drying on freeze-thaw durability of concrete. From the experiments conducted on small-scale concrete slabs, they concluded that:

- Although air-entrained admixtures are used, concrete may be affected by freezing and thawing
- Freeze-thaw durability of concrete, which was wet-dry-wet cured, was significantly greater than the one, which was continuously wet cured.
- Drying is stated to be important in terms of durability, if it is applied 3-5 days after the 7 days of wet-curing

Freeze-thaw experiments are extreme cases, which cause deterioration in the concrete. They are durability-based tests. Without going these extremes, the

influence of thermal loading at which temperatures were always above the freezing temperature was studied by Vecchio and Sato [52]. They tested three reinforced concrete portal frames under thermal and mechanical loading. The frames were built in real size and rotated 180 degrees to form a tank. After sealing the open parts, water was filled in the tank and thermal loading was applied through heating and cooling the water. Thermal loading was applied between 15°C and 95°C. Thermal gradients were recorded via thermocouples. After different thermal and mechanical loadings, they observed that:

- Thermal gradient was non-linear shortly after loading but became linear when the temperature held constant for a long period (18 h).
- Strain gradient followed the same trend as the thermal gradient. Strains corresponding to high temperature were high and tensile in nature whereas they were compression and relatively low at lower temperature. From the strain readings it was stated that beam and columns bended due to the thermal loading.
- New cracks during thermal loadings were not reported, however, from strain readings, they noticed that internal cracks were developed
- Increasing the number of internal steels would not enhance the resistance of concrete to thermal loading, rather it increased the thermal loading developed in the concrete

***b) Fiber Reinforced Polymer***

The influence of environmental exposure on FRP composite depends on the resistance of fibers and the matrix material. It was reported that since matrix is highly vulnerable to environmental exposure, mechanical properties depending mainly on matrix change significantly.

The effect of moisture absorbtion on mechanical properties of FRP has been studied by several researchers. Cohen et al. [53] tested CFRP, GFRP and KFRP (Kevlar Fiber Reinforced Polymer) to identify the behavior under hygrothermal conditions.

Besides the absorbtion tests, they also performed flexural tests on these materials. Flexural specimens were also immersed in water and thermal cycling was applied. They found that:

- KFRP absorbed the highest amount of water, whereas GFRP absorbed the least amount of water when they were kept in water under room temperature
- If the specimens were subjected to hot temperature-room temperature cycle in water the absorbtion of GFRP and KFRP increased
- CFRP was not affected from that thermal cycling
- Although CFRP and KFRP specimens experienced a slight decrease in flexural capacity under hot temperature exposures, the more pronounced reduction was observed in GFRP
- CFRP is not sensitive to hot temperature immersion

Selzer and Friedrich [54] tested CFRP composites to determine the effect of moisture on their mechanical properties. Three different epoxies, in which two of them were thermosetting (EP and $EP_{mod}$) and the other was thermoplastic (PEEK), were used. The authors prepared unidirectional ($[0]_{16}$, $[90]_{16}$), bidirectional ($[0, 90]_{4s}$) and multidirectional ($[0, \pm45, 90]_{2s}$) laminates. The laminates were tested under dry, semi saturated and fully saturated conditions under three different temperature ranges of 23, 70 and 100°C. The main results are summarized below:

- Since thermoplastic epoxy (CF/PEEK) absorbed less moisture (0.3 wt%), its glass transition temperature ($T_g$) did not change as compared to the others (CF/EP-1.6 wt% and CF/$EP_{mod}$-2.5 wt%)
- Tensile strength of unidirectional laminates showed no degradation since the load carrying fibers were in the loading direction
- If the orientation of the fibers with respect to the loading direction changed, tensile strength would become dependent on epoxy. Epoxy showed softening with increase in moisture content. Tensile strength in this type of laminates was inversely proportional to the moisture absorbtion. The higher the moisture intake, the lower the tensile strength

- Like tensile strength, elongation also depended on moisture content, which influenced the resistance of epoxy. Higher moisture content resulted in lower elongation.

Al-Salehi et al. [55] prepared angle-ply CFRP tubes, which were tested to find the effect of temperature changes on their tensile strength under hoop loading. The CFRP tubes had a winding angel of 25°, 55° and 75° with respect to the tube axis. In other words, 75° winding angle was close to a laminate constructed by [0] angle and 25° was close to [90] angle. Tubes were subjected to 3 different temperatures; -46°C, 20°C and 70°C in water. After each exposure, specimens were burst by applying internal pressure and their mechanical properties were recorded. According to the findings, they concluded that:

- Tubes with a winding angle of 75° failed by CFRP rupture whereas 25° failed by weeping since it was loaded from weak axis
- No apparent difference in mechanical properties such as hoop strength, strain, modulus was observed in 75° angle tubes at either temperature exposures
- No significant change was seen in 25° tubes because these specimens were weak in hoop direction.
- Hoop strength and secant hoop modulus of 55° tubes were found to decrease with increase in temperature

Rivera and Karbhari [56] tested CFRP flat plates and hollow cylindrical specimens, which were prepared using vinylester epoxy resin under the combined effect of humidity or salt water with freeze-thaw conditions, which were applied as decreasing temperature to -10°C and increasing to 22.5°C, for 100 days. They reported that, exposure to -10°C decreased the ductility of the matrix. Freeze-thaw cycling was seen to affect the fiber-matrix bond negatively, which became significant with moisture absorbtion. Tensile strength of CFRP specimens was observed to slightly

increase with freezing, but a considerable decrease was noted under freeze-thaw effect in water and freeze-thaw effect in salt water.

The researches dealing with moisture absorbtion and temperature effects that were performed afterwards mostly end up with the same aforementioned results in which the main effect was found to be on matrix, i.e., CFRP was not significantly affected [57-60].

In addition to the above experiments, Labossiere et al. [61] tried to understand the effect of ambient environment on CFRP and epoxy. They prepared one ply and four plies of CFRP sheets and 5 mm epoxy resin. All specimens were placed in direct exposure of sunlight under actual climatic conditions in different countries. After 1, 3, 5, 7, and 10 years of exposure, they conducted monotonic tests to clarify the difference in the mechanical properties. After 3 years of exposure, they found that tensile strength of CFRP plates had a tendency to decrease with the climatic exposures. The maximum reduction in tensile strength was observed to be 16%. Homam [4] exposed the CFRP plates to ultraviolet radiation using effective fluorescent lamps. He realized that tensile strength and stiffness of CFRP slightly increase after 4800 h exposure but its strain capacity reduced which increased the brittleness.

***c) FRP-Confined Concrete***

When the deterioration of FRP reinforced concrete members are examined under environmental effects, several studies revealed that FRP wrapped concrete members could exhibit reduction in strength and strain capacities. Among those, Toutanji and Balaguru [62] and Toutanji [63] tested CFRP and GFRP confined cylindrical specimens of 76 mm in diameter and 305 mm in length under 300 wet-dry cycles using salt water and freeze-thaw conditions. 28-day concrete strength was 30 MPa and two layers of FRP were applied as strengthening. They reported that:

- GFRP confined specimens experienced a strength reduction under wet-dry cycles in the order of 3 to 18% depending on the epoxy resin

- When specimens confined with CFRP were of concern under wet-dry cycles, the decrease in strength was almost 5%. In this case, the effect of epoxy resin was not significant
- An increase in the ductility (5 to 15%) was observed in CFRP confined specimens, however, GFRP specimens were observed to have a reduction in the ductility (20 to 42%) after the exposures.

Karbhari et al. [64] used 56 MPa cyindrical specimens wrapped with three layers of CFRP or GFRP and seven layers of GFRP. Specimens were subjected to dry freeze-thaw cycles between -20°C and 22.5°C. After 201 cycles, they concluded that:

- Freeze-thaw exposure resulted in a matrix hardening and softening which created microcracks at the fiber-matrix interphase.
- The exposure affected the mechanical properties and failure type of FRP confined concrete
- Strength was seen to be slightly decreased due to freeze-thaw cycles
- Hoop strain was observed to decrease after freeze-thaw cycles

Kshirsagar et al. [65] tested 28 plain and 54 GFRP wrapped concrete cylindrical specimens (102x204 mm) of 38 MPa strength under environmental aging such as exposure of alkaline solutions at room temperature and at 66°C, water at 66°C and freeze-thaw between -29 and 49°C. After 1000 h, 3000 h and 8000 h of exposures they tested specimens to see the progress of the change in mechanical properties. The observations were summarized below:

- Although the shape of the stress-strain curves were similar as the reference ones, the transition stress (stress at which a considerable decrease was seen in the slope) reduced with the environmental exposure. They attributed this to the residual hoop strains developed due to hygrothermal swelling which may result in a decrease in the confining action
- The ultimate strength and strain was found to reduce but the reduction was not pH dependent

- Freeze-thaw exposures and dry heating tests did not resulted in a change in mechanical properties

Karbhari [66] utilized 41 MPa cylindrical concrete specimens wrapped with three layers of CFRP. He prepared a set of tests to understand the effects of freeze-thaw, saturated freeze and saturated freeze-thaw on the mechanical properties. The aging cycles were performed continuously for 150, 300 and 450 days/cycles. Based on these tests he drew the conclusions as follows:

- 450 freeze-thaw cycles resulted in a 19.8% decrease in strength.
- The dry freeze made CFRP-confined concrete more brittle.
- Different from dry freeze tests, saturated freeze tests showed that fiber-matrix debonding developed and circumferential cracking occurred.
- Modulus of the FRP composite was not affected by any of the exposures.

Micelli et al. [67] conducted an experimental program to identify the change in mechanical properties of CFRP wrapped concrete cylinders having 43 MPa strength when they were subjected to NaCl, HCl and water solutions for 2000 h. CFRP was applied either one layer or four layers in which all plies had different orientations. Water immersion at 40°C revealed almost 2.5% weight increase in the epoxy resin. After 2000 h of exposures, no significant change was observed in strength and strain capacities of CFRP confined concrete.

Bae [68] and Belarbi and Bae [69] studied the various environmental exposures on the mechanical properties of reinforced concrete columns confined with FRP. They prepared small scale (150x450 mm) and mid scale (150x900) RC columns wrapped with CFRP or GFRP. Specimens were subjected to freeze-thaw, high temperature and high humidity cycles, UV radiation and saline solution. They found that:

- Freeze-thaw exposures resulted in a slight increase in compressive strength (4 to 7%) which could be attributed to the matrix hardening

- Whereas ductility was observed to decrease in the order of 1 to 4% which was believed to occur due to the debonding in matrix-fiber interface
- The combined effects of environmental exposure (freeze-thaw, high temperature, high humidity) was not significant in CFRP confined specimens whereas it was significant in GFRP confined specimens.
- Saline solution exposure was found to be the most adverse effect which resulted in a 14% reduction in the strength of GFRP confined specimens and at most 5% decrease in the strength of CFRP confined specimens. This exposure also negatively affected the ductility of the GFRP confined specimens by 26%. No reduction was mentioned on the ductility of CFRP confined specimens.

Saenz et al. [70] tested CFRP and GFRP-confined cylindrical concrete specimens under several environmental exposures such as interior, exterior and freeze-thaw cycling in saltwater with a 23% concentration. 28-day concrete strengths were 33 and 38 MPa. After exposure tests, they conducted uniaxial compression tests to determine the change in the mechanical properties. The results showed that:

- Although strength and strain were affected by the exposures, the overall behavior, i.e., stress-strain diagram, was similar to the reference ones.
- The reason for having relatively low strength and strain was attributed to the microcrakings developed due to the environmental exposures leading to internal damage in the concrete which resulted in an early initiation of volumetric dilation response of FRP composite.

Al-Salloum et al. [71] tested 100x200 mm cylindrical concrete specimens wrapped with one layer of CFRP or GFRP under 100°C and 200°C for 1, 2 and 3 h to determine the relation between high temperature and the mechanical properties. The concrete strength was 38 MPa. The results of their experiments revealed that:

- CFRP confined specimens subjected to 200°C experienced slightly higher strains than the ones at 100°C which was attributed to the softening of FRP and the reduction in the confinement.
- For each temperature range, strength of CFRP confined specimens reduced by increase in exposure time
- Rate of loss in strength was found to be great when the temperature was above the glass transition temperature

## 2.5 STUDIES OF SIMULTANEOUS EXPOSURE OF ENVIRONMENTAL EFFECTS AND SL ON FRP-CONFINED CONCRETE

In the abovementioned studies, researchers dealt with the environmental exposure and sustained loading separately. However, most of the structures are under the combined effects of temperature, load, and humidity. Therefore, the questions raised from the behavior under combined effects should be answered. To answer this question Kong [72] and Kong et al. [73] tested GFRP and CFRP confined cylindrical concrete specimens under freeze-thaw and/or sustained loading. For freeze-thaw cycles, they followed ASTM C666 procedure. The sustained load level was chosen to be 45% of the ultimate axial load capacity. All specimens were preloaded and immersed in water to increase the moisture content in the specimens. By this procedure, they aimed to create the worst-case scenario during freeze-thaw experiments. After 300 freeze–thaw cycles they reported that:

- CFRP confined normal weight specimens were slightly affected by the simultaneous exposure of freeze-thaw and sustained loading. The reduction in strength was noted as 3%.
- Freeze-thaw exposure was observed to have adverse effect on the specimens wrapped with CFRP. Three of the four specimens failed before the completion of 300 cycles. The reason was attributed to non-uniform bending created during freezing and thawing process, which creates longitudinal deformation in the concrete.

- The transition stress of the CFRP confined specimens subjected to sustained load was found to be higher when compared to the reference. This was stated to be because of the creep effect, which resulted in an increase in both axial and radial strains due to Poisson's effect.
- As for the GFRP confined specimens that were subjected to simultaneous exposures, only 3 % strength reduction was recorded. However, 7% reduction was noted when specimens were exposed to freeze-thaw only.

Green et al. [74] performed similar tests on 150x300 mm cylindrical specimens that were wrapped with one layer of CFRP or GFRP. The compressive strength of the lightweight specimens was 40 MPa. Before the exposure tests, specimens were preloaded to 45% of their strength to create cracking and then they were placed in water for one week. The freeze-thaw was applied such that temperature was reduced to -18° and then raised to 15°C. They applied a sustained load level as the 45% of the ultimate strength. The findings were given below:

- Simultaneous exposure of freeze-thaw and sustained loading resulted in a 2% decrease in CFRP confined lightweight specimens whereas the reduction was 9% for the ones wrapped with GFRP
- When the effect of only freeze-thaw was of concern, the reductions were found to be higher. CFRP confined specimens lost 5% of their strength and 16% drop was observed in GFRP confined specimens.
- The sustained load was believed to be beneficial because it prevented free expansion in longitudinal direction due to freeze-thaw action.

The effect of simultaneous exposure of freeze-thaw and sustained loading (SL) on CFRP-concrete bond was studied by Krishnaswamy and Lopez [75]. They bonded CFRP strips to concrete having 40 MPa at the time of bond tests. The sustained loading was applied as 7.5% and 15% of the failure load. Following the completion of 80 freeze-thaw cycles, specimens were subjected to monotonic loading until

failure and their mechanical properties were recorded. The experimental results were indicated that:

- Freeze-thaw exposure had no significant effect on mechanical properties of concrete and CFRP strips. However, 16% reduction in failure strength was observed in epoxy coupons.
- Failure types in bond tests were defined as the combination of concrete-failure and the failure of interface at concrete and adhesive layer.
- The reduction was observed in failure loads, when specimens exposed to sustained load. It was mentioned that the reduction was proportional to the sustained load level (1% reduction at 7.5% SL and 10% decrease at 15% SL)
- The simultaneous exposure was observed to reduce the failure load by 2.8% for the specimens loaded to 7.5% and 4.2% for the ones loaded to 15%.

# CHAPTER 3

# EXPERIMENTAL PROGRAM

## 3.1 INTRODUCTION

The main objective of this dissertation is to determine the change in the mechanical properties of CFRP-confined concrete columns under heating-cooling cycles and sustained loads. The experimental program consisted of two phases. In the first phase, specimens were exposed to accelerated aging. After aging (Phase 2), uniaxial compression tests were performed to determine the mechanical properties, such as strength, strain capacity, modulus of elasticity etc.

In order to understand the effects of exposures, aging tests were decided to be performed in four groups. First group of specimens were used as control specimens. In the second group, specimens were subjected to heating-cooling (H-C) cycles under approximately 40% relative humidity. Specimens were exposed to simultaneous exposure of heating-cooling cycles and sustained loading (SL) in Group 3. As for the last group, Group 4, specimens were only subjected to SL. In each group, the effect of a specific exposure was investigated. In addition to these tests, it was decided to construct two more groups to account for the different H-C procedures; i.e., specimens were either tested in water while being subjected to H-C cycles (Group 5) or kept under direct sunlight to investigate the effect of outdoor environment (Group 6). Table 3.1 summarizes the description of test groups.

**Table 3.1 Definition of the test groups**

| Test Group | Definition of the test group |
|---|---|
| Group 1 | Control specimens |
| Group 2 | H-C cycles under approximately 40% of RH |
| Group 3 | Simultaneous exposure of SL and H-C cycles under approximately 40% of RH |
| Group 4 | Sustained loading |
| Group 5 | H-C cycles in water |
| Group 6 | Outdoor environment under direct sunlight |

## 3.2 MATERIAL PROPERTIES

Concrete, primer, putty, epoxy and CFRP were the materials used and tested. Their properties were explained in the following sections.

### 3.2.1. Concrete

CFRP wrapping is widely used in strengthening of RC columns. In Turkey, most of the vulnerable buildings and bridges have very low concrete strength. Recent study on concrete quality showed that, the quality of concrete in Turkey was very close to the ones used in this dissertation. It was found out that the mean compressive strength was 5.38 MPa for public structures, 8.96 MPa for residential structures and 14.80 MPa for military structures located mainly in Istanbul [8].

Three different concrete strengths were aimed in this dissertation. 10 MPa strength was selected to represent the low strength concrete, 15 MPa strength was used to have specimens between low and medium strength and 20 MPa strength, which is the lower value stated in Turkish EQ Code-2007 [7], was chosen to represent the medium strength concrete.

Before the design of concrete mix, physical properties of aggregates were determined as shown in Table 3.2. The result of sieve analysis is given in Figure 3.1. For cement type, CEM II/B-M (P-L) 32.5 R Portland Composite Cement was used.

**Table 3.2 Physical properties of aggregates**

| | Coarse Aggregate (7-19 mm) | Coarse Aggregate (3-7 mm) | Fine Aggregate (0-3 mm) |
|---|---|---|---|
| Specific Gravity (Dry) | 2.69 | 2.79 | 2.32 |
| Specific Gravity (SSD*) | 2.70 | 2.82 | 2.43 |
| Water Absorption (%) | 0.30 | 1.40 | 4.80 |

* SSD: Saturated Surface Dry

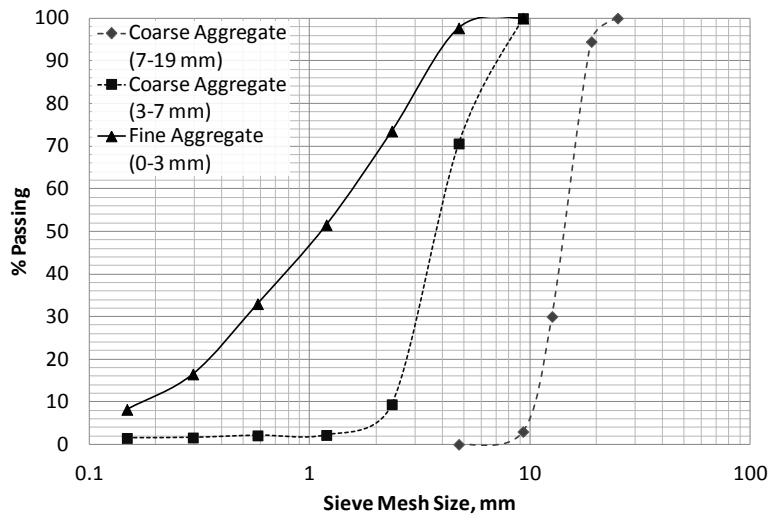


**Figure 3.1 Sieve analysis results of the aggregates**

Representative figures of concrete mixing, specimen preparation, curing and tests to determine the physical properties of aggregates are given in Figure 3.2.

**Figure 3.2 Preparation of the cylindrical concrete specimens; a-b) Tests to determine the physical properties of aggregates, c) Concrete was mixed via mixer and then poured into cylindrical moulds, d) Slump and air content of the mix were determined, e) Cylindrical specimens in the mould, f) In order to prevent rapid evaporation, specimens covered with wet burlap**

After determining the material properties mentioned above, concrete was prepared considering the mixing proportions given in Table 3.3. As shown in the table, for 10 MPa concrete water/cement ratio was 0.92, for 15 MPa concrete water/cement ratio was 0.74 and for 20 MPa the ratio was 0.64. Coarse aggregates were only used to prepare 10 MPa concrete. No air-entrainment was used in the mix design, as the freeze-thaw resistance of the concrete specimens is not to be determined.

**Table 3.3 Concrete mix proportions**

| **Material** | **Amount (kg/m$^3$)** | | |
|---|---|---|---|
| | **10 MPa** | **15 MPa** | **20 MPa** |
| 0-3 (Fine Aggregate) | 436 | 781 | 792 |
| 3-7 (Coarse Aggregate ) | 873 | 918 | 931 |
| 7-19 (Coarse Aggregate) | 459 | --- | --- |
| CEM II/B-M(P-L) 32,5 R | 275 | 344 | 349 |
| Water | 253 | 253 | 224 |
| **Water/Cement Ratio** | **0.92** | **0.74** | **0.64** |

Concrete specimens were cast in three types of moulds as listed in Table 3.4. The moulds were either cylindrical or prismatic in shape. Cylindrical moulds were 150 mm in diameter and 300 mm in height. Although all prismatic moulds had a cross-sectional dimension of 150x150 mm, they differed from each other in terms of corner radii.

Cylindrical specimens were prepared vertically while prismatic specimens were casted horizontally as shown in Figure 3.3. A single prismatic mould consisted of three long side plates and two wooden plates to cover the ends. Corners were

rounded by using plastic pipes. Plastic pipes were cut in four to be used in all corners. 50 mm pipe with 1 mm thickness were used to have 25 mm corner radius and 75 mm pipe with 2 mm thickness were used to have 37.5 mm corner radius. The reason for choosing 25 mm and 37.5 mm corner radii was to achieve an adequate confinement since corner radius was known to be one of the main parameter in prismatic specimens. The other reason was to understand the effect of corner radius on the behavior.

Thus, the effects of following parameters were aimed to be discussed;

- Shape effect (cylindrical and prismatic)
- Corner radius effect (same strength with different corner radius)
- Effect of concrete strength (same corner radius with different strength)

**Table 3.4 Specimen shapes used in the dissertation**

| **Concrete strength** | **Cylindrical** (150x300 mm) | **Prismatic** (150x150x300 mm, corner radius: 25 mm) | **Prismatic** (150x150x300 mm, corner radius: 37.5 mm) |
|---|---|---|---|
| 10 MPa | ✓ | ✓ | ✓ |
| 15 MPa | | | ✓ |
| 20 MPa | ✓ | | ✓ |

Specimens were removed from the moulds after 2 days and 5-day curing was applied at room temperature. During the curing period, concrete was kept moist by wrapping the specimens with wet burlap.

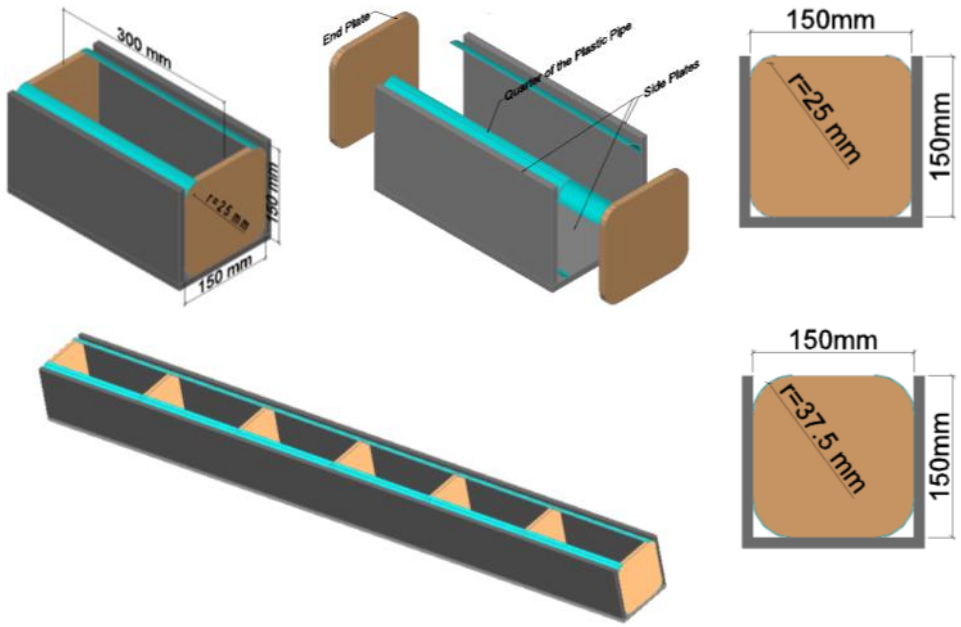


**Figure 3.3 Moulds for prismatic specimens**

### 3.2.2. Carbon Fiber Reinforced Polymer (CFRP)

Carbon fiber reinforced polymer (CFRP) is made of carbon fibers, which have micro-graphite crystal structures. CFRP sheets have high tensile strength and elastic modulus while being lightweight. Besides these mechanical properties, it has low thermal expansion coefficient [76].

In this dissertation, sheets with unidirectional carbon fibers (MBrace C1-30) were used. The material has high tensile strength and elastic modulus. Mechanical properties supplied by the manufacturer [77] were given in Table 3.5.

**Table 3.5 Mechanical and Physical Properties of the CFRP (MBrace C1-30)**

| Material Property | Amount | |
|---|---|---|
| Density of fiber | 1820 | kg/m³ |
| Effective Thickness | 0.165 | mm |
| Tensile Strength | 3430 | MPa |
| Tensile Modulus of Elasticity | 230 | GPa |
| Ultimate Strain | 0.015 | mm/mm |
| Coefficient of Thermal Expansion | $-1x10^{-7}$ | 1/°C |
| Thermal Conductivity | 17 | J/msK |
| Electrical resistivity | $2.6x10^{-5}$ (Conductive) | Ω-m |

To determine the tensile strength of CFRP, coupon tests were performed as shown in Figure 3.5. Single ply CFRP coupon specimens were prepared with a length of 300 mm and width of 25 mm. They were either coated with epoxy or kept uncoated as shown in Figure 3.4. Ends of coupons were strengthened using thick plastics to avoid the failure at the ends.

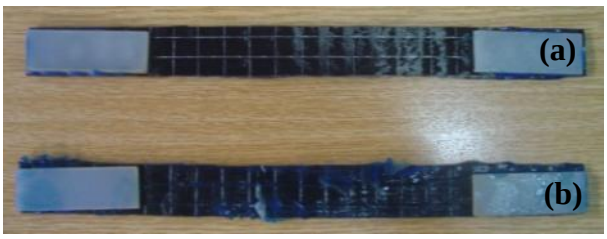


**Figure 3.4 Specimens for coupon tests; a) CFRP, b) CFRP with epoxy**

**Figure 3.5 Tensile test machine and coupon test specimen**

Failure types were observed to be different for epoxy coated specimens and specimens without epoxy. While epoxy coated specimens experienced brittle failure, specimens without epoxy failed in ductile manner.

After coupon tests, ultimate load and corresponding ultimate tensile strength were determined. As it is seen from the Table 3.6, average ultimate tensile strength of epoxy-coated specimens was calculated as 3013 MPa. This value was 12% lower than the value supplied by the manufacturer.

**Figure 3.6 Failure types of coupon test specimens**

**Table 3.6 Coupon test results for specimens coated with epoxy**

| Specimen | Length (mm) | Width (mm) | Ultimate Load (N) | Ultimate Strength (MPa) |
|---|---|---|---|---|
| 1 | 300 | 26.0 | 14943 | 3483 |
| 2 | 300 | 25.5 | 12459 | 2961 |
| 4 | 300 | 25.0 | 11085 | 2687 |
| 5 | 300 | 22.6 | 11282 | 3025 |
| 6 | 300 | 26.2 | 12361 | 2860 |
| 7 | 300 | 26.4 | 13342 | 3060 |
| **Average** | **300** | **25.3** | **12578** | **3013** |
| COV, % | | | 11.3 | 8.9 |

### 3.2.3. Primer, Putty and Epoxy

Primer layer was the first adhesive layer used in the CFRP wrapping process. It was applied on a clean concrete surface, penetrated into the surface of concrete, and increased the bond between the following adhesive layers and concrete surface. The primer used in this dissertation was MBT-MBrace Primer. It was composed of two components namely A and B. Component A was the epoxy resin and component B was the epoxy hardener. The mixture was prepared such that component A covered the 75% of the mixture by volume. Material properties of the primer were given in Table 3.7 as supplied by the manufacturer.

Putty layer was the second adhesive layer. It was applied on top of the primer layer and was used to fix the damaged parts of the concrete and to create a smooth surface before the CFRP application. Concresive 1406 was used as the putty layer. This material was composed of two components which were mixed 1/3 by weight, i.e., in

the mixture 25% of weight was component B and 75% was component A. Material properties of Concresive 1406 was given in Table 3.8.

**Table 3.7 Material properties of the primer [77]**

| Material Property | Amount | |
|---|---|---|
| Density of the mixture | 1080 | kg/m³ |
| Tensile Strength | 12 | MPa |
| Flexural Strength (7 days) | 24 | MPa |
| Bonding Strength (Concrete) (7 days) | $\sigma_{tc}$ | MPa (concrete tensile strength) |
| Tensile Modulus of Elasticity (7 days) | 700 | MPa |
| Flexural Modulus of Elasticity (7 days) | 580 | MPa |
| Ultimate Strain | 3 | % |

**Table 3.8 Material Properties of the putty [77]**

| Material Property | Amount | |
|---|---|---|
| Density of the mixture | 1700 | kg/m³ |
| Compressive Strength (7 days) | 75 | MPa |
| Flexural Strength (7 days) | 25 | MPa |
| Bonding strength to Concrete (7 days) | 3.5 | MPa (concrete failure) |

Epoxy was the last layer of adhesive that was applied on both the putty layer and CFRP material to create full bond. In this dissertation, MBT-MBrace Adesivo Saturant was used as the epoxy. Like the other adhesives, this material was also composed of two components and the mix ratio was 1/3 by volume, i.e., component

A (epoxy resin) covered the 75% of the volume. Material properties supplied by the manufacturer were presented in Table 3.9.

**Table 3.9 Material Properties of the epoxy [77]**

| Material Property | Amount | |
|---|---|---|
| Density of the mixture | 1020 | kg/m³ |
| Flexural Strength (7 days) | 70 | MPa |
| Compressive Strength (7 days) | 70 | MPa |
| Bonding Strength to Concrete (7 days) | 3 | MPa |
| Tensile Elastic Modulus (7 days) | 3000 | MPa |
| Flexural Elastic Modulus (7 days) | 3500 | MPa |
| Ultimate Strain | 2.5% | |

### 3.2.4. CFRP Wrapping and Specimen Preparation

Concrete specimens were either confined with one layer of CFRP or left unconfined. The confinement was achieved by wet-layup wrapping process (Figure 3.7). The process composed of:

- Cleaning the surface of the concrete specimen - surface was cleaned and dust was removed in order to improve the bond between first layer of adhesive and concrete,
- Primer layer - a thin layer of primer was applied by means of a roller and specimens were cured for a day,
- Putty layer - putty layer was applied on the primer layer in order to create a smooth surface between concrete and CFRP,
- Epoxy layer – CFRP sheets were cut in a desired length using scissors and

after 2 hours from the putty application epoxy was applied by means of a roller on concrete and CFRP sheet,

- CFRP wrapping - finally concrete was wrapped with CFRP providing an overlapping length of 11% of the perimeter of the specimen. CFRP's strong axis was decided to be perpendicular to the longitudinal axis of the specimen in order to ensure confining action. During the wrapping process of the specimens, special care was given to eliminate the voids between concrete and CFRP.

In the application guide, the manufacturer recommended to use a minimum of 100 mm as the overlap. However, in previous studies it was shown that strain distribution in cylindrical specimen was not uniform considering whole circumference. Strain was low at overlapping zone while high outside that zone [21]. Therefore, if overlapping zone were kept shorter, it would not be so wrong to assume a uniform strain distribution along the circumference. However, in prismatic concrete specimens, a uniform strain distribution assumption is not possible. Considering the strain distribution along the circumference, the reason for supplying relatively short overlapping was to simulate one layer strengthening without introducing lengthy stiff parts. Initial trials with 6% revealed the failure of confined specimens under heating-cooling and sustained loading without surviving to the end of the test. For the specimens with 6% overlapping all failures were due to the delamination and this was attributed to the inadequate overlapping. For that reason, the overlapping region was kept 11% of the perimeter.

Specimens were allowed to cure under ambient lab conditions for at least 5 days. Following this curing period, specimen ends were capped either with sulphur mortar (especially cylindrical specimens) or with a mixture of gypsum and cement (prismatic specimens).

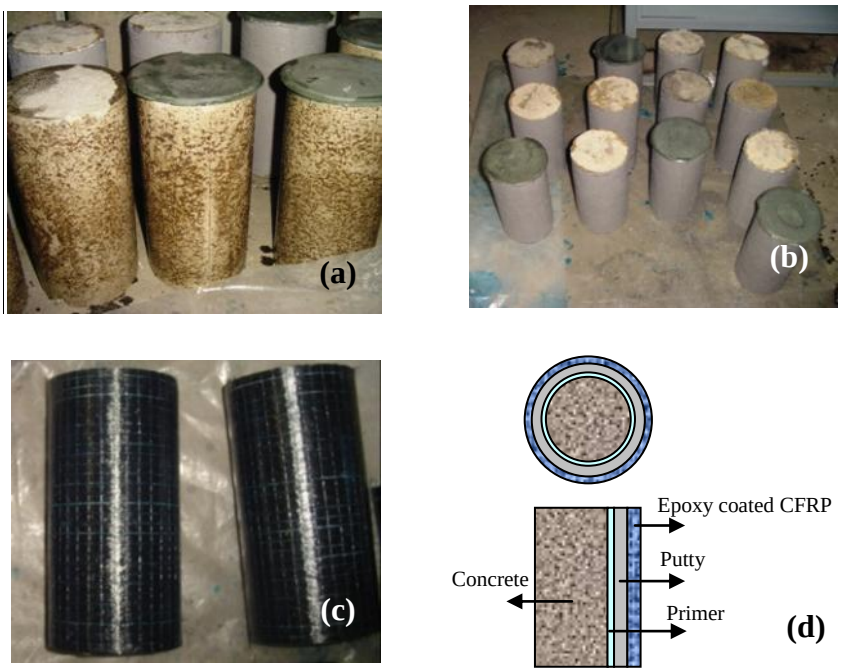


**Figure 3.7 CFRP wrapping process; a) Primer layer, b) Putty layer c) Epoxy coated CFRP application, d) Schematic view of the wrapping sequence**

## 3.3 TEST PROCEDURE

Experimental studies were performed at both Structural Mechanics Laboratory and Materials of Construction Laboratory of Civil Engineering Department of Middle East Technical University.

Specimens were tested in two-phases. First phase was called “Exposure Test”. In this phase, specimens were exposed to heating-cooling cycles and/or sustained loading. After the exposure tests, specimens were subjected to uniaxial compressive loading in the second phase until failure to determine the mechanical properties, such as strength, strain capacity, modulus of elasticity, axial stress-strain behavior.

In aging tests, specimens were tested in six groups as shown in Table 3.10. Specimens in the first group were kept at room temperature and used as control specimens. In the second group, specimens were exposed to heating-cooling cycles in the specially designed environmental test chamber. Specimens in the third group were loaded to a desired sustained load level while simultaneously being exposed to heating-cooling cycles; however, in the fourth group specimens were only exposed to sustained loads under room temperature. Fifth group was similar to the second group except that in this group specimens were kept in water while simultaneously being subjected to heating-cooling cycles in the environmental test chamber. Finally, the last group specimens were kept outside of the lab to determine the outdoor environmental effect.

Before starting the tests, specimens were coded to be distinguished from each other. The coding scheme was given in Table 3.11. Based on this scheme, for example, the fifth cylindrical confined specimen of 300 mm height having 10 MPa strength, which was exposed to only heating-cooling cycles (Group 2) was coded as "C10-C300-205". As for prismatic specimens, if it was coded as "C20-S300-25-301", this meant that it was a prismatic confined specimen of 20 MPa strength, its height was 300 mm, it had a corner radius of 25 mm and it was the first specimen of Group 3. Besides specimens' codes, the group codes were also defined as shown in Table 3.12. Group codes represent the average of all the specimens in the group. For example, C10-G1-S-25 shows the confined prismatic specimens in Group 1 having 10 MPa strength and 25 mm corner radius.

**Table 3.10 Test matrix for Phase 1-Exposure Test**

| | | 10 MPa | | | 15 MPa | 20 MPa | |
|---|---|---|---|---|---|---|---|
| | | Cylindrical | Prismatic | | Prismatic | Cylindrical | Prismatic |
| | | r=75 mm | r=25 mm | r=37.5 mm | r=37.5 mm | r=75 mm | r=37.5 mm |
| **Group1 Reference** | **Unconfined** | ✓ | ✓ | ✓ | ✓ | ✓ | ✓ |
| | **CFRP-Confined** | ✓ | ✓ | ✓ | ✓ | ✓ | ✓ |
| **Group2 Heating-Cooling** | **Unconfined** | ✓ | ✓ | | ✓ | ✓ | |
| | **CFRP-Confined** | ✓ | ✓ | ✓ | ✓ | ✓ | ✓ |
| **Group3 Sustained Load and Heating-Cooling** | **Unconfined** | ✓ | ✓ | | ✓ | | |
| | **CFRP-Confined** | ✓ | ✓ | ✓ | ✓ | ✓ | ✓ |
| **Group4 Sustained Load** | **CFRP-Confined** | ✓ | ✓ | ✓ | ✓ | | |
| **Group5 Heating-Cooling in Water** | **CFRP-Confined** | | | ✓ | ✓ | | |
| **Group6 Outdoor Exposure** | **CFRP-Confined** | ✓ | ✓ | ✓ | ✓ | | |

**Table 3.11 Coding scheme for the specimens**

| Confinement | Strength (MPa) | Cross Section | Height (mm) | Corner radius (mm) | Group No. | Specimen No. |
|---|---|---|---|---|---|---|
| C (Confined) | 10 | S (Square) | 300 | 25 | 1 | 01 |
| | 15 | | | 37.5 | 2 | 02 |
| U (Unconfined) | 20 | C (Cylinder) | | (null for Cylinders) | 3 | etc. |
| | | | | | 4 | |
| | | | | | 5 | |
| | | | | | 6 | |

**Table 3.12 Coding scheme for the groups**

| Confinement | Strength (MPa) | Group No. | Cross Section | Corner radius in prism specimens (mm) |
|---|---|---|---|---|
| C (Confined) | 10 | G1 | S (Square) | 25 |
| | 15 | G2 | | 37.5 |
| U (Unconfined) | 20 | G3 | C (Cylinder) | (null for Cylinders) |
| | | G4 | | |
| | | G5 | | |
| | | G6 | | |

### 3.3.1 Heating-Cooling Tests

Heating-cooling cycles were performed in a specially designed environmental test chamber. The main properties of the chamber are as follows:

- The chamber was manufactured from polyurethane panels having 38-42 kg/m³ density. The inner surface of the chamber was made of stainless steel while the outer surface was of PVC panels.
- Operating temperature was in between -10±5°C and +50±5°C and relative humidity could be 80% at 50°C
- The cooling system was a split system with hermetic compressor
- Heating and cooling cycles were controlled via PLC (Programmable Logical Controller) screen
- The control of heating and cooling systems had a process speed of 0.5 microseconds.
- The chamber was 200x400x200 cm (width*length*height) in dimension and it had an inner volume of 16 m³.

The cooling system was placed at the outside of the chamber while the heating system was kept inside as shown in Figure 3.8. a and d.

Heating-cooling cycles and the relative humidity level can be adjusted from the PLC screen placed outside of the chamber. However, the adjustment should be made manually. Considering the high number of cycles, manual control becomes unfeasible. Therefore, PLC screen was connected to a computer and software was written to enable the online control of the screen.

The data transfer from inside to outside was carried out via terminals. One of the terminals was attached inside and the other one kept outside (Figure 3.8. b-c). The hole between terminals was filled with insulating foam.

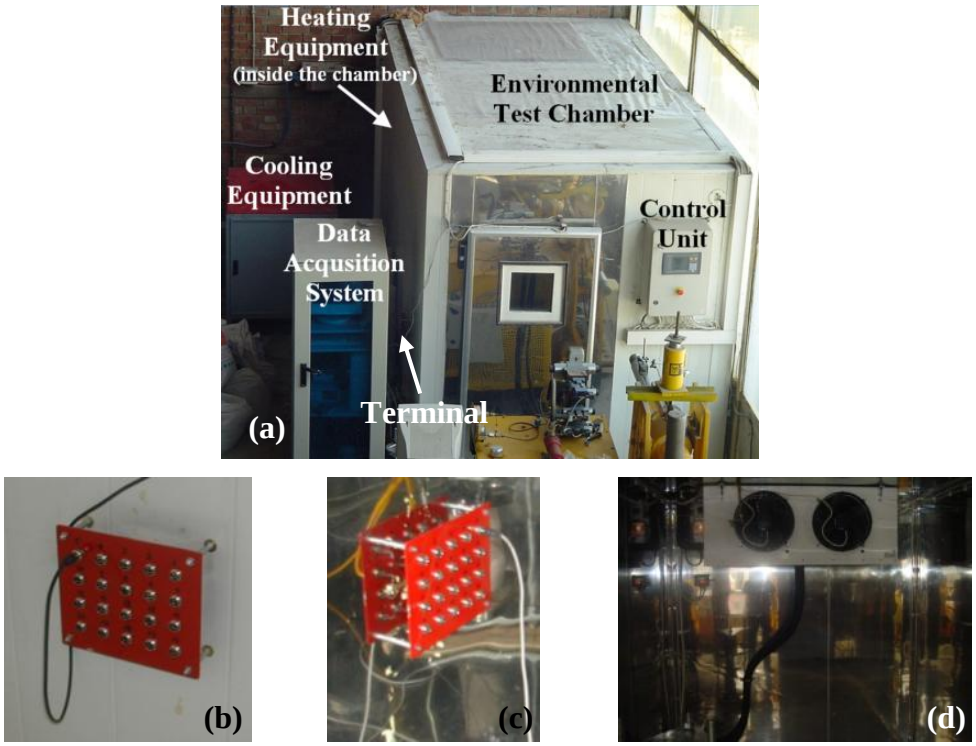


**Figure 3.8 a) Environmental Test Chamber, b) Terminal outside the chamber, c) Terminal inside the chamber, d) Heating equipment**

In this dissertation, a new test procedure for heating-cooling cycles was defined based on the data recorded by Turkish State Meteorological Service [79]. Maximum and minimum temperature values for 200 points in Turkey, which was recorded between 1975 and 2005, were taken as given in Figure 3.9. As it can be seen from the figure, the average minimum temperature was found to be -14.3°C and the average maximum temperature was determined as 41.4°C. In addition to these values, yearly maximum temperature differences for 200 points recorded in 30 years were presented in Figure 3.10. In this figure, yearly average temperature range was calculated as 56°C. With the help of these data, it was decided to apply a temperature range of 60°C. Considering the heating-cooling capacity of the environmental test chamber, minimum temperature was selected as -10°C and maximum temperature as 50°C. Those temperature values were selected because one of the aims of this

dissertation was to understand the effect of heating-cooling cycles on the mechanical properties of CFRP-confined concrete not the unfavorable situations under freeze-thaw cycles.

The number of cycles that would be repeated during the tests was searched and it was found out that the total number of temperature cycles varies between 100 and 450 [41, 43, 62-66, 70, 72-74]. Since there was no unique number of cycles, it was decided to determine the number of cycles considering the freeze-thaw characteristics of Turkey. In order to determine the freeze-thaw characteristics of Turkey, daily maximum and minimum temperatures of all cities for the period of 2000 and 2006 were obtained from Turkish State Meteorological Service [79]. In Table 3.13, freeze-thaw cycles for different regions considering each year were given. Based on the values presented in the table it was detected that an average of 45 freeze-thaw cycles occurred in a year. From this table it was decided to perform 200 heating-cooling cycles which could be regarded to correspond to the 4-year of the exposure period.

**Table 3.13 Freeze-thaw cycles for different regions considering the period of 2000-2006**

| **Region** | **2000** | **2001** | **2002** | **2003** | **2004** | **2005** | **2006** | **Average** |
|---|---|---|---|---|---|---|---|---|
| Marmara | 32 | 21 | 26 | 40 | 34 | 26 | 33 | **30** |
| Ege | 35 | 21 | 26 | 26 | 32 | 26 | 30 | **28** |
| Akdeniz | 38 | 22 | 30 | 30 | 29 | 27 | 30 | **30** |
| İç Anadolu | 95 | 71 | 70 | 84 | 86 | 86 | 91 | **83** |
| Karadeniz | 37 | 21 | 28 | 29 | 34 | 27 | 39 | **31** |
| Doğu Anadolu | 85 | 70 | 67 | 79 | 82 | 75 | 89 | **78** |
| Güney Doğu Anadolu | 42 | 23 | 43 | 34 | 43 | 34 | 36 | **36** |
| **Average** | **52** | **35** | **42** | **46** | **49** | **43** | **50** | **45** |

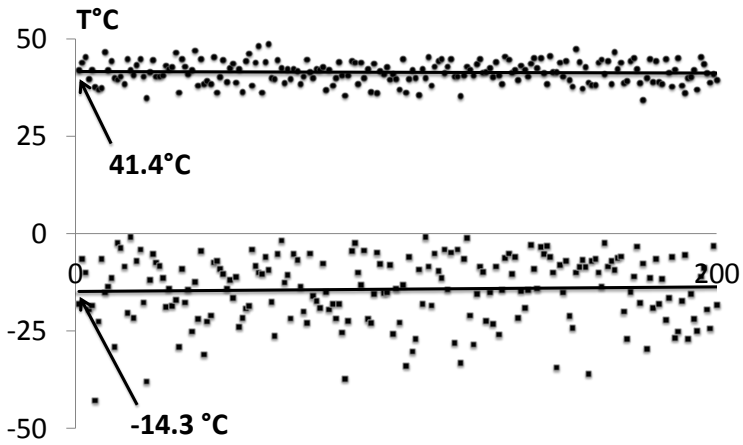


**Figure 3.9 Yearly maximum and minimum temperature values between 1975-2005 for 200 data points in Turkey**

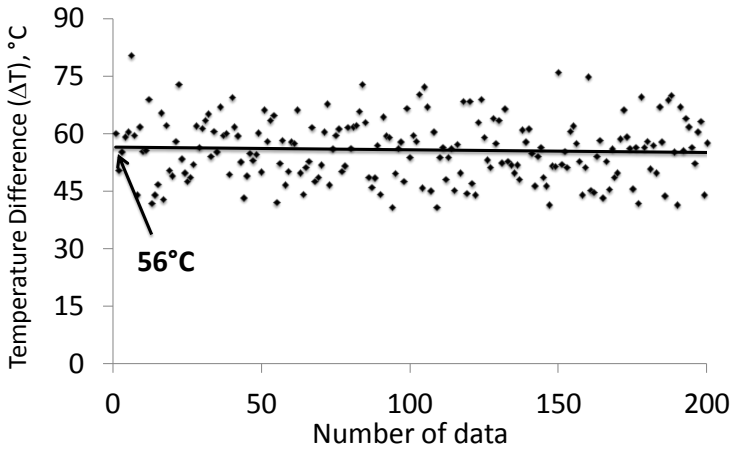


**Figure 3.10 Maximum temperature differences between 1975-2005 for 200 data points in Turkey**

After determining the maximum and minimum temperature values and the number of cycles, heating-cooling procedure that would be followed during tests was

established. According to this procedure, inside temperature of the environmental test chamber was increased to 50°C and maintained at that level for 30 min. and heating period is later followed by a cooling period, in which temperature was dropped down to -10°C and this temperature was kept constant for an hour. While performing the heating-cooling cycles it was found that a typical cycle approximately lasted for 9 hours as shown in Figure 3.11. In the figure, relative humidity in the ETC during the applied heating-cooling cycles was also presented.

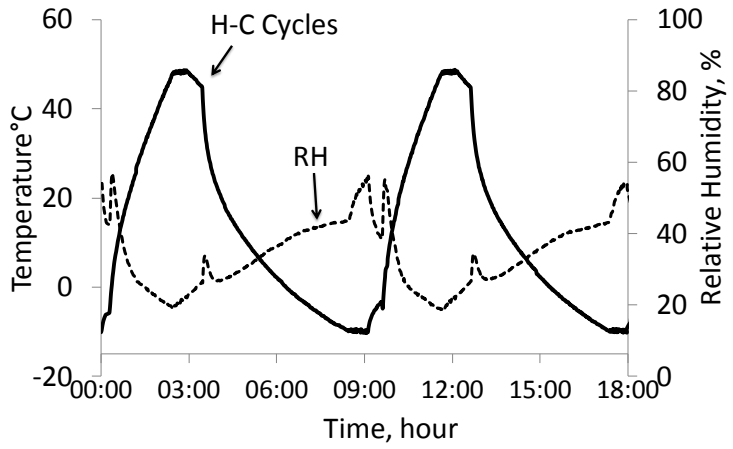


**Figure 3.11 Typical H-C cycles and relative humidity in the ETC**

To determine the temperature gradient in concrete, one thermocouple was inserted in the core of the specimen and the other one was attached at the interface between concrete and CFRP. In Figure 3.12, thermocouple recordings were plotted comparatively with the ambient temperature. It was revealed that although the temperature difference in the ETC was 60°C (from -10°C to 50°C), it was almost 30°C (from -3°C to 27°C) in the concrete core. The temperature at the interface between concrete and CFRP was observed to be greater as compared to the core, but

again the temperature difference was lower (39°C; from -5°C to 34°C) than the ambient temperature difference.

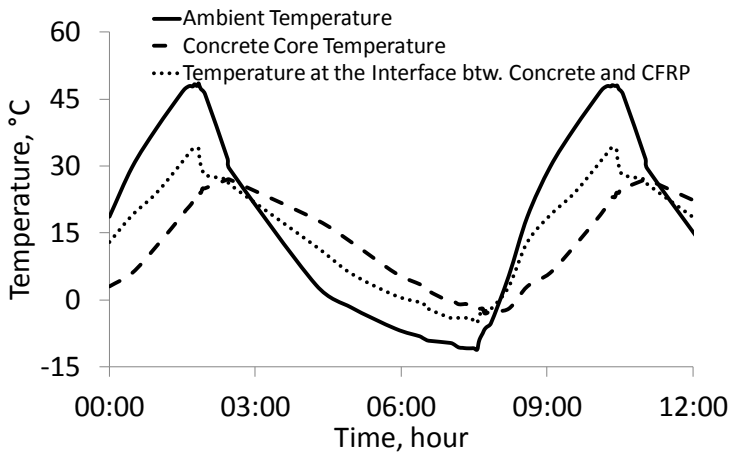


**Figure 3.12 Typical temperature variations in a specimen under H-C cycles**

### 3.3.2 Outdoor-Exposure Tests

Outdoor exposure tests were performed at the outside of the laboratory under actual environmental conditions. Specimens were kept under direct sunlight for 530 days. During this period, the daily maximum-minimum temperatures and relative humidity were recorded [80]. Figure 3.13 shows the daily maximum and minimum temperatures. From the figure, it can be seen that considering the 530 days of exposure the maximum temperature was recorded to be 41°C and the minimum temperature was found to be -11°C. Specimens were subjected to 61 freeze and thaw cycles in 530 days of outdoor exposure. During freeze-thaw exposures, four successive days were noted to be below minus degree.

The average relative humidity (RH) values were presented in Figure 3.14. RH values were observed to get lower during May to November as compared to the other months. In 530 days, 222 days were recorded to have RH higher than 80%.

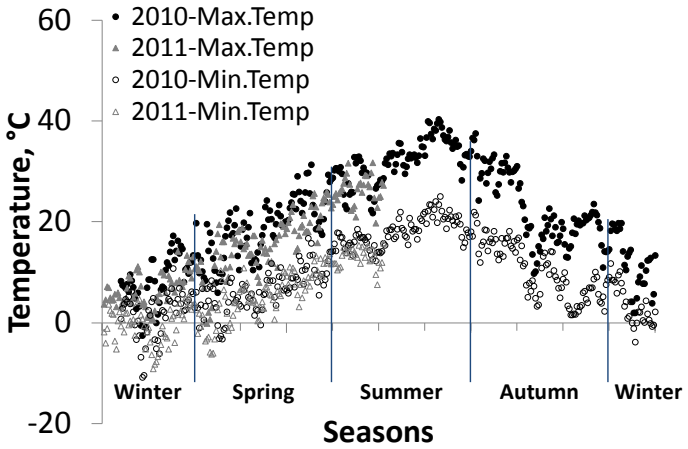


**Figure 3.13 Recorded temperature values during the exposure tests**

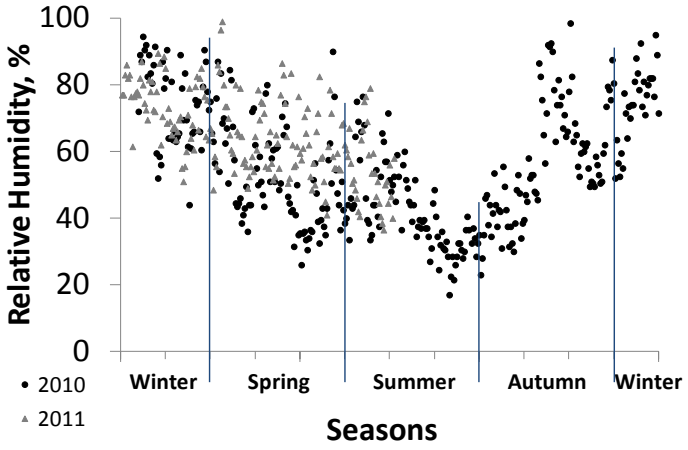


**Figure 3.14 Recorded average relative humidity values during the exposure tests**

### 3.3.3 Sustained Loading Tests

Sustained loading tests were performed using specially designed loading frames. Six loading frames were designed and manufactured as shown in Figure 3.15. Loading frames were designed such that they could retain 800 kN of uniaxial load.

A typical loading frame consisted of three main thick plates of triangular shape and three rods. A ball and socket system was attached to the lower main plate and test specimen was placed on the top of that plate. A thin plate was put on the specimen and a load cell was settled on the thin plate to continuously record the load on the specimen. On the load cell there was another main plate. This plate was pushed downwards by a hydraulic jack. While loading the system with hydraulic jack, the load on the specimen was recorded with load cell. When the desired load level was reached, nuts were tightened to keep the load on the specimen and hydraulic jack was removed to be used in other loading frames.

Load cells were manufactured so that they could be operational inside the environmental test chamber under heating-cooling cycles. They were calibrated and placed in the loading frame. Sustained load on each specimen was monitored continuously via a data acquisition system integrated to the environmental test chamber.

Both unconfined and confined specimens were loaded to 40% of their axial load capacity. Due to the limitations in the loading frames, confined specimens were loaded after being wrapped with CFRP. No load was applied before the CFRP application.

Specimens were either subjected to heating-cooling cycles or left under ambient lab temperature. For the axial load level, the starting point was the limiting value of TEC2007 [7] ($0.5f_{co}A_c$). This value was modified by replacing unconfined concrete strength ($f_{co}$) with confined concrete strength ($f_{cc}$) and reducing 0.5 to 0.4. The

reason for that modification was that; $0.5f_{co}A_c$ correspond to a low level of axial load when the CFRP-confined concrete was of concern. Since it was known that for low level of axial load, CFRP was passive in nature, it was decided to apply higher axial stress to trigger CFRP activation (Figure 3.17).

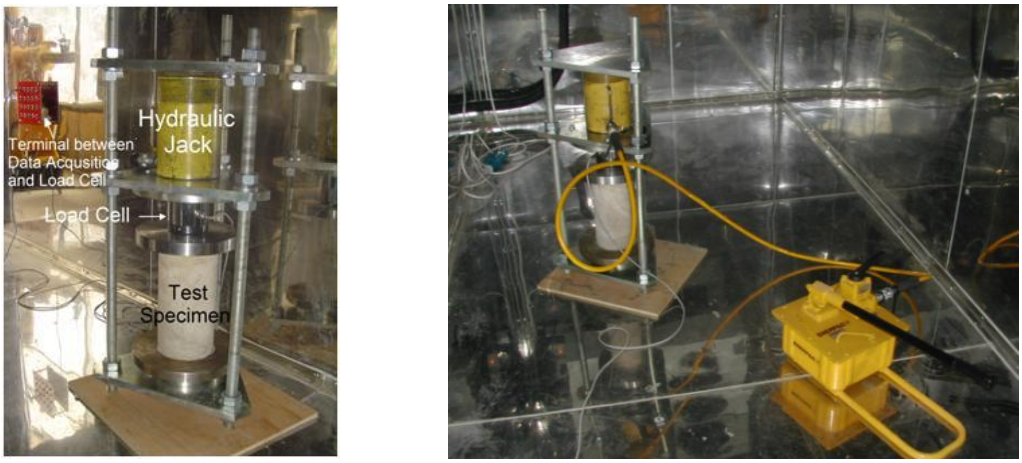


**Figure 3.15 Specially designed loading frame**

**Figure 3.16 Loading Frames in the ETC**

As it can be seen from Figure 3.17 the small curve (unconfined concrete behavior) and the large curve (CFRP-confined concrete behavior) had similar behaviors up to 70-80% of $f_{co}$. It can be inferred from this observation that up to this point, concrete was the dominant material and CFRP was not effective. CFRP started to be active at a stress level of 80-90% of $f_{co}$. Considering these situations sustained load level was chosen as $0.4f_{cc}A_c$ which almost correspond to $0.9f_{co}A_c$ as shown in Table 3.14. This load level was the minimum value to keep the stress in the concrete-dominant part of axial stress-axial strain diagram but triggering the CFRP activation slightly.

Before the sustained loading tests, one reference specimen in each set was tested under uniaxial compression to determine the axial load capacity. From this axial load capacity, the sustained load was calculated. In Table 3.14, $f_{ccr}$ is the strength of the confined reference specimen, $f_{co}$ is the average strength of the unconfined specimen, $P_{unconfined}$ is the axial load capacity of the unconfined specimen, $P_{confined}$ is the axial load capacity of the confined specimen and $A_c$ is the gross area of the specimen.

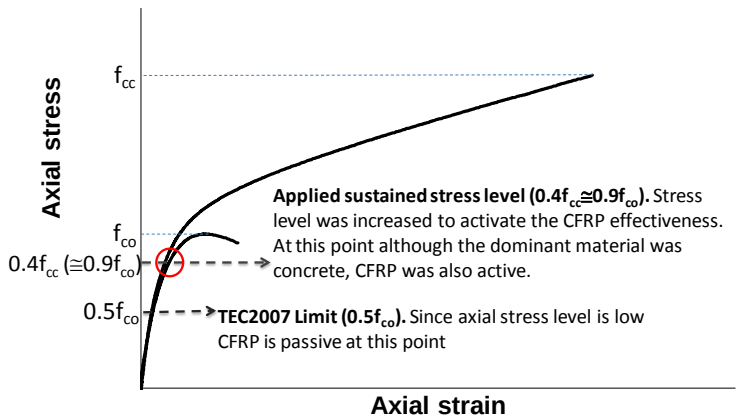


**Figure 3.17 Applied sustained stress level**

**Table 3.14 Sustained load level on specimens**

| Specimen | $f_{co}$ (MPa) | $f_{ccr}$ (MPa) | $P_{unconfined}$ (kN) | $P_{confined}$ (kN) | $0.4f_{ccr}A_c$ (kN) | $n = \frac{0.4f_{ccr}A_c}{f_{co}A_c}$ |
|---|---|---|---|---|---|---|
| 10 MPa Cylinder | 11.1 | 28.6 | 196.2 | 505.9 | 202.4 | 1.03 |
| 10 MPa Square | 10.0 | 20.7 | 219.6 | 455.1 | 182.0 | 0.83 |
| 20 MPa Cylinder | 20.8 | 38.5 | 367.6 | 680.4 | 272.1 | 0.74 |
| | | | | | AVERAGE | 0.87 |

Specimens were loaded by a hydraulic jack and when the desired load level was reached, nuts were tightened and hydraulic jack was removed from the frame. The load was monitored continuously via a load cell and a data acquisition system. It was observed that after 3 days from loading, sustained loads on the specimens dropped due to the relaxation of the loading frame. The relaxation may be due to heating-cooling cycles, which resulted in a dynamic loading other than static sustained loading. As it can be seen from Figure 3.18, load on the specimen reduced with increasing temperature. Since steel had a positive thermal expansion coefficient, which was slightly greater than the one for concrete, it expanded with increase in temperature. On the other hand, steel would shrink if the temperature decreased. Because of this shrinking phenomenon, the loading frame started to squeeze the specimen and resulted in an increase in the load on the specimen. The sustained load on the specimen was determined by drawing a linear trend line, which took the average of a typical cycle.

When the decrease in the sustained load reached 10-15% of the initial load, hydraulic jack again was placed in the loading frame and specimen was loaded to attain the desired load (Figure 3.18). This procedure was followed until the trend of the sustained load was determined to be constant. After 10 days, it was seen that the

sustained load level was almost constant and no adjustments were made afterwards (Figure 3.19).

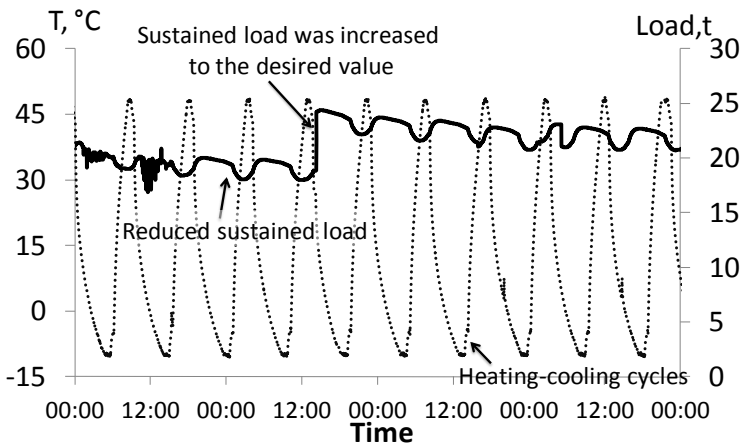


**Figure 3.18 Relaxation and an attempt to increase the sustained load**

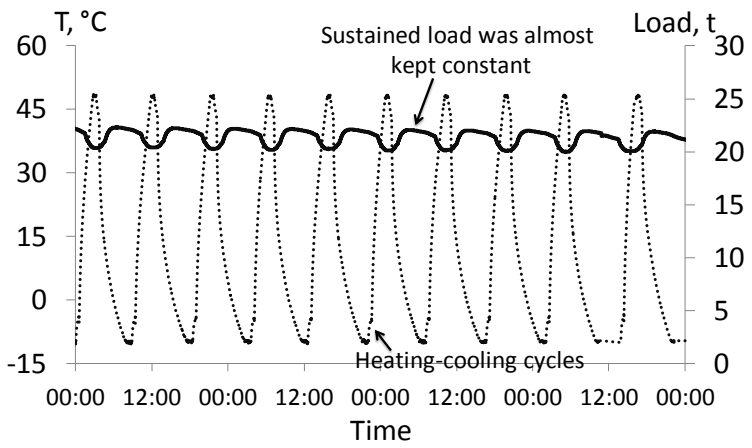


**Figure 3.19 Sustained load was almost constant after 10 days**

### 3.3.4 Uniaxial Compression Tests

Exposure tests were finished when the desired heating-cooling cycles were reached. The heating-cooling procedure in the ETC was stopped and specimens were unloaded. If necessary, caps at the end of the specimens were renewed and they were carried to the Materials of Construction Laboratory to test under uniaxial compression, which was also called as Phase 2 Test. Uniaxial compression tests were performed in between 3-7 days after the end of the exposure tests. Load-controlled procedure was followed until the failure

Uniaxial compression tests were performed in accordance with ASTM C469 [81]. Since the load rate was stated to be around 241±34 kPa/s, it was taken as 5.2 kN/s in the tests. Testing machine was ELE Autotest Compression Machine with a capacity of 3000 kN (Figure 3.20). The machine was connected to a data acquisition system and the readings were calibrated before each test group. The load values during the compression test were recorded continuously and converted to the stress values.

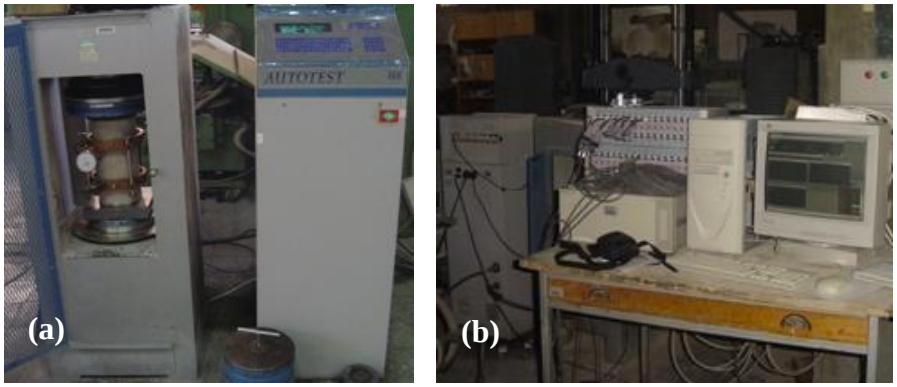


**Figure 3.20 a) ELE Autotest compression testing machine**
**b) Data Acquisition system connected to the testing machine**

The compressometer was employed to record displacements during the test and then displacements were converted to strains to obtain axial stress-axial strain diagram of each specimen. Two different compressometers were used in the tests. The first one was the same as explained in ASTM C469 [81] and it was utilized to conduct tests for cylindrical specimens (Figure 3.21). It had two rings with an inner diameter of 17 cm, which were placed 13.5 cm apart vertically. The upper ring had two yokes, which were attached at two opposite points to enable the ring to rotate freely. However, the lower ring had three yokes that ensured the connection to the specimen be rigid. Two rings were connected to each other via a stiff steel bar (pivot rod) and a dial gage, which was shown in Figure 3.21. Pivot rod provided constant distance between upper and lower yokes. The dial gage having a capacity of 20 mm at the opposite side was used to measure the change in the distance between the yokes. Since the dial gage was located away from the upper yokes, calibration was necessary to find the displacement at the center. The calibration was done according to Figure 3.22 and Eqn. 3.1. Strains at each load level were calculated by dividing the displacement at point b by the distance between upper and lower yokes (Eqn. 3.2).

$$d = \frac{g.e_r}{(e_r + e_g)} \tag{3. 1}$$

$$\varepsilon_d = \frac{d}{h} \tag{3. 2}$$

where, $e_r$ is the perpendicular distance from the pivot rod to the vertical plane passing through the two support points of the rotating yokes, and $e_g$ is the perpendicular distance from the gage to the vertical plane passing through the two support points of the rotating yokes, $\varepsilon_g$ is the strain measured at point a and $\varepsilon_d$ is the strain measured at point b.

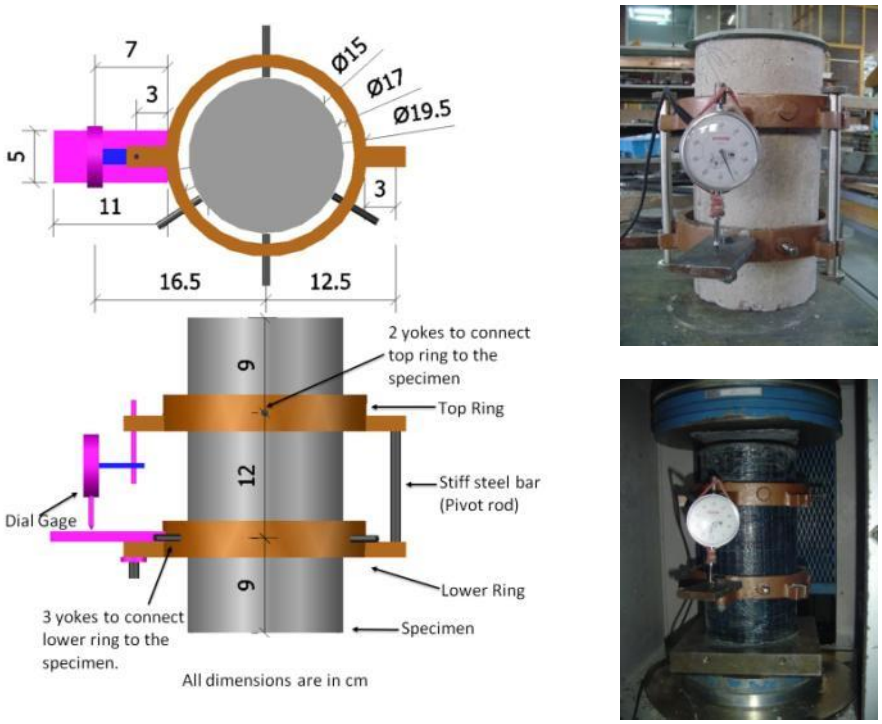


**Figure 3.21 The compressometer used to test cylindrical specimens**

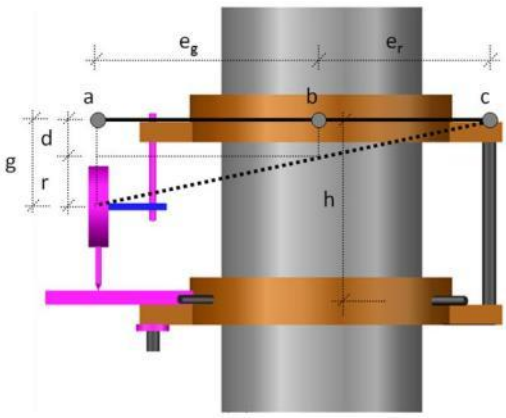


**d** = displacement due to specimen deformation
**r** = displacement due to rotation of the yoke about the pivot rod
**a** = location of gage
**b** = support point of the rotating yoke
**c** = location of pivot rod
**g** = gage reading
**h** = distance between upper yokes and lower yokes

**Figure 3.22 Working principle of the compressometer used to test cylindrical specimens**

Home-made compressometer was used to test prismatic specimens under uniaxial compression (Figure 3.23). The compressometer differed from the one used for cylindrical specimens in terms of the working principle. This setup included two rings, which were manufactured from 50x5 equal-leg-angle steel sections. Angles were cut in a desired length and welded to form a ring. 4 yoke locations were drilled on the vertical leg, which corresponds to the center of each face of the specimen. Moreover, 4 dial gage locations were drilled on the horizontal leg. At the lower ring the point that corresponds to the dial gage's tip were lengthened by additional steel plate, because dial gage did not fit in between the rings and it had to be placed away from the rings. In order to keep the distance between upper and lower yokes the same and keep the rings at the horizontal level, 4 bars were placed at the tip of horizontal legs. Those bars were only used to adjust the compressometer and they were removed before the test.

During the test, load and displacement measurements were recorded continuously. Load values were divided by the cross-sectional area of the specimen to calculate the stress values. Displacements were recorded by two opposite dial gages with a gage length of 20 mm. The average of two readings was considered as the actual displacement (Figure 3.24 and Eqn. 3.3). Actual displacements were then divided by the distance between upper and lower yokes to find the strains (Eqn. 3.4).

$$d = \frac{d_1 + d_2}{2} \tag{3. 3}$$

$$\varepsilon_d = \frac{d}{h} \tag{3. 4}$$

where, $d$ is the displacement due to specimen deformation, $d_1$ is the displacement measured by the left dial gage, $d_2$ is the displacement measured by the right dial gage, $h$ is the distance between upper yokes and lower yokes and $\varepsilon_d$ is the strain at the midpoint of the specimen.

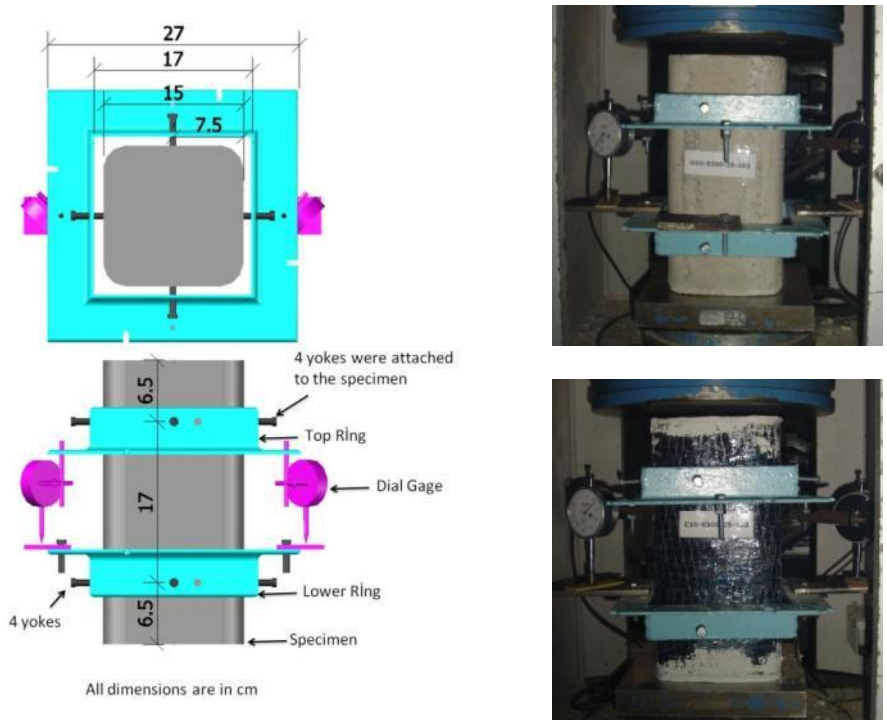


**Figure 3.23 The compressometer used to test prismatic specimens**

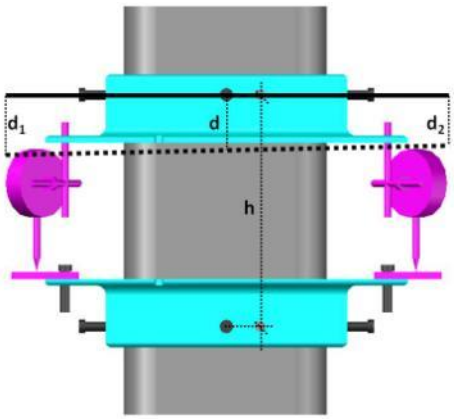


**Figure 3.24 Working principle of the compressometer used to test prismatic specimens**

Besides the abovementioned compressometers strain gages were used in some prismatic specimens (Figure 3.25). Four uniaxial strain gages with a gage length of 10 mm were placed at each corner to determine the lateral strains at these locations. Two triaxial rosette strain gages with a gage length of 10 mm were attached at the sides of the specimen to record axial shortening and lateral expansion. One of the rosette strain gages was placed at the overlapping zone and the other one was placed at the opposite side. With these measuring devices, it was aimed to record axial and lateral strains, circumferential strain distribution and the relationship with strain and failure. In some specimens four triaxial rosette strain gages were used at each side of the specimen. All strain gages were placed at the midheight of the specimen.

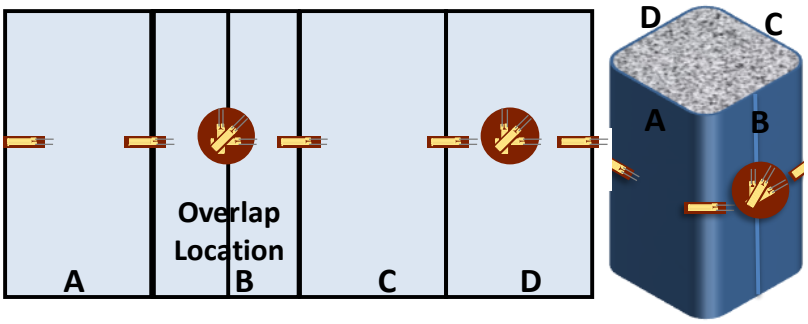


**Figure 3.25 Schematic view of the strain gage locations**

# CHAPTER 4

# TEST RESULTS

## 4.1 INTRODUCTION

In this chapter, results of the experimental work were presented in detail, since the aim of this study was to identify the effect of exposure tests on the mechanical properties of CFRP-confined concrete columns, results were presented accordingly. They were included failure types of specimens, axial stress-strain diagrams and a summary of mechanical properties. In each group, results for all specimens were presented comparatively in order to understand the variation in the group.

In the following sections, figures and tables include both specimens' data and the average of the group. The name of the average of the group is given at the end of the legend in the figures and at the end of the table with bold characters. The codes used for the averages differed from that of specimens as explained in Table 3.11 and Table 3.12.

## 4.2 MECHANICAL PROPERTIES OF CFRP-CONFINED CONCRETE COLUMNS

Mechanical properties of CFRP-confined concrete are illustrated in Figure 4.1, where $f_{co}$ represents the unconfined concrete strength, $\varepsilon_{co}$ stands for strain corresponding to the $f_{co}$ and $E_1$ is the Secant Modulus of Elasticity calculated at $0.4f_{co}$, $E_2$ is used to

describe the slope of the linear part, $f_{cc}$ is the CFRP-confined concrete strength and $\varepsilon_{cc}$ is the ultimate strain of CFRP-confined concrete.

Axial stress-strain diagram of a CFRP-confined concrete consists of two parts. First part is an unconfined concrete dominant zone, which ends at a point close to $f_{co}$. This part is a parabolic curve and reflects the mechanical properties of unconfined concrete. After that, point since unconfined concrete reached the ultimate strength it cannot carry further load without any help. CFRP starts to be active at this point where unconfined concrete exhausted. CFRP having linear material properties influences the second part of the diagram. This part is almost linear and can be said that CFRP dominant zone. Between first and second part of the diagram there exists a transition zone.

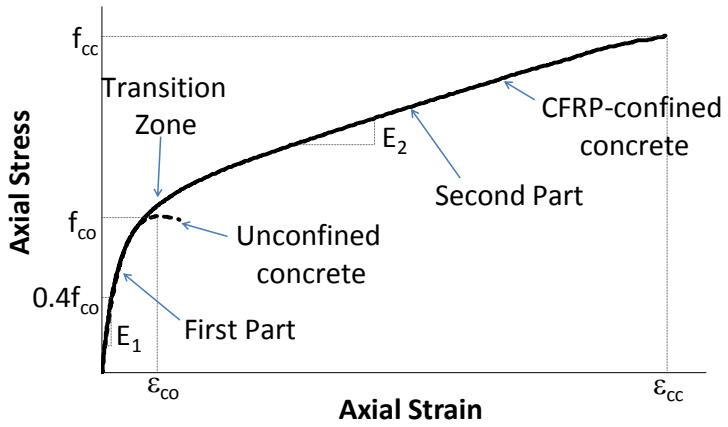


**Figure 4.1. Axial stress-strain diagram and mechanical properties of CFRP-confined concrete**

## 4.3 CONCRETE SPECIMENS HAVING 10 MPa STRENGTH

In this part, specimens were cast in both cylindrical and prismatic forms. Cylindrical specimens were prepared in two sets whose CFRP-overlap length and loading-rate differed from each other. Prismatic specimens were again prepared in two sets and the main difference was in the corner radius.

Both cylindrical and prismatic specimens were 300 mm tall. Side dimensions of prismatic specimens were chosen to be 150 mm, which was equal to the diameter of the cylindrical specimens.

### 4.3.1 Cylindrical Specimens

Cylindrical specimens were prepared in two different sets, which are summarized in Table 4.1. In the first set, the overlap length was chosen to be 6% of the perimeter (30 mm) whereas in the second set it was 11% of the perimeter. Since the main aim was to keep the overlap length short enough to achieve the uniform stress distribution around the perimeter, this length was first provided to be 30 mm. However, in specimens of Group 3, which were under sustained loading (SL) while being subjected to heating-cooling (H-C) cycles, premature failures were observed to be due to the delamination of the CFRP at the overlap zone. As the failures were attributed to the bad workmanship, new specimens with the same overlap length (30 mm) were prepared meticulously. Nevertheless, the premature failure was again occurred while the specimens were under both sustained loading and heating-cooling cycles. Based on these observations, overlap length was blamed to be the reason of these failures. Therefore, new set was prepared in which specimens had an increased overlap length (11%).

The other difference was the loading rate during uniaxial compression test. In SET 1, specimens were tested with a loading rate of 1.5 kN/s. Since this value was well below the one stated in ASTM C469 [81], tests on this set were kept separate. SET 2 was tested under 5.2 kN/s.

## Table 4.1 Summary of the 10 MPa cylindrical specimens

| Specimen Code | Confinement | $f_{co}$ (MPa) | Type | Overlap % | Group No | # of H-C cycles | SL, % | Outdoor Exposure |
|---|---|---|---|---|---|---|---|---|
| U10-C300-101 | Unconfined | 10 | Cylinder | 6 | 1 | | | |
| U10-C300-102 | Unconfined | 10 | Cylinder | 6 | 1 | | | |
| C10-C300-101 | CFRP-confined | 10 | Cylinder | 6 | 1 | | | |
| C10-C300-102 | CFRP-confined | 10 | Cylinder | 6 | 1 | | | |
| C10-C300-103 | CFRP-confined | 10 | Cylinder | 6 | 1 | | | |
| C10-C300-104 | CFRP-confined | 10 | Cylinder | 6 | 1 | | | |
| U10-C300-201 | Unconfined | 10 | Cylinder | 6 | 2 | 200 | | |
| U10-C300-202 | Unconfined | 10 | Cylinder | 6 | 2 | 200 | | |
| U10-C300-203 | Unconfined | 10 | Cylinder | 6 | 2 | 200 | | |
| C10-C300-201 | CFRP-confined | 10 | Cylinder | 6 | 2 | 200 | | |
| C10-C300-202 | CFRP-confined | 10 | Cylinder | 6 | 2 | 200 | | |
| C10-C300-203 | CFRP-confined | 10 | Cylinder | 6 | 2 | 200 | | |
| C10-C300-204 | CFRP-confined | 10 | Cylinder | 6 | 2 | 200 | | |
| C10-C300-205 | CFRP-confined | 10 | Cylinder | 6 | 2 | 200 | | |
| U10-C300-301 | Unconfined | 10 | Cylinder | 6 | 3 | 200 | 40 | |
| U10-C300-302 | Unconfined | 10 | Cylinder | 6 | 3 | 200 | 40 | |
| U10-C300-303 | Unconfined | 10 | Cylinder | 6 | 3 | 200 | 40 | |
| C10-C300-301 | CFRP-confined | 10 | Cylinder | 6 | 3 | 200 | 40 | |
| C10-C300-302 | CFRP-confined | 10 | Cylinder | 6 | 3 | 200 | 40 | |
| C10-C300-303 | CFRP-confined | 10 | Cylinder | 6 | 3 | 200 | 40 | |
| C10-C300-304 | CFRP-confined | 10 | Cylinder | 6 | 3 | 200 | 40 | |
| C10-C300-305 | CFRP-confined | 10 | Cylinder | 6 | 3 | 200 | 40 | |
| U10-C300-103 | Unconfined | 10 | Cylinder | 11 | 1 | | | |
| U10-C300-104 | Unconfined | 10 | Cylinder | 11 | 1 | | | |
| U10-C300-105 | Unconfined | 10 | Cylinder | 11 | 1 | | | |
| C10-C300-105 | CFRP-confined | 10 | Cylinder | 11 | 1 | | | |
| C10-C300-106 | CFRP-confined | 10 | Cylinder | 11 | 1 | | | |
| C10-C300-107 | CFRP-confined | 10 | Cylinder | 11 | 1 | | | |
| C10-C300-206 | CFRP-confined | 10 | Cylinder | 11 | 2 | 200 | | |
| C10-C300-207 | CFRP-confined | 10 | Cylinder | 11 | 2 | 200 | | |
| C10-C300-208 | CFRP-confined | 10 | Cylinder | 11 | 2 | 200 | | |
| C10-C300-306 | CFRP-confined | 10 | Cylinder | 11 | 3 | 200 | 40 | |
| C10-C300-307 | CFRP-confined | 10 | Cylinder | 11 | 3 | 200 | 40 | |
| C10-C300-308 | CFRP-confined | 10 | Cylinder | 11 | 3 | 200 | 40 | |
| C10-C300-309 | CFRP-confined | 10 | Cylinder | 11 | 3 | 200 | 40 | |
| C10-C300-401 | CFRP-confined | 10 | Cylinder | 11 | 4 | | 40 | |
| C10-C300-402 | CFRP-confined | 10 | Cylinder | 11 | 4 | | 40 | |
| C10-C300-403 | CFRP-confined | 10 | Cylinder | 11 | 4 | | 40 | |
| C10-C300-601 | CFRP-confined | 10 | Cylinder | 11 | 6 | | | Yes |
| C10-C300-602 | CFRP-confined | 10 | Cylinder | 11 | 6 | | | Yes |

#### *4.3.1.1 SET 1 – Specimens with 6% overlap length*

##### *4.3.1.1.1 Group-1: Reference Specimens*

In this group, specimens were kept under ambient lab conditions without being subjected to any sustained loading. They were tested under uniaxial compression after the completion of tests in the Environmental Test Chamber.

***Unconfined Specimens***

Two unconfined specimens were used as reference specimens. Axial stress-strain diagrams of the specimens were presented in Figure 4.2 and mechanical properties were summarized in Table 4.3. Coefficients of variation (COV) were also calculated to understand the dispersion for the group, i.e., to identify the quality control. Although the quality limits were previously defined for concrete strength [36], same limits may be used for ultimate strain also. The limits were presented in Table 4.2.

**Table 4.2. The limits to identify the quality control of concrete**

| Range of COV | Quality Control |
|---|---|
| COV≤0.10 | Excellent |
| 0.10<COV≤0.15 | Good |
| 0.15<COV≤0.20 | Average |
| 0.20≤COV | Bad |

As it is seen from Table 4.3, the average strength of the unconfined specimens was determined to be 10.5 with a COV of 2.2%, which could be regarded as good. The strain corresponding to the strength was found to be 0.005 and the COV was calculated as 9.2%.

**Table 4.3. Mechanical properties of unconfined cylindrical specimens in Group-1 (SET1 - $f_{co}$=10 MPa)**

| Specimen | $f_{co}$ , MPa | $\varepsilon_{co}$ | $E_1$ , GPa |
|---|---|---|---|
| U10-C300-101 | 10.7 | 0.004 | 10.37 |
| U10-C300-102 | 10.3 | 0.005 | 11.63 |
| **U10-G1-C_SET1** | **10.5** | **0.005** | **11.00** |

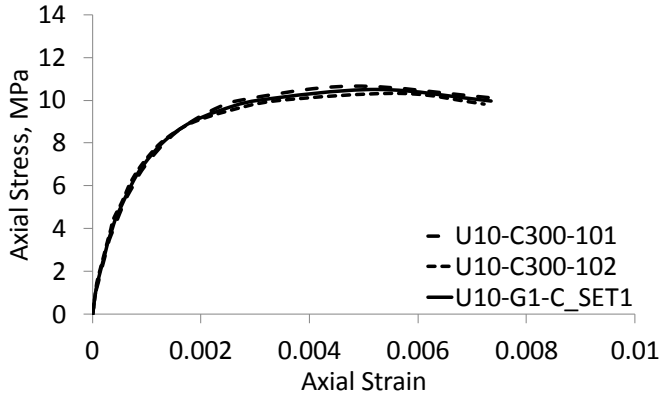


**Figure 4.2. Axial stress-strain diagrams of unconfined cylindrical specimens in Group-1 (SET1 - $f_{co}$=10 MPa)**

***CFRP-Confined Specimens***

In this group, four specimens were wrapped with one-layer of CFRP providing 30 mm overlap length. All specimens were kept outside the curing room under ambient lab condition until the end of the exposure tests. After that period, specimens were tested under uniaxial compression and their axial stress-strain behaviors were recorded.

Failure characteristics of the CFRP-wrapped specimens were given in Figure 4.3. As it is seen, all specimens failed due to CFRP rupture. The rupture was observed to extend to full height of the specimen. All failures were sudden and brittle. No signs had been observed before the failure except the low cracking sound during the lateral expansion. Upon reaching the ultimate strength, there heard a popping sound, which was because of the CFRP rupture. Following the CFRP rupture since the stress level was well above the unconfined concrete strength, a sharp decrease observed in the stress level and specimen was not able to carry any load afterwards.

In Figure 4.4, axial stress-strain diagrams of the specimens were presented and their mechanical properties were tabulated in Table 4.4. The axial stress-strain diagrams consisted of two ascending parts. The first part was a parabolic curve, which was controlled by concrete and the other one, in which CFRP was dominant, was a linear curve. From Table 4.4, the average strength was calculated to be 33.5 MPa and $E_1$ was evaluated as 10 GPa.

**(a) C10-C300-101** **(b) C10-C300-102** **(c) C10-C300-103** **(c) C10-C300-104**

**Figure 4.3. Failure types of CFRP-confined cylindrical specimens in Group-1 (SET1 - $f_{co}$=10 MPa)**

**Table 4.4. Mechanical properties of CFRP-confined cylindrical specimens in Group-1 (SET1-$f_{co}$=10 MPa)**

| Specimen | $f_{cc}$ , MPa | $\varepsilon_{cc}$ | $E_1$ , GPa | $E_2$ , GPa | $E_1/E_2$ |
|---|---|---|---|---|---|
| C10-C300-101 | 33.6 | 0.042 | 11.03 | 0.45 | 24.7 |
| C10-C300-102 | 33.4 | 0.044 | 9.68 | 0.41 | 23.7 |
| C10-C300-103 | 34.9 | 0.045 | 9.68 | 0.46 | 21.3 |
| C10-C300-104 | 32.1 | 0.043 | 9.68 | 0.38 | 25.2 |
| **C10-G1-C_SET1** | **33.5** | **0.043** | **10.02** | **0.42** | **23.7** |
| COV, % | 3.5 | 3.6 | | | |

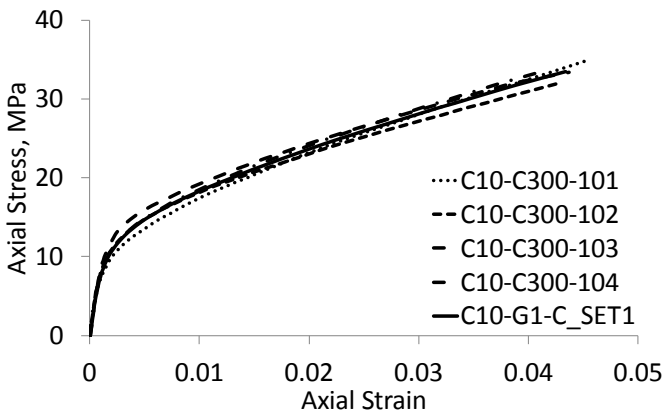


**Figure 4.4. Axial stress-strain diagrams of CFRP-confined cylindrical specimens in Group-1 (SET 1 - $f_{co}$=10 MPa)**

#### *4.3.1.1.2 Group-2: Specimens exposed to H-C Cycles*

In this group, three unconfined and five CFRP-confined specimens were tested. Specimens were kept in the Environmental Test Chamber (ETC) and exposed to heating-cooling (H-C) cycles as stated in Chapter 3, Section 3.3.1.

***Unconfined Specimens***

Three unconfined specimens were tested to determine the change in mechanical properties under heating-cooling cycles. Axial stress-strain diagrams of these specimens were given in Figure 4.5 and the corresponding mechanical properties were summarized in Table 4.5. From the figure and the table, it was observed that all of the specimens behaved differently. The main difference was in strain corresponding to the ultimate strength. The COV for strain was calculated as 30%. As for secant moduli of elasticity, the reason for having low modulus was attributed to the low rate of loading.

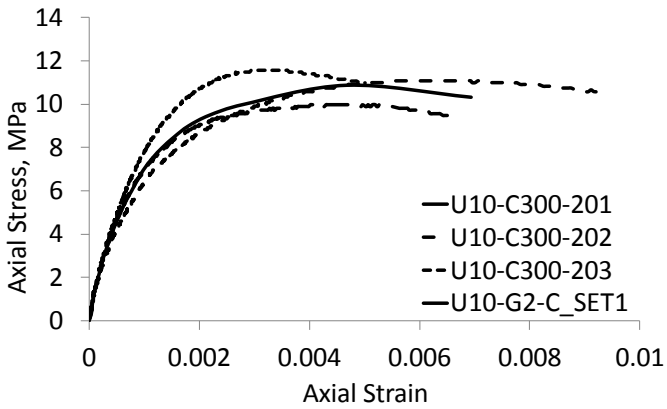


**Figure 4.5. Axial stress-strain diagrams of unconfined cylindrical specimens in Group-2 (SET1 - $f_{co}$=10 MPa)**

**Table 4.5. Mechanical properties of unconfined cylindrical specimens in Group-2 (SET1 - $f_{co}$=10 MPa)**

| Specimen | H-C Cycles | $f_{co}$ , MPa | $\varepsilon_{co}$ | $E_1$ , GPa |
|---|---|---|---|---|
| U10-C300-201 | 200 | 10.0 | 0.004 | 9.85 |
| U10-C300-202 | 200 | 11.1 | 0.005 | 8.28 |
| U10-C300-203 | 200 | 11.6 | 0.003 | 10.01 |
| **U10-G2-C_SET1** | | **10.9** | **0.004** | **9.38** |
| COV, % | | 7.4 | 30.2 | |

***CFRP-Confined Specimens***

Five specimens were utilized in two sets to determine the change in mechanical properties. Specimens were exposed to heating-cooling cycles and then they were tested under uniaxial compression. In Figure 4.6 failure patterns of the specimens were given. In the figures, CFRP rupture was localized at the midheight in some specimens (C10-C300-201, C10-C300-204, and C10-C300-206) but it had no effect on the axial stress-strain diagrams as indicated in Figure 4.7. Mechanical properties of these specimens were given in Table 4.6.

**(a) C10-C300-201** **(b) C10-C300-202** **(c) C10-C300-203** **(d) C10-C300-204**

**Figure 4.6. Failure types of CFRP-confined cylindrical specimens in Group-2 (SET1 - $f_{co}$=10 MPa)**

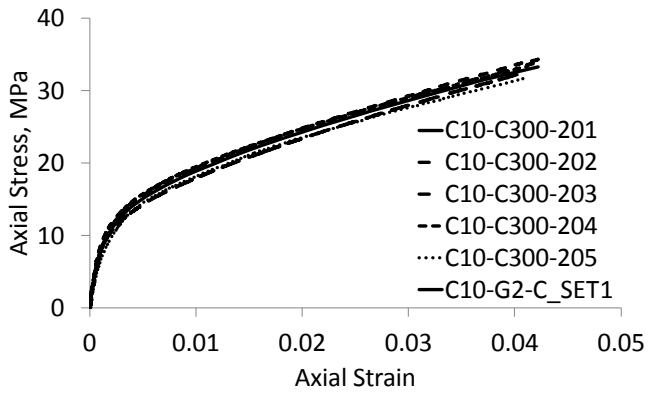


**Figure 4.7. Axial stress-strain diagrams of CFRP-confined cylindrical specimens in Group-2 (SET1 - $f_{co}$=10 MPa)**

**Table 4.6. Mechanical properties of CFRP-confined cylindrical specimens in Group-2 (SET 1 - $f_{co}$=10 MPa)**

| Specimen | H-C Cycles | $f_{cc}$ , MPa | $\varepsilon_{cc}$ | $E_1$ , GPa | $E_2$ , GPa | $E_1/E_2$ |
|---|---|---|---|---|---|---|
| C10-C300-201 | 200 | 32.6 | 0.044 | 11.00 | 0.43 | 25.6 |
| C10- C300-202 | 200 | 34.1 | 0.042 | 8.60 | 0.42 | 20.3 |
| C10- C300-203 | 200 | 34.6 | 0.043 | 12.80 | 0.44 | 28.8 |
| C10- C300-204 | 200 | 33.4 | 0.041 | 11.00 | 0.41 | 26.7 |
| C10- C300-205 | 200 | 31.7 | 0.041 | 7.80 | 0.38 | 20.3 |
| **C10-G2-C_SET1** | | **33.3** | **0.042** | **10.24** | **0.42** | **24.4** |
| COV, % | | 3.5 | 2.6 | | | |

#### *4.3.1.1.3 Group-3: Specimens Exposed to H-C Cycles and SL*

Specimens in this group were loaded to 40% of their axial load capacity while being subjected to H-C cycles. Three unconfined and five CFRP-confined specimens were utilized.

***Unconfined Specimen***

Three unconfined specimens were used in this group. After being subjected to 200 H-C cycles they were unloaded, removed from the loading frame and tested under uniaxial compression. The axial stress-strain diagrams were plotted as shown in Figure 4.8 and mechanical properties based on these curves were summarized in Table 4.7. As it is seen from the table, the average strength was found to be 11.7 MPa, average strain corresponding that value was evaluated as 0.003 and modulus of elasticity was calculated as 14.88 MPa.

**Table 4.7. Mechanical properties of unconfined cylindrical specimens in Group-3 ( SET 1 - $f_{co}$=10 MPa)**

| Specimen | H-C Cycles | SL % | $f_{co}$ , MPa | $\varepsilon_{co}$ | $E_1$ , GPa |
|---|---|---|---|---|---|
| U10-C300-301 | 200 | 40 | 11.8 | 0.002 | 17.24 |
| U10-C300-302 | 200 | 40 | 11.7 | 0.004 | 11.86 |
| U10-C300-303 | 200 | 40 | 11.7 | 0.003 | 15.54 |
| **U10-G3-C_SET1** | | | **11.7** | **0.003** | **14.88** |
| COV, % | | | 0.7 | 30.7 | |

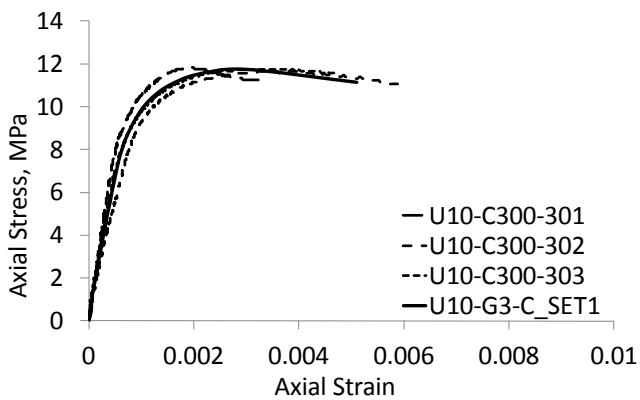


**Figure 4.8. Axial stress-strain diagrams of unconfined cylindrical specimens in Group-3 (SET 1 - $f_{co}$=10 MPa)**

***CFRP-Confined Specimens***

Five CFRP-confined specimens with 30 mm (6%) overlap were tested under simultaneous exposure of sustained loading (SL) and heating-cooling (H-C) cycles. At first, two specimens were prepared and placed in the loading frame. Sustained loading level was applied as the 40% of the axial load capacity while being exposed to H-C cycles. It was observed that C10-C300-304 failed at the 11$^{th}$ cycle due to the delamination at the overlap location. After that, when C10-C300-303 failed at 36$^{th}$ cycle because of the same problem, it was decided to prepare new specimens having better bond at the overlap location. Three additional specimens with identical properties were prepared. However, those specimens were also observed to fail prematurely due to the delamination problem as seen in Figure 4.10. C10-C300-305 failed at the 4$^{th}$ H-C cycle, C10-C300-301and C10-C300-302 failed at the 42$^{nd}$ cycle (Figure 4.9). Premature failures due to delamination were attributed to the insufficient overlap.

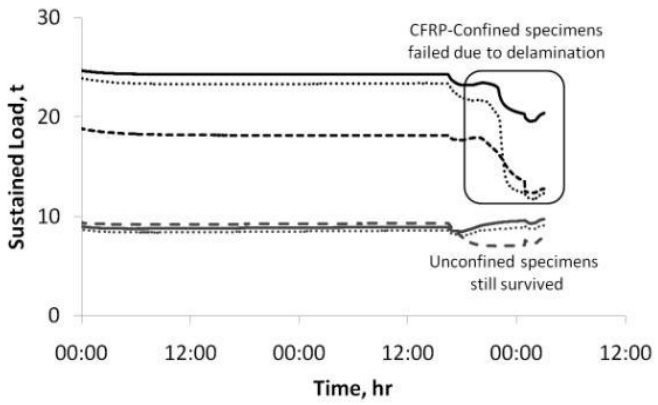


**Figure 4.9. The moment at which CFRP-confined specimens failed under sustained loading**

**(a) C10-C300-301** **(b) C10-C300-302** **(c) C10-C300-303** **(d) C10-C300-304**

**Figure 4.10. Failure of CFRP-confined specimens due to delamination**

#### *4.3.1.2 SET 2 – Specimens with 11% overlap length*

##### *4.3.1.2.1 Group-1: Reference Specimens*

***Unconfined Specimens***

In this group, three specimens were used as reference specimens. Figure 4.11 shows the axial stress-strain diagrams of the specimens and Table 4.8 summarizes their mechanical properties. As it is seen from the table, the average strength was determined to be 11.1 with a COV of 13.3%. The strain corresponding to the strength was found to be 0.003 and the COV was calculated as 16.1%, which was in the range of average quality. As for the Secant Modulus of Elasticity, the average was determined as 14.8 GPa.

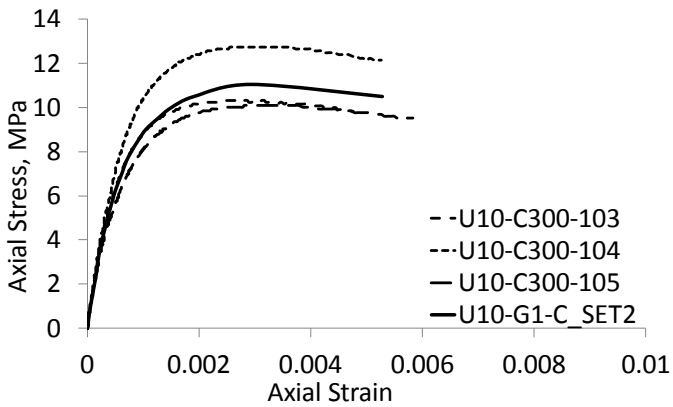


**Figure 4.11. Axial stress-strain diagrams of unconfined cylindrical specimens in Group-1 (SET 2 - $f_{co}$=10 MPa)**

**Table 4.8. Mechanical properties of unconfined cylindrical specimens in Group-1 (SET2 - $f_{co}$=10 MPa)**

| Specimen | $f_{co}$ , MPa | $\varepsilon_{co}$ | $E_1$ , GPa |
|---|---|---|---|
| U10-C300-103 | 10.3 | 0.002 | 15.81 |
| U10-C300-104 | 12.8 | 0.003 | 15.25 |
| U10-C300-105 | 10.1 | 0.003 | 13.21 |
| **U10-G1-C_SET2** | **11.1** | **0.003** | **14.75** |
| COV, % | 13.3 | 16.1 | |

***CFRP-Confined Specimens***

Three specimens were kept outside the curing room under ambient lab condition until the end of the exposure tests. After that period, specimens were tested under uniaxial compression and their axial stress-strain behaviors were recorded. In Figure 4.11, failure types of CFRP-confined specimens were given. Ruptures were seen to be localized at the midheight. However, since specimens failed due to CFRP rupture,

this localization did not affect the behavior as shown in Figure 4.13. Mechanical properties of the specimens were tabulated in Table 4.9. From the table, it can be seen that the average strength was 33 MPa and strain corresponding to this value was 0.042. The ratio of the slope in second part to the first part of the curve is calculated as 36, which shows that upon reaching unconfined concrete strength, the slope of the curve reduces 36 times.

**(a) C10-C300-105** **(b) C10-C300-106** **(c) C10-C300-107**

**Figure 4.12. Failure types of CFRP-confined cylindrical specimens in Group-1 (SET 2 - $f_{co}$=10 MPa)**

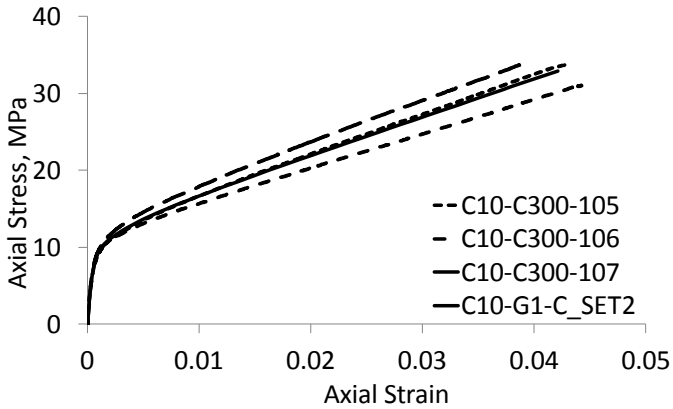


**Figure 4.13. Axial stress-strain diagrams of CFRP-confined cylindrical specimens in Group-1 ( SET 2 - $f_{co}$=10 MPa)**

**Table 4.9. Mechanical properties of CFRP-confined cylindrical specimens in Group-1 (SET 2 - $f_{co}$=10 MPa)**

| Specimen | $f_{cc}$, MPa | $\varepsilon_{cc}$ | $E_1$ , GPa | $E_2$ , GPa | $E_1/E_2$ |
|---|---|---|---|---|---|
| C10-C300-105 | 33.7 | 0.043 | 19.79 | 0.52 | 38.1 |
| C10-C300-106 | 31.0 | 0.044 | 17.63 | 0.45 | 39.5 |
| C10-C300-107 | 34.0 | 0.040 | 17.63 | 0.55 | 32.3 |
| **C10-G1-C_SET2** | **32.9** | **0.042** | **18.35** | **0.48** | **36.4** |
| COV, % | 5.1 | 5.8 | | | |

#### *4.3.1.2.2 Group-2: Specimens exposed to H-C Cycles*

Unconfined specimens were not tested in this group because the difference in SET1 and SET2 was at the overlap length. Since unconfined specimens did not include CFRP, they were not utilized in this group.

***CFRP-Confined Specimens***

Three specimens were wrapped with one-layer of CFRP providing 11% overlap length. They were put in the ETC and subjected to 200 H-C cycles. Failures of the specimens were illustrated in Figure 4.14. All specimens failed due to CFRP rupture. Axial stress-strain diagrams were given in Figure 4.15. From the figures, it can be seen that although two specimens showed almost identical behavior, C10-C300-206 differed slightly. However, this difference is not significant. From Table 4.10, the average strength was found as 33 MPa with a COV of 15% and the average strain was evaluated to be 0.04 with a COV of 7%

**(a) C10-C300-206** **(b) C10-C300-207** **(c) C10-C300-208**

**Figure 4.14. Failure types of CFRP-confined cylindrical specimens in Group-2 (SET 2 - $f_{co}$=10 MPa)**

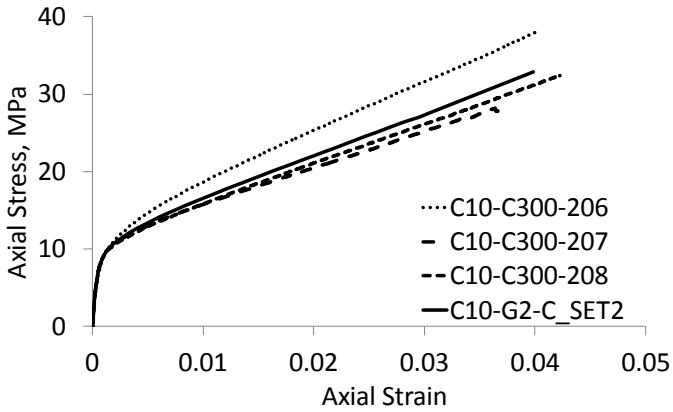


**Figure 4.15. Axial stress-strain diagrams of CFRP-confined cylindrical specimens in Group-2 (SET 2 - $f_{co}$=10 MPa)**

**Table 4.10. Mechanical properties of CFRP-confined cylindrical specimens in Group-2 (SET 2 - $f_{co}$=10 MPa)**

| Specimen | H-C Cycles | $f_{cc}$ , MPa | $\varepsilon_{cc}$ | $E_1$ , GPa | $E_2$ , GPa | $E_1/E_2$ |
|---|---|---|---|---|---|---|
| C10-C300-206 | 200 | 38.1 | 0.040 | 15.89 | 0.65 | 24.5 |
| C10- C300-207 | 200 | 28.0 | 0.037 | 22.56 | 0.47 | 48.0 |
| C10- C300-208 | 200 | 32.4 | 0.042 | 17.54 | 0.51 | 34.6 |
| **C10-G2-C_SET2** | | **32.9** | **0.040** | **18.66** | **0.54** | **34.4** |
| COV, % | | 15.3 | 7.0 | | | |

#### *4.3.1.2.3 Group-3: Specimens Exposed to H-C Cycles and SL*

Because of the same reason described in Group2, only CFRP-confined specimens were used in this group. Specimens were loaded to 40% of their axial load capacity while being subjected to H-C cycles.

***CFRP-Confined Specimens***

Since none of the CFRP-confined specimens with 30 mm overlap was survived when subjected to sustained loading and H-C cycles, new specimens with relatively long overlap length were prepared. Four specimens were wrapped with one layer of CFRP providing 50 mm overlap (11% of the perimeter). It was observed that all of the specimens survived during exposure tests. After the completion of exposure test in, specimens were tested under uniaxial compression and their failure types were observed to be due to the rupture of CFRP (Figure 4.16). The axial stress-strain diagrams for the remaining three specimens were plotted in Figure 4.17 and their mechanical properties were presented in Table 4.11. As it is seen from the table, the average strength was found as 35.9 MPa and the ultimate strain was calculated as 0.03 with a COV of 5%.

Overlap length was seen to be one of the main parameters in CFRP-confined specimens. As noted before, specimens with an overlap length of 6% of the perimeter failed due to delamination, but specimens survived when it was increased to 11%. It was believed that 11% was the lower limit to guarantee the confinement. Therefore, this overlap length was used in the entire tests performed afterwards.

**(a) C10-C300-306** **(b) C10-C300-307** **(c) C10-C300-308** **(c) C10-C300-309**

**Figure 4.16. Failure types of CFRP-confined cylindrical specimens in Group-3 (SET 2 - $f_{co}$=10 MPa)**

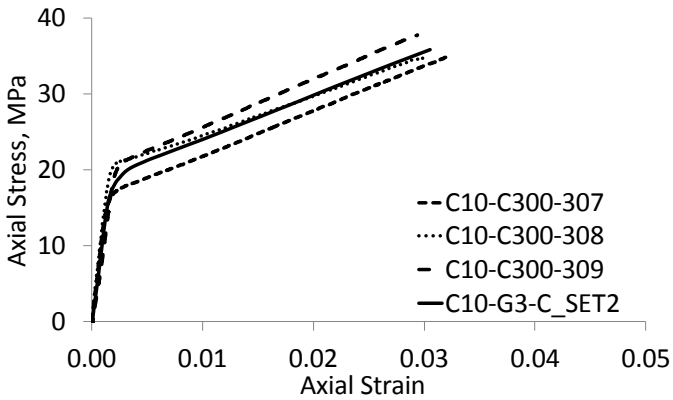


**Figure 4.17. Axial stress-strain diagrams of CFRP-confined cylindrical specimens in Group-3 (SET 2 - $f_{co}$=10 MPa)**

**Table 4.11. Mechanical properties of CFRP-confined cylindrical specimens in Group-3 (SET 2 - $f_{co}$=10 MPa)**

| Specimen | H-C cycles | SL, % | $f_{cc}$ , MPa | $\varepsilon_{cc}$ | $E_1$ , GPa | $E_2$ , GPa | $E_1/E_2$ |
|---|---|---|---|---|---|---|---|
| C10-C300-307 | 200 | 40 | 35.1 | 0.032 | 12.07 | 0.67 | 18.1 |
| C10-C300-308 | 200 | 40 | 34.7 | 0.030 | 14.46 | 0.52 | 27.9 |
| C10-C300-309 | 200 | 40 | 37.8 | 0.029 | 8.36 | 0.64 | 13.1 |
| **C10-G3-C_SET2** | | | **35.9** | **0.030** | **11.63** | **0.59** | **19.1** |
| COV, % | | | 4.8 | 5.1 | | | |

#### *4.3.1.2.4 Group-4: Specimens Subjected to SL*

***CFRP-Confined Specimens***

Three specimens were loaded axially to a sustained loading level of 40% of the axial capacity for 530 days. During this period, they were kept under ambient lab conditions. After 530 days, specimens were removed from the loading frame and tested under uniaxial compression to determine the change in mechanical properties.

Failure types of all specimens were given in Figure 4.18. All specimens were seen to fail due to the CFRP rupture extended to full height. Figure 4.19 shows the axial stress-strain diagrams of all specimens and Table 4.12 summarizes their mechanical properties. Unlike the ones in Group 3, there exists a smooth transition between first and second part of the curves. The average confined concrete strength was found to be 36.1 MPa with a relatively good COV. Confined concrete strain was evaluated as 0.027. The modulus of elasticity in the first part was calculated as 8.87 MPa and in the second part slope decreased to 0.62 MPa.

**(a) C10-C300-401** **(b) C10-C300-402** **(c) C10-C300-403**

**Figure 4.18. Failure types of CFRP-confined cylindrical specimens in Group-4 (SET 2 - $f_{co}$=10 MPa)**

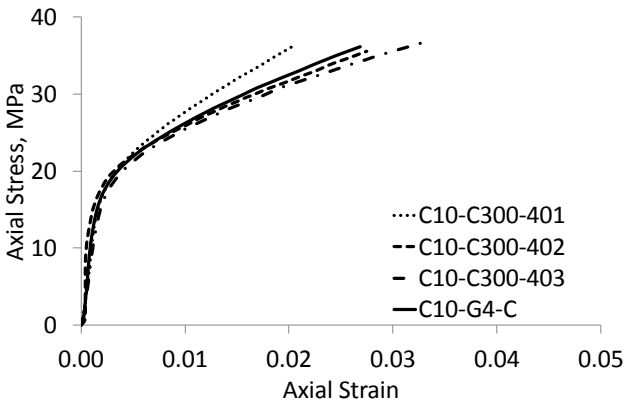


**Figure 4.19. Axial stress-strain diagrams of CFRP-confined cylindrical specimens in Group-4 (SET 2 - $f_{co}$=10 MPa)**

**Table 4.12. Mechanical properties of CFRP-confined cylindrical specimens in Group-4 (SET 2 - $f_{co}$=10 MPa)**

| Specimen | SL, % | $f_{cc}$, MPa | $\varepsilon_{cc}$ | $E_1$ , GPa | $E_2$ , GPa | $E_1/E_2$ |
|---|---|---|---|---|---|---|
| C10-C300-401 | 40 | 36.2 | 0.020 | 8.34 | 0.83 | 10.1 |
| C10-C300-402 | 40 | 35.6 | 0.028 | 10.32 | 0.54 | 19.2 |
| C10-C300-403 | 40 | 36.6 | 0.033 | 7.95 | 0.48 | 16.4 |
| **C10-G4-C** | | **36.1** | **0.027** | **8.87** | **0.62** | **14.4** |
| COV, % | | 1.4 | 23.4 | | | |

#### *4.3.1.2.5 Group-6: Specimens Subjected to Outdoor Exposure*

***CFRP-Confined Specimens***

Three specimens were kept outside the laboratory and subjected to outdoor exposure for 530 days. During this period, daily maximum and minimum temperatures and the humidity values were recorded as stated in Chapter 3, Section 3.3.2. All specimens failed due to the CFRP rupture as shown in Figure 4.20. The rupture extended to full height except for the last specimen in this group. For this specimen rupture was observed to occur at the upper midheight level.

Axial stress-strain diagrams of specimens were plotted in Figure 4.21 and their mechanical properties were summarized in Table 4.13. Since the readings of C10-C300-603 were not reliable, this specimen has discarded. Two specimens seem to behave identically. As it can be seen from the table, the average strength was 36.1 MPa and the confined concrete strain was calculated as 0.029 MPa.

**(a) C10-C300-601** **(b) C10-C300-602** **(c) C10-C300-603**

**Figure 4.20. Failure types of CFRP-confined cylindrical specimens in Group-6 (SET 2 - $f_{co}$=10 MPa)**

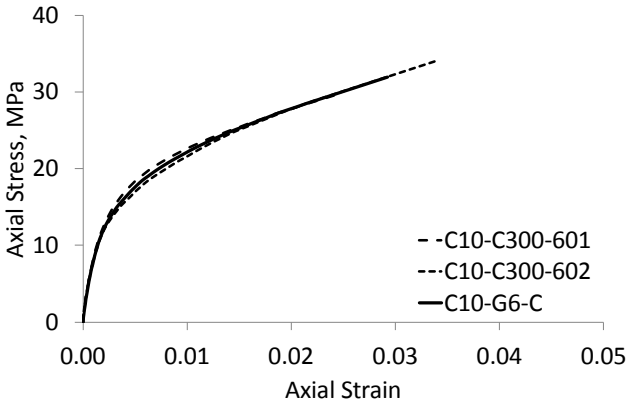


**Figure 4.21. Axial stress-strain diagrams of CFRP-confined cylindrical specimens in Group-6 (SET 2 - $f_{co}$=10 MPa)**

**Table 4.13. Mechanical properties of CFRP-confined cylindrical specimens in Group-6 (SET 2 - $f_{co}$=10 MPa)**

| Specimen | $f_{cc}$, MPa | $\varepsilon_{cc}$ | $E_1$ , GPa | $E_2$ , GPa | $E_1/E_2$ |
|---|---|---|---|---|---|
| C10-C300-601 | 29.8 | 0.025 | 10.22 | 0.46 | 22.2 |
| C10-C300-602 | 34.0 | 0.034 | 10.55 | 0.52 | 20.2 |
| **C10-G6-C** | **36.1** | **0.029** | **10.39** | **0.49** | **21.1** |

### 4.3.2 Prismatic Specimens

It is known that CFRP strengthening is more effective in cylindrical members [17, 18, 21, 82, 83]. The reason is that in cylindrical members, the confining stress is almost uniform (Figure 4.22-c) [21] along the circumference. However, if this confining stress is localized at some points (Figure 4.22-a and b), as in prismatic members, effectiveness of the confining material will change.

FRP-confined prismatic members having sharp corners behave almost the same as the unconfined members. Since the confining stress is only effective at the corners for these members, no apparent improvement in strength and strain capacity is possible. If the corners are rounded in such a way that the confining stress spreads over a larger area, strength and strain capacity are observed to increase. Therefore, corner radius was found to be the main parameter to ensure an effective strengthening [15, 16, 33].

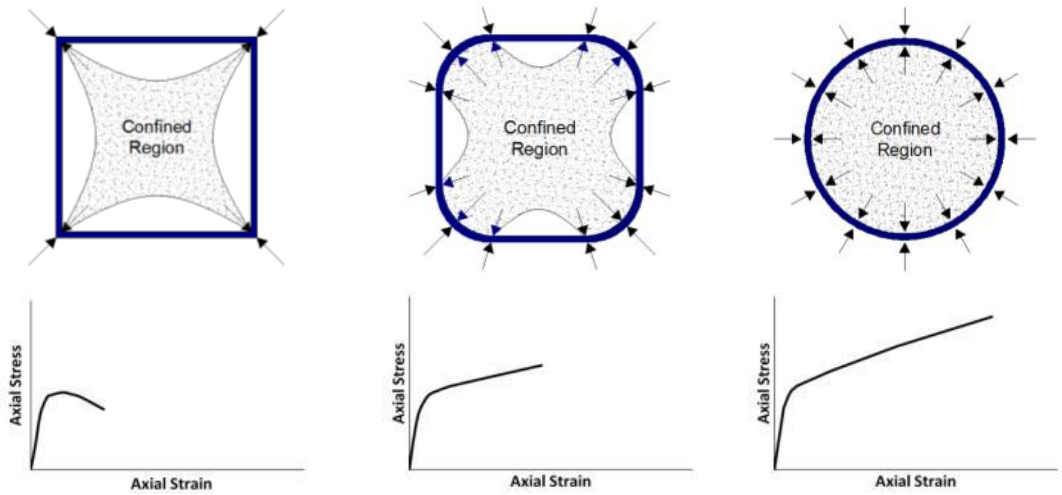


*(a) Prismatic specimen with sharp corners* *(b) Prismatic specimen with rounded corners* *(c) Cylindrical specimen*

**Figure 4.22 The effectiveness of the FRP in concrete**

Several authors studied the effect of corner radius on the effectiveness of the FRP material and based on their experiments they proposed equations to reflect this relationship. Among those authors, the equation proposed by Mirmiran et al. [16] seems to be well defined. They suggested "Modified Confinement Ratio" (Eqn. 4.1) which considers the corner radius, unconfined concrete strength, specimen width and the confining stress. A specified limit was introduced to account for the change in behavior. They stated that, if MCR was greater than 0.15, the concrete column would be properly confined, i.e. increase in the strength and strain capacity would be possible. However, below that limit effect of the confinement would not be seen.

$$MCR = \frac{2.r.f_{conf}}{b.f_{co}} \tag{4.1}$$

$$f_{conf} = \frac{2.t_{FRP}.f_{FRP}}{b} \tag{4.2}$$

In these equations, $r$ is the corner radius, $b$ is the specimen width, $f_{co}$ is the unconfined concrete strength, $t_{FRP}$ is the thickness of the FRP material used in strengthening and $f_{FRP}$ is the tensile strength of the FRP.

Based on the discussions above, in this dissertation prismatic specimens having square sections were carefully selected so that confinement would be effective, i.e. they were prepared to have an MCR factor greater than 0.15. In this respect, two sets of specimens were decided to be tested. In the first set specimens had 25 mm corner radius, which corresponded to an MCR factor of 0.25. The corner radius in the second set was 37.5 mm and it gave an MCR factor of 0.38. Corner radii were selected such that they could be in relationship with the specimen width, i.e. 25 mm corresponded to 1/6$^{th}$ of the width, 37.5 mm gave a ratio of ¼ and 75 mm (cylinder) corresponded to ½ of the specimen width (Table 4.14).

**Table 4.14. Relationship between corner radius, specimen width and the MCR**

| $f_{co}$, MPa | r, mm | b, mm | r/b ratio | MCR |
|---|---|---|---|---|
| 10 | 25 | 150 | 1/6 | 0.25 |
| 10 | 37.5 | 150 | 1/4 | 0.38 |
| 10 | 75.0 (cylinder) | 150 | 1/2 | 0.75 |

Prismatic specimens having 10 MPa strength were tested in two different sets, namely SET3 and SET4, in which corner radius was the main difference in the specimens. The experimental program for these specimens was summarized in Table 4.15. In the following sections, cylinder strength is denoted by $f_{co}$ and prismatic strength is represented by $f_{cop}$.

## Table 4.15 Summary of the 10 MPa prismatic specimens with r=25 mm

| Specimen Code | Confinement | $f_{co}$ (MPa) | Type | Overlap % | r, mm | Group No | # of H-C cycles | SL, % | Outdoor Exposure |
|---|---|---|---|---|---|---|---|---|---|
| U10-S300-25-101 | Unconfined | 10 | Prism | 11 | 25 | 1 | | | |
| U10-S300-25-102 | Unconfined | 10 | Prism | 11 | 25 | 1 | | | |
| U10-S300-25-103 | Unconfined | 10 | Prism | 11 | 25 | 1 | | | |
| C10-S300-25-101 | CFRP-Confined | 10 | Prism | 11 | 25 | 1 | | | |
| C10-S300-25-102 | CFRP-Confined | 10 | Prism | 11 | 25 | 1 | | | |
| C10-S300-25-103 | CFRP-Confined | 10 | Prism | 11 | 25 | 1 | | | |
| U10-S300-25-201 | Unconfined | 10 | Prism | 11 | 25 | 2 | 200 | | |
| U10-S300-25-202 | Unconfined | 10 | Prism | 11 | 25 | 2 | 200 | | |
| U10-S300-25-203 | Unconfined | 10 | Prism | 11 | 25 | 2 | 200 | | |
| C10-S300-25-201 | CFRP-Confined | 10 | Prism | 11 | 25 | 2 | 200 | | |
| C10-S300-25-202 | CFRP-Confined | 10 | Prism | 11 | 25 | 2 | 200 | | |
| C10-S300-25-203 | CFRP-Confined | 10 | Prism | 11 | 25 | 2 | 200 | | |
| C10-S300-25-204 | CFRP-Confined | 10 | Prism | 11 | 25 | 2 | 200 | | |
| U10-S300-25-301 | Unconfined | 10 | Prism | 11 | 25 | 3 | 200 | 40 | |
| U10-S300-25-302 | Unconfined | 10 | Prism | 11 | 25 | 3 | 200 | 40 | |
| U10-S300-25-303 | Unconfined | 10 | Prism | 11 | 25 | 3 | 200 | 40 | |
| C10-S300-25-301 | CFRP-Confined | 10 | Prism | 11 | 25 | 3 | 200 | 40 | |
| C10-S300-25-302 | CFRP-Confined | 10 | Prism | 11 | 25 | 3 | 200 | 40 | |
| C10-S300-25-303 | CFRP-Confined | 10 | Prism | 11 | 25 | 3 | 200 | 40 | |
| C10-S300-25-304 | CFRP-Confined | 10 | Prism | 11 | 25 | 3 | 200 | 40 | |
| C10-S300-25-305 | CFRP-Confined | 10 | Prism | 11 | 25 | 3 | 200 | 40 | |
| C10-S300-25-306 | CFRP-Confined | 10 | Prism | 11 | 25 | 3 | 200 | 55 | |
| C10-S300-25-307 | CFRP-Confined | 10 | Prism | 11 | 25 | 3 | 200 | 55 | |
| C10-S300-25-401 | CFRP-Confined | 10 | Prism | 11 | 25 | 4 | | 40 | |
| C10-S300-25-402 | CFRP-Confined | 10 | Prism | 11 | 25 | 4 | | 40 | |
| C10-S300-25-403 | CFRP-Confined | 10 | Prism | 11 | 25 | 4 | | 40 | |
| C10-S300-25-601 | CFRP-Confined | 10 | Prism | 11 | 25 | 6 | | | Yes |
| C10-S300-25-602 | CFRP-Confined | 10 | Prism | 11 | 25 | 6 | | | Yes |
| C10-S300-25-603 | CFRP-Confined | 10 | Prism | 11 | 25 | 6 | | | Yes |
| C10-S300-25-604 | CFRP-Confined | 10 | Prism | 11 | 25 | 6 | | | Yes |

**Table 4.16 Summary of the 10 MPa prismatic specimens with r=37.5 mm**

| Specimen Code | Confinement | $f_{co}$ (MPa) | Type | Overlap % | r, mm | Group No | # of H-C cycles | SL, % | Outdoor Exposure |
|---|---|---|---|---|---|---|---|---|---|
| U10-S300-37.5-101 | Unconfined | 10 | Prism | 11 | 37.5 | 1 | | | |
| U10-S300-37.5-102 | Unconfined | 10 | Prism | 11 | 37.5 | 1 | | | |
| U10-S300-37.5-103 | Unconfined | 10 | Prism | 11 | 37.5 | 1 | | | |
| C10-S300-37.5-101 | CFRP-Confined | 10 | Prism | 11 | 37.5 | 1 | | | |
| C10-S300-37.5-102 | CFRP-Confined | 10 | Prism | 11 | 37.5 | 1 | | | |
| C10-S300-37.5-201 | CFRP-Confined | 10 | Prism | 11 | 37.5 | 2 | 200 | | |
| C10-S300-37.5-301 | CFRP-Confined | 10 | Prism | 11 | 37.5 | 3 | 200 | 50 | |
| C10-S300-37.5-302 | CFRP-Confined | 10 | Prism | 11 | 37.5 | 3 | 200 | 50 | |
| C10-S300-37.5-303 | CFRP-Confined | 10 | Prism | 11 | 37.5 | 3 | 200 | 40 | |
| C10-S300-37.5-304 | CFRP-Confined | 10 | Prism | 11 | 37.5 | 3 | 200 | 40 | |
| C10-S300-37.5-401 | CFRP-Confined | 10 | Prism | 11 | 37.5 | 4 | | 40 | |
| C10-S300-37.5-402 | CFRP-Confined | 10 | Prism | 11 | 37.5 | 4 | | 40 | |
| C10-S300-37.5-403 | CFRP-Confined | 10 | Prism | 11 | 37.5 | 4 | | 40 | |
| C10-S300-37.5-501 | CFRP-Confined | 10 | Prism | 11 | 37.5 | 5 | 200 wet | | |
| C10-S300-37.5-502 | CFRP-Confined | 10 | Prism | 11 | 37.5 | 5 | 200 wet | | |
| C10-S300-37.5-503 | CFRP-Confined | 10 | Prism | 11 | 37.5 | 5 | 200 wet | | |
| C10-S300-37.5-601 | CFRP-Confined | 10 | Prism | 11 | 37.5 | 6 | | | Yes |
| C10-S300-37.5-602 | CFRP-Confined | 10 | Prism | 11 | 37.5 | 6 | | | Yes |
| C10-S300-37.5-603 | CFRP-Confined | 10 | Prism | 11 | 37.5 | 6 | | | Yes |

#### *4.3.2.1. SET 3: Prismatic Specimens with r = 25 mm*

In this set, a total of 31 specimens were tested. The cylinder strength was found to be 10.9 MPa.

##### *4.3.2.1.1. Group-1: Reference Specimens*

***Unconfined Specimens***

Four specimens were kept unloaded in the ambient lab condition until the end of exposure tests conducted in the environmental test chamber. In Phase 2 test (uniaxial compression test), those specimens were axially loaded to failure and their

mechanical properties were recorded. The axial stress-strain diagrams for three specimens were presented in Figure 4.24 and their mechanical properties were tabulated in Table 4.17. From the failure types given in Figure 4.23, it can be seen that all specimens failed in shear mode as described in ASTM C39/C39M-01 [84].

As it is seen from Figure 4.24, all of the three specimens showed different behavior. In Table 4.17, it can be clearly seen that, coefficient of variations were in the bad region for modulus of elasticity and strain corresponding to stress. The reason can be attributed to the stress concentrations at the corners and the distribution of the coarse aggregates. However, as for strength, they are relatively good and it can be said that, the average strength was 10 MPa.

**(a) U10-S300-25-101** **(b) U10-S300-25-102** **(c) U10-S300-25-103** **(c) U10-S300-25-104**

**Figure 4.23. Failure types of unconfined prismatic specimens in Group-1 (SET 3 – $f_{co}$=10 MPa and r=25mm)**

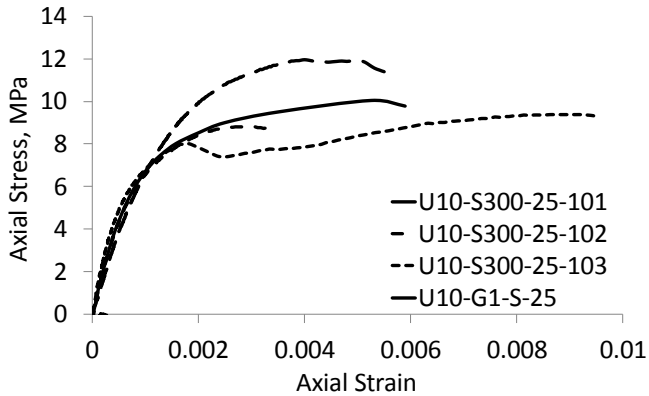


**Figure 4.24. Axial stress-strain diagrams of unconfined prismatic specimens in Group-1 (SET 3 - $f_{co}$=10 MPa and r=25 mm)**

**Table 4.17. Mechanical properties of unconfined prismatic specimens in Group-1 (SET 3 - $f_{co}$=10 MPa and r=25 mm)**

| Specimen | $f_{cop}$ , MPa | $\varepsilon_{co}$ | $E_1$ , GPa |
|---|---|---|---|
| U10-S300-25-101 | 11.9 | 0.004 | 7.45 |
| U10-S300-25-102 | 8.8 | 0.003 | 9.31 |
| U10-S300-25-103 | 9.4 | 0.009 | 11.29 |
| **U10-G1-S-25** | **10.0** | **0.005** | **9.35** |
| COV, % | 16.6 | 61.0 | |

***CFRP-Confined Specimens***

Specimens in this group were used as control specimens and wrapped with one layer of CFRP providing an overlap length of 11% of the perimeter. As it is seen from the failure types given in Figure 4.25, both C10-S300-25-101 and C10-S300-25-103 failed due to the CFRP rupture at the corner near the midheight. Different from these specimens, the rupture in C10-S300-25-102 was at the side of the specimen and localized at a point, which seem to occur due to the out of plane forces exerted from

the local concrete failure. Axial stress-strain behaviors were given in Figure 4.26 and mechanical properties were summarized in Table 4.18. From the table it can be seen that the average strength was found to be 25.8 MPa with a COV of 5% and confined concrete strain was evaluated to be 0.026 with a COV of 24.3, which shows that wrapping specimens with CFRP decreases the dispersion as compared to the COVs calculated for unconfined concrete specimens.

**(a) C10-S300-25-101** **(b) C10-S300-25-102** **(c) C10-S300-25-103**

**Figure 4.25. Failure types of CFRP-confined prismatic specimens in Group-1 (SET 3 - $f_{co}$=10 MPa and r=25mm)**

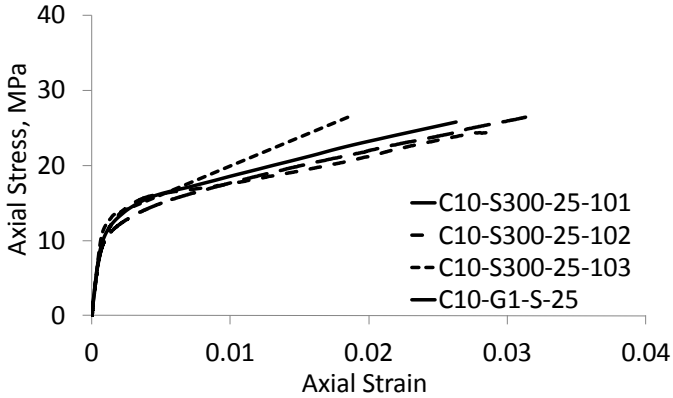


**Figure 4.26. Axial stress-strain diagrams of CFRP-confined prismatic specimens in Group-1 (SET 3 - $f_{co}$=10 MPa and r=25 mm)**

**Table 4.18 Mechanical properties of CFRP-confined prismatic specimens in Group-1 (SET 3 - $f_{co}$=10 MPa and r=25 mm)**

| Specimen | $f_{cc}$, MPa | $\varepsilon_{cc}$ | $E_1$ , GPa | $E_2$ , GPa | $E_1/E_2$ |
|---|---|---|---|---|---|
| C10-S300-25-101 | 26.4 | 0.031 | 16.39 | 0.44 | 37.4 |
| C10-S300-25-102 | 24.4 | 0.029 | 16.81 | 0.38 | 43.7 |
| C10-S300-25-103 | 26.6 | 0.019 | 17.00 | 0.74 | 23.1 |
| **C10-G1-S-25** | **25.8** | **0.026** | **16.73** | **0.52** | **32.2** |
| COV, % | 4.7 | 24.3 | | | |

Specimen C10-S300-25-103 was tested using strain gages as shown in Figure 4.27. Four uniaxial strain gages with a gage length of 10 mm were placed at each corner to determine the lateral strains at these locations. Two triaxial rosette strain gages with a gage length of 10 mm were attached at the sides of the specimen to record axial shortening, lateral expansion and shear strains. One of the rosette strain gages was placed at the overlapping zone and the other one was placed at the opposite side. Besides the strain gages, two dial gages with a gage length of 20 mm were used to record the axial deformations and thus axial strains. They were placed at the other two sides. With these measuring devices, it was aimed to record axial and lateral strains, circumferential strain distribution and the relationship with strain and failure.

In Figure 4.27, schematic view of the gages is illustrated. Gage numbers were the channel numbers in data acquisitions system. While performing uniaxial compression test, it was realized that two strain gages (108 and 109) were not in function because of the cable problems. In addition to these strain gages, 106 and 102 were also discarded because they record shear strains. Only axial and lateral strains were processed and used in here.

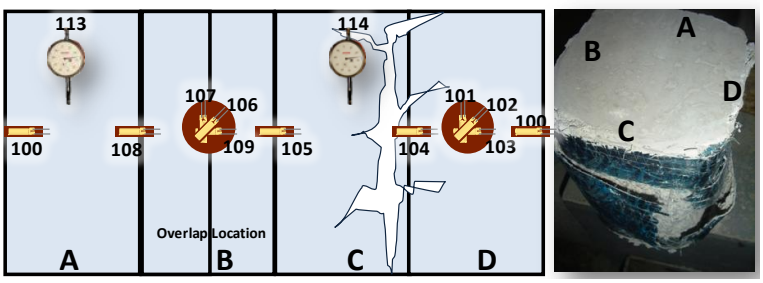


**Figure 4.27 Schematic view of the gages used in C10-S300-25-103**

In Figure 4.28, failure type of C10-S300-25-103 was presented. As previously stated, this specimen failed due to the CFRP rupture at the corner. In the figure, (a) and (b) shows the deformation in CFRP, (c) shows the deformation in concrete and (d) illustrates the lateral stress distribution in CFRP and concrete due to the expansion phenomenon. The internal stress in concrete seems to localize at corners (d). Therefore, corners can be regarded as the vulnerable parts of a rectangular concrete member. This was verified in figure (c) which shows that concrete experiences extensive crushing at the corners. The stress concentrations at the corners lead to crushing and thus crushing leads to out-of-plane stresses developed in CFRP. Since CFRP is weak in shear, confinement effectiveness decreases and CFRP fails at relatively low strain. In Figure 4.30, stress-strain behaviors in both axial and lateral directions were presented. Although lateral strains at the sides were greater than the ones at the corners, CFRP rupture occurred at the corner. Another reason to answer why CFRP failed at the corner was that, fibers may be weakened due to the curvature of the CFRP material at the corners [82].

Figure 4.29 shows the axial and lateral strain distribution along the perimeter. As it is seen, axial stain distribution is not uniform. It is 0.0136 at face A and almost doubles at face C, which is the indication of bending. The specimen bends about -x-axis. It was observed that during tests, the axial load was almost concentric up to a stress level close to the ultimate strength. Therefore, the bending in the specimen is

believed to be due to the non-uniform deformation caused by the irregularities in the concrete. Bending results in a nonuniform squeezing thus nonuniform expansion. Nonuniform expansion can be seen form lateral strain distribution as presented in Figure 4.29. The rupture strain was recorded to be 0.0072, which was 48% of the strain provided by the manufacturer.

(a) (b) (c) (d)

**Figure 4.28 Failure of C10-S300-25-103 (a, b and c) and confining stresses (d)**

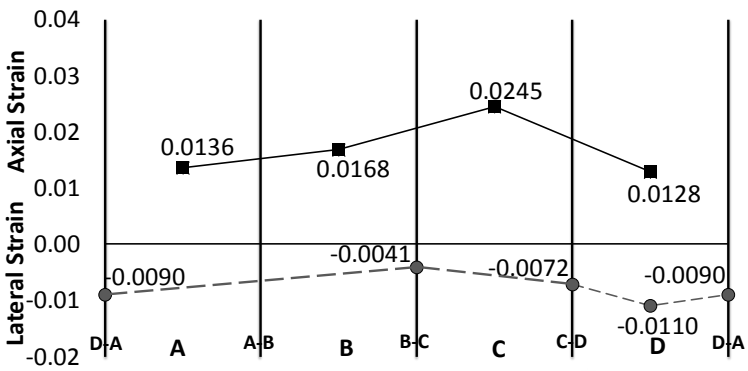


**Figure 4.29 Axial and lateral strain distributions in C10-S300-25-103**

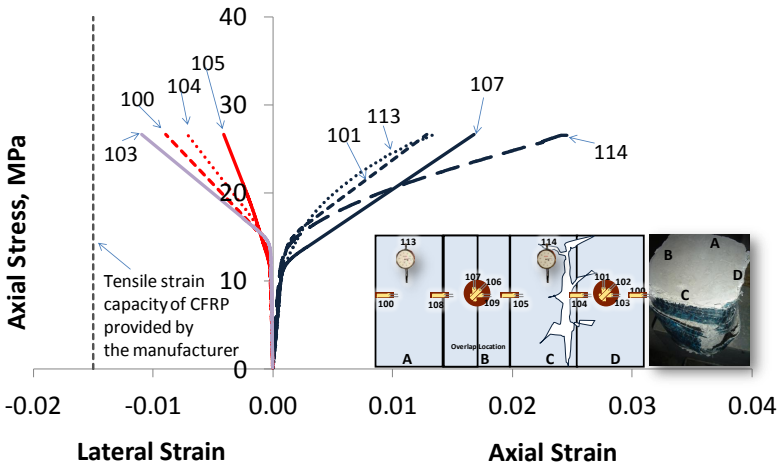


**Figure 4.30 Stress-strain behavior of C10-S300-25-103**

#### *4.3.2.1.2. Group-2: Specimens exposed to H-C Cycles*

***Unconfined Specimens***

Three unconfined prismatic specimens were exposed to 200 heating-cooling cycles in Phase 1 test and after that, they were removed from the environmental test chamber. In Phase 1 test, they were loaded uniaxially to failure to determine the effect of heating-cooling cycles on the mechanical properties.

In Figure 4.31, failure types of the specimens were presented. Failure types were mostly in cone and shear type as described in [84]. From the axial stress-strain diagrams given in Figure 4.32, it can be seen that all specimens behaved differently. The main difference is at the strength level. The strength of U10-S300-25-201 was found to be 6.5 MPa, which was much lower than the target strength of 10 MPa. This may be attributed to the nonuniform expansion and contraction under heating and cooling cycles. Since specimens in this group were free to expand under heating cycles and contract under cooling cycles, the deformations developed during these cycles may cause the strength reduction.

Mechanical properties of the specimens were tabulated in Table 4.19. As it can be seen, the coefficients of variations seem to be bad which makes the mechanical properties difficult to estimate. The average strength was calculated to be 8.0 MPa and the corresponding strain was estimated to be 0.003.

**(a) U10-S300-25-201**

**(b) U10-S300-25-202**

**(c) U10-S300-25-203**

**Figure 4.31. Failure types of unconfined prismatic specimens in Group-2 (SET 3 - $f_{co}$=10 MPa and r=25mm)**

**Table 4.19. Mechanical properties of unconfined prismatic specimens in Group-2 (SET 3 - $f_{co}$=10 MPa and r=25 mm)**

| Specimen | H-C Cycles | $f_{cop}$ , MPa | $\varepsilon_{co}$ | $E_1$ , GPa |
|---|---|---|---|---|
| U10-S300-25-201 | 200 | 6.5 | 0.003 | 9.6 |
| U10-S300-25-202 | 200 | 9.5 | 0.002 | 14.2 |
| U10-S300-25-203 | 200 | 7.9 | 0.004 | 10.8 |
| **U10-G2-S-25** | | **8.0** | **0.003** | **11.6** |
| COV, % | | 18.8 | 34.2 | |

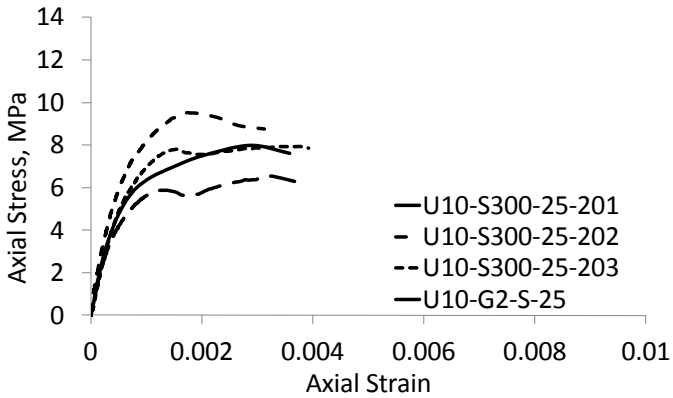


**Figure 4.32. Axial stress-strain diagrams of unconfined prismatic specimens in Group-2 (SET 3 - $f_{co}$=10 MPa and r=25 mm)**

***CFRP-Confined Specimens***

CFRP confined prismatic specimens were subjected to 200 heating-cooling cycles in the environmental test chamber and after the completion of exposure test their mechanical properties were determined.

Failure types of the specimens were presented in Figure 4.33. All specimens failed due to the CFRP rupture at the corner. Although CFRP rupture occurred at the midheight of the specimens, it occurred below the midheight in C10-S300-25-202 and there was not a clear rupture. However, this did not affect the behavior as shown in Figure 4.34. In this figure, it is seen that all specimens followed the same path except C10-S300-25-204 in which CFRP rupture extended to a relatively longer height.

Mechanical properties of the specimens were summarized in Table 4.20. After 200 heating-cooling cycles the average strength was calculated as 23.9 with a COV of 5% and confined concrete strain was found to be 0.025 with a COV of 22%.,

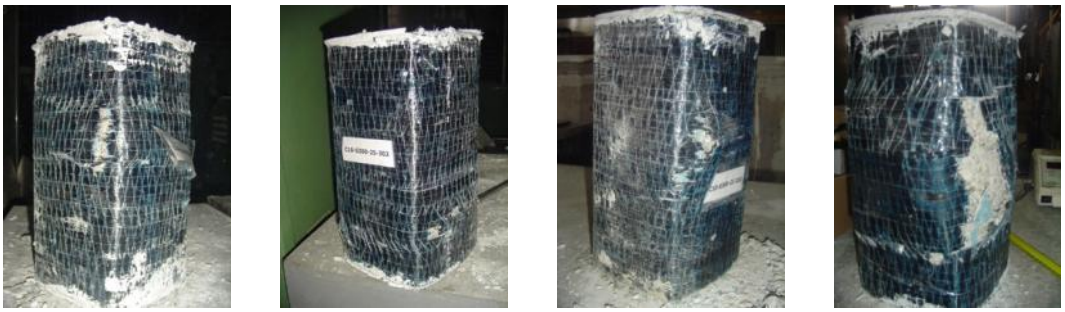

**(a) C10-S300-25-201** **(b) C10-S300-25-202** **(c) C10-S300-25-203** **(d) C10-S300-25-204**

**Figure 4.33. Failure types of CFRP-confined prismatic specimens in Group-2 (SET 3 - $f_{co}$=10 MPa and r=25mm)**

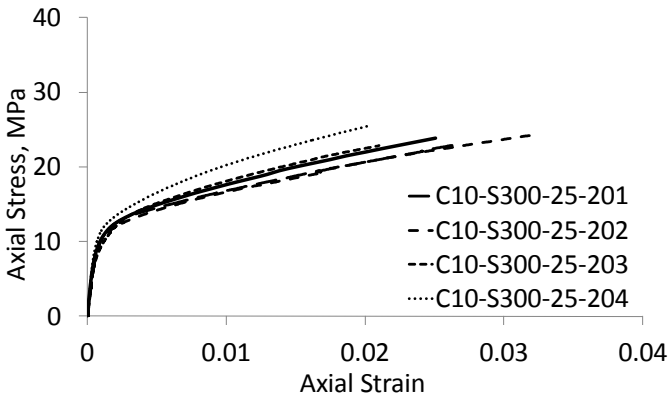


**Figure 4.34. Axial stress-strain diagrams of CFRP-confined prismatic specimens in Group-2 (SET 3 - $f_{co}$=10 MPa and r=25 mm)**

Similar to Group 1, one specimen in this group (C10-S300-25-204) was tested using additional gages. As illustrated in Figure 4.35, two uniaxial strain gages were attached to the corners and one triaxial rosette strain gage was placed at the side where the overlap was provided. One of the dial gages was placed at the overlap location to understand the difference in the readings recorded from dial gage and the strain gage. The other dial gage was provided at the opposite face of the specimen.

**Table 4.20. Mechanical properties of CFRP-confined prismatic specimens in Group-2 (SET 3 - $f_{co}$=10 MPa and r=25 mm)**

| Specimen | H-C Cycles | $f_{cc}$, MPa | $\varepsilon_{cc}$ | $E_1$ , GPa | $E_2$ , GPa | $E_1/E_2$ |
|---|---|---|---|---|---|---|
| C10-S300-25-201 | 200 | 22.9 | 0.026 | 16.44 | 0.37 | 40.3 |
| C10-S300-25-202 | 200 | 24.2 | 0.032 | 19.17 | 0.36 | 44.7 |
| C10-S300-25-203 | 200 | 22.9 | 0.021 | 18.36 | 0.45 | 21.9 |
| C10-S300-25-204 | 200 | 25.5 | 0.021 | 22.82 | 0.63 | 28.6 |
| **C10-G2-S-25** | | **23.9** | **0.025** | **19.20** | **0.45** | **31.0** |
| COV, % | | 5.1 | 21.9 | | | |

Figure 4.36 shows the stress-strain diagrams plotted from the recordings of each gage. As it is seen, both the strain gage (100) and the dial gage (114) at the overlap region recorded almost the same axial strains. The dial gage 113 at the opposite face recorded relatively higher axial strains, which was the indication of bending. Similar to the one observed in Group 1, CFRP rupture in this specimen occurred at the corner close to the higher axial strain zone. Since there were not enough gages at the lateral direction, it was hard to say anything about the strain distribution along the circumference. However, since there was a strain gage at the failure zone, it can be said that the rupture strain was 0.0079, which was the 53% of the tensile strain capacity provided by the manufacturer (Figure 4.37).

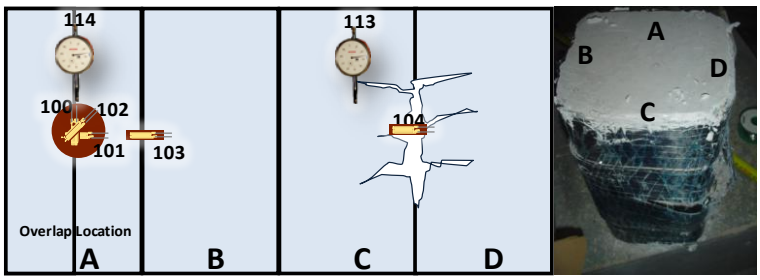


**Figure 4.35 Schematic view of the gages used in C10-S300-25-204**

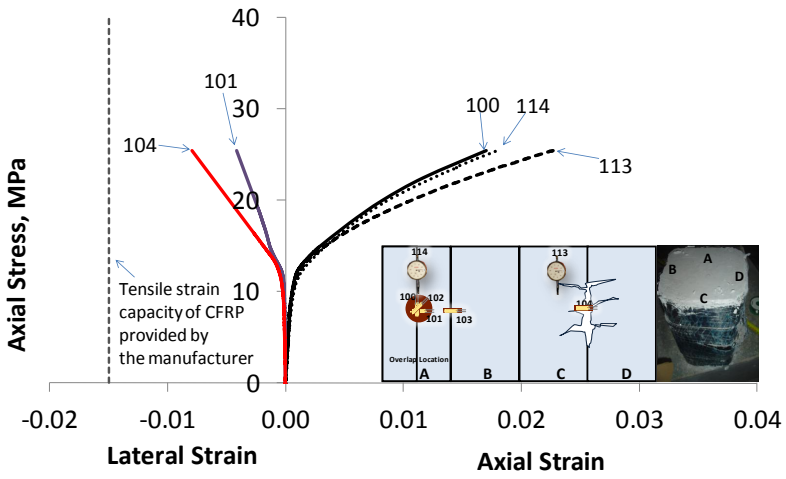


**Figure 4.36 Stress-strain behavior of C10-S300-25-204**

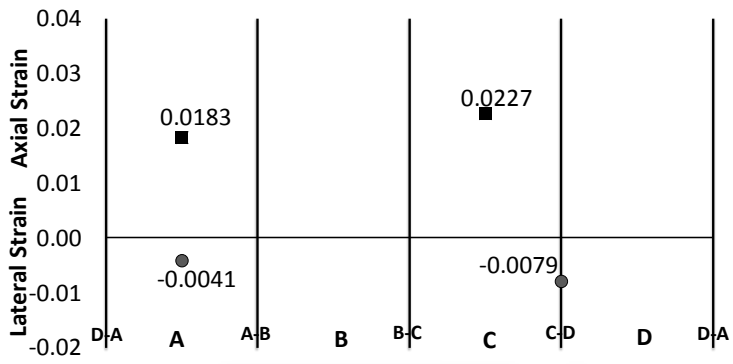


**Figure 4.37 Axial and lateral strain distributions in C10-S300-25-204**

#### *4.3.2.1.3. Group-3: Specimens Exposed to H-C Cycles and SL*

***Unconfined Specimens***

Unconfined specimens in this group were loaded to 40% of their axial load capacity and subjected to heating-cooling cycles. After reaching 200 cycles, heating-cooling procedure was stopped; specimens were unloaded and then tested under uniaxial compression to determine the change in their mechanical properties. As it is seen from the failure types given in Figure 4.38, all specimens failed in shear mode. The axial stress-strain diagrams were presented in Figure 4.39 and their mechanical properties were tabulated in Table 4.21. From the table, it can be seen that the average strength was 9.2 and average strain was 0.004.

**(a) U10-S300-25-301** **(b) U10-S300-25-302** **(c) U10-S300-25-303**

**Figure 4.38. Failure types of unconfined prismatic specimens in Group-3 (SET 3 - $f_{co}$=10 MPa and r=25mm)**

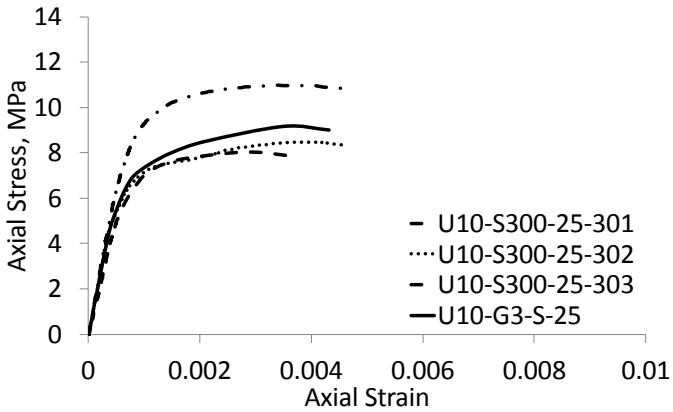


**Figure 4.39. Axial stress-strain diagrams of unconfined prismatic specimens in Group-3 (SET 3 - $f_{co}$=10 MPa and r=25 mm)**

**Table 4.21. Mechanical properties of unconfined prismatic specimens in Group-3 (SET 3 - $f_{co}$=10 MPa and r=25 mm)**

| Specimen | H-C Cycles | SL, % | $f_{cop}$, MPa | $\varepsilon_{co}$ | $E_1$ , GPa |
|---|---|---|---|---|---|
| U10-S300-25-301 | 200 | 40 | 11.0 | 0.004 | 13.2 |
| U10-S300-25-302 | 200 | 40 | 8.5 | 0.004 | 13.1 |
| U10-S300-25-303 | 200 | 40 | 8.0 | 0.003 | 10.2 |
| **U10-G3-S-25** | | | **9.2** | **0.004** | **12.2** |
| COV, % | | | 17.3 | 12.2 | |

***CFRP-Confined Specimens***

Seven specimens were tested in this group. Five of them were loaded to 40% of their axial load capacity ($0.4f_{cc}$), and the remaining two were loaded to 55% of their axial load capacity ($0.55f_{cc}$) to determine the effect of the sustained loading level. All specimens were also subjected to heating-cooling cycles as mentioned previously. In Figure 4.40, failure types of the specimens subjected to simultaneous exposure of a

sustained loading of $0.4f_{cc}$ and heating-cooling cycles were presented. All specimens failed due to the CFRP rupture at the end of the radius provided at the corner.

Axial stress-strain diagrams recorded after the exposure test were plotted in Figure 4.41. Table 4.22 summarizes the mechanical properties of the specimens. As it is seen, the average strength was 24.8 MPa with a COV of 11.5% and confined concrete strain was calculated to be 0.022 with a COV of 37.7. As for modulus of elasticity in the first and second part, the drastic drop can be seen easily. Modulus of elasticity dropped from 19.9 GPa to 0.43 GPa

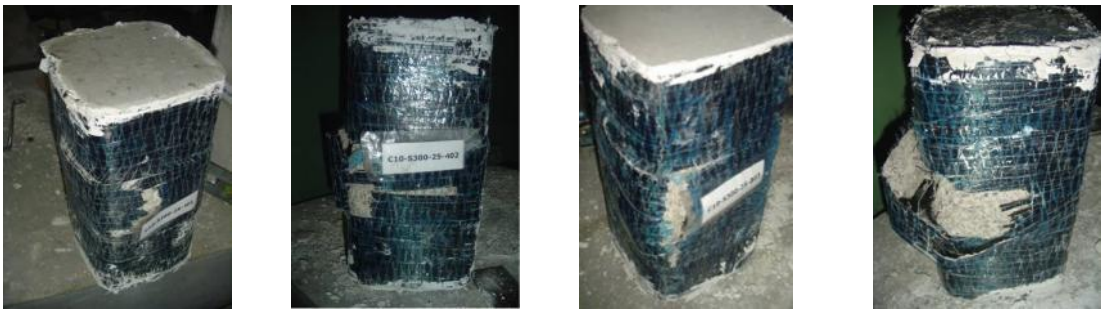

**(a) C10-S300-25-301** **(b) C10-S300-25-302** **(c) C10-S300-25-303** **(d) C10-S300-25-304**

**Figure 4.40. Failure types of CFRP-confined prismatic specimens in Group-3 (SET 3 - $f_{co}$=10 MPa, r=25mm and SL=0.4$f_{cc}$)**

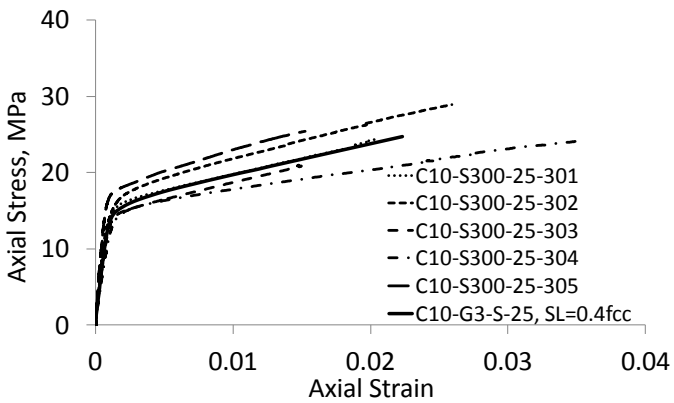


**Figure 4.41. Axial stress-strain diagrams of CFRP-confined prismatic specimens in Group-3 (SET 3 - $f_{co}$=10 MPa, r=25mm and SL=0.4$f_{cc}$)**

**Table 4.22. Mechanical properties of CFRP-confined prismatic specimens in Group-3 (SET 3 - $f_{co}$=10 MPa, r=25 mm and SL=0.4$f_{cc}$)**

| Specimen | H-C Cycles | SL, % | $f_{cc}$, MPa | $\varepsilon_{cc}$ | $E_1$, GPa | $E_2$, GPa | $E_1/E_2$ |
|---|---|---|---|---|---|---|---|
| C10-S300-25-301 | 200 | 40 | 24.4 | 0.021 | 15.63 | 0.43 | 36.7 |
| C10-S300-25-302 | 200 | 40 | 28.9 | 0.026 | 18.93 | 0.49 | 38.8 |
| C10-S300-25-303 | 200 | 40 | 21.0 | 0.015 | 20.23 | 0.44 | 46.5 |
| C10-S300-25-304 | 200 | 40 | 24.1 | 0.035 | 12.98 | 0.26 | 50.6 |
| C10-S300-25-305 | 200 | 40 | 25.4 | 0.015 | 31.64 | 0.56 | 56.3 |
| **C10-G3-S-25_%40** | | | **24.8** | **0.022** | **19.9** | **0.43** | **45.9** |
| COV, % | | | 11.5 | 37.7 | | | |

In Figure 4.42, failure types of the remaining specimens, i.e., specimens subjected to $0.55f_{cc}$ sustained load and heating-cooling cycles, were given. Failures were due to the CFRP rupture at the end of the radius at the corner as similar to the ones given

above. As seen from the axial stress-strain curves plotted in Figure 4.43, two specimens behaved almost identically. As given in Table 4.23, the average strength, which was calculated as 28.6 MPa, was a bit greater than the previous ones. However, this was not the case in strain capacity, which was much lower than the other one. In this case, it was 0.015. Modulus of elasticity in the first part was also lower. It can be said that increase in sustained load level resulted in an increase in both strength and modulus of elasticity in the second part of the curve but a decrease in both strain capacity and modulus of elasticity in the first part of the curve.

**(a) C10-S300-25-306**

**(b) C10-S300-25-307**

**Figure 4.42. Failure types of CFRP-confined prismatic specimens in Group-3 (SET 3 - $f_{co}$=10 MPa, r=25mm and SL=0.55$f_{cc}$)**

**Table 4.23. Mechanical properties of CFRP-confined prismatic specimens in Group-3 (SET 3 - $f_{co}$=10 MPa, r=25 mm and SL=0.55$f_{cc}$)**

| Specimen | H-C Cycles | SL, % | $f_{cc}$, MPa | $\varepsilon_{cc}$ | $E_1$, GPa | $E_2$, GPa | $E_1/E_2$ |
|---|---|---|---|---|---|---|---|
| C10-S300-25-306 | 200 | 55 | 29.7 | 0.015 | 7.82 | 0.63 | 12.4 |
| C10-S300-25-307 | 200 | 55 | 27.5 | 0.015 | 7.00 | 0.59 | 11.8 |
| **C10-G3-S-25_%55** | | | **28.6** | **0.015** | | | |

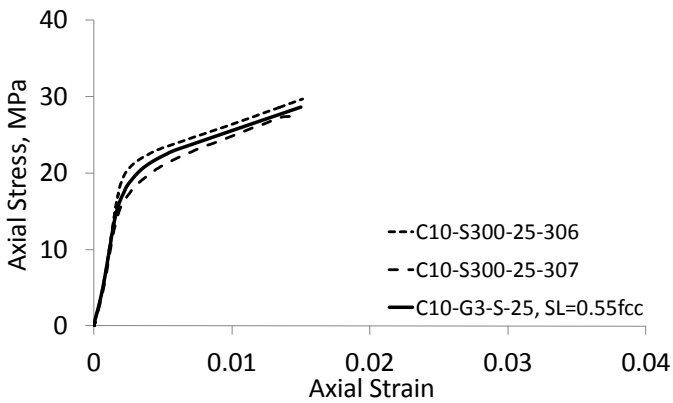


**Figure 4.43. Axial stress-strain diagrams of CFRP-confined prismatic specimens in Group-3 (SET 3 - $f_{co}$=10 MPa, r=25mm and SL=0.55$f_{cc}$)**

One specimen (C10-S300-25-305) in this group was also tested using several gages as shown in Figure 4.44. In this case, four uniaxial strain gages to record lateral strains were attached to each corner; two triaxial rosette strain gages to record strains in both axial and lateral directions were placed at the opposite sides of the specimen. One of these rosette dial gages was at the overlap zone. Besides strain gages, two dial gages were utilized at the faces where there were no strain gages. All strain gages were placed close to the midheight of the specimen. Unlike the ones presented in previous groups, all gages on this specimen worked and recordings were meaningful as presented in Figure 4.45. As previously stated the recordings from the diagonal strain gages were not processed and used.

As the detailed stress-strain curves plotted for each gage was investigated, it can be clearly seen that axial strains were not the same for each side of the specimen (Figure 4.45). Strains at face A and B were less than the other two faces, which can be regarded as the sign of bending. Figure 4.46 summarizes the ultimate strains to understand the strain distribution along the circumference. Neither axial nor lateral strains were uniform. Axial strains were high in the failure zone. However, lateral

strains were not high at this zone. Since at the sides, CFRP was straight and stress concentrations were not as high as the ones at the corners i.e. out-of plane shear was not effective, it showed good resistance. However, it is known that corners are the critical parts due to the reasons described above and the rupture takes place at this region, which experiences lower strains. The failure strain was found to be 0.0063, which was 42% of the tensile strain capacity of CFRP.

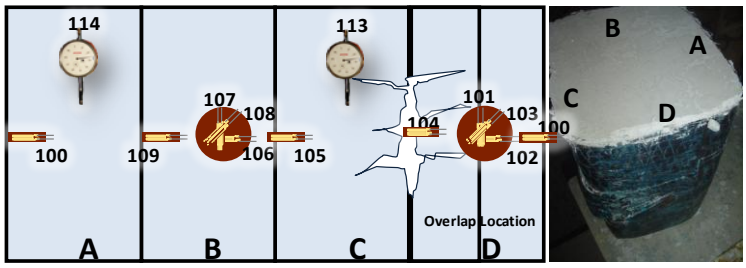


**Figure 4.44 Schematic view of the gages used in C10-S300-25-305**

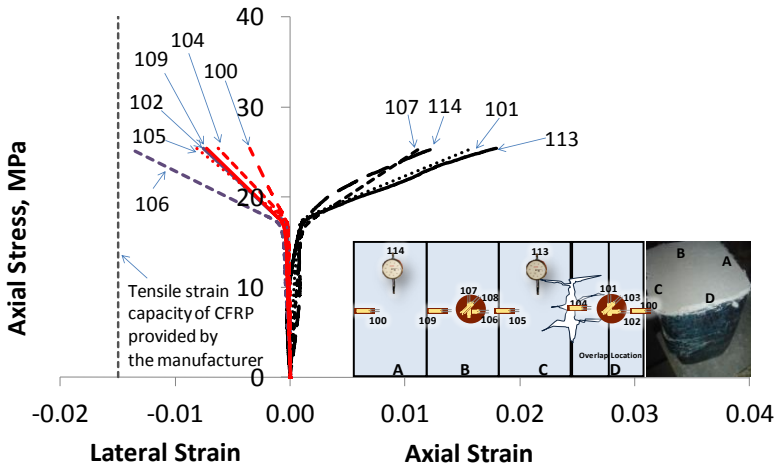


**Figure 4.45 Stress-strain behavior of C10-S300-25-305**

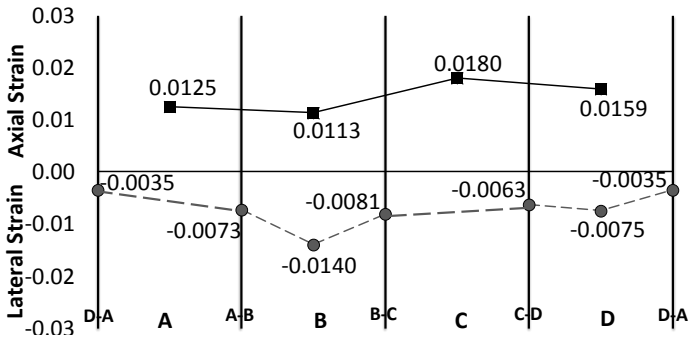


**Figure 4.46 Axial and lateral strain distributions in C10-S300-25-305**

### *4.3.2.1.4. Group-4: Specimens Subjected to SL*

***CFRP-Confined Specimens***

Three CFRP-confined specimens were tested in this group. They were kept under a sustained load level of 40% of the axial load capacity for 530 days. Failure types after the uniaxial compression test were presented in Figure 4.47. From the figure, it is seen that specimens failed due to the CFRP rupture near the corner. The rupture extended to full height.

Axial stress-strain diagrams were plotted in Figure 4. 48 and the mechanical properties were tabulated in Table 4.24. Axial stress-strain diagrams followed the same trend in the first part but they diverged from each other in the second part. Difference in the slope in the second part resulted in different strain capacities. Maximum strain was found to be 0.020 and minimum strain was 0.012. The average strain was calculated as 0.018 with a COV of 26.7%. However, difference in the second slope of the curve did not affect the strength of CFRP-confined concrete. The average strength was found to be 33.1 MPa with a COV of 3.2%.

**(a) C10-S300-25-401** **(b) C10-S300-25-402** **(c) C10-S300-25-403**

**Figure 4.47. Failure types of CFRP-confined prismatic specimens in Group-4 (SET 3 - $f_{co}$=10 MPa, r=25mm and SL=0.4$f_{cc}$)**

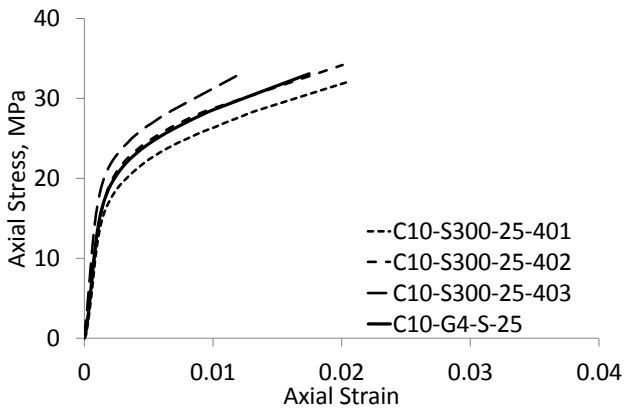


**Figure 4. 48. Axial stress-strain diagrams of CFRP-confined prismatic specimens in Group-4 (SET 3 - $f_{co}$=10 MPa, r=25mm and SL=0.4$f_{cc}$)**

**Table 4.24. Mechanical properties of CFRP-confined prismatic specimens in Group-4 (SET 3 - $f_{co}$=10 MPa, r=25 mm and SL=0.4$f_{cc}$)**

| Specimen | SL, % | $f_{cc}$, MPa | $\varepsilon_{cc}$ | $E_1$ , GPa | $E_2$ , GPa | $E_1/E_2$ |
|---|---|---|---|---|---|---|
| C10-S300-25-401 | 40 | 32.1 | 0.020 | 8.60 | 0.69 | 12.5 |
| C10-S300-25-402 | 40 | 34.2 | 0.020 | 10.00 | 0.91 | 11.0 |
| C10-S300-25-402 | 40 | 33.1 | 0.012 | 15.50 | 1.25 | 12.4 |
| **C10-G4-S-25** | | **33.1** | **0.018** | **11.3** | **0.95** | **11.9** |
| COV, % | | 3.2 | 26.7 | | | |

#### *4.3.2.1.5. Group-6: Specimens Subjected to Outdoor Exposure*

***CFRP-Confined Specimens***

Four CFRP-confined specimens were placed at the outside of the laboratory and subjected to outdoor exposure for 530 days and then they were tested under uniaxial compression to determine the mechanical properties. When the failure types were investigated it can be clearly seen that all specimens failed due to the CFRP rupture close to the corner as seen in Figure 4.49.

The axial stress-strain diagrams were presented in Figure 4.50. All specimens except C10-S300-25-602 behaved identical. In C10-S300-25-602, CFRP seem to be active in earlier phase. This may be due to the problem in the unconfined concrete strength, which was assumed to be low as compared to the others. However, this problem did not affect the CFRP-confined concrete strength and strain capacity. From the tabulated mechanical properties given in Table 4.25, it can be seen that the average strength was 32.1 MPa and the corresponding strain was 0.032.

**(a) C10-S300-25-601** **(b) C10-S300-25-602** **(c) C10-S300-25-603** **(d) C10-S300-25-604**

**Figure 4.49. Failure types of CFRP-confined prismatic specimens in Group-6 (SET 3 - $f_{co}$=10 MPa, r=25mm)**

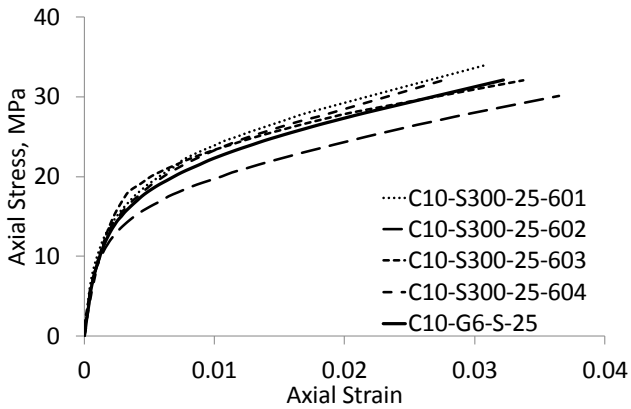


**Figure 4.50. Axial stress-strain diagrams of CFRP-confined prismatic specimens in Group-6 (SET 3 - $f_{co}$=10 MPa, r=25mm)**

Figure 4.51 illustrates the schematic view of the gages used in C10-S300-25-601, which was tested with additional gages. For this specimen, rosette strain gages at three faces of the specimen were used. In addition to these, two dial gages were placed at opposite faces as shown in the figure. No gages were provided at the corners.

**Table 4.25. Mechanical properties of CFRP-confined prismatic specimens in Group-6 (SET 3 - $f_{co}$=10 MPa, r=25 mm)**

| Specimen | $f_{cc}$ , MPa | $\varepsilon_{cc}$ | $E_1$ , GPa | $E_2$ , GPa | $E_1/E_2$ |
|---|---|---|---|---|---|
| C10-S300-25-601 | 34.1 | 0.031 | 13.57 | 0.56 | 24.4 |
| C10-S300-25-602 | 30.1 | 0.037 | 10.72 | 0.37 | 29.4 |
| C10-S300-25-603 | 32.1 | 0.034 | 13.10 | 0.42 | 31.5 |
| C10-S300-25-604 | 32.2 | 0.028 | 9.56 | 0.48 | 20.1 |
| **C10-G6-S-25** | **32.1** | **0.032** | **11.74** | **0.45** | **25.9** |
| COV, % | 5.0 | 11.8 | | | |

Stress-strain diagrams in axial and lateral directions can be seen in Figure 4.53. Axial strain recorded from the strain gage at face C was expected to be the close to the one recorded by dial gage E1. However, they were differed too much. Other than this gage, no strain data could be recorded in axial direction. This problem did not affect the lateral direction. In lateral direction, two strain readings were meaningful and they were provided in the figure. The ultimate strains were summarized in Figure 4.52 to understand the strain distribution. As it can be seen, at the failure zone the lateral strain was 0.011which was 76% of the ultimate strain of CFRP provided by the manufacturer.

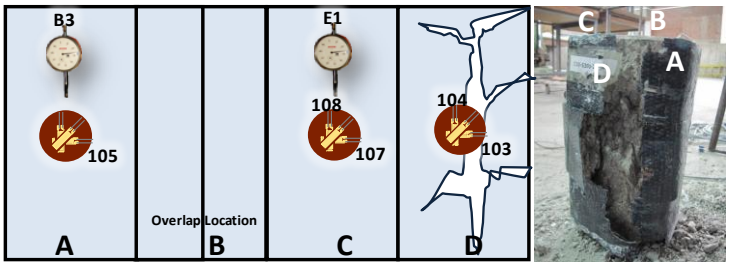


**Figure 4.51 Schematic view of the gages used in C10-S300-25-601**

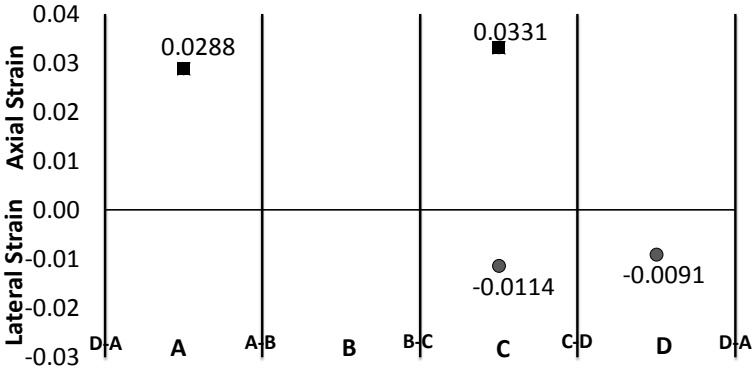


**Figure 4.52 Axial and lateral strain distributions in C10-S300-25-601**

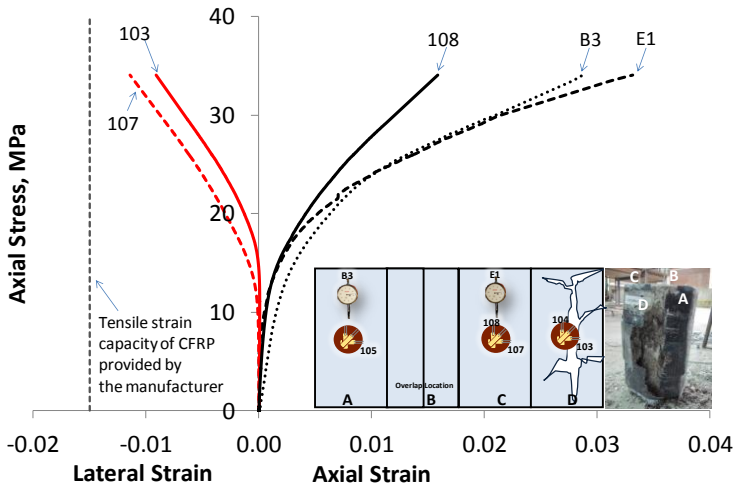


**Figure 4.53 Axial stress-axial strain and axial stress-lateral strain behavior of C10-S300-25-601**

#### *4.3.2.2. SET 4: Prismatic Specimens with r = 37.5 mm*

Besides the specimens in previous section having 25 mm corner radius, specimens in this set were prepared with 37.5 mm corner radius, i.e., 1/4$^{th}$ of the width, to correlate the CFRP effectiveness with different corner radii. Nineteen specimens in which only three of them were unconfined were prepared and tested. Unconfined specimens were only used in Group 1 as control specimens. Although the target strength was 10 MPa, the average cylinder strength was calculated to be 14.7 MPa.

##### *4.3.2.2.1. Group-1: Reference Specimens*

***Unconfined Specimens***

Three unconfined control specimens were kept outside the environmental chamber until the end of exposure test and tested under uniaxial compression. The axial stress-strain diagrams were presented in Figure 4.54 and the mechanical properties taken from these curves were tabulated in Table 4.26. The average strength was evaluated to be 12.5 MPa, which was the 85% of the cylinder strength. The average strain corresponding to the strength was 0.002 and the secant modulus of elasticity was about 17.6 GPa.

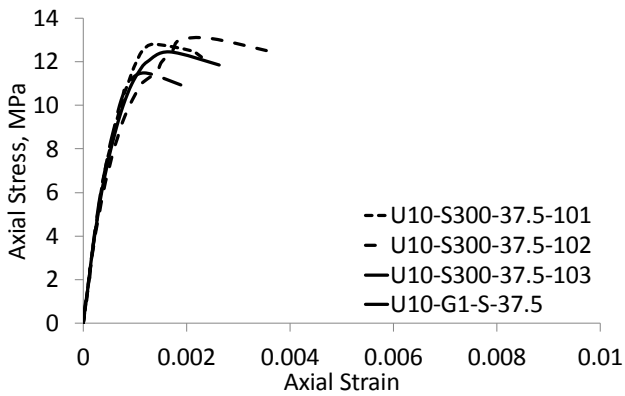


**Figure 4.54. Axial stress-strain diagrams of unconfined prismatic specimens in Group-1 (SET 4 - $f_{co}$=10 MPa and r=37.5mm)**

**Table 4.26. Mechanical properties of unconfined prismatic specimens in Group-1 (SET 4 - $f_{co}$=10 MPa and r=37.5 mm)**

| Specimen | $f_{cop}$ , MPa | $\varepsilon_{co}$ | $E_1$ , GPa |
|---|---|---|---|
| U10-S300-37.5-101 | 12.8 | 0.001 | 18.05 |
| U10-S300-37.5-102 | 13.1 | 0.003 | 16.25 |
| U10-S300-37.5-103 | 11.5 | 0.001 | 18.38 |
| **U10-G1-S-37.5** | **12.5** | **0.002** | **17.56** |
| COV, % | 6.8 | 41.2 | |

***CFRP-Confined Specimens***

Two CFRP-confined specimens were utilized as control specimens. Their failure types were illustrated in Figure 4.55. As it is seen from the figure, specimens failed due to the CFRP rupture close to the end of the radius at the corner. The rupture extended throughout the height of the specimen, which was similar to the failure of cylindrical specimens. The increase in the corner radius seems to affect the failure type.

As the axial stress-strain diagrams in Figure 4.56 are investigated, it can be seen that two curves are almost matched. No apparent difference can be observed. From the summarized mechanical properties presented in Table 4.27, it was clear that two specimens behaved identically. The average strength was evaluated as 37.4 MPa and the average strain was 0.024. The secant modulus of elasticity was less than the one for unconfined specimen but the difference was not so significant. Comparing the moduli of elasticity calculated in the first and second part of the diagram, it was observed that first part was 17.1 times greater than the second part.

**(a) C10-S300-37.5-101**

**(b) C10-S300-37.5-102**

**Figure 4.55. Failure types of CFRP-confined prismatic specimens in Group-1 (SET 4 - $f_{co}$=10 MPa and r=37.5mm)**

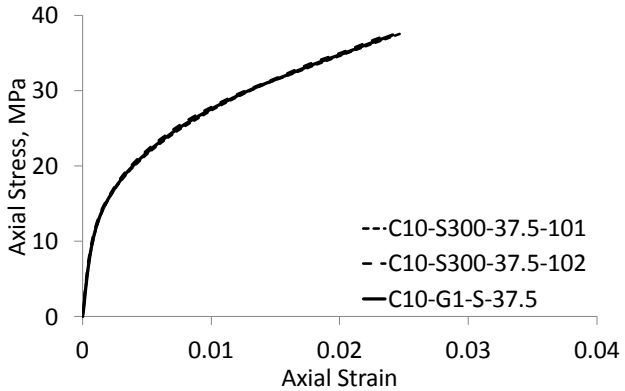


**Figure 4.56. Axial stress-strain diagrams of CFRP-confined prismatic specimens in Group-1 (SET 4 - $f_{co}$=10 MPa and r=37.5mm)**

**Table 4.27. Mechanical properties of CFRP-confined prismatic specimens in Group-1 (SET 4 - $f_{co}$=10 MPa and r=37.5 mm)**

| Specimen | $f_{cc}$, MPa | $\varepsilon_{cc}$ | $E_1$ , GPa | $E_2$ , GPa | $E_1/E_2$ |
|---|---|---|---|---|---|
| C10-S300-37.5-101 | 37.5 | 0.025 | 14.60 | 0.92 | 15.8 |
| C10-S300-37.5-102 | 37.3 | 0.024 | 16.82 | 0.91 | 18.5 |
| **C10-G1-S-37.5** | **37.4** | **0.024** | **15.71** | **0.92** | **17.1** |

#### *4.3.2.2.2. Group-2: Specimens Exposed to H-C Cycles*

***CFRP-Confined Specimens***

Only one specimen could be tested in this group and its axial stress-strain diagram was presented in Figure 4.57. Specimen failed due to CFRP at the lower midheight as shown in the figure. Strength of this specimen was 28.5 MPa and its strain was 0.016 (Table 4.28).

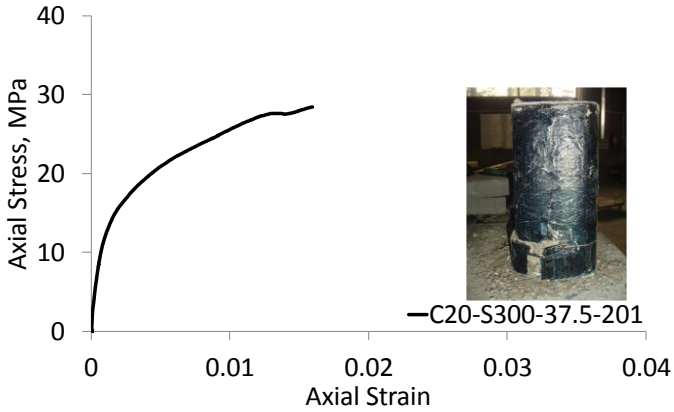


**Figure 4.57. Axial stress-strain diagram of CFRP-confined prismatic specimen in Group-2 (SET 4 - $f_{co}$=10 MPa and r=37.5mm)**

**Table 4.28. Mechanical properties of CFRP-confined prismatic specimen in Group-2 (SET 4 - $f_{co}$=10 MPa, r=37.5 mm and SL=0.5$f_{cc}$)**

| Specimen | H-C Cycles | $f_{cc}$ , MPa | $\varepsilon_{cc}$ | $E_1$ , GPa | $E_2$ , GPa | $E_1/E_2$ |
|---|---|---|---|---|---|---|
| C10-S300-37.5-201 | 200 | 28.5 | 0.016 | 21.48 | 0.78 | 27.5 |

#### *4.3.2.2.3. Group-3: Specimens Exposed to H-C Cycles and SL*

***CFRP-Confined Specimens***

Four specimens were utilized in this group. They were divided into two, in which two of them were loaded to $0.4f_{cc}$ (C10-S300-37.5-303 and C10-S300-37.5-304) and the remaining were loaded to $0.5f_{cc}$ (C10-S300-37.5-301 and C10-S300-37.5-302). The change in the behavior under different sustained loading levels was investigated via axial stress-strain diagrams.

All specimens failed due to the CFRP rupture close to the end of the corner radius (Figure 4.58). The rupture extended throughout the specimen height. This failure type was studied in detail for a specimen as shown in Figure 4.59. CFRP was detached from the specimen to understand the deformations in CFRP and concrete. As seen from the figure, CFRP was not delaminated after the failure. While pealing CFRP from the specimen, concrete layer at the surface was also detached. This could be the indication of perfect bond between CFRP and concrete. As from the same figure, concrete experienced too much deformation at corners. Deformations were not uniform throughout the height. They were small at the end but large at the midheight.

Axial stress-strain diagrams were presented in Figure 4.60. As previously stated, two specimens were loaded to a sustained load level of $0.4f_{cc}$ and the other two were loaded to $0.5f_{cc}$ while being subjected to heating-cooling cycles. From the figure it can be seen that, the difference in sustained loading seem to affect the behavior. The higher the sustained load level, the higher the strength was. However, increase in the sustained loading level seems to decrease the strain capacity.

From the summarized mechanical properties presented in Table 4.29 the average strength for specimens loaded to $0.5f_{cc}$ was found to be 32.8 MPa with a strain capacity of 0.011. As for the specimens loaded to $0.4f_{cc}$, it can be seen from Table 4.30, the average strength was 29.9 MPa and average strain at ultimate

strength was calculated as 0.015. The secant modulus of elasticity in the first part seems to be influenced by the sustained load level, too. Although a slight increase in the modulus of elasticity was anticipated, reduction was observed with the increase in sustained load. This was not the case in the second part of the diagram. From the table, it is seen that slopes of the second part are almost the same. The ratio of $E_1$ to $E_2$ is 17 and 21 for specimens loaded to $0.5f_{cc}$ and $0.4f_{cc}$, respectively.

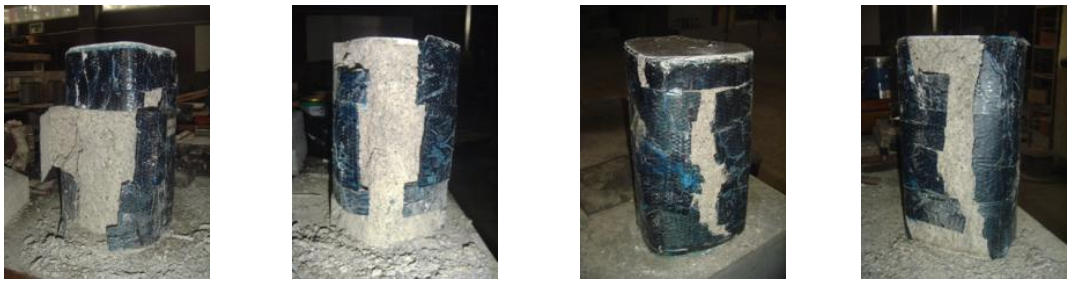

**(a) C10-S300-37.5-301** **(b) C10-S300-37.5-302** **(c) C10-S300-37.5-303** **(d) C10-S300-37.5-304**

**Figure 4.58. Failure types of CFRP-confined prismatic specimens in Group-3 (SET 4 - $f_{co}$=10 MPa and r=37.5mm)**

**(a) Failure of the specimen** **(b) Failure of CFRP** **(c) Failure of concrete**

**Figure 4.59. Failure of C10-S300-37.5-302**

**Table 4.29. Mechanical properties of CFRP-confined prismatic specimens in Group-3 (SET 4 - $f_{co}$=10 MPa, r=37.5 mm and SL=0.5$f_{cc}$)**

| Specimen | H-C Cycles | SL, % | $f_{cc}$, MPa | $\varepsilon_{cc}$ | $E_1$, GPa | $E_2$, GPa | $E_1/E_2$ |
|---|---|---|---|---|---|---|---|
| C10-S300-37.5-301 | 200 | 50 | 30.6 | 0.008 | 11.81 | 0.76 | 15.5 |
| C10-S300-37.5-302 | 200 | 50 | 35.0 | 0.013 | 15.24 | 0.83 | 18.3 |
| **C10-G3-S-37.5_%50** | | | **32.8** | **0.011** | **13.52** | **0.80** | **16.9** |

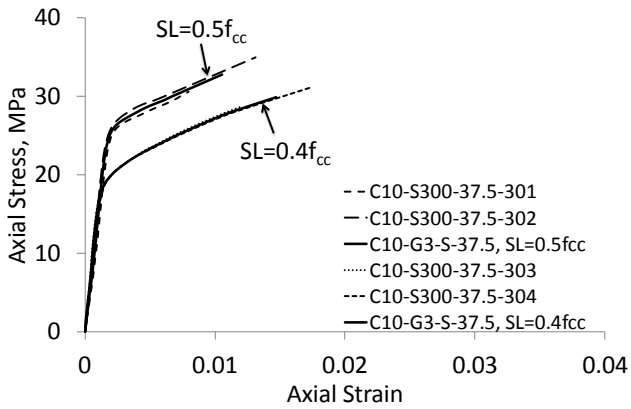


**Figure 4.60. Axial stress-strain diagrams of CFRP-confined prismatic specimens in Group-3 (SET 4 - $f_{co}$=10 MPa and r=37.5mm)**

**Table 4.30. Mechanical properties of CFRP-confined prismatic specimens in Group-3 (SET 4 - $f_{co}$=10 MPa, r=37.5 mm and SL=0.4$f_{cc}$)**

| Specimen | H-C Cycles | SL, % | $f_{cc}$, MPa | $\varepsilon_{cc}$ | $E_1$, GPa | $E_2$, GPa | $E_1/E_2$ |
|---|---|---|---|---|---|---|---|
| C10-S300-37.5-303 | 200 | 40 | 28.8 | 0.012 | 20.79 | 0.85 | 24.4 |
| C10-S300-37.5-304 | 200 | 40 | 31.1 | 0.017 | 13.83 | 0.79 | 17.6 |
| **C10-G3-S-37.5_%40** | | | **29.9** | **0.015** | **17.31** | **0.82** | **21.0** |

Specimen C10-S300-37.5-303 was tested with additional gages. As seen from Figure 4.61, four triaxial rosette strain gages at each face and a uniaxial strain gage at a corner were utilized to study the axial and lateral strain distribution along the circumference. From the strain and dial gages strain were recorded and then used to draw the stress-strain diagrams as shown in Figure 4.63. From the figure, ultimate strains were collected and summarized in Figure 4.62. In this figure, one can see that lateral strain was low at the failure zone. The failure strain was 36% of the ultimate tensile strain capacity of CFRP. The reason may be due to the non-uniform settlement of concrete, non-uniform stress distribution.

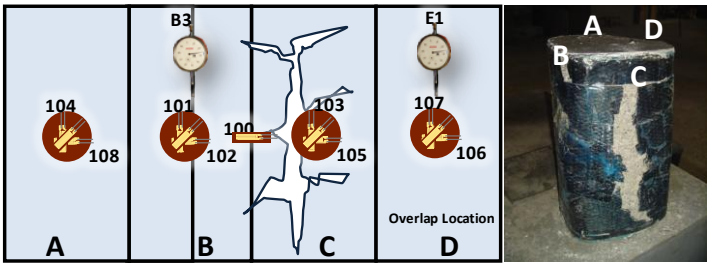


**Figure 4.61 Schematic view of the gages used in C10-S300-37.5-303**

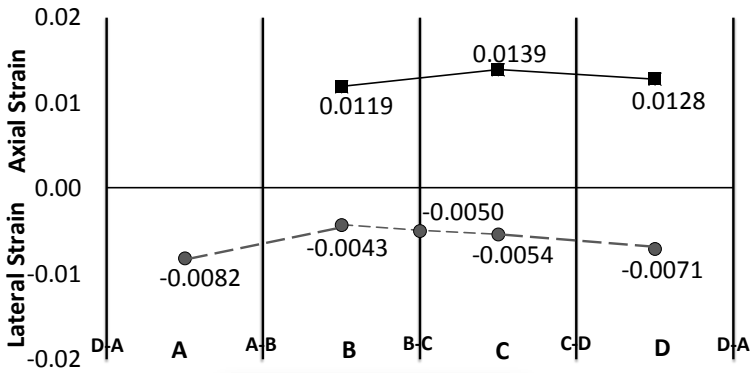


**Figure 4.62 Axial and lateral strain distributions in C10-S300-37.5-303**

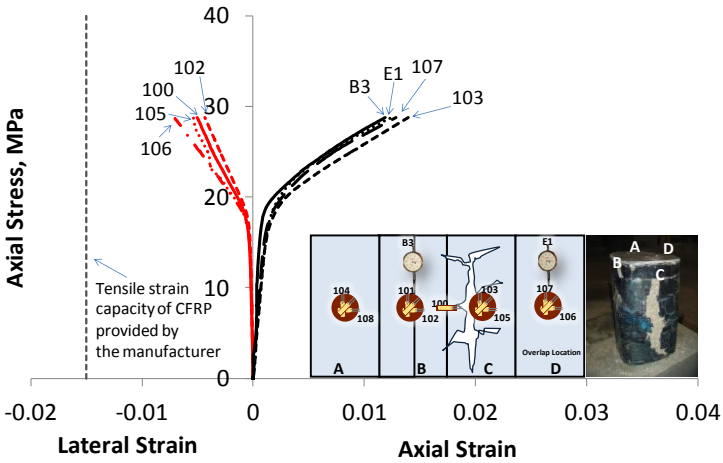


**Figure 4.63 Stress-strain behavior of C10-S300-37.5-303**

### *4.3.2.2.4. Group-4: Specimens Subjected to SL*

#### *CFRP-Confined Specimens*

Three specimens were loaded to 40% of their axial load capacity and kept under sustained load for 530 days. After that, they were tested under uniaxial compression to failure and their axial stress- strain diagrams were plotted as shown in Figure 4.65.

All three specimens failed because of the CFRP rupture near the corner where the radius ends (Figure 4.64). The rupture extended to full height. As it can be seen from Figure 4.65, all specimens experienced different strains. The average strain was calculated as 0.016 with a COV of 29% (Table 4.31). Difference in strains was the result of the second slope of the curves ($E_2$). Although strains differed too much, it was not the case in strength. Strengths of all specimens were close to each other and the average strength was found to be 32.8 MPa with a COV of 1.3%.

**(a) C10-S300-37.5-401** **(b) C10-S300-37.5-402** **(c) C10-S300-37.5-403**

**Figure 4.64. Failure types of CFRP-confined prismatic specimens in Group-4 (SET 4 - $f_{co}$ =10 MPa and r=37.5mm)**

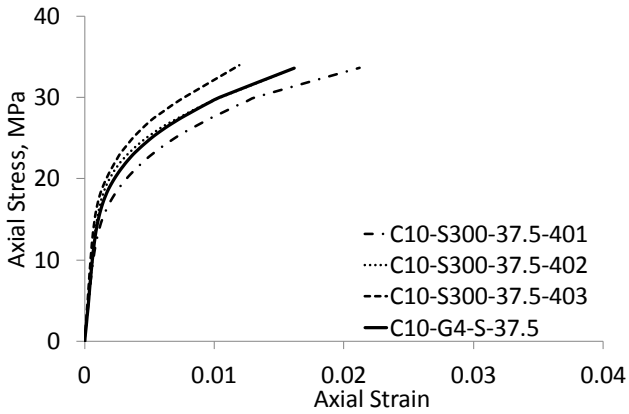


**Figure 4.65. Axial stress-strain diagrams of CFRP-confined prismatic specimens in Group-4 (SET 4 - $f_{co}$=10 MPa and r=37.5mm)**

**Table 4.31. Mechanical properties of CFRP-confined prismatic specimens in Group-4 (SET 4 - $f_{co}$=10 MPa, r=37.5 mm and SL=0.5$f_{cc}$)**

| Specimen | SL, % | $f_{cc}$, MPa | $\varepsilon_{cc}$ | $E_1$ , GPa | $E_2$ , GPa | $E_1/E_2$ |
|---|---|---|---|---|---|---|
| C10-S300-37.5-401 | 40 | 33.7 | 0.021 | 16.04 | 0.81 | 19.9 |
| C10-S300-37.5-402 | 40 | 33.1 | 0.015 | 15.32 | 0.88 | 17.4 |
| C10-S300-37.5-403 | 40 | 34.0 | 0.012 | 20.32 | 1.27 | 16.1 |
| **C10-G4-S-37.5** | | **32.8** | **0.016** | **17.22** | **0.98** | **17.5** |
| COV, % | | 1.3 | 29.1 | | | |

Third specimen in this group was tested with attached strain gages and two dial gages in order to record lateral and axial strains. Uniaxial strain gages were provided at each corner and two triaxial rosette strain gages were placed at two faces as shown in Figure 4.66. Strains were recorded and stress-strain diagrams for each strain gages were plotted in Figure 4.67. Using these diagrams, ultimate strain values were picked and presented in Figure 4.68 to study the strain distribution along the circumference. As it is seen from the figure, ultimate axial strain at face C is greater than the one at face A. Specimen bended about +x-axis that increased the lateral strains at face A relative due to the opposite face. This can be seen from the lateral strain distribution. Strain at face C is lower than the strain at face A. It is interesting to note that failure occurred at face C, which experienced lower strains. The reason for this failure at lower strains may be attributed to the internal failure of concrete, which may create out-of plane shear at the CFRP material.

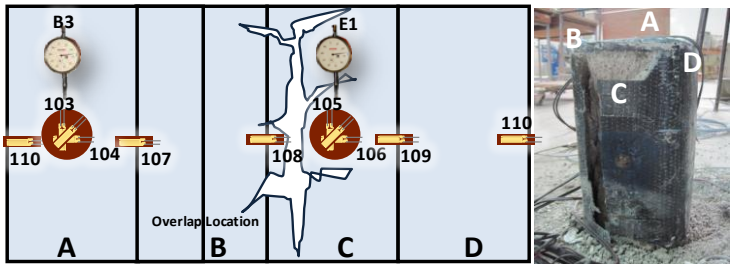


**Figure 4.66 Schematic view of the gages used in C10-S300-37.5-403**

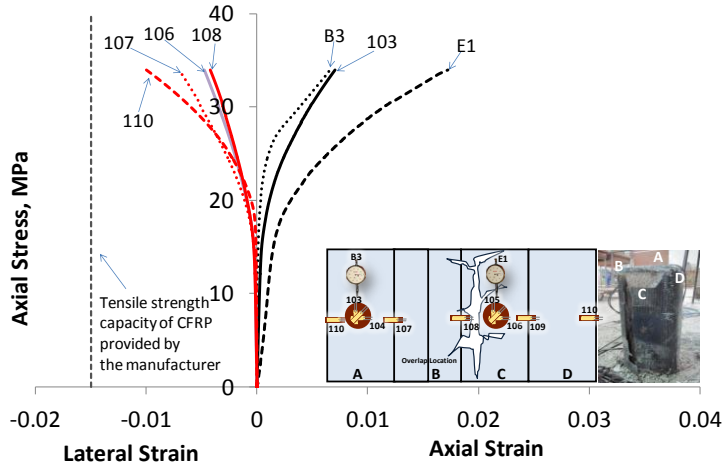


**Figure 4.67 Stress-strain behavior of C10-S300-37.5-403**

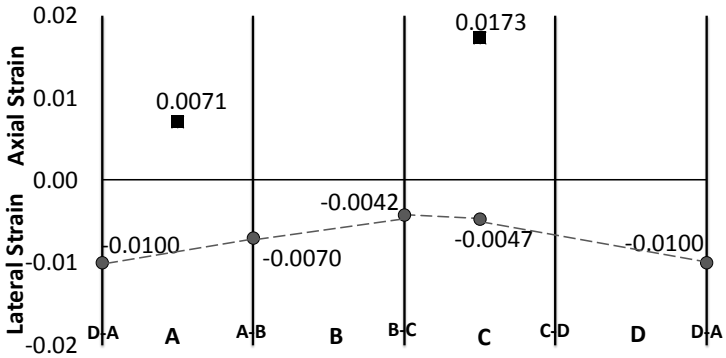


**Figure 4.68 Axial and lateral strain distributions in C10-S300-37.5-403**

#### *4.3.2.2.5. Group-5: Specimens kept in water and exposed to H-C Cycles*

***CFRP-Confined Specimens***

This group of specimens was tested under only heating-cooling cycles while being kept in water, i.e., they were exposed to wet heating-cooling cycles. Other than the wet environment, the procedure was identical to the one carried out in Group 2.

Three specimens were confined with a single layer of CFRP. They were capped, carried into the environmental test chamber (ETC) and placed in a basin full of water. Heating-cooling cycles were started. After applying 200 cycles, specimens were taken out of the basin and kept outside of the ETC for one week to make them dry before the uniaxial compression test.

The change in the behavior under wet heating-cooling exposure was investigated after the uniaxial compression test. As from the failure types shown in Figure 4.69, specimens in this group were also failed due to the CFRP rupture close to the end of the corner.

Axial stress-strain diagrams were illustrated in Figure 4.70 and mechanical properties derived from these diagrams were summarized in Table 4.32. The average strength was found as 28 MPa with a COV of 7.7% and the strain corresponding to this strength was evaluated as 0.021. The ratio of the modulus of elasticity calculated in the first part of the diagram to the second part ($E_1/E_2$) was found to be 26.5.

**(a) C10-S300-37.5-501** **(b) C10-S300-37.5-502** **(c) C10-S300-37.5-503**

**Figure 4.69. Failure types of CFRP-confined prismatic specimens in Group-5 (SET 4 - $f_{co}$=10 MPa and r=37.5mm)**

**Table 4.32. Mechanical properties of CFRP-confined prismatic specimens in Group-5 (SET 4 - $f_{co}$=10 MPa and r=37.5 mm)**

| Specimen | H-C Cycles | $f_{cc}$, MPa | $\varepsilon_{cc}$ | $E_1$ , GPa | $E_2$ , GPa | $E_1/E_2$ |
|---|---|---|---|---|---|---|
| C10-S300-37.5-501 | 200 | 27.2 | 0.019 | 17.94 | 0.63 | 28.3 |
| C10-S300-37.5-502 | 200 | 26.5 | 0.019 | 16.63 | 0.54 | 30.7 |
| C10-S300-37.5-503 | 200 | 30.5 | 0.024 | 12.15 | 0.59 | 20.7 |
| **C10-G5-S-37.5** | | **28.0** | **0.021** | **15.57** | **0.59** | **26.5** |
| COV, % | | 7.7 | 13.2 | | | |

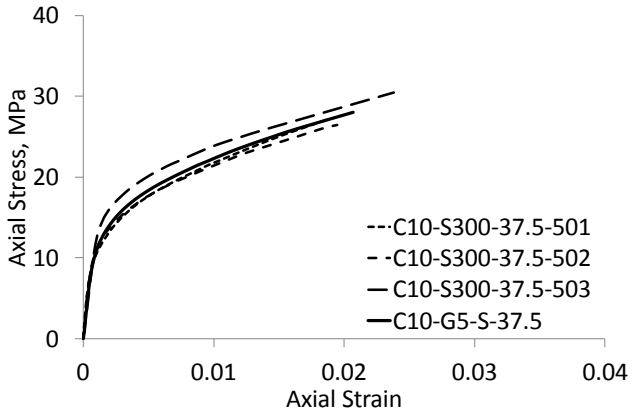


**Figure 4.70. Axial stress-strain diagrams of CFRP-confined prismatic specimens in Group-5 (SET 4 - $f_{co}$=10 MPa and r=37.5mm)**

#### *4.3.2.2.6. Group-6: Specimens Subjected to Outdoor Exposure*

***CFRP-Confined Specimens***

Specimens in this group were kept outside of the laboratory to make them expose to outdoor environmental conditions. They were kept under outdoor exposure for 530 days and after that, they were carried to the laboratory, kept for one week and then tested under uniaxial compression to determine the mechanical properties.

All specimens failed because of the CFRP rupture at the corner close to the end of the radius at this location (Figure 4.71). Failures were clear rupture, which extended to full height of the specimens. While being under uniaxial compression test, their axial stress-strain diagrams were recorded and plotted as shown in Figure 4.72. From the figure, it can be said that although there exists slight difference, all specimens behaved identically. The COVs provided in Table 4.33 were below 10% for strength and strain. The main differences were observed to be at the first slope of the curves, i.e., secant modulus of elasticity.

**(a) C10-S300-37.5-601** **(b) C10-S300-37.5-602** **(c) C10-S300-37.5-603**

**Figure 4.71. Failure types of CFRP-confined prismatic specimens in Group-6 (SET 4 - $f_{co}$=10 MPa and r=37.5mm)**

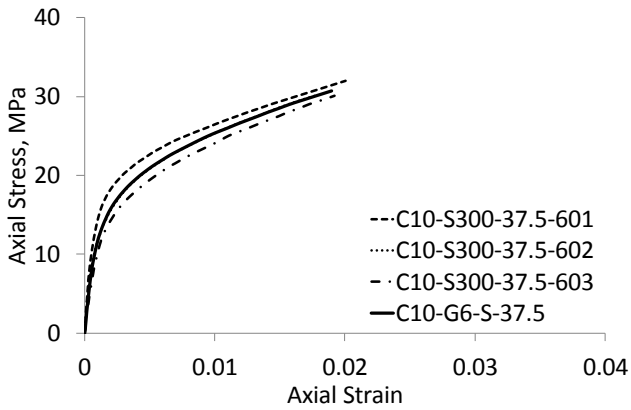


**Figure 4.72. Axial stress-strain diagrams of CFRP-confined prismatic specimens in Group-6 (SET 4 - $f_{co}$=10 MPa and r=37.5mm)**

**Table 4.33. Mechanical properties of CFRP-confined prismatic specimens in Group-6 (SET 4 - $f_{co}$=10 MPa, r=37.5 mm and SL=0.5$f_{cc}$)**

| Specimen | $f_{cc}$, MPa | $\varepsilon_{cc}$ | $E_1$ , GPa | $E_2$ , GPa | $E_1/E_2$ |
|---|---|---|---|---|---|
| C10-S300-37.5-601 | 32.0 | 0.020 | 20.91 | 0.60 | 34.8 |
| C10-S300-37.5-602 | 30.1 | 0.018 | 19.68 | 0.65 | 30.5 |
| C10-S300-37.5-603 | 30.1 | 0.019 | 12.05 | 0.63 | 19.1 |
| **C10-G6-S-37.5** | **30.7** | **0.019** | **17.55** | **0.63** | **28.0** |
| COV, % | 3.5 | 6.4 | | | |

## 4.4 CONCRETE SPECIMENS HAVING 15 MPa STRENGTH

This part was aimed to fill the gap between low (10 MPa) and medium strength (20 MPa) concrete. Eighteen prismatic concrete specimens with square in cross-section were prepared. Dimensions were the same as the other prismatic specimens, such that they were 150x150 mm in cross-section and 300 mm in height. Since specimens were in prismatic form, in order to ensure proper confinement, corners were rounded. The corner radius of 37.5 mm, which corresponded to an MCR factor of 0.25, was decided to be applied.

Specimens were tested in six groups as shown in Table 4.34. In the following sections, results of each group were presented separately. Cylindrical strength of unconfined concrete was calculated as 16.3 MPa.

**Table 4.34 Summary of the 15 MPa prismatic specimens**

| Specimen Code | Confinement | $f_{co}$ (MPa) | Type | Overlap % | r, mm | Group No | # of H-C cycles | SL, % | Outdoor Exposure |
|---|---|---|---|---|---|---|---|---|---|
| U15-S300-37.5-101 | Unconfined | 15 | Prism | 11 | 37.5 | 1 | | | |
| U15-S300-37.5-102 | Unconfined | 15 | Prism | 11 | 37.5 | 1 | | | |
| U15-S300-37.5-103 | Unconfined | 15 | Prism | 11 | 37.5 | 1 | | | |
| C15-S300-37.5-101 | CFRP-Confined | 15 | Prism | 11 | 37.5 | 1 | | | |
| C15-S300-37.5-102 | CFRP-Confined | 15 | Prism | 11 | 37.5 | 1 | | | |
| C15-S300-37.5-103 | CFRP-Confined | 15 | Prism | 11 | 37.5 | 1 | | | |
| U15-S300-37.5-201 | Unconfined | 15 | Prism | 11 | 37.5 | 2 | 200 | | |
| U15-S300-37.5-202 | Unconfined | 15 | Prism | 11 | 37.5 | 2 | 200 | | |
| C15-S300-37.5-201 | CFRP-Confined | 15 | Prism | 11 | 37.5 | 2 | 200 | | |
| C15-S300-37.5-202 | CFRP-Confined | 15 | Prism | 11 | 37.5 | 2 | 200 | | |
| U15-S300-37.5-301 | Unconfined | 15 | Prism | 11 | 37.5 | 3 | 200 | 40 | |
| U15-S300-37.5-302 | Unconfined | 15 | Prism | 11 | 37.5 | 3 | 200 | 40 | |
| C15-S300-37.5-301 | CFRP-Confined | 15 | Prism | 11 | 37.5 | 3 | 200 | 40 | |
| C15-S300-37.5-302 | CFRP-Confined | 15 | Prism | 11 | 37.5 | 3 | 200 | 40 | |
| C15-S300-37.5-303 | CFRP-Confined | 15 | Prism | 11 | 37.5 | 3 | 200 | 40 | |
| C15-S300-37.5-401 | CFRP-Confined | 15 | Prism | 11 | 37.5 | 4 | | 40 | |
| C15-S300-37.5-402 | CFRP-Confined | 15 | Prism | 11 | 37.5 | 4 | | 40 | |
| C15-S300-37.5-501 | CFRP-Confined | 15 | Prism | 11 | 37.5 | 5 | 200 wet | | |
| C15-S300-37.5-502 | CFRP-Confined | 15 | Prism | 11 | 37.5 | 5 | 201 wet | | |
| C15-S300-37.5-503 | CFRP-Confined | 15 | Prism | 11 | 37.5 | 5 | 202 wet | | |
| C15-S300-37.5-601 | CFRP-Confined | 15 | Prism | 11 | 37.5 | 6 | | | Yes |
| C15-S300-37.5-602 | CFRP-Confined | 15 | Prism | 11 | 37.5 | 6 | | | Yes |

### 4.4.1. Group-1: Reference Specimens

***Unconfined Specimens***

Control specimens in this group were failed in columnar type (Figure 4.73). Although failure types were the same, their axial stress-strain behaviors were different from each other (Figure 4.74). The difference was mainly on the strength values. The dispersion in the strength values was found to be 17.2% as presented in Table 4.35. As compared to the cylindrical strength, from the average strength point

of view, it can be said that strength of prismatic specimens in this group was almost 85% of the cylindrical strength.

**(a) U15-S300-37.5-101** **(b) U15-S300-37.5-102** **(c) U15-S300-37.5-103**

**Figure 4.73. Failure types of unconfined prismatic specimens in Group-1 ($f_{co}$=15 MPa and r=37.5mm)**

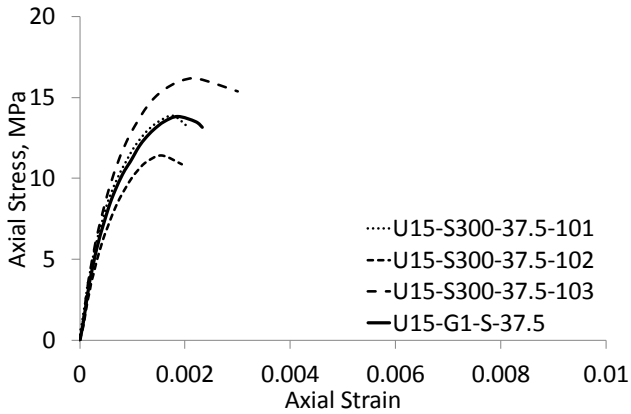


**Figure 4.74. Axial stress-strain diagrams of unconfined prismatic specimens in Group-1 ($f_{co}$=15 MPa and r=37.5mm)**

**Table 4.35. Mechanical properties of unconfined prismatic specimens in Group-1 ($f_{co}$=15 MPa and r=37.5 mm)**

| Specimen | $f_{cop}$, MPa | $\varepsilon_{co}$ | $E_1$ , GPa |
|---|---|---|---|
| U15-S300-37.5-101 | 13.9 | 0.002 | 20.03 |
| U15-S300-37.5-102 | 11.4 | 0.002 | 15.40 |
| U15-S300-37.5-103 | 16.2 | 0.002 | 19.58 |
| **U15-G1-S-37.5** | **13.8** | **0.002** | **18.34** |
| COV, % | 17.2 | 11.9 | |

***CFRP-Confined Specimens***

Three CFRP-confined specimens were used as control specimens. Their failure types were illustrated in Figure 4.75. Failures were due to the CFRP rupture close to the end of the corner radius, which was the case in 10 MPa prismatic specimens with a corner radius of 37.5 mm also. Furthermore, CFRP-ruptures were observed to extend throughout the height of the specimen.

Axial stress-strain diagrams were plotted in Figure 4.76. All specimens showed almost the same behavior up to 22 MPa; however, after that point they diverged with a different slope. Unlike that, the difference in strength and strain capacity was not so significant. This can be seen in Table 4.36 more clearly. The COV for strength was about 6% and for strain about 10%. The main difference was at the second slope where modulus of elasticity in second part was calculated.

**(a) C15-S300-37.5-101** **(b) C15-S300-37.5-102** **(c) C15-S300-37.5-103**

**Figure 4.75. Failure types of CFRP-confined prismatic specimens in Group-1 ($f_{co}$=15 MPa and r=37.5mm)**

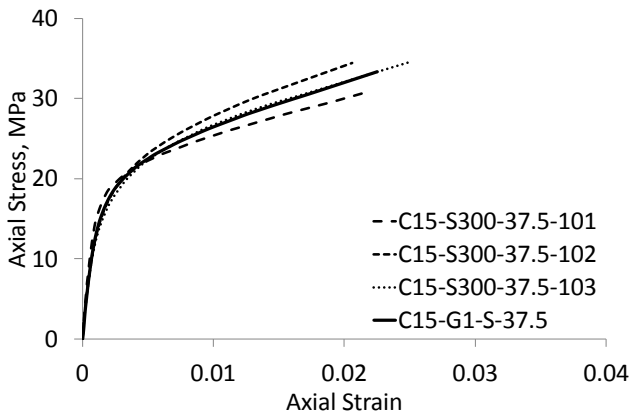


**Figure 4.76. Axial stress-strain diagrams of CFRP-confined prismatic specimens in Group-1 ($f_{co}$=15 MPa and r=37.5mm)**

**Table 4.36. Mechanical properties of CFRP-confined prismatic specimens in Group-1 ($f_{co}$=15 MPa and r=37.5 mm)**

| Specimen | $f_{cc}$, MPa | $\varepsilon_{cc}$ | $E_1$ , GPa | $E_2$ , GPa | $E_1/E_2$ |
|---|---|---|---|---|---|
| C15-S300-37.5-101 | 30.9 | 0.022 | 19.52 | 0.47 | 41.5 |
| C15-S300-37.5-102 | 34.5 | 0.021 | 15.95 | 0.79 | 20.2 |
| C15-S300-37.5-103 | 34.6 | 0.025 | 15.41 | 0.63 | 24.5 |
| **C15-G1-S-37.5** | **33.3** | **0.023** | **16.96** | **0.63** | **26.9** |
| COV, % | 6.2 | 9.8 | | | |

### 4.4.2. Group-2: Specimens exposed to H-C Cycles

***Unconfined Specimens***

Two specimens were exposed to 200 heating-cooling cycles. After exposure tests, they were tested under uniaxial compression to determine the change in mechanical properties. Both specimens showed almost the same behavior as seen from Figure 4.78. The average strength was calculated as 11.6 MPa (Table 4.37), which was lower than the one in control specimens.

**(a) U15-S300-37.5-201**

**(b) U15-S300-37.5-202**

**Figure 4.77. Failure types of unconfined prismatic specimens in Group-2 ($f_{co}$=15 MPa and r=37.5mm)**

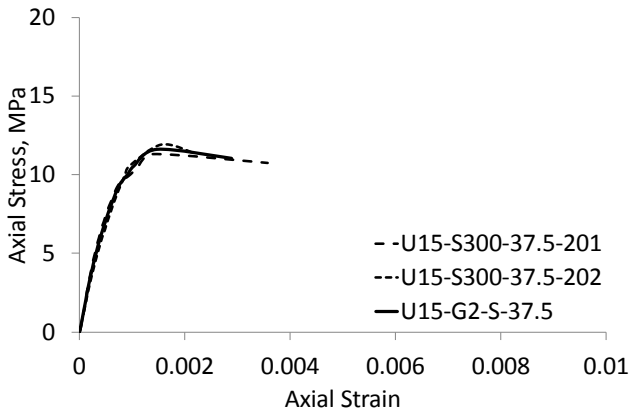


**Figure 4.78. Axial stress-strain diagrams of unconfined prismatic specimens in Group-2 ($f_{co}$=15 MPa and r=37.5mm)**

**Table 4.37. Mechanical properties of unconfined prismatic specimens in Group-2 ($f_{co}$=15 MPa and r=37.5 mm)**

| Specimen | H-C Cycles | $f_{cop}$ , MPa | $\varepsilon_{co}$ | $E_1$ , GPa |
|---|---|---|---|---|
| U15-S300-37.5-201 | 200 | 11.3 | 0.002 | 17.84 |
| U15-S300-37.5-202 | 200 | 11.9 | 0.002 | 14.96 |
| **U15-G2-S-37.5** | | **11.6** | **0.002** | **16.40** |

***CFRP-Confined Specimens***

The effect of heating-cooling cycles on mechanical properties of CFRP-confined concrete specimens was studied in this group. As it is seen from the failure types given in Figure 4.79, specimens failed due to the CFRP-rupture close to the end of the corner radius and rupture was extended to the full height of the specimen.

From the axial stress-strain diagrams shown in Figure 4.80, it is seen that both specimens behaved identical. This can be clearly seen from the collected mechanical properties presented in Table 4.38. The average strength was calculated as 27.8 MPa and strain corresponding to this strength value was found to be 0.019. In modulus of elasticity point of view, it can be seen that after reaching unconfined concrete strength, modulus of elasticity dropped to 0.57 GPa which was 34.6 times less than the one calculated in first part.

**(a) C15-S300-37.5-201** **(b) C15-S300-37.5-202**

**Figure 4.79. Failure types of CFRP-confined prismatic specimens in Group-2 ($f_{co}$=15 MPa and r=37.5mm)**

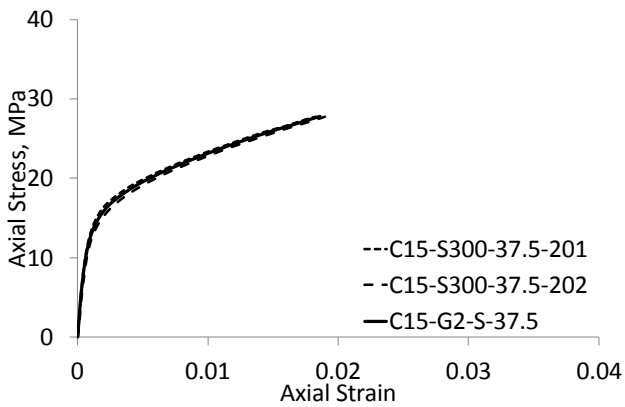


**Figure 4.80. Axial stress-strain diagrams of CFRP-confined prismatic specimens in Group-2 ($f_{co}$=15 MPa and r=37.5mm)**

**Table 4.38. Mechanical properties of CFRP-confined prismatic specimens in Group-2 ($f_{co}$=15 MPa and r=37.5 mm)**

| Specimen | H-C Cycles | $f_{cc}$, MPa | $\varepsilon_{cc}$ | $E_1$ , GPa | $E_2$ , GPa | $E_1/E_2$ |
|---|---|---|---|---|---|---|
| C15-S300-37.5-201 | 200 | 27.8 | 0.018 | 21.93 | 0.57 | 38.7 |
| C15-S300-37.5-202 | 200 | 27.8 | 0.019 | 17.33 | 0.57 | 30.7 |
| **C15-G2-S-37.5** | | **27.8** | **0.019** | **19.63** | **0.57** | **34.6** |

### 4.4.3. Group-3: Specimens Exposed to H-C Cycles and SL

***Unconfined Specimens***

Failure types of the specimens, which were exposed to simultaneous exposure of heating-cooling cycles and sustained loading were given in Figure 4.81 and their axial stress-strain behaviors were plotted in Figure 4.82. Both specimens showed similar behaviors. The average strength was evaluated as 13.2 MPa, which was almost equal to the strength of control specimens (Table 4.39). Simultaneous exposure seems to affect the strain capacity more, because strain capacity decreased from 0.002 to 0.001. Actually, sustained loading was the cause of that decrease because no apparent change was observed when specimens exposed to only heating-cooling cycles.

**Table 4.39. Mechanical properties of unconfined prismatic specimens in Group-3 ($f_{co}$=15 MPa and r=37.5 mm)**

| Specimen | H-C Cycles | SL, % | $f_{cop}$ , MPa | $\varepsilon_{co}$ | $E_1$ , GPa |
|---|---|---|---|---|---|
| U15-S300-37.5-301 | 200 | 40 | 13.1 | 0.001 | 21.0 |
| U15-S300-37.5-302 | 200 | 40 | 13.3 | 0.001 | 17.1 |
| **U15-G3-S-37.5** | | | **13.2** | **0.001** | **19.1** |

**(a) U15-S300-37.5-301** **(b) U15-S300-37.5-302**

**Figure 4.81. Failure types of unconfined prismatic specimens in Group-3 ($f_{co}$=15 MPa and r=37.5mm)**

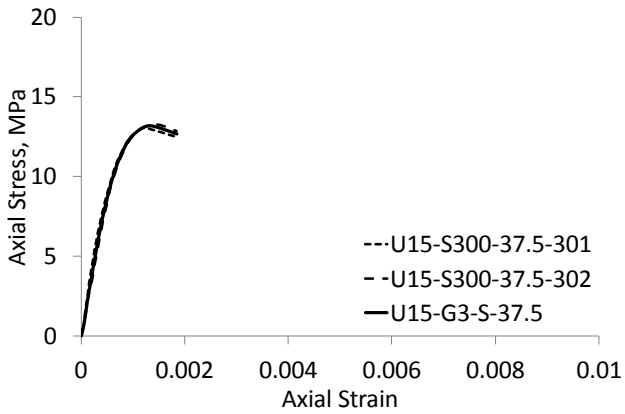


**Figure 4.82. Axial stress-strain diagrams of unconfined prismatic specimens in Group-3 ($f_{co}$=15 MPa and r=37.5mm)**

***CFRP-Confined Specimens***

Three CFRP-confined specimens were exposed to 200 heating-cooling cycles and sustained loading level of $0.4f_{cc}$. After exposure tests they were tested under uniaxial compression to determine the change in mechanical properties. Failure types were presented in Figure 4.83. Failures were similar to the control specimens; they were

due to the CFRP rupture close to the end of the corner radius. Axial stress-strain diagrams were illustrated in Figure 4.84 and mechanical properties were presented in Table 4.40. From the table, the average was seen to be 29.3 MPa and corresponding strain was found to be 0.009. In the table, slopes at the first and second part of the curves were also provided.

**(a) C15-S300-37.5-301** **(b) C15-S300-37.5-302** **(c) C15-S300-37.5-303**

**Figure 4.83. Failure types of CFRP-confined prismatic specimens in Group-3 ($f_{co}$=15 MPa and r=37.5mm)**

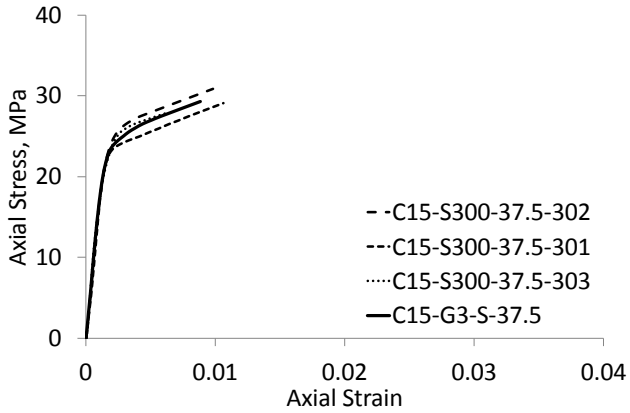


**Figure 4.84. Axial stress-strain diagrams of CFRP-confined prismatic specimens in Group-3 ($f_{co}$=15 MPa and r=37.5mm)**

**Table 4.40. Mechanical properties of CFRP-confined prismatic specimens in Group-3 ($f_{co}$=15 MPa and r=37.5 mm)**

| Specimen | H-C Cycles | SL, % | $f_{cc}$, MPa | $\varepsilon_{cc}$ | $E_1$, GPa | $E_2$, GPa | $E_1/E_2$ |
|---|---|---|---|---|---|---|---|
| C15-S300-37.5-301 | 200 | 40 | 29.1 | 0.011 | 14.22 | 0.65 | 21.9 |
| C15-S300-37.5-302 | 200 | 40 | 30.9 | 0.010 | 16.37 | 0.99 | 16.6 |
| C15-S300-37.5-303 | 200 | 40 | 27.8 | 0.006 | 17.63 | 0.63 | 27.9 |
| **C15-G3-S-37.5** | | | **29.3** | **0.009** | **16.07** | **0.76** | **21.2** |
| COV, % | | | 5.2 | 27.4 | | | |

### 4.4.4. Group-4: Specimens Subjected to SL

***CFRP-confined Specimens***

In this group, two CFRP-confined specimens were subjected to a sustained loading level of 40% of their axial load capacity. They were kept under ambient lab condition for 530 days and then tested under uniaxial compression to determine the mechanical behavior. After uniaxial compression test, it was observed that both specimens failed due to CFRP-rupture close to the corner and the rupture extended to full height as given in Figure 4.85.

Axial stress-strain behaviors of both specimens seem to be similar as illustrated in Figure 4.86. They followed the same trend until failure. This similarity can be clearly seen in Table 4.41. They almost had the same strength and experienced the same strain. The average strength was calculated as 32.8 MPa and the confined concrete strain was found as 0.019.

**(a) C15-S300-37.5-401** **(b) C15-S300-37.5-402**

**Figure 4.85. Failure types of CFRP-Confined prismatic specimens in Group-4 ($f_{co}$=15 MPa and r=37.5mm)**

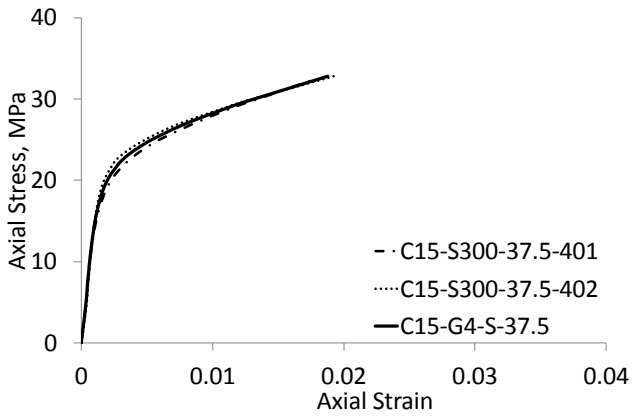


**Figure 4.86. Axial stress-strain diagrams of CFRP-Confined prismatic specimens in Group-4 ($f_{co}$=15 MPa and r=37.5mm)**

**Table 4.41. Mechanical properties of CFRP-confined prismatic specimens in Group-4 ($f_{co}$=15 MPa and r=37.5 mm)**

| Specimen | SL, % | $f_{cc}$ , MPa | $\varepsilon_{cc}$ | $E_1$ , GPa | $E_2$ , GPa | $E_1/E_2$ |
|---|---|---|---|---|---|---|
| C15-S300-37.5-401 | 40 | 32.7 | 0.018 | 15.02 | 0.67 | 22.5 |
| C15-S300-37.5-402 | 40 | 33.0 | 0.020 | 12.30 | 0.61 | 20.0 |
| **C15-G4-S-37.5** | | **32.8** | **0.019** | **13.66** | **0.64** | **21.3** |

C15-S300-37.5-401 was attached strain gages to determine the strain distribution along the circumference (Figure 4.87). Three uniaxial strain gages were used at the corners to record lateral strains and two triaxial rosette dial gages were placed at two opposite faces to record both axial and lateral strains. The recorded values were presented in Figure 4.88 as the stress-strain diagrams. As it can be observed from the figure, strains were almost uniform in this specimen. As for the ultimate strains presented in Figure 4.89, the rupture strain was 0.0084, which was the 56% of the ultimate tensile strength of CFRP.

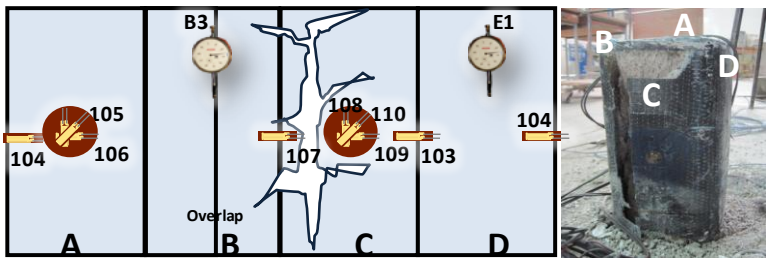


**Figure 4.87 Schematic view of the gages used in C15-S300-37.5-401**

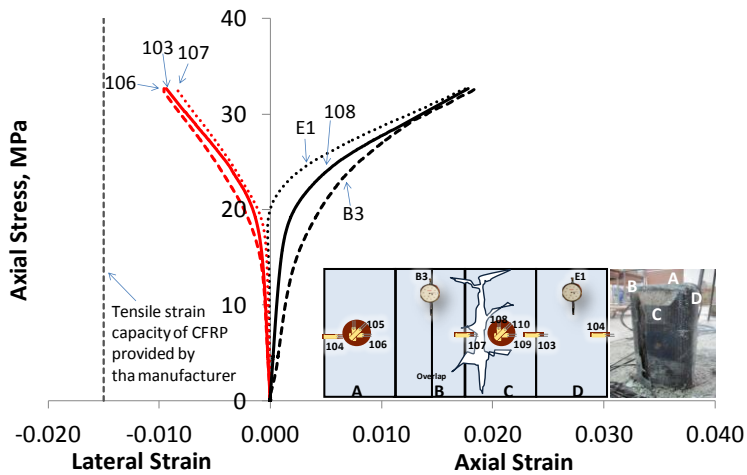


**Figure 4.88 Stress-strain behavior of C15-S300-37.5-401**

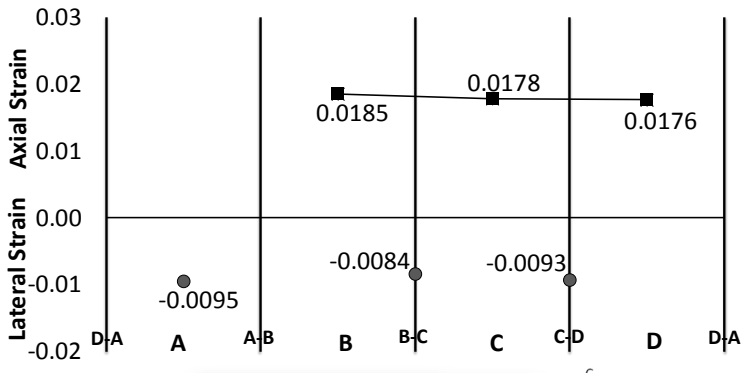


**Figure 4.89 Axial and lateral strain distributions in C15-S300-37.5-401**

### 4.4.5. Group-5: Specimens kept in water and exposed to H-C Cycles

***CFRP-confined Specimens***

Three specimens were kept in the water and exposed to 200 heating-cooling cycles in the environmental test chamber. After the exposure test, they were uniaxially loaded to failure to determine the mechanical properties.

Failure types were illustrated in Figure 4.90. All specimens failed due to the CFRP rupture close to the corner. The axial stress-strain behaviors were presented in Figure 4.91. As it is seen, specimens showed almost the same behavior. The difference in the mechanical properties can be seen in Table 4.42. From the table it is concluded that, the average strength was 26.1 MPa with a COV of 4.3%. Secant modulus of elasticity ($E_1$) values differed too much for all specimens. However, considering the average behavior it can be said that axial stress-strain behavior started with a slope of 15.8 GPa in the first part and ended with a slope of 0.62 in the second part.

**(a) C15-S300-37.5-501** **(b) C15-S300-37.5-502** **(c) C15-S300-37.5-503**

**Figure 4.90. Failure types of CFRP-Confined prismatic specimens in Group-5 ($f_{co}$=15 MPa and r=37.5mm)**

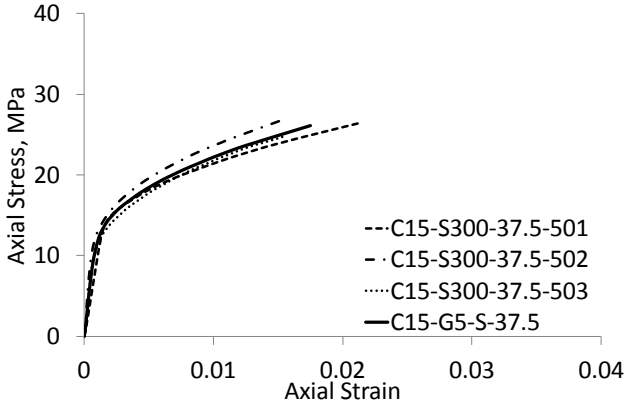


**Figure 4.91. Axial stress-strain diagrams of CFRP-Confined prismatic specimens in Group-5 ($f_{co}$=15 MPa and r=37.5mm)**

**Table 4.42. Mechanical properties of CFRP-confined prismatic specimens in Group-5 ($f_{co}$=15 MPa and r=37.5 mm)**

| Specimen | $f_{cc}$, MPa | $\varepsilon_{cc}$ | $E_1$ , GPa | $E_2$ , GPa | $E_1/E_2$ |
|---|---|---|---|---|---|
| C15-S300-37.5-501 | 26.4 | 0.021 | 9.64 | 0.51 | 19.1 |
| C15-S300-37.5-502 | 27.0 | 0.016 | 21.94 | 0.76 | 28.9 |
| C15-S300-37.5-503 | 24.9 | 0.016 | 15.81 | 0.61 | 26.0 |
| **C15-G5-S-37.5** | **26.1** | **0.018** | **15.80** | **0.62** | **25.3** |
| COV, % | 4.3 | 18.3 | | | |

### 4.4.6. Group-6: Specimens subjected to outdoor exposure

***CFRP-confined Specimens***

In order to understand the effect of outdoor exposure two specimens were placed at the outside of the laboratory and kept under environmental exposure for 530 days. After the exposure test, they were tested under uniaxial compression. The failure types shown in Figure 4.92 were in CFRP rupture close to the corner. Since two specimens experienced the same failure characteristic, their axial stress-strain behaviors were seen to be identical as illustrated in Figure 4.93. The collected and summarized mechanical properties were presented in Table 4.43. As it can be seen from the table, the average strength was 30.5 MPa and the average strain was 0.018.

**(a) C15-S300-37.5-601** **(b) C15-S300-37.5-602**

**Figure 4.92. Failure types of CFRP-confined prismatic specimens in Group-6 ($f_{co}$=15 MPa and r=37.5mm)**

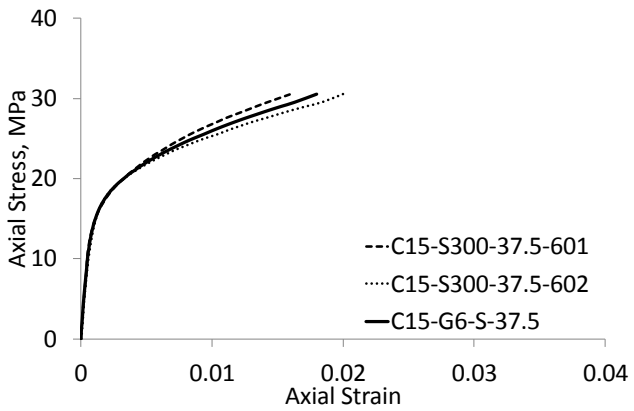


**Figure 4.93. Axial stress-strain diagrams of CFRP-confined prismatic specimens in Group-6 ($f_{co}$=15 MPa and r=37.5mm)**

**Table 4.43. Mechanical properties of CFRP-confined prismatic specimens in Group-6 ($f_{co}$=15 MPa and r=37.5 mm)**

| Specimen | $f_{cc}$ , MPa | $\varepsilon_{cc}$ | $E_1$ , GPa | $E_2$ , GPa | $E_1/E_2$ |
|---|---|---|---|---|---|
| C15-S300-37.5-601 | 30.5 | 0.016 | 26.65 | 0.70 | 38.3 |
| C15-S300-37.5-602 | 30.6 | 0.020 | 20.00 | 0.50 | 39.7 |
| **C15-G6-S-37.5** | **30.5** | **0.018** | **23.32** | **0.60** | **38.9** |

## 4.5 CONCRETE SPECIMENS HAVING 20 MPa STRENGTH

In this part, the main aim was to understand the effect of exposure tests on the mechanical behavior of CFRP-confined concrete specimens having 20 MPa strength, which was the minimum value for strengthening provided by the Turkish Earthquake Code 2007. The other aim was to determine the difference in the behavior when the strength of unconfined concrete increased to 20 MPa, i.e., to determine the effect of unconfined concrete strength on the behavior of CFRP-confined specimens.

Both cylindrical and prismatic specimens were tested in this part and the results were presented separately in the following sections.

### 4.5.1. Cylindrical Specimens

Cylindrical specimens were tested in three groups, i.e., specimens belonged to Group1, Group 2 and Group 3, as shown in Table 4.44.

**Table 4.44 Summary of the 20 MPa cylindrical specimens**

| Specimen Code | Confinement | $f_{co}$ (MPa) | Type | Overlap % | Group No | # of H-C cycles | SL, % | Outdoor Exposure |
|---|---|---|---|---|---|---|---|---|
| U20-C300-101 | Unconfined | 20 | Cylinder | 11 | 1 | | | |
| U20-C300-102 | Unconfined | 20 | Cylinder | 11 | 1 | | | |
| C20-C300-101 | CFRP-Confined | 20 | Cylinder | 11 | 1 | | | |
| C20-C300-102 | CFRP-Confined | 20 | Cylinder | 11 | 1 | | | |
| C20-C300-103 | CFRP-Confined | 20 | Cylinder | 11 | 1 | | | |
| U20-C300-201 | Unconfined | 20 | Cylinder | 11 | 2 | 200 | | |
| U20-C300-202 | Unconfined | 20 | Cylinder | 11 | 2 | 200 | | |
| U20-C300-203 | Unconfined | 20 | Cylinder | 11 | 2 | 200 | | |
| C20-C300-201 | CFRP-Confined | 20 | Cylinder | 11 | 2 | 200 | | |
| C20-C300-202 | CFRP-Confined | 20 | Cylinder | 11 | 2 | 200 | | |
| C20-C300-203 | CFRP-Confined | 20 | Cylinder | 11 | 2 | 200 | | |
| C20-C300-204 | CFRP-Confined | 20 | Cylinder | 11 | 2 | 200 | | |
| C20-C300-301 | CFRP-Confined | 20 | Cylinder | 11 | 3 | 200 | 40 | |
| C20-C300-302 | CFRP-Confined | 20 | Cylinder | 11 | 3 | 200 | 40 | |
| C20-C300-303 | CFRP-Confined | 20 | Cylinder | 11 | 3 | 200 | 40 | |
| C20-C300-304 | CFRP-Confined | 20 | Cylinder | 11 | 3 | 200 | 40 | |
| C20-C300-305 | CFRP-Confined | 20 | Cylinder | 11 | 3 | 200 | 40 | |
| C20-C300-306 | CFRP-Confined | 20 | Cylinder | 11 | 3 | 200 | 40 | |
| C20-C300-307 | CFRP-Confined | 20 | Cylinder | 11 | 3 | 200 | 40 | |
| C20-C300-308 | CFRP-Confined | 20 | Cylinder | 11 | 3 | 200 | 40 | |
| C20-C300-309 | CFRP-Confined | 20 | Cylinder | 11 | 3 | 200 | 40 | |
| C20-C300-310 | CFRP-Confined | 20 | Cylinder | 11 | 3 | 200 | 40 | |
| C20-C300-311 | CFRP-Confined | 20 | Cylinder | 11 | 3 | 200 | 40 | |

#### *4.5.1.1 Group-1: Reference Specimens*

***Unconfined Specimens***

Three unconfined specimens were used as reference specimens. Since the data for one of the specimen was not meaningful, it was discarded. After the axial compression test, it was found that the average strength was 20.8 MPa and average strain corresponding to strength was 0.003 as shown in Figure 4.94 and Table 4.45.

**Table 4.45. Mechanical properties of unconfined cylindrical specimens in Group-1 ($f_{co}$=20 MPa)**

| Specimen | $f_{co}$ , MPa | $\varepsilon_{co}$ | $E_1$ , GPa |
|---|---|---|---|
| U20-C300-101 | 21.4 | 0.003 | 17.09 |
| U20-C300-102 | 20.2 | 0.003 | 18.52 |
| **U20-G1-C** | **20.8** | **0.003** | **17.80** |

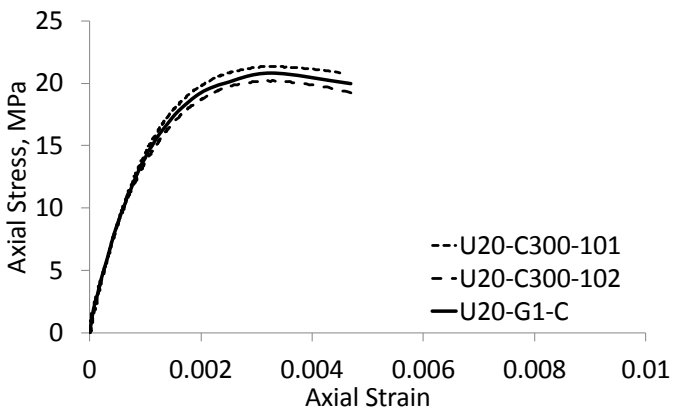


**Figure 4.94. Axial stress-strain diagrams of unconfined cylindrical specimens in Group-1 ($f_{co}$=20 MPa)**

***CFRP-Confined Specimens***

In this group, seven specimens were tested. First four specimens were experienced lower confined concrete strain. The reason was attributed to the problem in dial gage. Afterwards, three additional specimens were prepared to be used as reference specimens. The dial gage was renewed. It was found that new specimens behaved quite well and the recorded strains were meaningful. Therefore, only three successful specimens were presented below.

All three specimens were failed due to CFRP rupture. Ruptures were found to occur at the midheight of the specimens as shown in Figure 4.95. Like the rupture type, they also experienced the same behavior as given in Figure 4.96. The similarity can be seen clearly in Table 4.46 in which mechanical properties were summarized. The average strength was calculated as 47.5 MPa with a COV of 2.8%. The corresponding strain was found to be 0.035 with a COV of 9.9%. As for the slope of the curves, it can be said that curves started with a slope of 19 GPa (secant modulus of elasticity) in the first part and this slope dropped gradually afterwards. In the second part of the curve, the decrease in the slope reached to 25 times and curve continued with almost the same slope (0.75 GPa) until failure.

**(a) C20-C300-101** **(b) C20-C300-102** **(c) C20-C300-103**

**Figure 4.95. Failure types of CFRP-confined cylindrical specimens in Group-1 ($f_{co}$=20 MPa)**

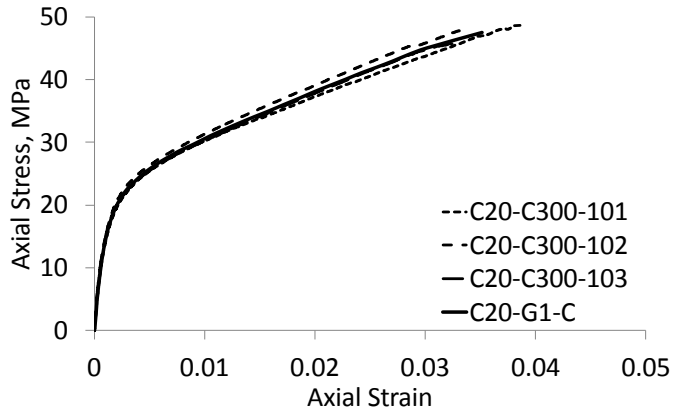


**Figure 4.96. Axial stress-strain diagrams of CFRP-confined cylindrical specimens in Group-1 ($f_{co}$=20 MPa)**

**Table 4.46. Mechanical properties of CFRP-confined cylindrical specimens in Group-1 ($f_{co}$=20 MPa)**

| Specimen | $f_{cc}$, MPa | $\varepsilon_{cc}$ | $E_1$ , GPa | $E_2$ , GPa | $E_1/E_2$ |
|---|---|---|---|---|---|
| C20-C300-101 | 48.7 | 0.039 | 17.53 | 0.69 | 25.4 |
| C20-C300-102 | 47.8 | 0.034 | 18.54 | 0.79 | 23.5 |
| C20-C300-103 | 46.0 | 0.033 | 20.82 | 0.76 | 27.6 |
| **C20-G1-C** | **47.5** | **0.035** | **18.97** | **0.75** | **25.4** |
| COV, % | 2.8 | 9.9 | | | |

### *4.5.1.2. Group-2: Specimens Exposed to H-C Cycles*

***Unconfined Specimens***

Three unconfined specimens were exposed to 200 heating-cooling cycles. Their behaviors after the exposure test were illustrated in Figure 4.97 and mechanical properties were summarized in Table 4.47. It can be seen from the table that, the average strength was 20.6 MPa and the corresponding strain was 0.003.

**Table 4.47. Mechanical properties of unconfined cylindrical specimens in Group-2 ($f_{co}$=20 MPa)**

| Specimen | H-C Cycles | $f_{co}$, MPa | $\varepsilon_{co}$ | $E_1$ , GPa |
|---|---|---|---|---|
| U20-C300-201 | 200 | 21.0 | 0.003 | 15.76 |
| U20-C300-202 | 200 | 21.6 | 0.003 | 34.96 |
| U20-C300-203 | 200 | 19.2 | 0.003 | 14.25 |
| **U20-G2-C** | | **20.6** | **0.003** | **21.66** |
| COV, % | | 6.2 | 9.2 | |

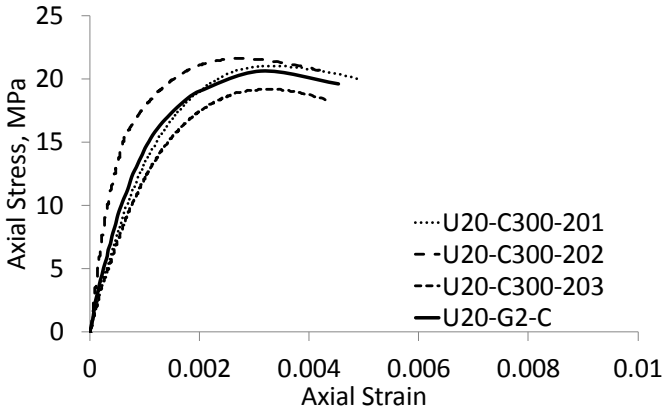


**Figure 4.97. Axial stress-strain diagrams of unconfined cylindrical specimens in Group-2 ($f_{co}$=20 MPa)**

***CFRP-Confined Specimens***

Four specimens were utilized to determine the effect of heating-cooling cycles on the mechanical properties of CFRP-confined specimens. In Figure 4.98, it can be seen that all specimens except C20-C300-201 failed due to the CFRP rupture at the midheight. In C20-C300-201, delamination was also observed in addition to the CFRP rupture. The difference in the failure type resulted in a reduced strength and

strain capacities. Since the reduction was not so different, this specimen was not discarded and taken into account in the comparison. Figure 4.99 illustrates the axial stress-axial strain behaviors of all specimens. From the figure, it can be seen that behaviors were almost identical. Mechanical properties of all specimens were tabulated in Table 4.48. In the table there also provided the average properties. It can be said that, average strength was 47.3 MPa, average strain was 0.033 when the specimens exposed to heating-cooling cycles.

**(a) C20-C300-201** **(b) C20-C300-202** **(c) C20-C300-203** **(d) C20-C300-204**

**Figure 4.98. Failure types of CFRP-confined cylindrical specimens in Group-2 ($f_{co}$=20 MPa)**

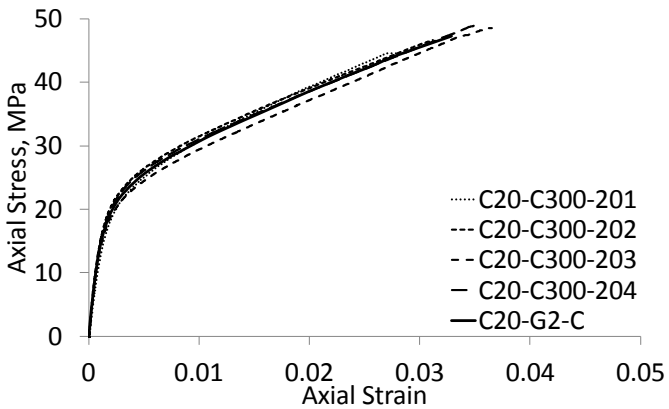


**Figure 4.99. Axial stress-strain diagrams of CFRP-confined cylindrical specimens in Group-2 ($f_{co}$=20 MPa)**

**Table 4.48. Mechanical properties of CFRP-confined cylindrical specimens in Group-2 ($f_{co}$=20 MPa)**

| Specimen | H-C Cycles | $f_{cc}$ , MPa | $\varepsilon_{cc}$ | $E_1$ , GPa | $E_2$ , GPa | $E_1/E_2$ |
|---|---|---|---|---|---|---|
| C20-C300-201 | 200 | 44.6 | 0.028 | 13.12 | 0.85 | 15.4 |
| C20-C300-202 | 200 | 46.6 | 0.031 | 18.41 | 0.77 | 24.0 |
| C20-C300-203 | 200 | 49.3 | 0.036 | 16.50 | 0.75 | 21.9 |
| C20-C300-204 | 200 | 48.6 | 0.037 | 16.57 | 0.76 | 21.7 |
| **C20-G2-C** | | **47.3** | **0.033** | **16.15** | **0.78** | **20.6** |
| COV, % | | 4.5 | 11.7 | | | |

#### *4.5.1.3. Group-3: Specimens Exposed to H-C Cycles and SL*

***CFRP-Confined Specimens***

In order to determine the change in the behavior of CFRP-confined specimens subjected to simultaneous exposure of heating-cooling cycles and sustained loading, eleven specimens were prepared and tested. Among those specimens, only three of them failed in a desired manner, which was the CFRP rupture at the midheight of the specimens. As it is seen from Figure 4.100 some specimens failed due to CFRP delamination and some failed due to CFRP rupture apart from the midheight. Those undesired failures resulted in an unreliable behavior as illustrated in Figure 4.101. Either strength or strain or both strength and strain were treated as wrong. As it is seen from the figure, delamination resulted in a reduced strength capacity while undesired CFRP rupture resulted in a reduced strain capacity. Since those specimens' data were not reliable, they were discarded. Apart from those specimens, some specimens failed due to CFRP rupture in a desired manner however; because of the problem in test setup, their data was also eliminated. The reliable specimens were presented in Figure 4.102. As it can be seen, all specimens failed due to CFRP rupture at midheight. The failure type influenced the axial stress-strain diagram as

given in Figure 4.103. For all specimens, axial stress-strain diagram composed of a clear first part and a clear second part. The average curve was also provided in the same figure. In addition to the curves, mechanical properties were tabulated and presented in Table 4.49. From the table, it can be seen that in this group specimens had an average strength of 48 MPa and an average strain of 0.028.

**(a) C20-C300-302** **(b) C20-C300-309** **(c) C20-C300-311**

**Figure 4.100. Undesired failure types of CFRP-confined cylindrical specimens in Group-3 ($f_{co}$=20 MPa)**

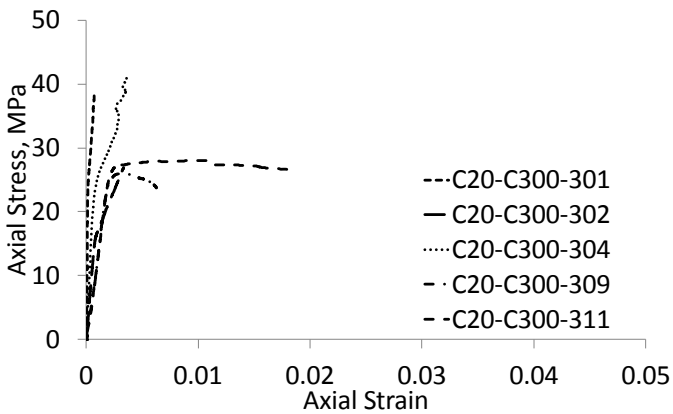


**Figure 4.101. Effect of undesired failure types on the axial stress-axial strain diagrams**

**(a) C20-C300-307** **(b) C20-C300-308** **(c) C20-C300-310**

**Figure 4.102. Desired failure types of CFRP-confined cylindrical specimens in Group-3 ($f_{co}$=20 MPa)**

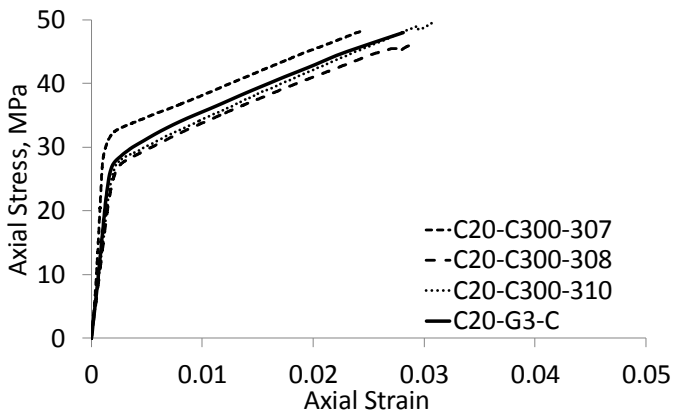


**Figure 4.103. Axial stress-strain diagrams of CFRP-confined cylindrical specimens in Group-3 ($f_{co}$=20 MPa)**

**Table 4.49. Mechanical properties of CFRP-confined cylindrical specimens in Group-3 ($f_{co}$=20 MPa)**

| Specimen | SL, % | H-C Cycles | $f_{cc}$, MPa | $\varepsilon_{cc}$ | $E_1$ , GPa | $E_2$ , GPa | $E_1/E_2$ |
|---|---|---|---|---|---|---|---|
| C20-C300-307 | 40 | 200 | 48.3 | 0.024 | 22.38 | 0.83 | 26.9 |
| C20-C300-308 | 40 | 200 | 46.2 | 0.029 | 13.12 | 0.73 | 18.0 |
| C20-C300-310 | 40 | 200 | 49.5 | 0.031 | 14.96 | 0.79 | 18.9 |
| **C20-G3-C** | | | **48.0** | **0.028** | **16.82** | **0.78** | **21.5** |
| COV, % | | | 3.5 | 12.2 | | | |

### 4.5.2. Prismatic Specimens

In order to understand the effect of heating-cooling cycles and/or sustained loading on the mechanical properties of CFRP-confined specimens which had an unconfined strength of 20 MPa, prismatic specimens were prepared and tested in three groups, i.e., specimens belonged to Group 1, Group 2 and Group 3. Specimens had a corner radius of 37.5 mm, which corresponded to an MCR factor of 0.19. Since MCR factor was greater than 0.15, which was the lower value to ensure proper confinement, it was believed that all specimens would be effectively confined.

Cylinder strength of this set was found as 27.9 MPa. In the following sections, results of each group were presented separately.

**Table 4.50 Summary of the 20 MPa prismatic specimens**

| Specimen Code | Confinement | $f_{co}$ (MPa) | Type | Overlap % | r, mm | Group No | # of H-C cycles | SL, % | Outdoor Exposure |
|---|---|---|---|---|---|---|---|---|---|
| U20-S300-37.5-101 | Unconfined | 20 | Prism | 11 | 37.5 | 1 | | | |
| U20-S300-37.5-102 | Unconfined | 20 | Prism | 11 | 37.5 | 1 | | | |
| C20-S300-37.5-101 | CFRP-Confined | 20 | Prism | 11 | 37.5 | 1 | | | |
| C20-S300-37.5-102 | CFRP-Confined | 20 | Prism | 11 | 37.5 | 1 | | | |
| C20-S300-37.5-201 | CFRP-Confined | 20 | Prism | 11 | 37.5 | 2 | 200 | | |
| C20-S300-37.5-202 | CFRP-Confined | 20 | Prism | 11 | 37.5 | 2 | 200 | | |
| C20-S300-37.5-301 | CFRP-Confined | 20 | Prism | 11 | 37.5 | 3 | 200 | 40 | |
| C20-S300-37.5-302 | CFRP-Confined | 20 | Prism | 11 | 37.5 | 3 | 200 | 40 | |
| C20-S300-37.5-303 | CFRP-Confined | 20 | Prism | 11 | 37.5 | 3 | 200 | 40 | |

#### *4.5.2.1 Group-1: Reference Specimens*

***Unconfined Specimens***

Two unconfined specimens were used as reference. Those specimens were not subjected to exposure tests. However, they were tested after the end of exposure tests. Axial stress-strain behaviors of unconfined reference specimens were plotted in Figure 4.104 and mechanical properties were provided in Table 4.51. As it is seen from the table, the average strength was found as 21.7 MPa, which was 78% of the cylinder strength.

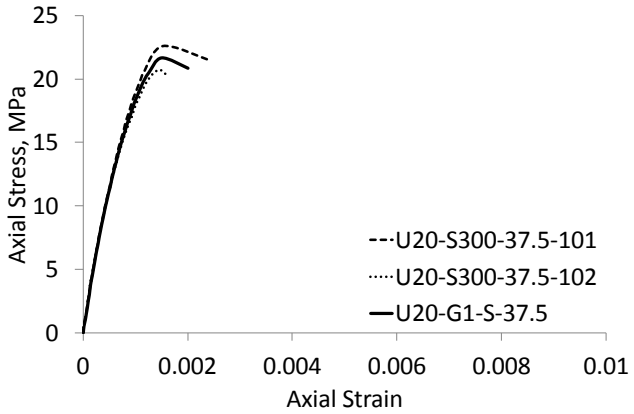


**Figure 4.104. Axial stress-strain diagrams of unconfined prismatic specimens in Group-1 ($f_{co}$=20 MPa)**

**Table 4.51. Mechanical properties of unconfined prismatic specimens in Group-1 ($f_{co}$=20 MPa)**

| Specimen | $f_{cop}$ , MPa | $\varepsilon_{co}$ | $E_1$ , GPa |
|---|---|---|---|
| U20-S300-37.5-101 | 22.6 | 0.002 | 23.92 |
| U20-S300-37.5-102 | 20.7 | 0.001 | 24.12 |
| **U20-G1-S-37.5** | **21.7** | **0.002** | **24.02** |

***CFRP-Confined Specimens***

In this group, two specimens wrapped with one layer of CFRP and used as reference specimens. They were kept inside the laboratory without any exposures. After the completion of exposure tests, which were the case in other groups, they were tested under uniaxial compression. Failure types were observed to be CFRP rupture close to the corner as seen in Figure 4.105. Failures were at the end of the curvature at the corner. Axial stress-strain diagrams were plotted in Figure 4.106 and mechanical

properties were summarized in Table 4.52. Figure 4.106 shows that, behaviors of both specimens differed from each other. Although strain capacities were close to each other, strength difference was quite high.

**(a) C20-S300-37.5-101**

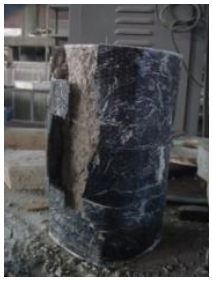

**(b) C20-S300-37.5-102**

**Figure 4.105. Failure types of CFRP-confined prismatic specimens in Group-1 ($f_{co}$=20 MPa)**

**Table 4.52. Mechanical properties of CFRP-confined prismatic specimens in Group-1 ($f_{co}$=20 MPa)**

| Specimen | $f_{cc}$ , MPa | $\varepsilon_{cc}$ | $E_1$ , GPa | $E_2$ , GPa | $E_1/E_2$ |
|---|---|---|---|---|---|
| C20-S300-37.5-101 | 37.4 | 0.012 | 25.74 | 1.02 | 25.3 |
| C20-S300-37.5-102 | 44.2 | 0.010 | 28.50 | 1.84 | 15.5 |
| **C20-G1-S-37.5** | **40.8** | **0.011** | **27.12** | **1.43** | **19.0** |

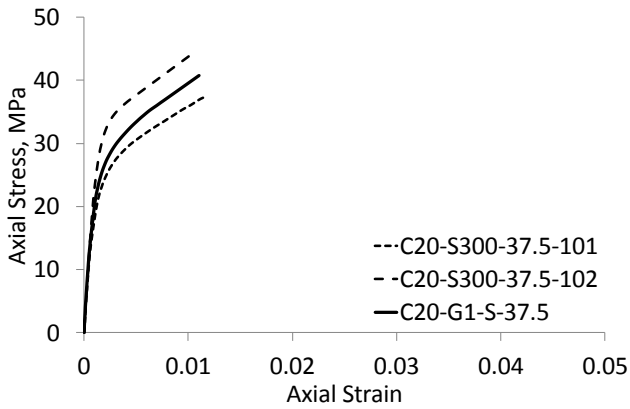


**Figure 4.106. Axial stress-strain diagrams of CFRP-confined prismatic specimens in Group-1 ($f_{co}$=20 MPa)**

### *4.5.2.2 Group-2: Specimens Exposed to H-C Cycles*

***CFRP-Confined Specimens***

Two CFRP-confined specimens were exposed to 200 heating-cooling cycles in order to understand the change in mechanical properties. As it is seen from Figure 4.107, failure patterns were not affected by the exposure. As the ones observed in reference specimens, failures were due to CFRP rupture close to the corner. Rupture extended to full height as well.

Figure 4.108 illustrates the axial stress-axial strain diagrams of both specimens as well as the average curve. No difference was observed in the behavior. Both specimens behaved almost the same. However, slight differences can be seen in Table 4.53. The average strength was calculated as 41.5 MPa and average strain was found as 0.011. The ratio of the slope in first part to the slope in the second part was evaluated as 21.3, which was almost equal to the ones calculated for reference specimens.

**(a) C20-S300-37.5-201** **(b) C20-S300-37.5-202**

**Figure 4.107. Failure types of CFRP-confined prismatic specimens in Group-2 ($f_{co}$=20 MPa)**

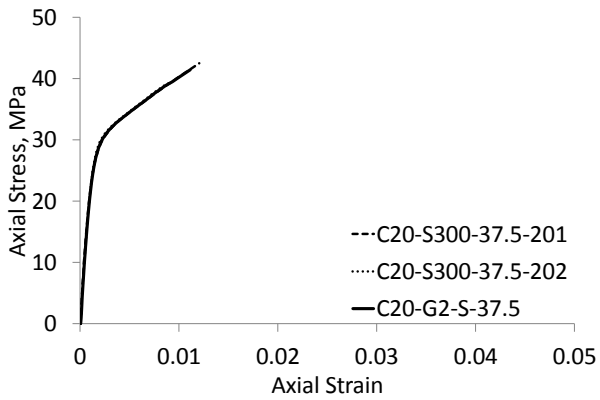


**Figure 4.108. Axial stress-strain diagrams of CFRP-confined prismatic specimens in Group-2 ($f_{co}$=20 MPa)**

**Table 4.53. Mechanical properties of CFRP-confined prismatic specimens in Group-2 ($f_{co}$=20 MPa)**

| Specimen | H-C Cycles | $f_{cc}$ , MPa | $\varepsilon_{cc}$ | $E_1$ , GPa | $E_2$ , GPa | $E_1/E_2$ |
|---|---|---|---|---|---|---|
| C20-S300-37.5-201 | 200 | 42.5 | 0.012 | 27.38 | 1.22 | 22.4 |
| C20-S300-37.5-202 | 200 | 40.5 | 0.010 | 25.34 | 1.25 | 20.3 |
| **C20-G2-S-37.5** | | **41.5** | **0.011** | **26.36** | **1.24** | **21.3** |

#### *4.5.2.3 Group-3: Specimens Exposed to H-C Cycles and SL*

***CFRP-Confined Specimens***

In order to determine the effect of simultaneous exposure of heating-cooling cycles (H-C cycles) and sustained loading, three specimens were wrapped with one-layer of CFRP and placed in environmental test chamber. They were loaded to 40% of their axial load capacity. After reaching 200 H-C cycles, exposure test was completed and specimens were tested under uniaxial compression. Figure 4.109 shows the failure types after the uniaxial compression test. The first and the third specimens failed due to CFRP rupture extending to full height, which was the desired failure type. However, although second specimen (C20-S300-37.5-302) failed due to CFRP rupture, rupture did not extend to full height. Besides, rupture was not seen at the midheight either. Therefore, since this type of failure affected the behavior, second specimen was discarded.

Axial stress-strain diagrams for two specimens were provided in Figure 4.110. As it can be seen, both specimens behaved almost the same. The similarity was clear in Table 4.54. Both specimens had strength of 37 MPa. Confined concrete strain and slope of the curves were also identical.

**(a) C20-S300-37.5-301** **(b) C20-S300-37.5-302** **(c) C20-S300-37.5-303**

**Figure 4.109. Failure types of CFRP-confined prismatic specimens in Group-3 ($f_{co}$=20 MPa)**

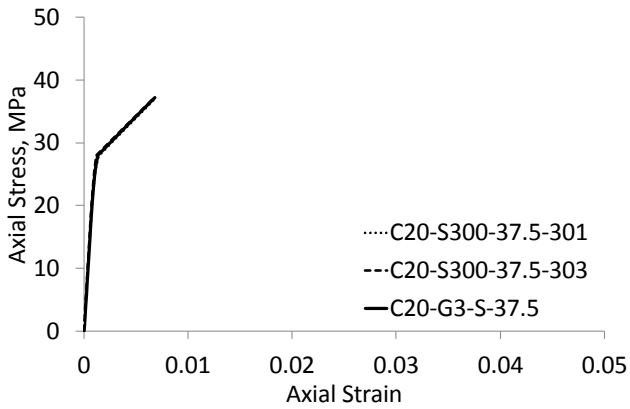


**Figure 4.110. Axial stress-strain diagrams of CFRP-confined prismatic specimens in Group-3 ($f_{co}$=20 MPa)**

**Table 4.54. Mechanical properties of CFRP-confined prismatic specimens in Group-3 ($f_{co}$=20 MPa)**

| Specimen | SL, % | H-C Cycles | $f_{cc}$, MPa | $\varepsilon_{cc}$ | $E_1$ , GPa | $E_2$ , GPa | $E_1/E_2$ |
|---|---|---|---|---|---|---|---|
| C20-S300-37.5-301 | 40 | 200 | 37.0 | 0.007 | 25.13 | 1.70 | 14.8 |
| C20-S300-37.5-303 | 40 | 200 | 37.4 | 0.007 | 26.40 | 1.66 | 15.9 |
| **C20-G3-S-37.5** | | | **37.2** | **0.007** | **25.76** | **1.68** | **15.3** |

C20-S300-37.5-303 was attached additional gages to study the axial and lateral strain distributions. Figure 4.111 shows the locations of each gage. From the figure, it can be seen that, two uniaxial strain gages for the lateral strains at the corners and four triaxial strain gages for the axial and lateral strains at the sides were utilized. As a result, six strain gages were used to record lateral strains and four strain gages plus two dial gages were utilized two record axial strains. During the test, two strain gages (at sides B and C) which were used to record axial strains broke out.

As it is seen from Figure 4.113, stress-strain diagrams were plotted for each part of the specimen. Axial strains were seen to be higher at the failure zone. At this location, however, lateral strains were lower as compared to other locations. If the figure was carefully studied, it could be seen that strain gage at this zone (gage 108) was not able to record reliable strains after reaching ~32 MPa. The other strain gage close to this zone (gage 101) experienced the higher lateral strain. Strain distribution along the circumference can be clearly seen in Figure 4.112. Lateral strain distribution was observed to be almost uniform except at the failure zone.

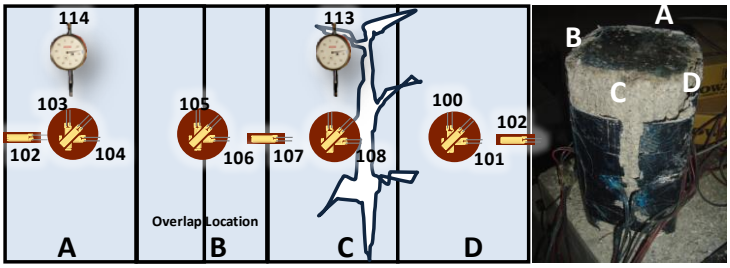


**Figure 4.111 Schematic view of the gages used in C20-S300-37.5-303**

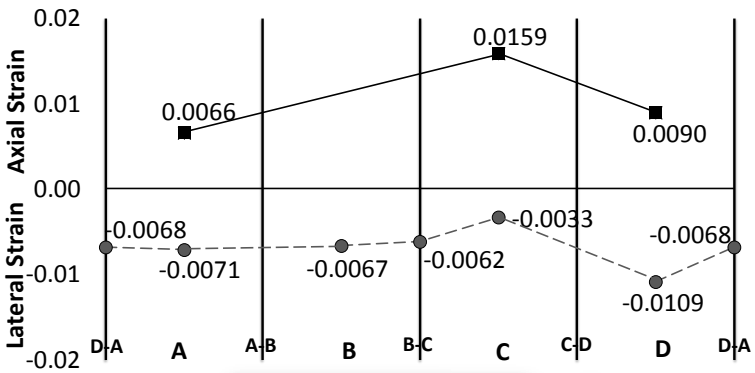


**Figure 4.112 Axial and lateral strain distributions in C20-S300-37.5-303**

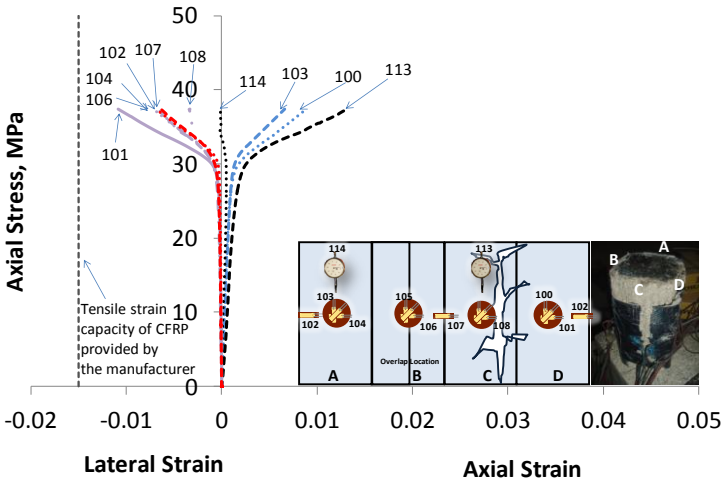


**Figure 4.113 Stress-strain behavior of C20-S300-37.5-303**

# CHAPTER 5

# DISCUSSION OF THE TEST RESULTS

## 5.1 INTRODUCTION

In this chapter, results of the tests are compared and discussed considering the axial stress-strain behavior and mechanical properties. First, effect of CFRP confinement on the behavior of concrete specimens is presented. Unconfined specimens' data are only used in this part. Then, only CFRP-confined specimen's data are presented and discussed. Second, effect of heating-cooling cycles (H-C cycles) on CFRP-confined specimens is discussed and then effect of outdoor exposure follows this section. Finally, effect of sustained loading is presented and discussed considering several parameters. Target strength for some specimens could not be reached. For example, in 10 MPa prismatic specimens with r=37.5 mm, cylinder strength was found to be 14.7 MPa not 10 MPa which was the target. In addition, for 20 MPa prismatic specimens, cylinder strength was 27.9 MPa. Although there existed those differences, specimens' codes were not changed and same coding was used throughout this dissertation.

## 5.2 EFFECT OF CFRP CONFINEMENT ON BEHAVIOR OF CONCRETE COLUMNS

Concrete columns under axial load exhibit contraction in axial direction but they expand in lateral direction due to Poisson's effect. This expansion creates tensile forces in the concrete. Since concrete has low tensile strength capacity, the expansion results in a lower compressive strength. To increase strength of the concrete

confinement is necessary. A proper confinement helps concrete to carry the tensile stresses in lateral direction and results in a higher compressive strength and strain capacity. CFRP is one of the effective confinement materials for strengthening of the members. If properly applied, CFRP leads to an improvement in the behavior, which ends up with a considerable increase in strength and strain capacities. The enhancement in strength and strain capacities however, depends on several factors, such as; unconfined concrete strength, number of FRP layers and its thickness, environmental factors, cross-section etc.

In this section, effect of CFRP-confinement on behavior of concrete columns is discussed. Considering that the CFRP material used in this study had high strength and strain capacities, specimens were designed so that they would exhibit improved behavior, i.e., the aim was to provide an adequate confinement to see the capacity increase. While wrapping specimens with CFRP two parameters were kept constant. The first one was the thickness of CFRP. It was known that confinement effectiveness increases with increase in CFRP thickness. However, since CFRP was relatively expensive with respect to other conventional materials, increase in thickness would result in an increase in the cost. As it was tried to establish an economical solution for strengthening and/or retrofitting applications, minimum thickness leading to an adequate confinement was the optimum solution. Therefore, it was decided to apply a single layer of CFRP, which had a thickness of 0.165 mm.

The other parameter was the overlap length, which was provided after a one full wrap of CFRP. The overlap length was chosen to be the 11% of the perimeter of the specimen. The reason for choosing such a short overlap length was to provide almost uniform strain distribution thus uniform stress distribution around the circumference. The uniform strain distribution was possible in cylindrical specimens. However, the study performed by [82] showed that at the overlap region (overlap length varied between 21% (100 mm) to 85% (400 mm) of the perimeter) strains were lower than the strains at the other regions (Figure 5.1). In other words, since FRP thickness was higher at this region, strains were lower when compared to the other regions, which

had low thickness. Hence, in order to minimize the difference in the strain distribution to end up with almost uniform distribution, overlap length was kept short enough. 11% of the perimeter as the overlap length was selected in this study because it was found that this ratio was the minimum value to prevent delamination and lead to a proper confinement.

When prismatic specimens are of concern, uniform strain distribution is not possible due to the strain or stress concentrations at the corners. However, if corners are rounded in such a way that those concentrations are extended to a wider areas, strain distribution may approach to a somehow uniform level. In Figure 5.1, the strain distribution along a prismatic specimen is given in comparison with cylindrical specimen. Although, the distribution in cylindrical specimens is almost uniform the overlap zone, it is not the case in prismatic members. Since it was hard to create a uniform strain distribution, the overlap length ratio used in cylindrical specimens was decided to be used in prismatic specimens also.

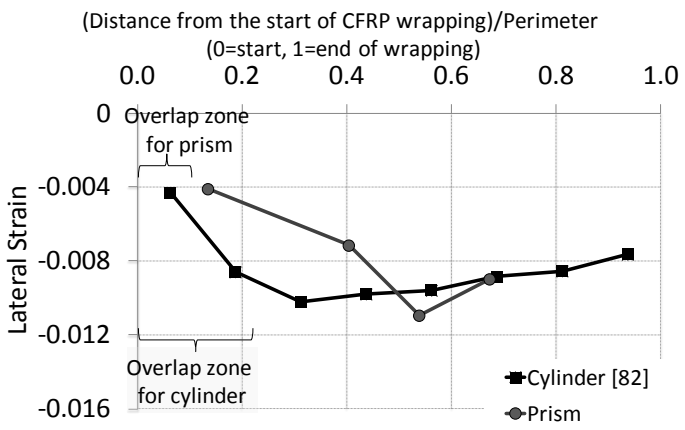


**Figure 5.1 Strain distribution around the circumference of cylindrical [82] and prismatic specimens**

Figure 5.3 illustrates the effect of CFRP-confinement on all specimens and the details of these figures were given in Figure 5.2. The curves given in Figure 5.3 represent the average curves. In order to see the effectiveness of CFRP application, behaviors of unconfined specimens were also provided in each figure.

Confinement behavior leads to strength and strain enhancement (Figure 5.3). The curves consisted of three parts. First part was in between the zero stress and $\sim 0.9f_{co}$ [31]. It was dominated by unconfined concrete and was a parabolic curve. The modulus of elasticity in this part was calculated at the $0.4f_{co}$ and called secant modulus of elasticity, $E_1$. The second part started at around $1.1\ f_{co} \sim 1.2f_{co}$ and ended at $f_{cc}$. It was almost a straight line and influenced by the effectiveness of CFRP. The linearity at this part reflected the behavior of CFRP, which is a linear elastic material. Since this part was beyond the unconfined concrete strength, it was a CFRP dominant region. The slope in this part is called $E_2$, which is much less as compared to secant modulus of elasticity calculated in the first part. The third part is in between first and second part and called as transition zone. This part connects the first and the second part smoothly by decreasing the slope of the curve from $E_1$ to $E_2$.

All CFRP-confined concrete specimens were observed to fail due to CFRP rupture. Ruptures took place at a region other than overlap zone where thickness of CFRP was less. For cylindrical specimens the place of rupture was not foreseen because it could be any place other than overlap zone. However, as for prismatic specimens failures were observed to occur at a place close to a corner. This place was observed to be the end of the curvature at the comer.

Mechanical properties of unconfined and CFRP-confined specimens are summarized in Table 5.1. In this table, mechanical properties are presented in terms of ultimate strength, strain corresponding to the ultimate strength and secant modulus of elasticity. For unconfined specimens, strength values are given in terms of cylinder strength and prism strength. As from the unconfined strength values, prism strength was found be lower than the cylindrical strength. The difference between confined

and unconfined specimens, which indicates the CFRP effectiveness, is also provided. Both strength and strain were observed to enhance with the application of CFRP.

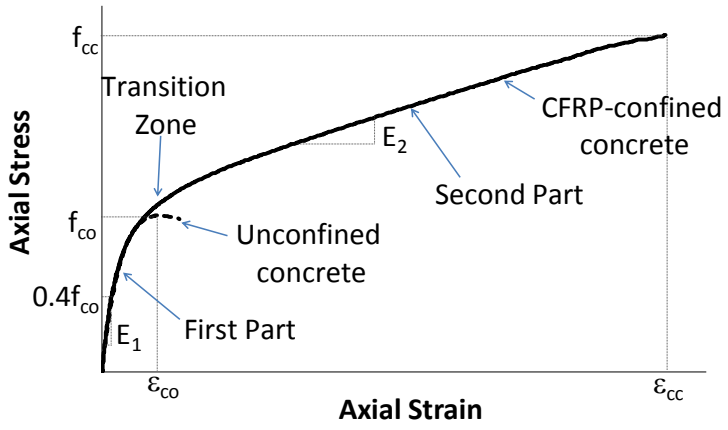


**Figure 5.2. Behavior of unconfined and CFRP-confined specimens under compression**

Degree of enhancement depends on unconfined concrete strength and cross-section as shown in Figure 5.4. In the figure, CFRP effectiveness is given in terms of MCR factor, which was explained in Chapter 4. Since MCR factor takes unconfined concrete strength and cross-section of the specimen into account, it is believed to be a reliable factor reflecting the CFRP effectiveness. From the figure, it is observed that the effectiveness is high in low strength concrete of both cylindrical and prismatic forms. The effectiveness however, reduces with the decrease in MCR factor.

Prismatic specimens were designed so that they would exhibit improvement in the behavior. In this respect, corners in 10 MPa specimens were rounded considering two different corner radii. 25 mm radius corresponded to 1/6th and 37.5 mm

corresponded to 1/4th of the side dimension of square section. In other words, considering that cylindrical specimens had a corner radius (r) to side dimension (a) ratio of a/2, specimen with 37.5 mm corner radius had a ratio of a/4 and specimen with 25 mm had a ratio of a/6. However, in 20 MPa specimens corners were only rounded to 37.5 mm. Effect of corner radius can be clearly seen in the figures.

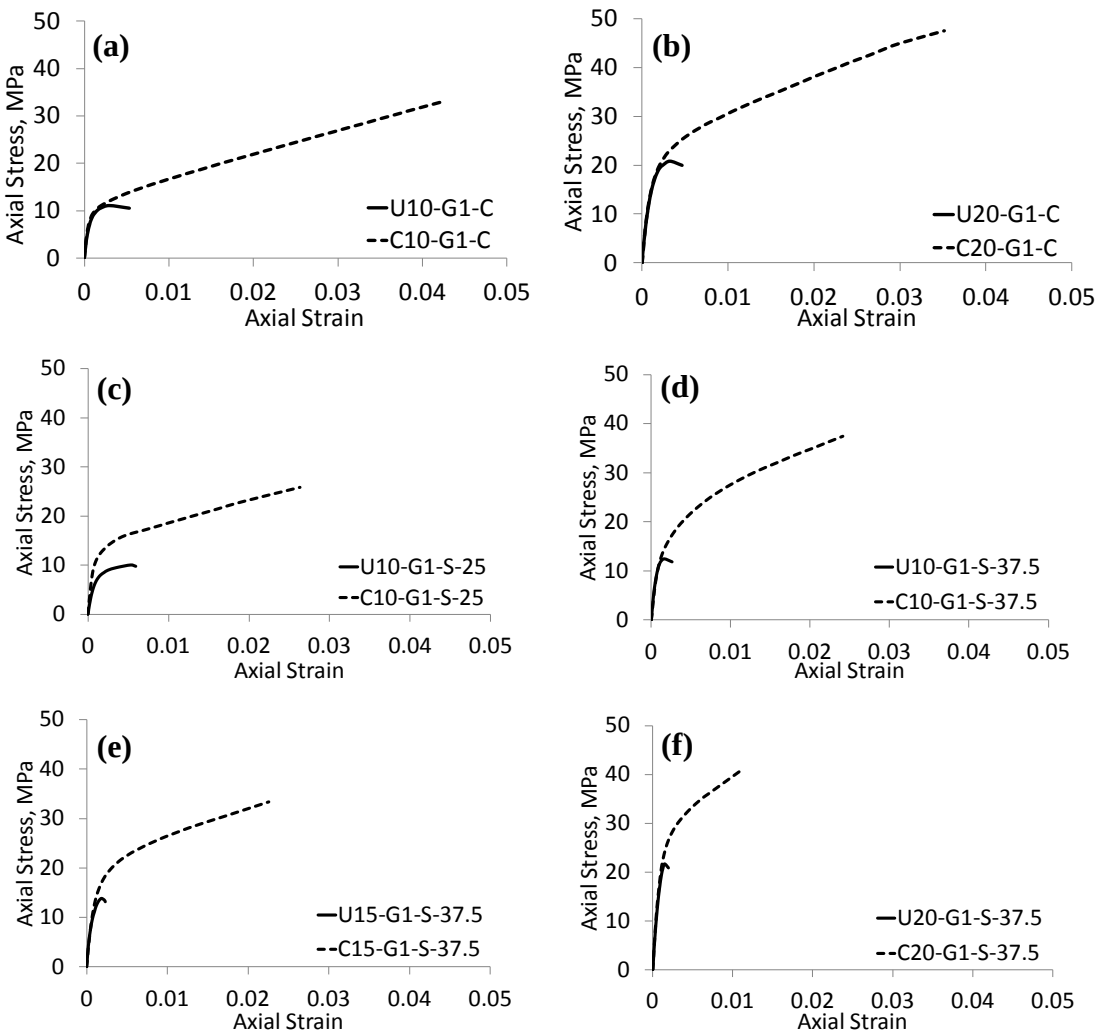


**Figure 5.3. Effect of CFRP confinement on behavior of concrete columns a) 10 MPa cylinder, b) 20 MPa cylinder, c) 10 MPa prismatic r=25 mm, d) 10 MPa prismatic r=37.5 mm, e) 15 MPa prismatic r=37.5 mm, f) 20 MPa prismatic r=37.5 mm**

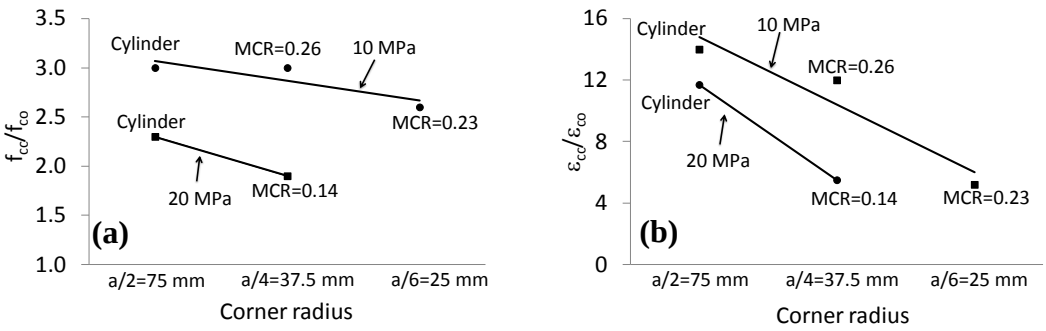


**Figure 5.4. Effect of corner radius on the mechanical properties of CFRP-confined specimens a) Effect on strength, b) Effect on strain**

One of the main effects on the effectiveness of CFRP-confined specimens is the workmanship. If the application is not good enough, CFRP will not take an active role in the confinement. Figure 5.5 shows the effect of workmanship on the failure types of CFRP-confined cylinders. The first specimen on the left failed due to delamination occurred in the bottom half of the specimen. In the second one, failure was at the top and localized at a small region. Although it failed due to CFRP rupture, it was still not the desired failure type. For both specimens the quality of workmanship was not good enough to create a sufficient confinement. As for the last specimen on the right failure was due to CFRP rupture, which extended to full height of the specimen. This failure type was the desired one because it ended up with relatively high strength and strain as shown in Table 5.2. In the table, mechanical properties are normalized with respect to the properties of reference specimen called C10-C300-101. Specimen C10-C300-R29, which failed due to delamination showed the worst performance in terms of both strength and strain. The strength was 58% and the strain corresponding to the strength was found to be 64% of the one given for reference specimen. Since the other specimen failed due to a localized CFRP rupture, its mechanical properties were relatively good but still lower than the reference.

**Table 5. 1 Effect of CFRP confinement on mechanical properties of concrete columns**

| Unconfined Concrete | | | | | | CFRP-Confined Concrete | | | | Difference | | | |
|---|---|---|---|---|---|---|---|---|---|---|---|---|---|
| **Test Group** | $f_{co}$ **(MPa)** | **MCR** | $f_{cop}$ **(MPa)** | $\varepsilon_{co}$ | $E_1$ **(GPa)** | **Test Group** | $f_{cc}$ **(MPa)** | $\varepsilon_{cc}$ | $E_1$ **(GPa)** | $\frac{f_{cc}}{f_{co}}$ | $\frac{f_{cc}}{f_{cop}}$ | $\frac{\varepsilon_{cc}}{\varepsilon_{co}}$ | $\frac{E_{1confined}}{E_{1unconfined}}$ |
| U10-G1-C | 11.1 | 1.00 | 11.1 [13.3]* | 0.003 [16.1] | 14.75 [9.3] | C10-G1-C | 32.9 [5.1] | 0.042 [5.8] | 18.35 [6.8] | 3.0 | 3.0 | 14.0 | 1.2 |
| U10-G1-S-25 | 10.9 | 0.23 | 10.0 [16.6] | 0.005 [61.0] | 9.35 [20.5] | C10-G1-S-25 | 25.8 [4.7] | 0.026 [24.3] | 16.73 [1.9] | 2.4 | 2.6 | 5.2 | 1.8 |
| U10-G1-S-37.5 | 14.7 | 0.26 | 12.5 [6.8] | 0.002 [41.2] | 17.56 [6.6] | C10-G1-S-37.5 | 37.4 [0.3] | 0.024 [3.1] | 15.71 [10.0] | 2.5 | 3.0 | 12.0 | 0.9 |
| U15-G1-S-37.5 | 16.3 | 0.23 | 13.8 [17.2] | 0.002 [11.9] | 18.34 [13.9] | C15-G1-S-37.5 | 33.3 [6.2] | 0.023 [9.8] | 16.96 [13.2] | 2.0 | 2.4 | 11.5 | 0.9 |
| U20-G1-C | 20.8 | 1.00 | 20.8 [3.8] | 0.003 [1.1] | 17.80 [5.7] | C20-G1-C | 47.5 [2.8] | 0.035 [9.9] | 18.97 [8.9] | 2.3 | 2.3 | 11.7 | 1.1 |
| U20-G1-S-37.5 | 27.9 | 0.14 | 21.7 [6.2] | 0.002 [2.1] | 24.02 [0.6] | C20-G1-S-37.5 | 40.8 [11.9] | 0.011 [8.5] | 27.12 [7.2] | 1.5 | 1.9 | 5.5 | 1.1 |

**Values in parenthesis show the coefficient of variation of the test group*

**(a) C10-C300-R29** **(b) C10-C300-R30** **(c) C10-C300-101**

**Figure 5.5. Effect of workmanship on the failure types of CFRP-confined cylinders**

**Table 5.2. Effect of workmanship on mechanical properties of CFRP-confined cylinders**

| Specimen | $f_{cc}$, MPa | Difference | $\varepsilon_{cc}$ | Difference |
|---|---|---|---|---|
| C10-C300-101 | 34.9 | 1.00 | 0.023 | 1.00 |
| C10-C300-R30 | 28.6 | 0.82 | 0.021 | 0.93 |
| C10-C300-R29 | 20.3 | 0.58 | 0.015 | 0.64 |

## 5.3 EFFECT OF HEATING-COOLING (H-C) CYCLES ON BEHAVIOR OF CFRP-CONFINED CONCRETE COLUMNS

Concrete is vulnerable to temperature cycles [85]. These cycles cause successive expansion and contraction. The expansion and contraction can be harmful if the voids in the concrete contain water. It is known that water expands 9% upon freezing. Since concrete contracts in freezing action, the expansion in water may

cause concrete to crack provided that the voids are not enough to take care of this expansion.

In this experimental program, concrete specimens were prepared without using air-entrained admixture to simulate the general concrete practice in Turkey. Therefore, they were kept susceptible to H-C cycles. After wrapping specimens with one layer of CFRP, tests were performed considering two cases. In the first case, specimens were exposed to dry H-C cycles under approximately 40% of relative humidity (RH), whereas in the second case specimens (10 and 15 MPa specimens having 37.5 mm corner radius) were subjected to wet H-C cycles. Dry cycles were performed in the Environmental Test Chamber (ETC) without introducing any RH changes. However, wet cycles were performed by keeping specimens in water bath in the ETC. In both procedures, same H-C procedures were repeated for 200 cycles.

The coefficient of thermal expansion ($\alpha$) of concrete is taken as $10x10^{-6}$/°C [86] whereas it is approximately $-1x10^{-6}$/°C to zero in CFRP in longitudinal direction [2]. The difference in $\alpha$ may have positive effect on CFRP-confined concrete when heated. Although concrete experiences expansion during heating process, CFRP contracts and prevents concrete to expand too much by activating the confining action. Concrete in this case will be under circumferential compression forces. On the contrary, during the cooling process, concrete tries to contract whereas CFRP tends to expand. This action may cause a bond problem between concrete and CFRP. Moreover, concrete will be exposed to circumferential tensile forces. Periodical H-C cycles create periodical tensile and compression forces in the concrete. If there exists any bond problem between concrete and CFRP, it may grow after each H-C cycle. Since the bond may be affected by H-C process, adhesives used in wet-layup process should be carefully applied in order to create an adequate bond.

Effect of H-C cycles on axial stress-strain diagram, ultimate strength and ultimate strain capacity is discussed separately in the following sections.

### 5.3.1 Effect of H-C cycles on axial stress-strain diagram

Figure 5.6 illustrates the effect of H-C cycles on behavior of CFRP-confined cylindrical specimens used in this dissertation. In the figures, codes with G1 represents the reference specimens, G2 denotes the specimens exposed to H-C cycles at approximately 40% of RH which is called dry H-C cycles. As it is seen from the, H-C cycles have almost no effect on the behavior of cylindrical specimens. Figures are matched and no apparent difference is observed.

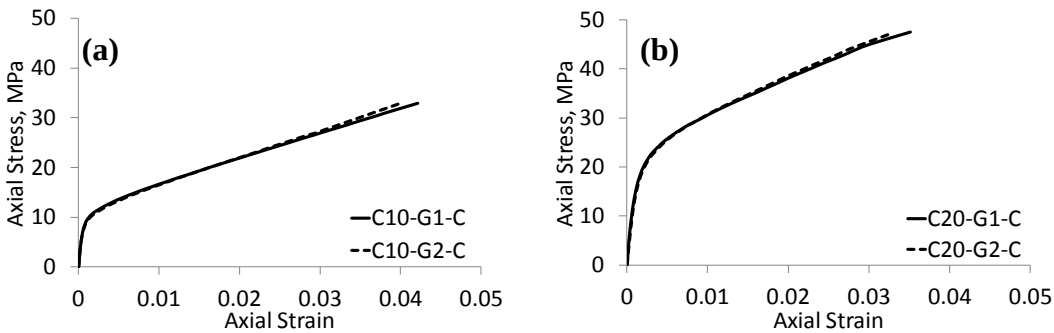


**Figure 5.6. Effect of dry H-C cycles on behavior of CFRP-confined cylindrical specimens a) 10 MPa, b) 20 MPa**

Figure 5.7 presents the effect of H-C cycles on $E_1$ and $E_2$. The differences in between the groups are given in terms of percentage at the right hand side of the table. The percentage shows the change with respect to reference specimens. The graphical representation of the table is provided in Figure 5.7. Although no apparent change is observed in the axial stress-strain diagram, Figure 5.7 reveals that $E_1$ of 20 MPa cylinder reduced 15% (Table 5.3) but 10 MPa cylinder showed no difference. The reason in the reduction of $E_1$ may be attributed to the durability of the concrete. Since

the first part (nonlinear part) of the curve is concrete dominant part, effect of H-C cycles in this part is apparent. Although the decrease was expected in the low strength concrete, it occurred in 20 MPa concrete. As for $E_2$ no significant difference is observed. Both specimens experienced a slight increase in the CFRP dominant second part.

Therefore, it can be inferred from the observations that H-C cycles performed between -10°C and 50°C on approximately 40% RH may affect the secant modulus of elasticity calculated at the first part of the curve but will not have any significant influence on the slope of the second part of the curve concerning cylindrical specimens.

**Table 5.3 Effect of dry H-C cycles on stiffness properties of CFRP-confined cylindrical specimens**

| Reference Specimens (Group1) | | | | Effect of Dry H-C Cycles (Group 2) | | | | % diff. w.r.t. Group 1 | |
|---|---|---|---|---|---|---|---|---|---|
| **Test Group** | ***$E_1$*, GPa** | ***$E_2$*, GPa** | ***$E_1/E2$*** | **Test Group** | ***$E_1$*, GPa** | ***$E_2$*, GPa** | ***E1/E2*** | ***$E_1$*** | ***$E_2$*** |
| C10-G1-C | 18.35 [6.8] | 0.50 [10.2] | 36.70 | C10-G2-C | 18.66 [18.6] | 0.54 [17.4] | 34.56 | 1.7 | 8.0 |
| C20-G1-C | 18.97 [8.9] | 0.75 [6.8] | 25.29 | C20-G2-C | 16.15 [13.7] | 0.78 [6.0] | 20.71 | -14.9 | 4.0 |

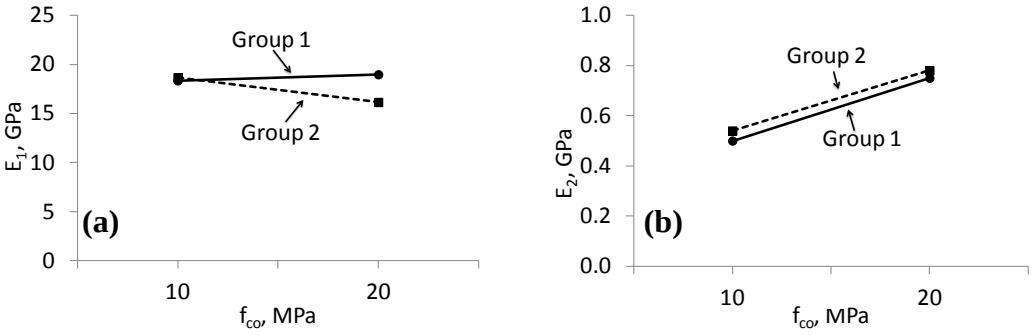


**Figure 5.7. Effect of dry H-C cycles on CFRP-confined cylindrical specimens a) Effect on $E_1$, b) Effect on $E_2$**

Figure 5.8 shows the axial stress-strain behaviors of CFRP-confined prismatic specimens subjected to H-C cycles with comparison with reference specimens. Two distinct behaviors were observed. Specimens with low confinement effectiveness, i.e., specimens with relatively low MCR factors, effect of dry H-C cycles on the behavior were not so significant. In other words, C10-G2-S-25 (MCR=0.23), C15-G2-S-37.5 (MCR=0.23) and C20-G2-S-37.5 (MCR=0.14) were affected slightly from the H-C cycles. The curves almost followed the same trend. As for the specimens having relatively high MCR factor (C10-G2-S-37.5) the effect of dry H-C cycles are more pronounced.

In the figure the effect of wet H-C cycles were also presented. Wet cycles were only performed on C10-G5-S-37.5 and C15-G5-S-37.5. As from the figure, wet H-C cycles affected the behavior of low strength concrete but its effect decreased when the concrete strength increased.

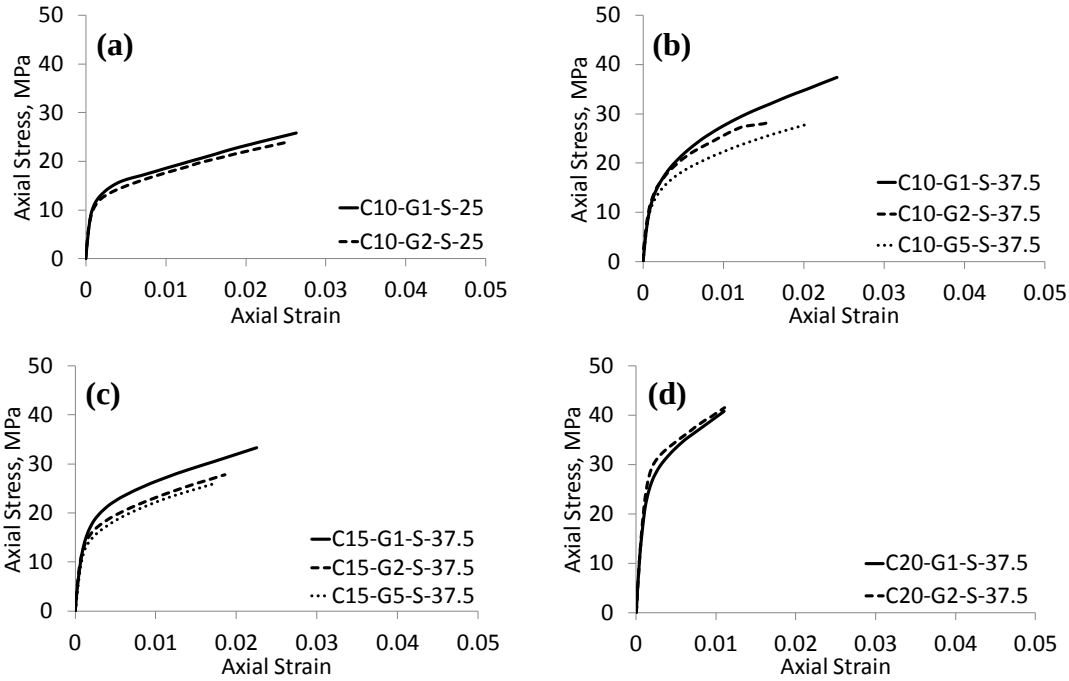


**Figure 5.8. Effect of H-C cycles on behavior of CFRP-confined prismatic specimens, a) 10 MPa with r=25 mm, b) 10 MPa with r=37.5 mm, c) 15 MPa with r=37.5 mm, d) 20 MPa with r=37.5 mm**

Table 5.4 summarizes the effect of dry H-C cycles on $E_1$ and $E_2$ and Figure 5.9 presents the results in a different way. From the figure, it is seen that the effect of dry H-C cycles on $E_1$ decreases with increase in concrete strength as expected. It is interesting to note that dry H-C cycles results in an increase in $E_1$. Specimens became stiffer after the exposures.

The slopes of the linear part were observed to experience approximately 15% reduction.

**Table 5.4 Effect of dry H-C cycles on stiffness properties of CFRP-confined prismatic specimens**

| Reference Specimens (Group1) | | | | Effect of Dry H-C Cycles (Group 2) | | | | % diff. w.r.t. Group 1 | |
|---|---|---|---|---|---|---|---|---|---|
| **Test Group** | ***$E_1$*, GPa** | ***$E_2$*, GPa** | ***$E_1/E2$*** | **Test Group** | ***$E_1$*, GPa** | ***$E_2$*, GPa** | ***E1/E2*** | ***$E_1$*** | ***$E_2$*** |
| C10-G1-S-25 (MCR=0.25) | 16.73 [1.9] | 0.52 [36.5] | 32.17 | C10-G2-S-25 | 19.20 [13.9] | 0.45 [27.6] | 42.67 | 14.8 | -13.5 |
| C10-G1-S-37.5 (MCR=0.38) | 15.71 [10.0] | 0.92 [1.2] | 17.08 | C10-G2-S-37.5 | 21.48 | 0.78 | 27.54 | 36.7 | -15.2 |
| C15-G1-S-37.5 (MCR=0.25) | 16.96 [13.2] | 0.63 [25.4] | 26.92 | C15-G2-S-37.5 | 19.63 [16.6] | 0.57 [0.4] | 34.44 | 15.7 | -9.5 |
| C20-G1-S-37.5 (MCR=0.19) | 27.12 [7.2] | 1.43 [40.8] | 18.97 | C20-G2-S-37.5 | 26.36 [5.5] | 1.24 [1.5] | 21.26 | -2.8 | -13.3 |

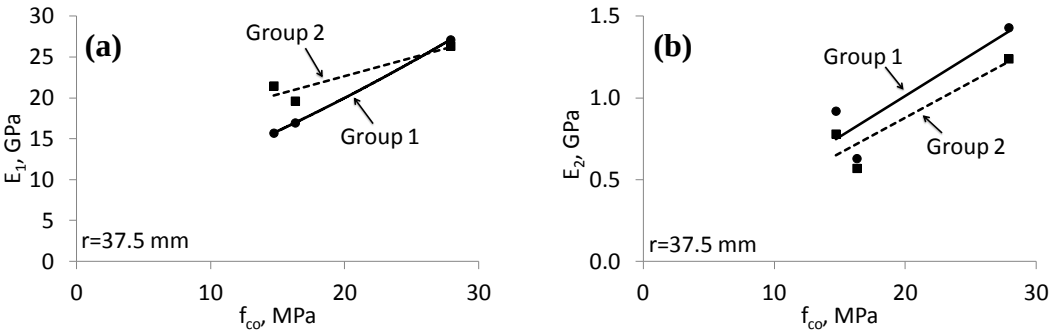


**Figure 5.9. Effect of dry H-C cycles on CFRP-confined prismatic specimens a) Effect on *$E_1$*, b) Effect on *$E_2$***

Effect of wet H-C cycles on *$E_1$* and *$E_2$* of prismatic specimens were tabulated in Table 5.5 and their effects are shown graphically in Figure 5.10. In the figure, effect of dry cycles was also provided. It is seen that effects of wet H-C cycles and dry H-C

cycles are totally different when $E_1$ is of concern. Wet H-C cycles slightly decreased $E_1$ whereas increase was noted in dry H-C cycles. Although $E_1$ was slightly affected from wet cycles, $E_2$ was found to decrease significantly in C10-G5-S-37.5. Almost no difference was recorded in higher concrete strength.

**Table 5.5 Effect of wet H-C cycles on stiffness properties of CFRP-confined prismatic specimens**

| Reference Specimens (Group1) | | | | Effect of Wet H-C Cycles (Group 5) | | | | % diff. w.r.t. Group 1 | |
|---|---|---|---|---|---|---|---|---|---|
| **Test Group** | ***$E_1$*, GPa** | ***$E_2$*, GPa** | ***E1/E2*** | **Test Group** | ***$E_1$*, GPa** | ***$E_2$*, GPa** | ***E1/E2*** | ***$E_1$*** | ***$E_2$*** |
| C10-G1-S-37.5 (MCR=0.38) | 15.71 [10.0] | 0.92 [1.2] | 17.08 | C10-G5-S-37.5 | 15.57 [19.5] | 0.59 [7.8] | 26.39 | -0.9 | -35.9 |
| C15-G1-S-37.5 (MCR=0.25) | 16.96 [13.2] | 0.63 [25.4] | 26.92 | C15-G5-S-37.5 | 15.80 [38.9] | 0.62 [20.5] | 25.48 | -6.8 | -1.6 |

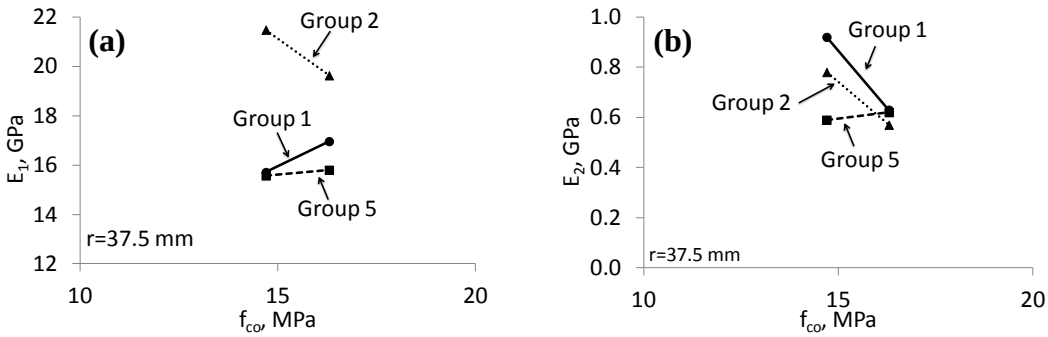


**Figure 5.10. Comparison of dry and wet H-C cycles a) $E_1$, b) $E_2$**

As a conclusion, it can be said that:

- Dry H-C cycles may result in an increase in $E_1$ for CFRP-confined prismatic specimens
- Increase in $E_1$ is proportional to confinement effectiveness. As effectiveness increases $E_1$ increases also.
- The slope in the linear part of the curves ($E_2$) depends on CFRP because concrete does not play an active role above the unconfined concrete strength.
- $E_2$ seems to decrease 10-15% in CFRP-confined prismatic specimens.
- Wet H-C cycles slightly affect $E_1$.

### 5.3.2 Effect of H-C cycles on ultimate strength ($f_{cc}$)

Ultimate strength of CFRP-confined cylindrical specimens was not affected from dry H-C cycles as shown in Table 5.17 and Figure 5.11.

**Table 5.6 Effect of dry H-C cycles on ultimate strength of CFRP-confined cylindrical specimens**

| Reference Specimens (Group1) | | Effect of Dry H-C Cycles (Group 2) | | % diff. w.r.t. Group 1 |
|---|---|---|---|---|
| **Test Group** | **$f_{cc}$ (MPa)** | **Test Group** | **$f_{cc}$ (MPa)** | |
| C10-G1-C | 32.9 [5.1] | C10-G2-C | 32.9 [15.3] | 0.0 |
| C20-G1-C | 47.5 [2.8] | C20-G2-C | 47.3 [4.5] | -0.4 |

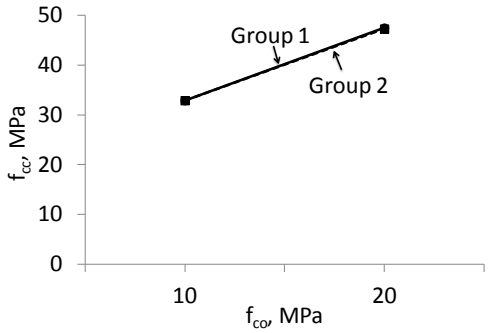


**Figure 5.11. Effect of dry H-C cycles on ultimate strength of CFRP-confined cylindrical specimens**

Effect of H-C cycles on ultimate strength of CFRP-confined prismatic specimens was summarized in Table 5.7. As it is seen, all specimens except C20-G1-S-37.5 exhibited a reduction in ultimate strength under dry H-C cycles. The reduction is high in specimens having relatively high MCR (MCR=0.26). Figure 5.12 shows the change in ultimate strength with unconfined concrete strength for the specimens with 37.5 mm corner radius. As it is seen from the Figure 5.12a, the negative effect of H-C cycles on ultimate strength diminishes with increase in unconfined concrete strength.

Ultimate strength further reduces when specimens are kept in water and exposed to 200 H-C cycles. Since top and bottom faces of those specimens were not sealed and were in direct contact with water, the moisture absorption through the unsealed concrete faces was not avoidable. The further reduction may be attributed to the increase in moisture content, which creates problems in concrete upon H-C process.

**Table 5.7 Effect of H-C cycles on ultimate strength of CFRP-confined prismatic specimens**

| Reference Specimens (Group1) | | Effect of Dry H-C Cycles (Group 2) | Effect of Wet H-C Cycles (Group 5) | Group1 vs Group2 % | Group1 vs Group5 % |
|---|---|---|---|---|---|
| **Test Group** | **$f_{cc}$ (MPa)** | **$f_{cc}$ (MPa)** | **$f_{cc}$ (MPa)** | | |
| C10-G1-S-25 (MCR=0.25) | 25.8 [4.7] | 23.9 [5.1] | --- --- | -7.4 | --- |
| C10-G1-S-37.5 (MCR=0.38) | 37.4 [0.3] | 28.5 --- | 28.0 [7.7] | -23.8 | -25.1 |
| C15-G1-S-37.5 (MCR=0.25) | 33.3 [6.2] | 27.8 [0.0] | 26.1 [4.3] | -16.5 | -21.6 |
| C20-G1-S-37.5 (MCR=0.19) | 40.8 [11.9] | 41.5 [3.5] | --- --- | 1.7 | --- |

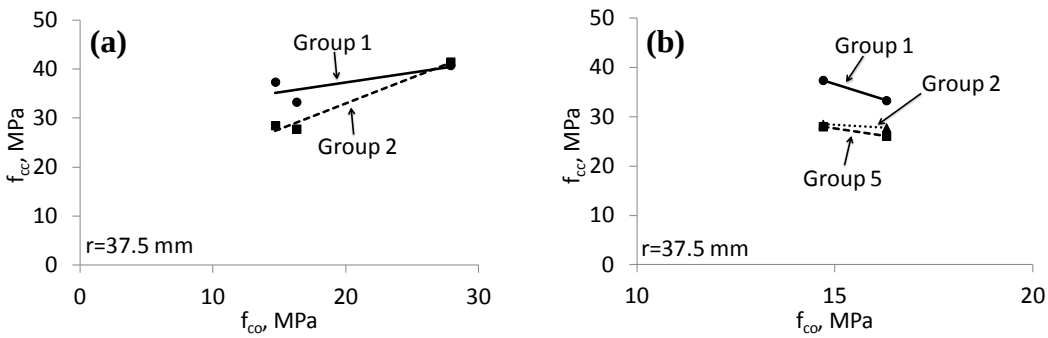


**Figure 5.12. Change in ultimate strength of CFRP-confined prismatic specimens with a) Dry H-C cycles, b) Wet H-C cycles**

CFRP-confined prismatic specimens were found to experience a strength reduction under H-C cycles. The increase in humidity level was observed to further decrease the ultimate strength.

### 5.3.3 Effect of H-C cycles on ultimate strain ($\varepsilon_{cc}$)

Ultimate strain of CFRP-confined cylindrical specimens was noticed to be almost insensitive to dry H-C cycles as seen from Table 5.8 and Figure 5.13. It was decreased 5% upon 200 H-C cycles.

**Table 5.8 Effect of dry H-C cycles on ultimate strain of CFRP-confined cylindrical specimens**

| Reference Specimens (Group1) | | Effect of Dry H-C Cycles (Group 2) | | % diff. w.r.t. Group 1 |
|---|---|---|---|---|
| **Test Group** | $\varepsilon_{cc}$ | **Test Group** | $\varepsilon_{cc}$ | |
| C10-G1-C | 0.042 [5.8] | C10-G2-C | 0.040 [7.0] | -4.8 |
| C20-G1-C | 0.035 [9.9] | C20-G2-C | 0.033 [11.7] | -5.7 |

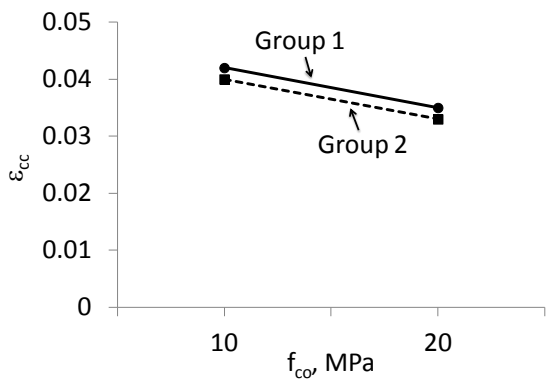


**Figure 5.13. Effect of dry H-C cycles on ultimate strain of CFRP-confined cylindrical specimens**

The effect of H-C cycles on ultimate strain of CFRP-confined prismatic specimens was given in Table 5.9. As it is seen in either dry or wet H-C cycles all specimens experienced a strain decrease except C20-G1-S-37.5. The decrease was well pronounced in 10 and 15 MPa specimens having 37.5 mm corner radius.

Figure 5.14 shows the variation of strain with unconfined concrete strength when specimens were subjected to H-C cycles. The influence of dry H-C cycles in Figure 5.14a was found to decrease with increase in unconfined concrete strength. As for wet H-C cycles, 10 MPa specimens with r=37.5 mm experienced less strain decrease when compared to dry H-C cycles. This can be attributed to the softening of the epoxy with increase in moisture content [54]. However, same conclusion is not valid for 15 MPa specimens.

Therefore, it can be generalized that H-C cycles has negative effect on ultimate strain of CFRP-confined prismatic specimens. The effect reduces with increase in unconfined concrete strength and may increase with humidity level.

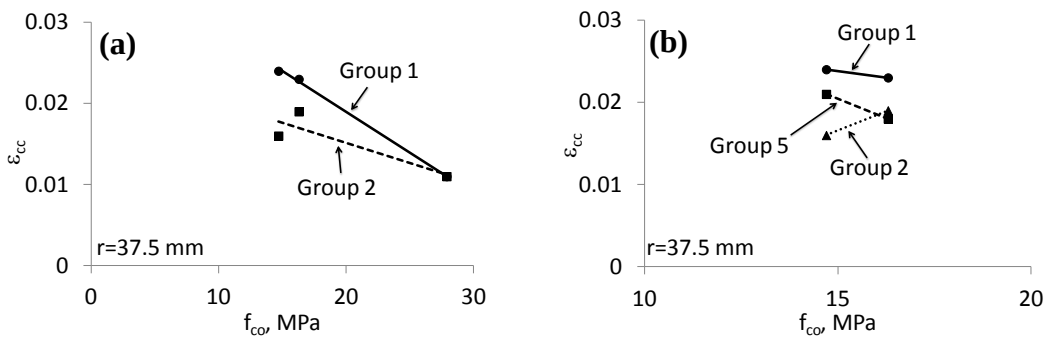


**Figure 5.14. Change in ultimate strain of CFRP-confined prismatic specimens with a) Dry H-C cycles, b) Wet H-C cycles**

**Table 5.9 Effect of H-C cycles on ultimate strain of CFRP-confined prismatic specimens**

| Reference Specimens (Group1) | | Effect of Dry H-C Cycles (Group 2) | Effect of Wet H-C Cycles (Group 5) | Group1 vs Group2 % | Group1 vs Group5 % |
|---|---|---|---|---|---|
| **Test Group** | $\varepsilon_{cc}$ | $\varepsilon_{cc}$ | $\varepsilon_{cc}$ | | |
| C10-G1-S-25 (MCR=0.25) | 0.026 [24.3] | 0.025 [21.9] | --- --- | -3.8 | --- |
| C10-G1-S-37.5 (MCR=0.38) | 0.024 [3.1] | 0.016 | 0.021 [13.1] | -33.3 | -12.5 |
| C15-G1-S-37.5 (MCR=0.25) | 0.023 [9.8] | 0.019 [2.7] | 0.018 [18.3] | -17.4 | -21.7 |
| C20-G1-S-37.5 (MCR=0.19) | 0.011 [8.5] | 0.011 [11.7] | --- --- | 0.0 | --- |

## 5.4 EFFECT OF OUTDOOR EXPOSURE ON BEHAVIOR OF CFRP-CONFINED CONCRETE COLUMNS

Structural elements located at the perimeter of a building are in direct contact with outdoor exposure such as UV radiation, heating-cooling cycles, freeze-thaw cycles, wet dry cycles etc. If these elements have proper protection, the effect of the exposures would reduce. However, if the protection is not sufficient, they may deteriorate and their performance may decrease [4, 53].

In this experimental study, it was assumed that concrete columns were in direct exposure of outdoor environment without having any protection such as plaster and paint. Four types of specimens were wrapped with one layer of CFRP as explained in previous chapters and exposed to outdoor exposure for 530 days under direct sunlight as given in Chapter3. During these exposures, specimens were exposed to 61 freeze-thaw cycles. 222 days were recorded to have RH greater than 80%. These

specimens included C10-G6-C, C10-G6-S-25, C10-G6-S-37.5 and C15-G6-S-37.5. 20 MPa specimens were not utilized in these tests.

### 5.4.1 Effect of outdoor exposure on axial stress-strain diagram

Figure 5.15 presents the axial stress-strain behaviors of the specimens exposed to outdoor exposure with the comparison of reference specimens. As seen from the figures, the diagrams of both 10 MPa cylindrical (C10-G6-C) and 10 MPa prismatic specimens with 25 mm corner radius (C10-G6-S-25) deviates after reaching the unconfined concrete strength. Both specimens experienced higher transition stresses, which can be attributed to the strength increase in unconfined concrete due to CFRP activation, which might be influenced by the increase in concrete strains due to the exposures.

In Figure 5.16, behaviors of all CFRP-confined specimens were given in the same figure. It is interesting to note that, all prismatic specimens behaved almost identical. Although, previously it was stated that CFRP effectiveness changes with the change in cross-section and unconfined concrete strength, no apparent difference due to these parameters was observed when they were subjected to outdoor exposure. All of the axial stress-strain diagrams followed almost the same path. However, cylindrical specimens were observed to behave differently.

The effect of outdoor exposure on $E_1$ and $E_2$ are summarized in Table 5.10. From the table it is seen that although 10 MPa cylindrical and 10 MPa prismatic specimens with r=25mm experienced a decrease in $E_1$, the other two had increase in modulus. In order to make a reasonable comparison, the effect of outdoor exposure was illustrated in Figure 5.17 for only 10 MPa specimens. As it is seen, prismatic specimen with r=25 mm showed decrease in $E_1$ but increase in $E_2$, which revealed that outdoor exposure had an adverse effect on this specimen. However reverse is true for specimen having 37.5 mm corner radius.

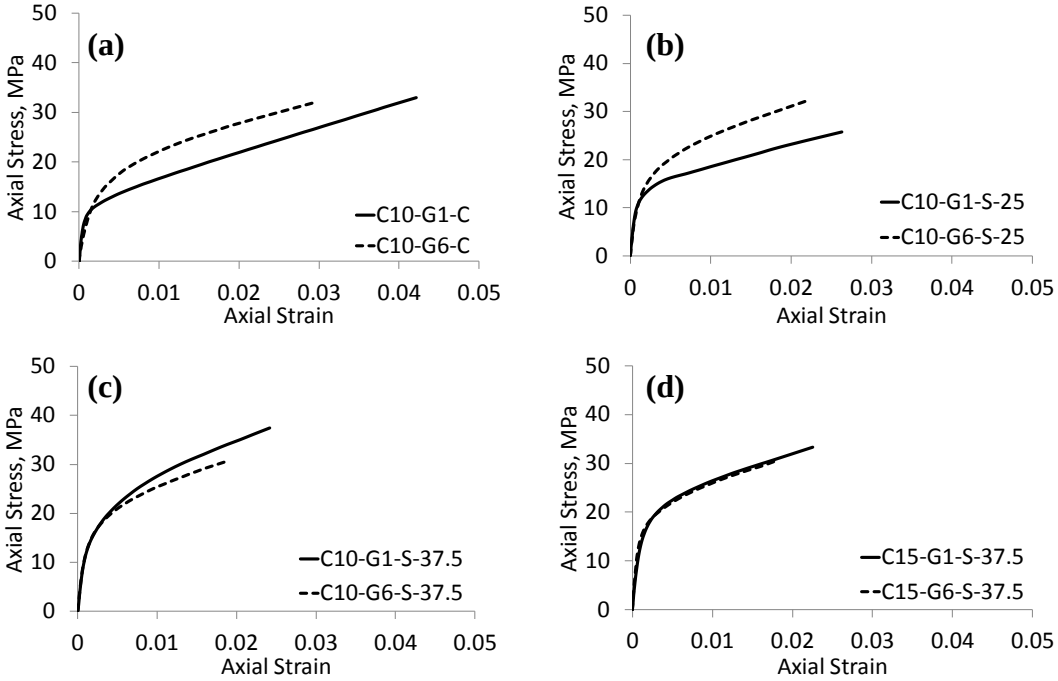


**Figure 5.15. Effect of outdoor exposure on behavior of CFRP-confined specimens a) 10 MPa cylinder, b) 10 MPa prismatic r=25 mm, c) 10 MPa prismatic r=37.5 mm, d) 15 MPa prismatic r=37.5 mm,**

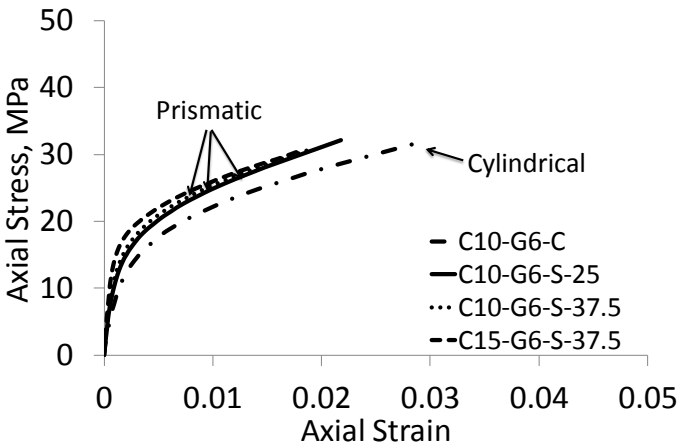


**Figure 5.16. Comparative presentation of the behaviors of CFRP-confined specimens subjected to outdoor exposure**

**Table 5.10 Effect of outdoor exposure on stiffness properties of CFRP-confined concrete**

| Reference Specimens (Group 1) | | | | Effect of Outdoor Exposure (Group 6) | | | | % diff. w.r.t. Group 1 | |
|---|---|---|---|---|---|---|---|---|---|
| **Test Group** | ***$E_1$*, GPa** | ***$E_2$*, GPa** | ***$E_1$/ $E_2$*** | **Test Group** | ***$E_1$*, GPa** | ***$E_2$*, GPa** | ***$E_1$/ $E_2$*** | ***$E_1$*** | ***$E_2$*** |
| C10-G1-C | 18.35 [6.8] | 0.50 [10.2] | 36.70 | C10-G6-C | 10.39 [2.2] | 0.49 [8.8] | 21.20 | -43.4 | -2.0 |
| C10-G1-S-25 | 16.73 [1.9] | 0.52 [36.5] | 32.17 | C10-G6-S-25 | 12.85 [24.3] | 0.66 [8.0] | 19.47 | -23.2 | 26.9 |
| C10-G1-S-37.5 | 15.71 [10.0] | 0.92 [1.2] | 17.08 | C10-G6-S-37.5 | 17.55 [27.3] | 0.63 [3.6] | 27.86 | 11.7 | -31.5 |
| C15-G1-S-37.5 | 16.96 [13.2] | 0.63 [25.4] | 26.92 | C15-G6-S-37.5 | 23.32 [20.2] | 0.60 [22.6] | 38.87 | 37.5 | -4.8 |

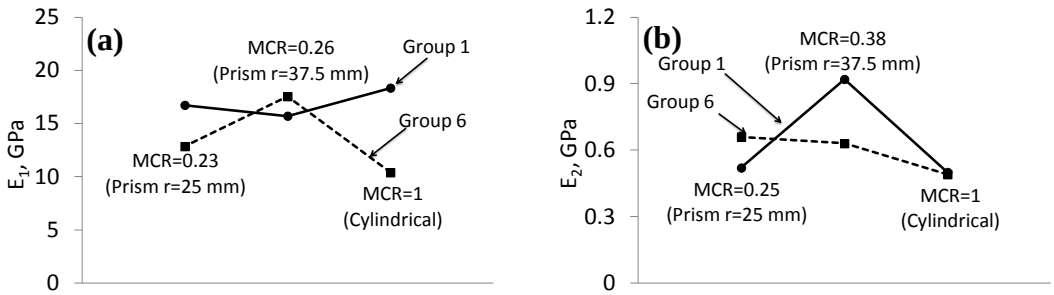


**Figure 5.17. Effect of outdoor exposure on a) *$E_1$*, b) *$E_2$***

### 5.4.2 Effect of outdoor exposure on ultimate strength ($f_{cc}$)

Outdoor exposure seems to reduce the ultimate strength of CFRP-confined specimens except 10 MPa prismatic specimens with r=25 mm, which experienced 24% increase (Table 5.11 and Figure 5.18). CFRP is known to be durable under UV

radiation, freeze-thaw and humidity changes, which are combined in the outdoor exposure. However, the adhesives that are used to bond CFRP to concrete are reported to be affected by these exposures [4, 53, 54]. Since those adhesives serve load transfer between concrete and CFRP, any degradation in their mechanical properties will lead to a reduced confinement effect, which has direct influence on confined concrete strength.

Therefore, the reduction in strength can be attributed to the degradation in bond between CFRP, epoxy based adhesives and concrete. However, further research is necessary to better understand the behavior.

**Table 5.11 Effect of outdoor exposure on ultimate strength of CFRP-confined specimens**

| Reference Specimens (Group1) | | Effect of Outdoor Exposure (Group 6) | | % diff. w.r.t. Group 1 |
|---|---|---|---|---|
| **Test Group** | **$f_{cc}$ (MPa)** | **Test Group** | **$f_{cc}$ (MPa)** | |
| C10-G1-C | 32.9 [5.1] | C10-G6-C | 31.9 [9.4] | -3.0 |
| C10-G1-S-25 | 25.8 [4.7] | C10-G6-S-25 | 32.1 [5.0] | 24.4 |
| C10-G1-S-37.5 | 37.4 [0.3] | C10-G6-S-37.5 | 30.7 [3.5] | -17.9 |
| C15-G1-S-37.5 | 33.3 [6.2] | C15-G6-S-37.5 | 30.5 [0.1] | -8.4 |

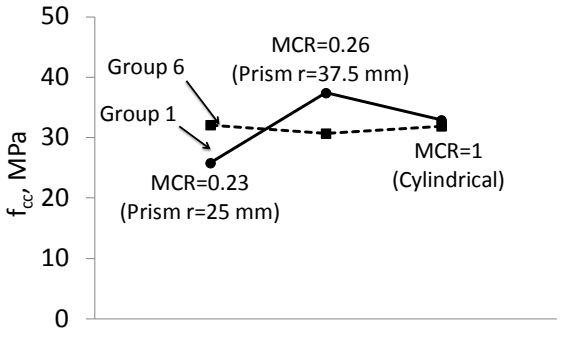


**Figure 5.18. Effect of outdoor exposure on ultimate strength of CFRP-confined specimens**

### 5.4.3 Effect of outdoor exposure on ultimate strain ($\varepsilon_{cc}$)

For specimens subjected to outdoor exposure, ultimate strains were found to be lower as compared to the reference one. In cylindrical specimens, strain decrease is more pronounced (Table 5.12 and Figure 5.19). Ultimate strains were all found to decrease around 15 and 30%. It should be kept in mind that top and bottom ends of the specimens were not sealed and they were in direct contact with environmental exposures. Specimens were subjected to moisture attack at these faces and increase in moisture content may result in deterioration during freeze-thaw action. Moreover, fiber-epoxy-concrete interaction may be weakened during the combined exposures, such as UV radiation, freeze-thaw, humidity etc.

As a conclusion, it can be said that, outdoor exposure reduces the ultimate strain of CFRP-confined specimens in the order of 15 to 30%.

**Table 5.12 Effect of outdoor exposure on ultimate strain of CFRP-confined specimens**

| Reference Specimens (Group1) | | Effect of Outdoor Exposure (Group 6) | | % diff. w.r.t. Group 1 |
|---|---|---|---|---|
| **Test Group** | $\varepsilon_{cc}$ | **Test Group** | $\varepsilon_{cc}$ | |
| C10-G1-C | 0.042 [5.8] | C10-G6-C | 0.029 [22.2] | -31.0 |
| C10-G1-S-25 | 0.026 [24.3] | C10-G6-S-25 | 0.022 [11.8] | -15.4 |
| C10-G1-S-37.5 | 0.024 [3.1] | C10-G6-S-37.5 | 0.019 [6.4] | -20.8 |
| C15-G1-S-37.5 | 0.023 [9.8] | C15-G6-S-37.5 | 0.018 [16.2] | -21.7 |

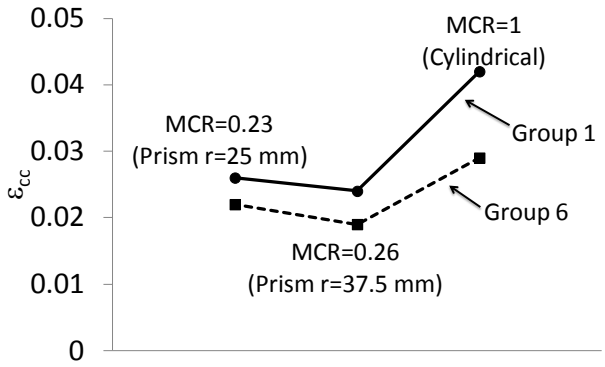


**Figure 5.19. Effect of outdoor exposure on ultimate strain of CFRP-confined specimens**

## 5.5 EFFECT OF SUSTAINED LOADING ON BEHAVIOR OF CFRP-CONFINED CONCRETE COLUMNS

The main aim of this experimental study was to understand the performance of CFRP-confined concrete columns when they were subjected to H-C cycles and sustained loading (SL). In this respect, first set of cylindrical specimens having 10 MPa strength were prepared and wrapped with one layer of CFRP providing an overlap of 6% of the perimeter. Specimens were then divided into several groups as described in previous chapters. During tests, it was observed that specimens under simultaneous exposure of H-C cycles and SL failed due to the delamination at the overlap region. Although new specimens with same overlap were prepared and tests were repeated, they again failed due to delamination. Therefore, the first observation was made about the overlap length: Overlap length in such specimens should be greater than 6% of the perimeter in order to ensure that delamination will not govern the failure.

### 5.5.1 Effect of SL on axial stress-strain diagram

Figure 5.20 illustrates the behavior of CFRP-confined cylindrical specimens after being subjected to SL (Group 4) and simultaneous exposure of SL and H-C cycles (Group 3). In the figure, results belonged to a sustained loading level of 40% of the axial load capacity. Axial stress-strain behaviors are compared with the reference ones and transition stresses are marked with dots.

The common behavior in specimens is seen in the shape of the axial stress-strain behavior. Although the curves for reference specimens have a smooth transition between first and second part, this transition becomes sharp and clear for the specimens being subjected to SL. As previously stated that the first part of the curve reflects the behavior of unconfined concrete and is governed by concrete itself. It has almost the same axial stiffness and ends about $0.9f_{co}$. Although CFRP has little effect on this part, it is not significant. It becomes active after the axial stress reaches *0.8-*

$0.9f_{co}$, which creates unbearable expansion in the concrete. Since concrete is not able to carry the tensile stresses developed due to this expansion, it redistributes tensile forces to CFRP. Therefore, $0.9f_{co}$ can be considered as the lowest stress level to trigger the CFRP activation. In this respect, in order to make CFRP active while keeping the concrete still dominant, specimens were loaded to a sustained load level of $0.9f_{co}A_c$, which corresponded to 40% of the axial load capacity of CFRP-confined concrete ($0.4f_{cc}A_c$). Transition zone starts at this stress level. As the CFRP is active beyond this zone, second part of the curve is mainly governed by CFRP.

Different from the behavior of reference specimens, transition stress increases when specimens are under sustained loading (SL). Under the SL, specimens contract in axial direction whereas they tend to expand in lateral direction due to Poisson's effect. Keeping the axial stress level in the concrete the same for a long time, specimens undergo creep effect. The increase in axial strains due to creep increases lateral expansion, thus it increases the tensile forces developed in CFRP. As the tensile stress increases in CFRP, confining stress in concrete increases also.

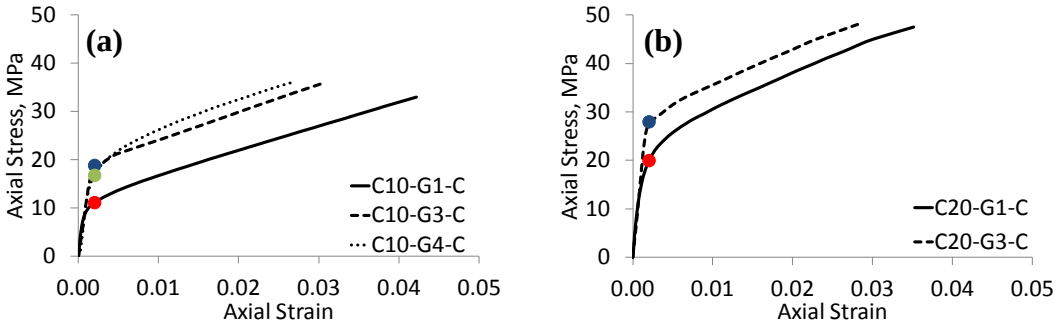


**Figure 5.20. Effect of SL on behavior of CFRP-confined cylindrical specimens a) 10 MPa, b) 20 MPa**

Secant moduli of elasticity ($E_1$) were found to decrease with simultaneous exposures of H-C cycles and SL as shown in Table 5.13. However, it was seen that, the reduction was less for higher strength concrete. Although in the literature $E_1$ for 40 and 50 MPa specimens was noted to increase under only SL [45], it was not the case in very low concrete strength (10 MPa).

The slope in linear part of the curve was observed to increase due to SL and simultaneous exposure of H-C cycles and SL, but the increase was less in higher strength concrete (Figure 5.21).

**Table 5.13 Effect of H-C cycles and SL on stiffness properties of CFRP-confined cylindrical specimens**

| Reference Specimens (Group 1) | | | | Effect of H-C and SL (Group 3) | | | | % diff. w.r.t. Group 1 | |
|---|---|---|---|---|---|---|---|---|---|
| **Test Group** | **$E_1$, MPa** | **$E_2$, MPa** | **$E_1/E_2$** | **Test Group** | **$E_1$, MPa** | **$E_2$, MPa** | **$E_1/E_2$** | **$E_1$** | **$E_2$** |
| C10-G1-C | 18.35 [6.8] | 0.50 [10.2] | 36.70 | C10-G3-C | 11.63 [26.4] | 0.61 [13.0] | 19.07 | -36.6 | 22.0 |
| C20-G1-C | 18.97 [8.9] | 0.75 [6.8] | 25.29 | C20-G3-C | 16.82 [29.1] | 0.78 [6.6] | 21.56 | -11.3 | 4.0 |

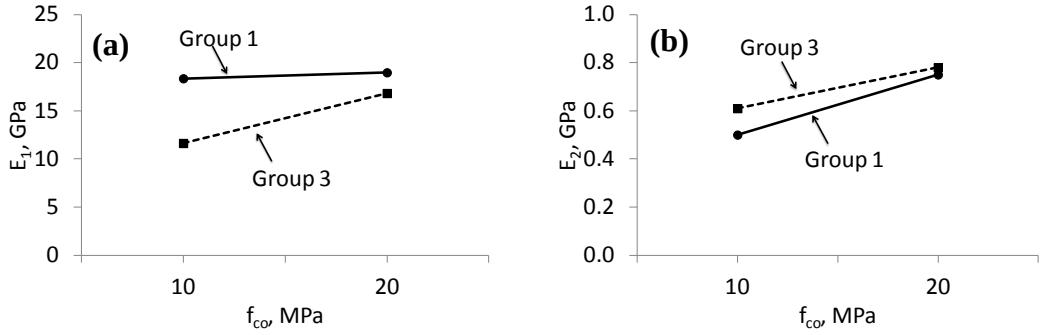


**Figure 5.21. Effect of H-C cycles and SL on stiffness properties of CFRP-confined cylindrical specimens a) Effect on $E_1$, b) Effect on $E_2$**

The axial stress-strain diagrams of prismatic specimens confined with CFRP were given in Figure 5.22. In the figure, the effect of SL and simultaneous exposure of H-C cycles and SL were provided in comparison with reference specimens. The curves were again observed to deviate from the reference ones as the case in cylindrical specimens. However, the deviation is not so clear in prismatic specimens exposed to H-C cycles and SL. The reason can be attributed to the non-uniform stress distribution in prismatic specimens. As from the effect of only SL, it is seen that although the curve for 10 MPa specimens with r=25 mm deviate too much, it is not valid for the others.

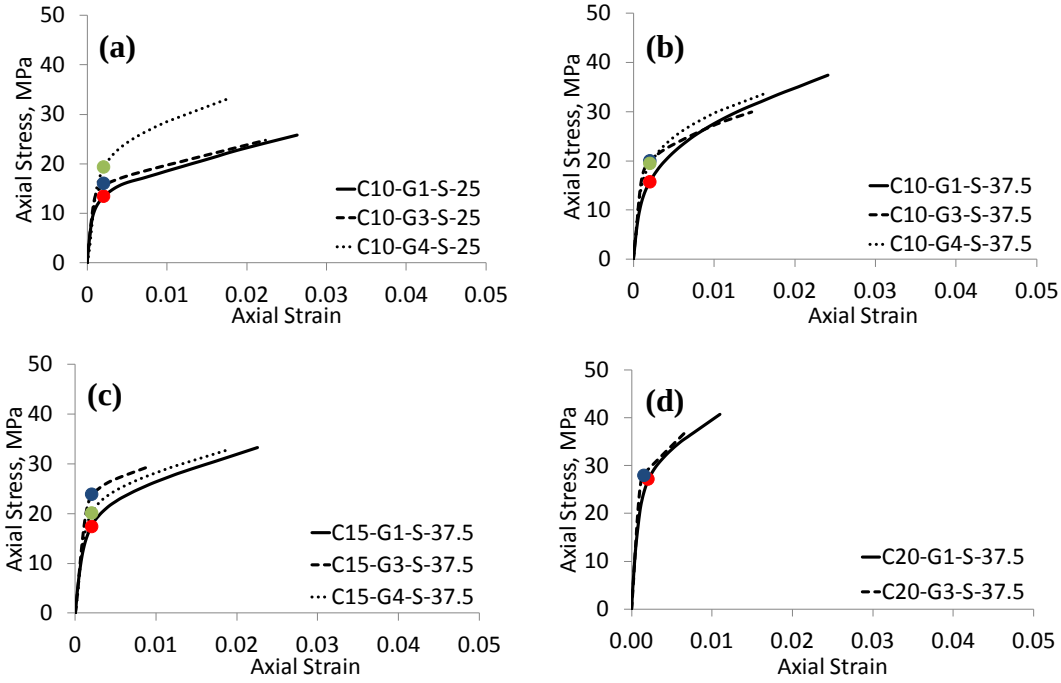


**Figure 5.22. Effect of SL on behavior of CFRP-confined prismatic specimens a) 10 MPa prismatic r=25 mm, b) 10 MPa prismatic r=37.5 mm, c) 15 MPa prismatic r=37.5 mm, d) 20 MPa prismatic r=37.5 mm**

Table 5.14 summarizes the change in $E_1$ and $E_2$ under simultaneous exposure of H-C cycles and SL. From the table, $E_1$ values of very low strength prismatic specimens were found to increase 10-19% under both exposures, whereas it tended to decrease 5% for relatively higher strengths. The reverse was observed for the slope of the linear part; as slope for higher strength concrete increased, it reduced in very low strength concrete. This can be explained by the fact that, CFRP undergoes active state early for very low concrete strength when it is under 40% of SL, which results in creep. Since CFRP become active early due to increase in creep strains, fiber matrix breakage may result in degradation in its stiffness, which directly influences the second part of the curve. As for relatively higher strengths, since creep effect

reduces, the force transfer between concrete and CFRP will not take place early, and CFRP will not experience high stresses.

**Table 5.14 Effect of H-C cycles and SL on stiffness properties of CFRP-confined prismatic specimens**

| Reference Specimens (Group 1) | | | | Effect of H-C cycles and SL (Group 3) | | | | % diff. w.r.t. Group 1 | |
|---|---|---|---|---|---|---|---|---|---|
| **Test Group** | ***$E_1$*, GPa** | ***$E_2$*, GPa** | ***$E_1/E_2$*** | **Test Group** | ***$E_1$*, GPa** | ***$E_2$*, GPa** | ***$E_1/E_2$*** | ***$E_1$*** | ***$E_2$*** |
| C10-G1-S-25 | 16.73 [1.9] | 0.52 [36.5] | 32.17 | C10-G3-S-25 | 19.88 [36.0] | 0.43 [26.0] | 46.23 | 18.8 | -17.3 |
| C10-G1-S-37.5 | 15.71 [10.0] | 0.92 [1.2] | 17.08 | C10-G3-S-37.5 | 17.31 [28.4] | 0.82 [5.4] | 21.11 | 10.2 | -10.9 |
| C15-G1-S-37.5 | 16.96 [13.2] | 0.63 [25.4] | 26.92 | C15-G3-S-37.5 | 16.07 [10.7] | 0.76 [26.5] | 21.14 | -5.2 | 20.6 |
| C20-G1-S-37.5 | 27.12 [7.2] | 1.43 [40.8] | 18.97 | C20-G3-S-37.5 | 25.76 [3.5] | 1.68 [1.7] | 15.33 | -5.0 | 17.5 |

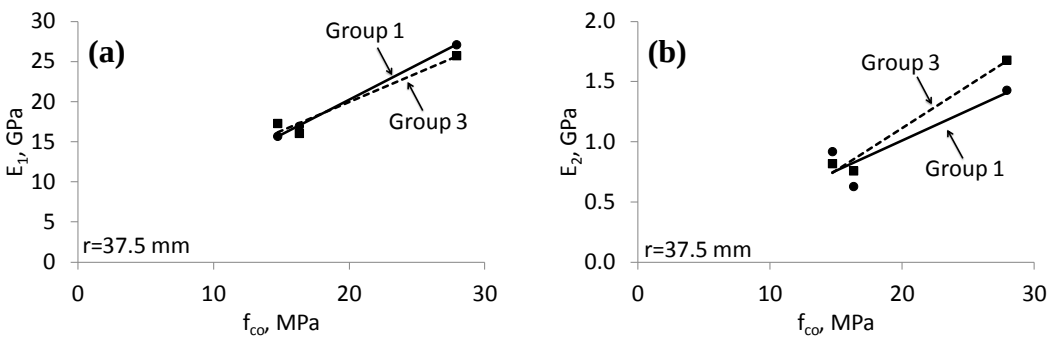


**Figure 5.23. Effect of H-C cycles and SL on stiffness properties of CFRP-confined prismatic specimens a) Effect on *$E_1$*, b) Effect on *$E_2$***

When the effect of only SL is of concern as given in Table 5.15, it is seen that $E_1$ of 10 MPa prismatic specimens with r=25 mm was affected significantly. However, the effect on other specimens was not so significant.

**Table 5.15 Effect of only SL on mechanical properties of CFRP-confined prismatic specimens**

| Reference Specimens (Group 1) | | | | Effect of SL (Group 4) | | | | % diff. w.r.t. Group 1 | |
|---|---|---|---|---|---|---|---|---|---|
| **Test Group** | **$E_1$, GPa** | **$E_2$, GPa** | **$E_1/E_2$** | **Test Group** | **$E_1$, GPa** | **$E_2$, GPa** | **$E_1/E_2$** | **$E_1$** | **$E_2$** |
| C10-G1-S-25 | 16.73 [1.9] | 0.52 [36.5] | 32.17 | C10-G4-S-25 | 11.34 [31.9] | 0.95 [0.95] | 11.94 | -32.2 | 82.7 |
| C10-G1-S-37.5 | 15.71 [10.0] | 0.92 [1.2] | 17.08 | C10-G4-S-37.5 | 17.20 [15.7] | 0.98 [25.1] | 17.55 | 9.5 | 6.5 |
| C15-G1-S-37.5 | 16.96 [13.2] | 0.63 [25.4] | 26.92 | C15-G4-S-37.5 | 13.66 [14.1] | 0.64 [6.0] | 21.34 | -19.5 | 1.6 |

As explained in Chapter 4, three CFRP-confined prismatic specimens were attached with strain gages to determine the axial and lateral strain distributions around the circumference. Results are given in Figure 5.24 in which Figure 5.24a shows the lateral strain distribution whereas Figure 5.24b illustrates the axial strain distribution. The distribution is given so that zero represents the corner at the start of the CFRP and 1 shows corner at the end of CFRP, which is wrapped around the specimen. As it is seen, although strains of all three specimens diverged at some points, they were generally close to each other. Strains at overlap region are marked as blue and strains at rupture zone are painted in red. It is seen that strain distribution is not uniform around the circumference. Although it was expected to have less lateral strains at the overlap region, strains after passing this region were found to be less. This

observation may be understandable together with the axial strain distribution. At the rupture zone, axial strains are higher than the other regions. The increase in axial strains may cause concrete to experience higher expansion thus higher tensile stresses. The increase in tensile stresses may force concrete to crack and exert out-of-plane stresses to CFRP. Since CFRP is weak in shear, the out-of-plane stresses may cause CFRP to fail at relatively low strains.

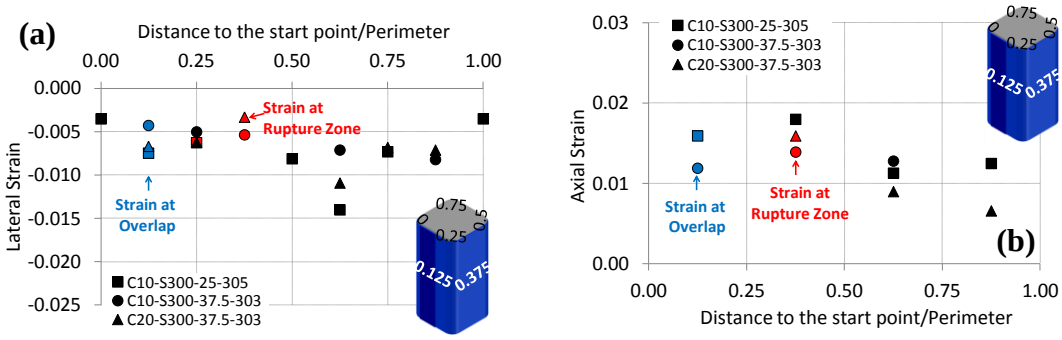


**Figure 5.24. Effect of H-C cycles and SL on strain distribution along the perimeter**

### 5.5.2 Effect of SL on transition stress ($f_{ct}$)

The effect of SL on transition zone is introduced in Table 5.16 for cylindrical specimens and in Table 5.17 for prismatic specimens. From Table 5.16, it is clear that SL which was applied as 40% of axial load capacity increases the transition zone considerably. The increase is almost 70% in 10 MPa specimens in which CFRP effectiveness is greater than the others. With the decrease in the effectiveness, the rate of increase in transition stress decreases. It is observed to be 40% for the higher concrete strength.

As for prismatic specimens, Table 5.17 reveals that SL had significant effect on transition stress. However, the transition zone is not as high as the ones in cylindrical specimens because CFRP is less effective in prismatic members. The less increase is observed to be in C20-G3-S-37.5, which have the lowest CFRP-effectiveness, i.e., MCR factor is 0.14 for those specimens.

Both tables were presented in a different way in Figure 5.25. Figure 5.25a shows the effect of corner radius on transition stress whereas Figure 5.25b illustrates the effect of unconfined concrete strength on the transition stress. The rate of increase in transition stress is directly related to some parameters. The first one is the corner radius. From Figure 5.25a, it is seen that the rate of increase in the transition stress reduces with decrease in corner radius. In other words, the rate of increase in transition stress decreases as the CFRP-effectiveness reduces. The other factor affecting this stress level is the unconfined concrete strength ($f_{co}$) as illustrated in Figure 5.25b. Since the effectiveness of CFRP is inversely proportional to $f_{co}$, the increase in $f_{co}$ results in a decrease in the rate of transition stress.

**Table 5.16 Effect of H-C cycles and SL on transition stress ($f_{ct}$) of CFRP-confined cylindrical specimens**

| Reference Specimens (Group 1) | | Effect of H-C cycles and SL (Group 3) | Group 3 vs Group 1 % |
|---|---|---|---|
| **Test Group** | **$f_{ct}$ (MPa)** | **$f_{ct}$ (MPa)** | |
| C10-G1-C | 11.1<br>[3.7] | 18.8<br>[9.3] | 69.4 |
| C20-G1-C | 20.0<br>[2.5] | 28.0<br>[14.2] | 40.0 |

**Table 5.17 Effect of H-C cycles and SL on transition stress ($f_{ct}$) of CFRP-confined prismatic specimens**

| Reference Specimens (Group 1) | | Effect of H-C cycles and SL (Group 3) | Effect of SL (Group 4) | Group 3 vs Group 1 % | Group 4 vs Group 1 % |
|---|---|---|---|---|---|
| **Test Group** | **$f_{ct}$ (MPa)** | **$f_{ct}$ (MPa)** | **$f_{ct}$ (MPa)** | | |
| C10-G1-S-25 | 13.5<br>[10.3] | 16.1<br>[8.5] | 19.4<br>[11.7] | 19.3 | 43.7 |
| C10-G1-S-37.5 | 15.8<br>[2.3] | 20.0<br>[0.0] | 19.5<br>[10.2] | 26.6 | 23.4 |
| C15-G1-S-37.5 | 17.4<br>[5.8] | 23.9<br>[2.7] | 20.1<br>[6.2] | 37.4 | 15.5 |
| C20-G1-S-37.5 | 27.3<br>[14.2] | 28.0<br>[0.1] | ---<br>--- | 2.7 | |

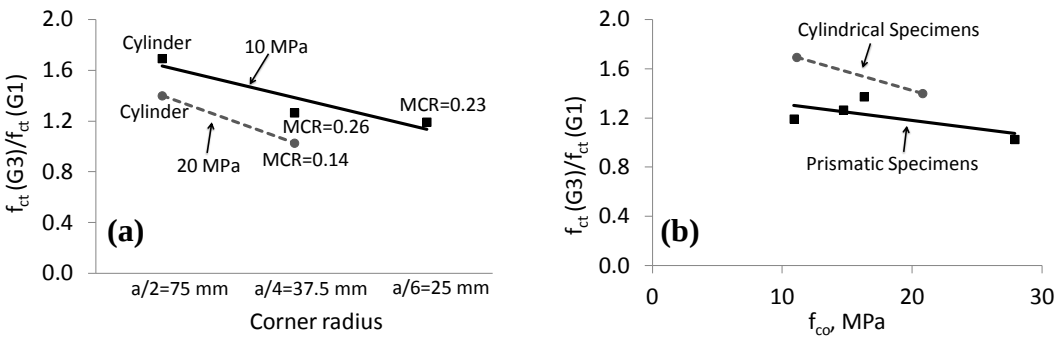


**Figure 5.25. Effect of simultaneous exposure of H-C cycles and SL on $f_{ct}$ a) Change with corner radius b) Change with $f_{co}$**

### 5.5.3 Effect of SL on ultimate strength ($f_{cc}$)

Table 5.18 and Table 5.19 summarize the effect of SL on $f_{cc}$ in cylindrical and prismatic specimens respectively. It was observed from Table 5.18 that, cylindrical specimens exhibited a slight increase in ultimate strength in which the rate of increase reduced with increase in strength. Ultimate strength of 10 MPa cylindrical specimens increased 9% whereas it is only 1% in 20 MPa specimens.

On the other hand, SL effect was noticed to have negative effect on the strength of prismatic specimens (Table 5.19). Although, strength of prismatic specimens reduced under both SL and simultaneous exposure of H-C cycles and SL, C10-G1-S-25 did not follow that trend. It experienced a considerable strength increase, which may be due to the increase in unconfined concrete as time passes because this set was tested 3 years after the preparation. From the table it can be said that, ultimate strength of CFRP-confined prismatic specimens reduces with SL, the reduction can be 20%.

**Table 5.18 Effect of SL on ultimate strength of CFRP-confined cylindrical specimens**

| Reference Specimens (Group 1) | | Effect of H-C cycles and SL (Group 3) | Effect of SL (Group 4) | Group 3 vs Group 1 % | Group 4 vs Group 1 % |
|---|---|---|---|---|---|
| **Test Group** | **$f_{cc}$ (MPa)** | **$f_{cc}$ (MPa)** | **$f_{cc}$ (MPa)** | | |
| C10-G1-C | 32.9 [5.1] | 35.9 [4.8] | 36.1 [1.4] | 9.1 | 9.7 |
| C20-G1-C | 47.5 [2.8] | 48.0 [3.5] | | 1.1 | |

**Table 5.19 Effect of SL on ultimate strength of CFRP-confined prismatic specimens**

| Reference Specimens (Group 1) | | Effect of H-C cycles and SL (Group 3) | Effect of SL (Group 4) | Group 3 vs Group 1 % | Group 4 vs Group 1 % |
|---|---|---|---|---|---|
| **Test Group** | **$f_{cc}$ (MPa)** | **$f_{cc}$ (MPa)** | **$f_{cc}$ (MPa)** | | |
| C10-G1-S-25 | 25.8 [4.7] | 24.8 [11.5] | 33.1 [3.2] | -3.9 | 28.3 |
| C10-G1-S-37.5 | 37.4 [0.3] | 29.9 [5.4] | 33.6 [1.3] | -20.1 | -10.2 |
| C15-G1-S-37.5 | 33.3 [6.2] | 29.3 [5.2] | 32.8 [0.7] | -12.0 | -1.5 |
| C20-G1-S-37.5 | 40.8 [11.9] | 37.2 [0.8] | | -8.8 | |

Figure 5.26 depicts the change in the strength of CFRP-confined specimens with corner radius and $f_{co}$ when they were subjected to both H-C cycles and SL. The values are given with respect to reference specimens. As it is seen from Figure 5.26a, the ultimate strength reduces with the decrease in corner radius. It is believed that the effect of SL is directly related to concrete properties. This can be seen in Figure 5.26b. As confinement effectiveness (MCR) reduces the effect of SL decreases, which shows that with decrease in confinement effectiveness unconfined concrete properties become important. If concrete has low confinement, the increase in unconfined concrete strength ($f_{co}$) results in a decrease in the effect of simultaneous exposure of H-C cycles and SL.

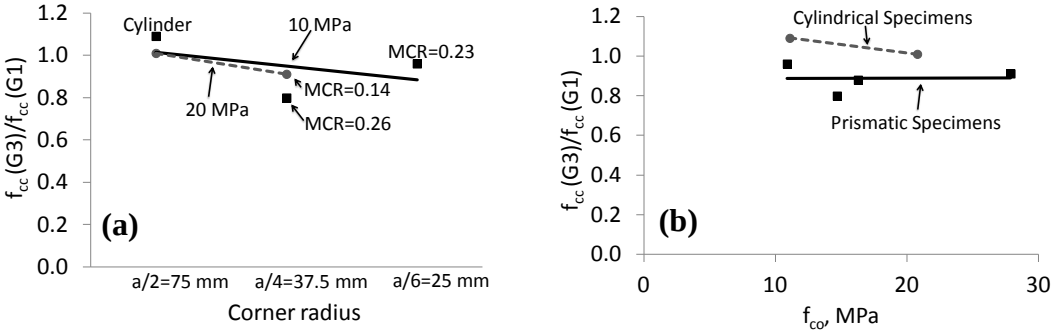


**Figure 5.26. Effect of SL on ultimate strength of CFRP-confined specimens a) Change with corner radius, b) Change with $f_{co}$**

### 5.5.4 Effect of SL on ultimate strain ($\varepsilon_{cc}$)

The drastic effect of SL on CFRP-confined specimens was seen in ultimate strain. Table 5.20 reveals that, ultimate strain of cylindrical specimens decreases 20-26% under simultaneous exposure of H-C cycles and SL. The decrease was observed to be less in higher strength concrete, which can be attributed to the creep properties. Therefore, it can be said that, SL of 40% of the axial load capacity will reduce the ultimate strain of cylindrical specimens confined with CFRP considerably depending on the unconfined concrete strength.

Similar behaviors were also seen in prismatic specimens as given in Table 5.21. 10 MPa prismatic specimens with 25 mm corner radius experienced a strain decrease about 15% when they were under simultaneous exposure, whereas the decrease was doubled when they kept under SL only. Specimens having same strength but greater corner radius (C10-G3-S-37.5) exhibited a 33 to 37% strain decrease. It is interesting to note that, 15 MPa prismatic specimens experienced 61% strain decrease under simultaneous exposure of H-C cycles and SL whereas it was about 17% under SL. In general, it can be said that, SL will results in a considerable decrease in ultimate

strain of CFRP-confined prismatic specimens. The decrease will be minimum 10% higher than that of cylindrical specimens.

The reason for the reduction of strain capacity may be attributed to the residual strains developed due to SL. SL, which was applied as $0.4f_{cc}A_c$, results in a compaction in the concrete, which is not allowed to freely expand laterally because of the CFRP material. The lateral expansion results in lateral strains in the CFRP material. Besides these lateral strains, CFRP may undergo out-of-plane strains due to the localized deformation of concrete, which is the result of the SL. This localized deformation may cause very thin and localized rupture in CFRP. Upon the removal of the load, it is known that elastic recovery takes place and following that, creep recovery occurs. However, some portion of the creep strain remains as residual strain [35]. Considering the CFRP wrapped concrete, because of the abovementioned reasons, deformations in the concrete and the CFRP material may be irrecoverable and results in a high residual strain. The deformations and the compaction action may be the cause of the lower ultimate strain capacities.

**Table 5.20 Effect of SL on ultimate strain of CFRP-confined cylindrical specimens**

| Reference Specimens (Group 1) | | Effect of H-C cycles and SL (Group 3) | Effect of SL (Group 4) | Group 3 vs Group 1 % | Group 4 vs Group 1 % |
|---|---|---|---|---|---|
| **Test Group** | $\varepsilon_{cc}$ | $\varepsilon_{cc}$ | $\varepsilon_{cc}$ | | |
| C10-G1-C | 0.042 [5.8] | 0.031 [5.1] | 0.027 [23.4] | -26.2 | -35.7 |
| C20-G1-C | 0.035 [9.9] | 0.028 [12.2] | | -20.0 | |

**Table 5.21 Effect of SL on ultimate strain of CFRP-confined prismatic specimens**

| Reference Specimens (Group 1) | | Effect of H-C cycles and SL (Group 3) | Effect of SL (Group 4) | Group 3 vs Group 1 % | Group 4 vs Group 1 % |
|---|---|---|---|---|---|
| **Test Group** | $\varepsilon_{cc}$ | $\varepsilon_{cc}$ | $\varepsilon_{cc}$ | | |
| C10-G1-S-25 | 0.026 [24.3] | 0.022 [37.7] | 0.018 [26.7] | -15.4 | -30.8 |
| C10-G1-S-37.5 | 0.024 [3.1] | 0.015 [24.7] | 0.016 [29.1] | -37.5 | -33.3 |
| C15-G1-S-37.5 | 0.023 [9.8] | 0.009 [27.4] | 0.019 [5.3] | -60.9 | -17.4 |
| C20-G1-S-37.5 | 0.011 [8.5] | 0.007 [1.0] | | -36.4 | |

Effect of corner radius and $f_{co}$ on the ultimate strain when specimens were subjected to both H-C cycles and SL was illustrated in Figure 5.27. The values again were given in terms of reference specimens. From Figure 5.27a, it can be said that SL effect increases with decrease in corner radius, i.e., confinement effectiveness. As for change in ultimate strain with $f_{co}$, it can be inferred from Figure 5.27b that unconfined concrete strength is not so effective on the ultimate strain. In other words, the effect of H-C cycles and SL does not change with $f_{co}$.

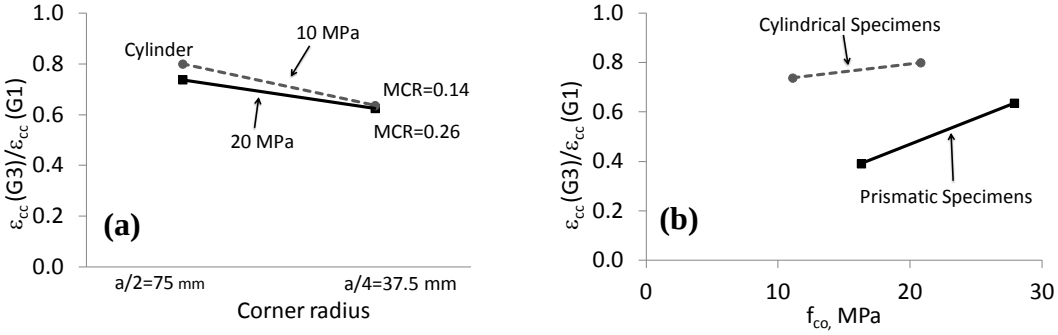


**Figure 5.27. Effect of SL on ultimate strain of CFRP-confined specimens a) Change with corner radius, b) Change with $f_{co}$**

### 5.5.4 Effect of different SL levels on behavior of CFRP-confined prismatic specimens

10 MPa prismatic specimens were tested under two different SL levels. Some specimens were subjected to 40% of their axial load capacity as explained above whereas the remaining was kept under 50-55%. Both set of specimens were also exposed to H-C cycles. Figure 5.28 shows the axial stress-strain behaviors of specimens comparatively. It can be clearly seen that, the transition stress becomes greater with increase in SL level. The other important effect is seen in the strain capacity. Increasing SL level seems to further decrease the ultimate strain. Decrease in ultimate strain makes CFRP-confined specimens more brittle.

The change in strength is not common for both specimens. Although specimens with a corner radius of 25 mm experienced a strength increase, it is not the case in the specimens with higher corner radius.

Table 5.22 summarizes the mechanical properties. Differences in the mechanical properties were calculated with respect to reference specimens. The table was

presented in a different way in Figure 5.29. The effect of SL level on ultimate strength, ultimate strain and transition stress were studied in the figures. From Figure 5.29a it can be seen that SL level slightly affects the ultimate strength of specimens. Although a decrease was noted at 40% of SL, it was found to be recovered at 50% of SL. Since 50% of SL created stresses above the unconfined concrete strength, CFRP would become active upon loading. In addition to the initial state, with creep, due to the stress redistribution between concrete and CFRP, tensile stresses in CFRP increased and higher levels of confinement was attained. However, the change in strength was not directly proportional to SL level

The effect of SL level on strain capacity was illustrated in Figure 5.29b. As previously stated, SL has drastic effect on strain capacity which decreases significantly with increase in SL level. From Table 5.22 it is seen that, the reduction for 10 MPa specimens with 25 mm corner radius is 15% for 40% of SL and 42% for 55% of SL. As for the other type of specimen, the decrease in strain capacity is 37% for 40% of SL and 54% for 50% of SL.

The change in transition stress versus SL level was given in Figure 5.29c. From the figure, it is clear that transition stress tends to increase with increase in SL level. The increase in this stress is attributed to the increase in concrete strength since CFRP becomes active in earlier stress levels due to creep effect. The increase is more pronounced in the specimens with a corner radius of 37.5 mm.

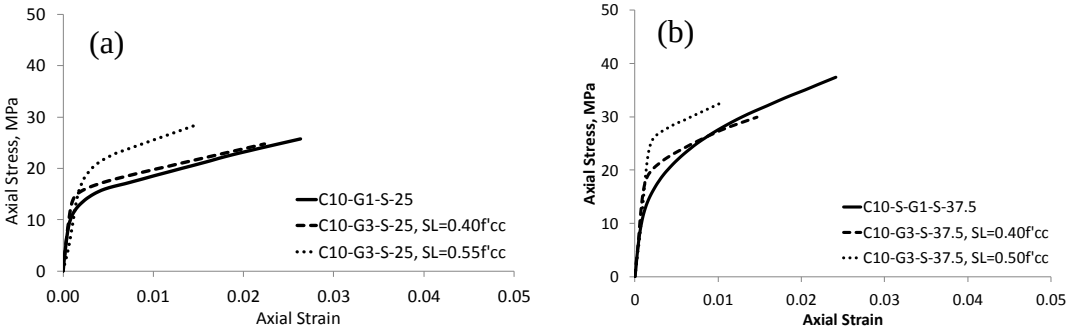


**Figure 5.28. Effect of SL level on behavior of CFRP-confined prismatic specimens**

**Table 5.22 Effect of SL level on mechanical properties of CFRP-confined prismatic specimens**

| Specimen | SL level % | $f_{ct}$ MPa | $f_{cc}$ MPa | $\varepsilon_{cc}$ | Difference % | | |
|---|---|---|---|---|---|---|---|
| | | | | | $f_{ct}$ | $f_{cc}$ | $\varepsilon_{cc}$ |
| 10 MPa Prism (r=25 mm) | 0 | 13.5 [10.3] | 25.8 [4.7] | 0.026 [24.3] | 0.0 | 0.0 | 0.0 |
| | 40 | 16.1 [8.5] | 24.8 [11.5] | 0.022 [37.7] | 19.3 | -3.9 | -15.4 |
| | 55 | 17.5 [12.1] | 28.6 [5.4] | 0.015 [1.4] | 29.6 | 10.9 | -42.3 |
| 10 MPa Prism (r=37.5 mm) | 0 | 15.8 [2.3] | 37.4 [0.3] | 0.024 [3.1] | 0.0 | 0.0 | 0.0 |
| | 40 | 20.0 [0.0] | 29.9 [5.4] | 0.015 [24.7] | 26.6 | -20.1 | -37.5 |
| | 50 | 25.3 [4.2] | 32.8 [9.5] | 0.011 [34.4] | 60.1 | -12.3 | -54.2 |

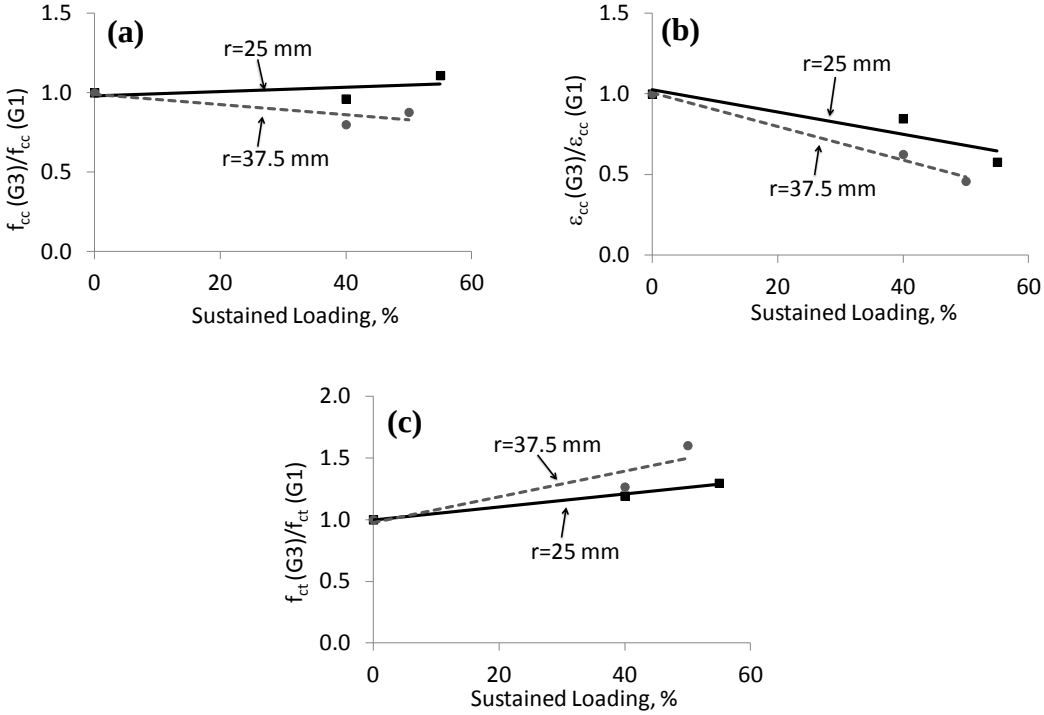


**Figure 5.29. Effect of SL level on a) $f_{cc}$ b) $\varepsilon_{cc}$ c) $f_{ct}$**

# CHAPTER 6

# ANALYTICAL STUDIES

## 6.1 INTRODUCTION

Experimental evaluation on FRP-confined concrete specimens has shown that their stress-strain behavior is significantly affected by many parameters such as, concrete strength and mechanical properties of FRP. Besides these parameters, in this study tests have shown that stress-strain diagram is also affected from temperature changes and sustained stress level. Therefore, sustained stress level and temperature changes should be available as separate parameters in the analytical models. In this chapter, parameters affecting the mechanical properties and stress-strain behavior of FRP-confined concrete are studied by experimental data, which were collected after an extensive literature review. Following the comments on parameters, a stress-strain model for FRP-confined concrete is proposed. In the model, three boundary points (BP) are established. The first one is the initial point of zero stress and zero strain. The second one is the transition point of the stress-strain curve. Finally, the third boundary point is the ultimate point of the curve, which corresponds to ultimate strength and strain. Then the model is compared with the experimental data and it is found that the behavior is predicted well.

## 6.2 BEHAVIOR OF FRP-CONFINED CONCRETE

After an extensive literature review and additional tests conducted in this study, 225 data for cylindrical specimens [16-22, 25, 72, 73, 82, 83, 87-108] and 149 data for prismatic specimens [14, 15, 26, 27, 29, 108, 109] were collected. Those data were sorted in order to study a single parameter while keeping the other parameters the same. Figures were presented such that horizontal axis showed the confinement effectiveness in terms of strength ($f_{cc}/f_{co}$) and strain capacity ($\varepsilon_{cc}/\varepsilon_{co}$), where $f_{co}$ is the unconfined concrete strength, $f_{cc}$ is the confined concrete strength, $\varepsilon_{co}$ represents the unconfined concrete strain corresponding to $f_{co}$ and $\varepsilon_{cc}$ denotes the ultimate strain of confined concrete.

The parameters of $f_{co}$, FRP thickness, diameter, overlap length were discussed in light of literature review whereas the remaining parameters such as heating-cooling cycles, sustained loading and outdoor exposure belong to this dissertation. Besides, effect corner radius includes both data belong to this dissertation and data collected from the literature.

### 6.2.1. Parameters affecting the strength and strain capacities of cylindrical specimens

Experiments related to cylindrical concrete members consist of concrete strength ranging from 6 MPa to 50 MPa. Those data were collected from the literature. In addition to the collected ones, the experimental data available in this dissertation are also used in the analytical studies. The wide variety of the tests is useful to understand the effectiveness of FRP at a wide range of concrete strength.

In Figure 6.1, the influence of unconfined concrete strength ($f_{co}$) on FRP effectiveness is shown, while keeping the FRP properties and specimen size the same [18, 19, 82, 87, 92, 93, 104-106, 108]. As it is seen, FRP effectiveness reduces with

increase in concrete strength, i.e., ultimate strength ($f_{cc}$) and ultimate strain ($\varepsilon_{cc}$) reduce with unconfined concrete strength if the confinement ratio is kept constant.

Figure 6.2 shows the effect of FRP thickness on confinement effectiveness [18, 19, 82]. From the figure, it is seen that, as FRP thickness or the number of FRP layers increases FRP becomes more effective. The effect of FRP thickness is more pronounced in low strength concrete than in high strength concrete.

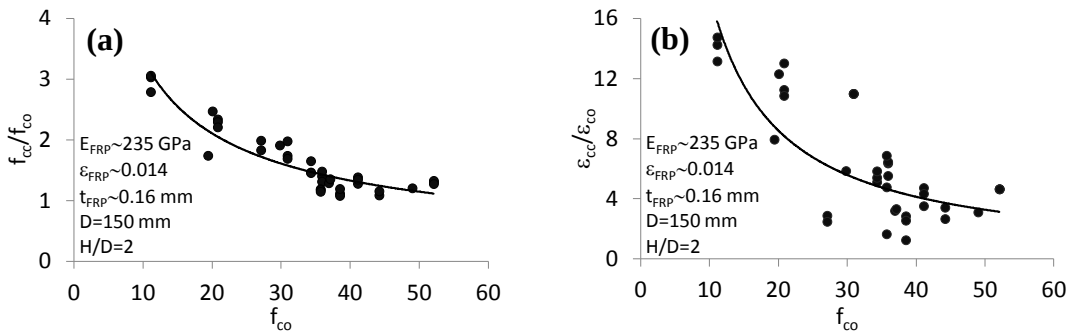


**Figure 6.1. Effect of $f_{co}$ on a) $f_{cc}$, b) $\varepsilon_{cc}$**

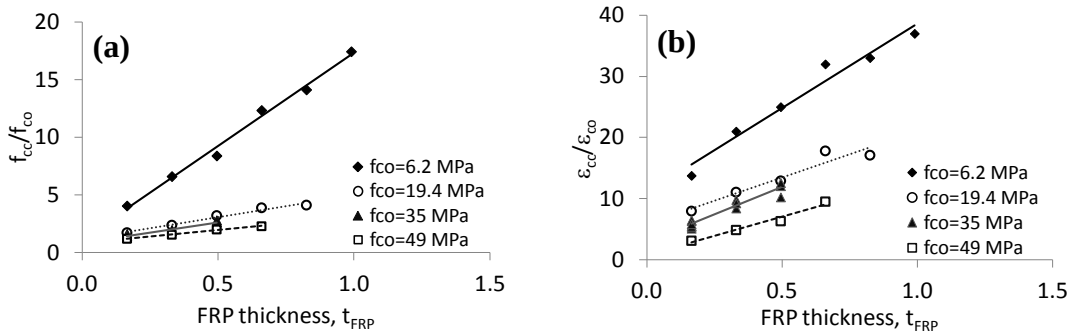


**Figure 6.2. Effect of FRP thickness ($t_{FRP}$) on a) $f_{cc}$, b) $\varepsilon_{cc}$**

Figure 6.3 reveals the relationship between overlap length and confinement effectiveness [82, 91]. Ultimate strength and ultimate strain slightly increase with increase in overlap length. Therefore, to establish a model, this length should also be taken into account.

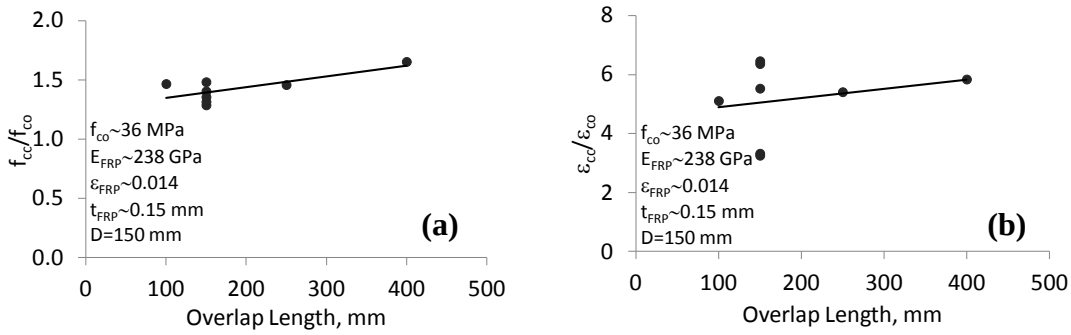


**Figure 6.3. Effect of overlap length on a) $f_{cc}$, b) $\varepsilon_{cc}$**

The effect of sustained loading (SL) level on CFRP-confined concrete strength and strain is shown in Figure 6.4. In these figures, data were taken from Chapter 5, i.e., all data belong to this dissertation. In the figure, two concrete grades are used and the SL is either 0% or 40% of the confined specimen's strength. As it is seen, confined concrete strength slightly increases with sustained stress level (Figure 6.4a), while strain capacity reduces significantly (Figure 6.4b).

Figure 6.5 shows the effect of heating-cooling (H-C) cycles on the ultimate strength and ultimate strain of CFRP-confined concrete. The H-C cycles were applied at a temperature difference of 60°C in which minimum temperature was -10°C and maximum was 50°C. After 200 cycles of H-C, it was observed that strength was not

sensitive to the H-C cycles, whereas strain capacity seemed to reduce with the cycles. However, the reduction is not so pronounced.

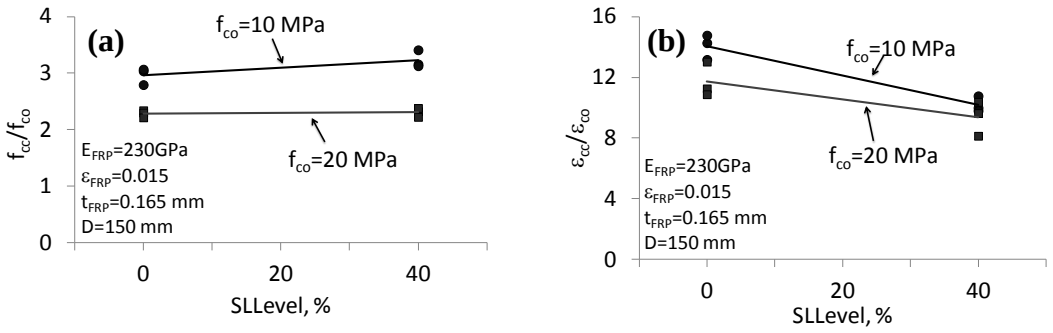


**Figure 6.4. Effect of SL on a) $f_{cc}$ and b) $\varepsilon_{cc}$**

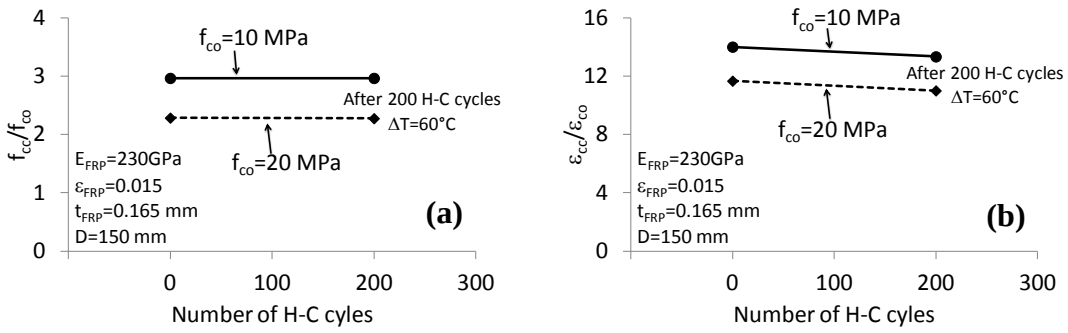


**Figure 6.5. Effect of H-C cycles on a) $f_{cc}$, b) $\varepsilon_{cc}$**

The effect of outdoor exposure on ultimate strength and ultimate strain of CFRP-confined concrete is shown in Figure 6.6. Specimens were kept outside of the laboratory for 530 days as explained in Chapter 3. From the figure, it is seen that

both ultimate strength and ultimate strain were affected from the outdoor exposure. Although the decrease in strain capacity is high, it is not valid for the strength.

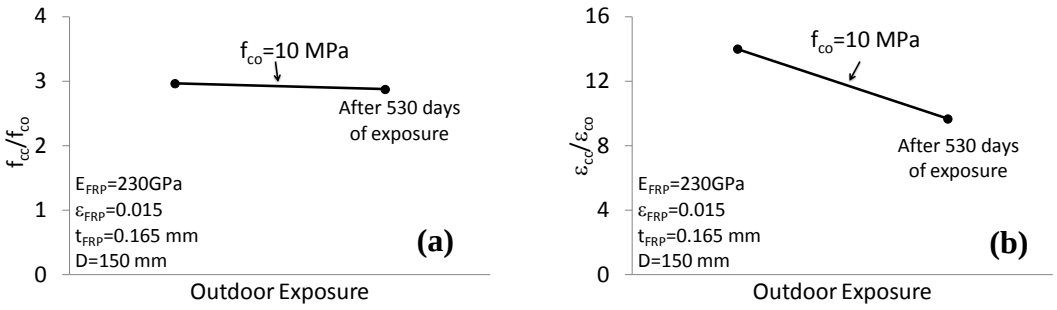


**Figure 6.6. Effect of Outdoor Exposure on a) $f_{cc}$, b) $\varepsilon_{cc}$**

### 6.2.2. Parameters affecting the ultimate strength and strain of square-section prismatic specimens

Behavior of FRP-confined prismatic specimens differs from that of the cylindrical ones. The difference is mainly due to the corner effect in prismatic members. Unlike the cylindrical specimens, whose hoop stress is said to be almost equal along the circumference, in prismatic specimens it is hard to say that equal lateral stress exists along the circumference. Although lateral stress distribution differs for these sections, their general behavior is affected by the same parameters, such as unconfined concrete strength and FRP thickness. Since corner effect is the main parameter for prismatic specimens, their effect on confinement effectiveness is investigated below.

Figure 6.7 shows the effect of corner radius and unconfined concrete strength on FRP effectiveness [99, 104-106, 108]. In the figure, hollow circles show the data belong to this dissertation. Since FRP effectiveness is inversely proportional to unconfined concrete strength, it is located in the denominator. It is seen from the figure that, to achieve strength and strain increase, corner radius should be carefully selected for different unconfined concrete strength; that is, as unconfined concrete strength increases so the corner radius should be.

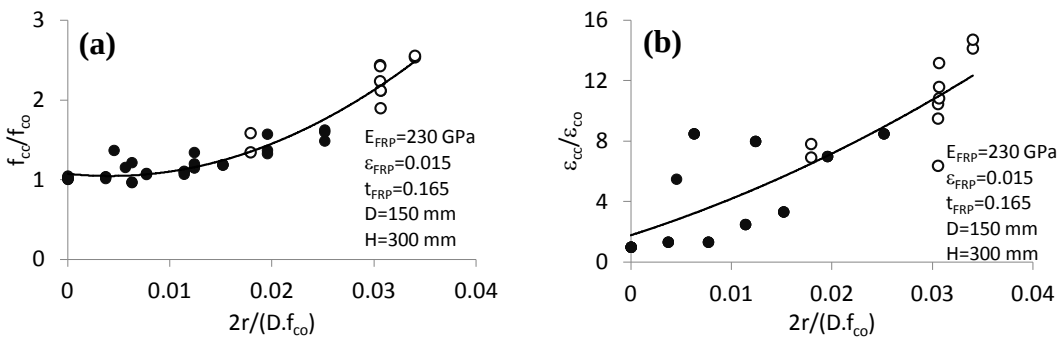


**Figure 6.7. Effect of [$2r/(D.f_{co})$] on a) $f_{cc}$, b) $\varepsilon_{cc}$**

Figure 6.8 shows the SL effect on CFRP-confined concrete strength and strain capacities in which data were taken from Chapter 5. Since SL effect was discussed in Chapter 5 in detail, it was summarized in here. Three grades of concrete (cylinder strengths: 10.9, 14.7 and 27.9 MPa) with two corner radius values (25 and 37.5 mm) were tested under 0, 40 and 50-55% of ultimate stress. From Figure 6.8a, it can be observed that SL effect on ultimate strength of 10.9 MPa specimens with 25 mm corner radius is not significant. However, a slight decrease is observed for both 14.7 and 27.9 MPa specimens with 37.5 mm corner radius. The drastic effect of sustained stress is shown in Figure 6.8b in which change in strain capacities under SL are

illustrated. As it is revealed, strain capacity reduces with increasing SL level. The decrease is observed to be almost 50% for a SL level of 50%.

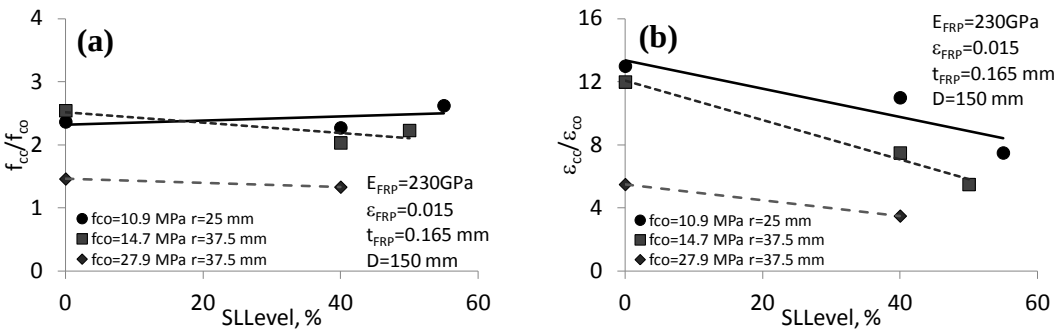


**Figure 6.8. Effect of SL level on a) $f_{cc}$, b) $\varepsilon_{cc}$**

Figure 6.9 reveals the effect of H-C cycles on CFRP-confined prismatic specimens. From Figure 6.9a, it is seen that the ultimate strength is inversely proportional to the temperature cycles for low strength concrete. Strain is also affected negatively from the H-C cycles for low strength concrete. However, the rate of reduction in both strength and strain capacities are not high and decreases with increase in concrete strength.

In Figure 6.10, the effect of outdoor exposure on strength and strain capacities of FRP-confined prismatic specimens are illustrated. After 530 days of exposure, although 10 MPa specimens have a tendency to show a strength increase, strength of 15 MPa specimens decreases. The decrease is found to be higher when compared to the effect H-C cycles because under outdoor exposure specimens were subjected to freeze-thaw cycles, humidity changes and UV radiation simultaneously. As for ultimate strain, it is found to reduce for all specimens after the exposure.

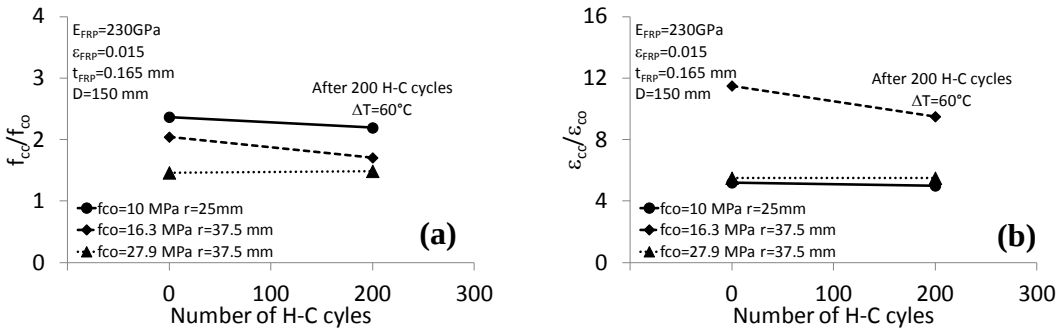


**Figure 6.9. Effect of H-C cycles on a) $f_{cc}$, b) $\varepsilon_{cc}$**

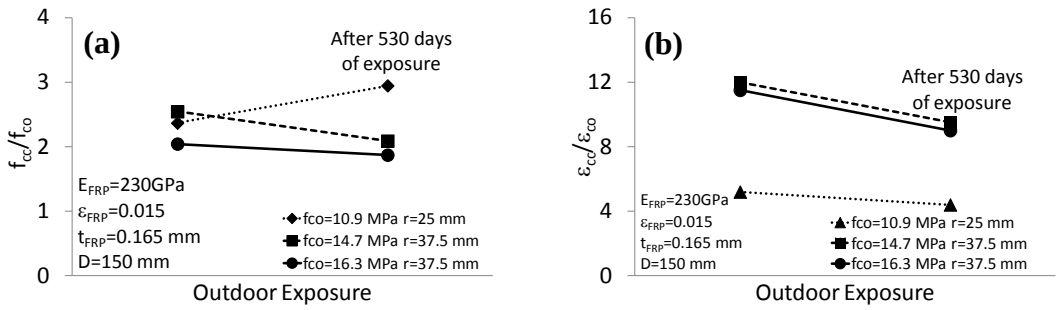


**Figure 6.10. Effect of outdoor exposure on a) $f_{cc}$, b) $\varepsilon_{cc}$**

### 6.2.3. Behavior under axial compression

The typical behavior of FRP-confined concrete and unconfined concrete under axial compression are illustrated in Figure 6.11. As it is seen, the curves have three main points, here called as boundary points (BP). The first BP represents the initial values of stress and strain, which are both zero. The second one is called transition BP, at which curves starts to deviate. The last one gives the ultimate values of strength and strain.

Both confined and unconfined specimens behave almost the same until near $f_{co}$, but after that (Point 2), two behaviors start to deviate from each other. Although unconfined concrete has descending branch after $f_{co}$, FRP-confined concrete shows an improved behavior depending on the parameters discussed in Sections 6.2.1 and 6.2.2. It can be said that first branch of the curve, i.e., up to $f_{co}$, is dominated by concrete since no apparent FRP-effectiveness is observed. After $f_{co}$, since concrete is not able to carry load, FRP becomes effective and enables concrete to show an improved behavior. The strength and ultimate strain depends on the degree of confinement (Point 3).

Figure 6.12 illustrates the effect of SL on FRP-confined concrete behavior. The given experimental curves belong to the specimens which were 150x150x300 mm in dimension with r= 37.5 mm and had 14.7 MPa concrete strength. From the figure, it is seen that, both Point 2 and Point 3 change with sustained stress level. At Point 2, the transition stress increases with increasing sustained stress. As for Point 3 although ultimate stress increases with increasing sustained stress, ultimate strain reduces significantly.

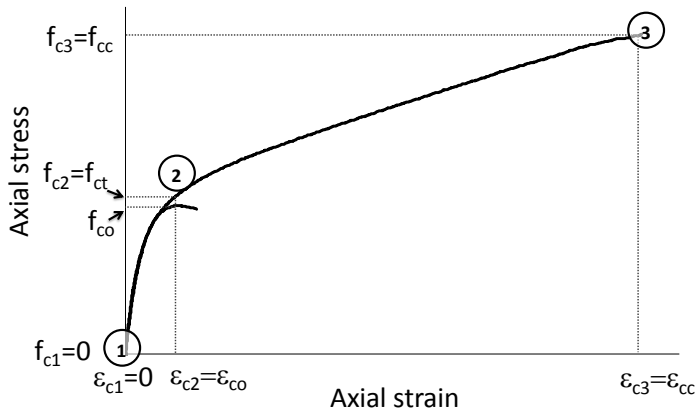


**Figure 6.11. Axial stress-strain behavior of unconfined and FRP-confined concrete under compression**

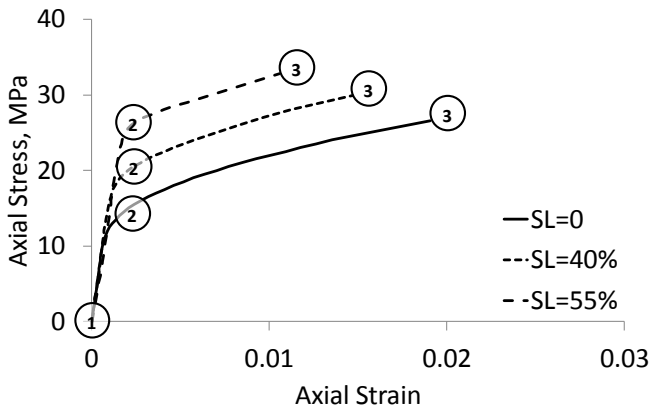


**Figure 6.12. Effect of SL level on FRP-reinforced concrete**

## 6.3 FRP-CONFINED CONCRETE MODEL INCLUDING CREEP AND TEMPERATURE EFFECTS

Modeling has two phases. In the first phase, good estimates of the stress and strain values for the determined BPs are searched via statistical study using the collected experimental data. The estimates are compared with the experimental data. In the second phase, the behavior of FRP-confined concrete is modeled using the stress and strain estimates found in the first part.

The proposed model has some limitations. It was developed for concretes having less than 50 MPa strength and FRP layer up to five plies. It should be noted that the equations given for prismatic columns were applicable to the columns with square-sections.

### 6.3.1. Point 1, Initial BP

Point 1 represents the initial BP at which both stress and strain are zero.

*Point 1 (Initial BP);* $f_{c1}=0$ (6.1)

$\varepsilon_{c1}=0$ (6.2)

### 6.3.2. Point 2, Transition BP

Point 2 denotes the transition BP at which the behavior of unconfined and confined concrete starts to deviate. This point becomes important especially when the specimen is under SL. The strain value at this point is assumed to be equal to *0.002*. However, as it is seen from Figure 6.12 a single value cannot be represented by the stress at this point. Therefore, for the stress value an expression is proposed after the regression analysis, which takes $f_{co}$, $f_{cc}$ and SL as the independent variables (Eq. 6.3). The figures given in Figure 6.13, show the variation of analytical data, which were calculated according to the equations given below, with the experimental data.

*Point 2 (Transition BP);* $$f_{c2} = f_{ct} = f_{co} + (f_{cc} - f_{co})\left(\frac{SL}{100}\right)^{0.75} \quad (6.3)$$

$$\varepsilon_{c2}=\varepsilon_{ct}=0.002 \quad (6.4)$$

In these equations, $f_{co}$ is the cylinder strength of unconfined concrete; $f_{cc}$ is the confined concrete strength and $SL$ is the sustained loading level in percent with respect to the ultimate axial strength.

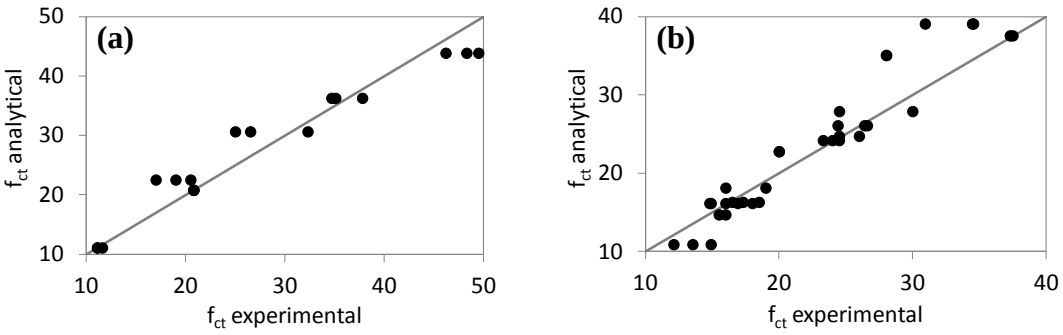


**Figure 6.13. Transition stress estimation of FRP-reinforced concrete**
**a) Cylindrical specimens b) Prismatic specimens**

### 6.3.3. Point 3, Final BP

Point 3 defines the ultimate strain value and corresponding stress value and is called final BP. These values are established using the collected experimental data.

#### *6.3.3.1. Ultimate axial strength estimation*

The general equation for strength of confined concrete was previously introduced by Richart et al. [9, 110] for reinforced concrete specimens as in Eqn. 6.5. In this equation, Richart et al. determined $k_1$ as *4.1* and *c* as *1.0* for reinforced concrete. This equation was taken as the basis for the estimate of the strength of confined concrete. Several authors modified the equation to model the strength of FRP-confined concrete [3, 13, 19, 83, 91-93, 111, 112]. The models either consist of two constants ($k_1$ and *c*) [13, 92, 111]; i.e., nonlinear relationship, or single constant ($k_1$, $c=1$) [3, 83, 91, 93, 112]; i.e., linear relationship.

$$f_{cc} = f_{co}\left[1 + k_1\left(\frac{f_l}{f_{co}}\right)^c\right] \tag{6.5}$$

While estimating the strength capacity of an FRP-confined concrete, parameters discussed in Sections 6.2.1 and 6.2.2 should be considered. From the abovementioned parameters, it can be said that corner radius, FRP thickness, overlap length and sustained stress level are proportional to FRP effectiveness whereas diameter of the specimen, unconfined concrete strength and environmental factors are inversely proportional.

Since the effect of FRP confinement is different for both cylindrical and prismatic members, a single equation is hard to be adapted. Therefore, in order to simplify the problem, the proposed strength equation consists of a constant that is different for cylindrical and prismatic specimens as shown in Eqn. 6.6.

$$f_{cc} = f_{co}\left[1 + k_1\left(\frac{2r}{D}\frac{f_l}{f_{co}}\right)^{1.3}\right]CT \tag{6.6}$$

$$f_l = \frac{2f_{FRP} * t_{eff}}{D} \tag{6.7}$$

$$t_{eff} = \left(nt_{FRP} + t_{FRP}\frac{l_{overlap}}{P}\right) \tag{6.8}$$

From the regression analysis, the unknown parameter $k_1$, which is the strength coefficient for Point 3, is found to be *2.7* for cylindrical specimens and *5* for square specimens. In the equations, $r$ is the corner radius of the prismatic specimen and it is the radius for cylindrical specimens, $D$ is the diameter of the specimen for cylinders and side width for the square section, $f_l$ is the confinement effectiveness, $f_{co}$ is the cylinder strength of unconfined concrete, $f_{FRP}$ is the tensile strength of FRP, $t_{FRP}$ is the thickness of FRP, $n$ is the number of FRP layers, $l_{overlap}$ is the overlap length of final wrapping, $P$ is the perimeter of the specimen, $C$ is the correction factor for creep effect and $T$ is the factor considering temperature effect.

Since strength of a confined concrete specimen is affected by sustained stress level, environmental exposure and temperature changes, those parameters were taken into

account by correction factors. Sustained stress level is introduced as the percentage of the axial strength. The correction for SL level (Eqn. 6.9) is found from linear regression analysis and is the same for both cylindrical and prismatic specimens. However, the correction factor for temperature changes is evaluated to be constant (Eqn. 6.10).

$$C = \left(1 + 0.3\frac{SL}{100}\right) \tag{6.9}$$

$$T = 0.95 \tag{6.10}$$

The main difference of Eqn. 6.6 is that, it uses effective thickness approach and considers the corrections for exposures. The equation is calibrated with the collected data points.

In Figure 6.14, the estimated strength of FRP-confined cylindrical specimens and the experimental data are given comparatively. Figure 6.14a shows all data that includes data from literature and data belong to this dissertation. Data from literature do not include any temperature and SL effect. It should be kept in mind that, the equation for strength is calibrated using all data. Figure 6.14b illustrates the data taken from this dissertation. As it is seen, the strength model gives conservative estimates for the data from this dissertation.

The strength estimates for prismatic specimens were given in Figure 6.15 considering all data and data from this dissertation separately. All data again includes data collected from literature and data taken from this dissertation. The prediction is conservative for the data belong to this study (Figure 6.15b).

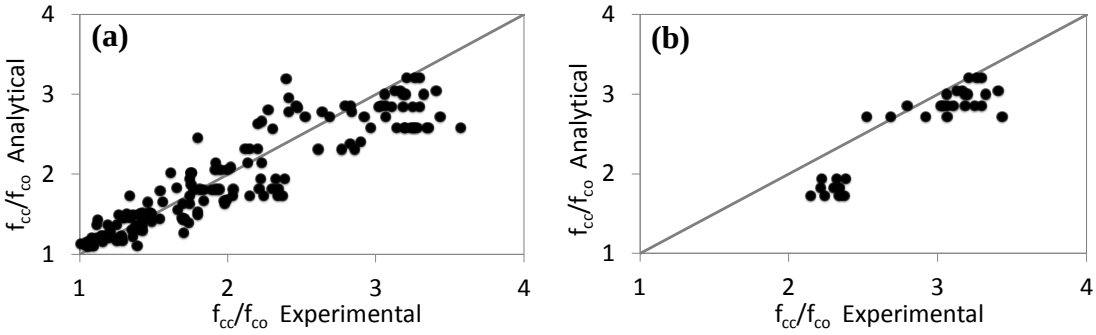


**Figure 6.14. Strength estimation of FRP-confined cylindrical specimens**

**a) All data b) Data from this dissertation**

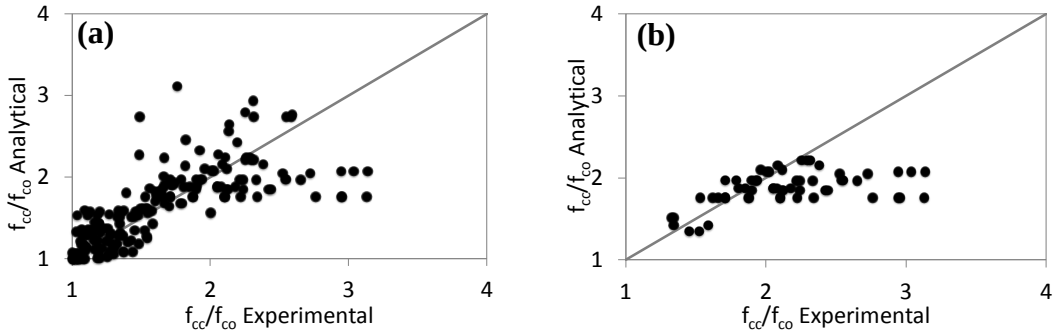


**Figure 6.15. Strength estimation of FRP-confined prismatic specimens**

**a) All data b) Data from this dissertation**

The root mean square error (RMS error) method given in Eqn. 6.12 is used to understand the difference between analytical and experimental data. RMS error of the proposed equation is compared with the available equations from the literature as shown in Figure 6.16. The proposed equation seems to better predict the FRP-confined concrete strength.

$$RMS\ error = \sqrt{\frac{\sum(x_a - x_e)^2}{n_d}} \tag{6.11}$$

Where $x_a$ is the analytical data, $x_e$is the experimental data and $n_d$ is the number of data points.

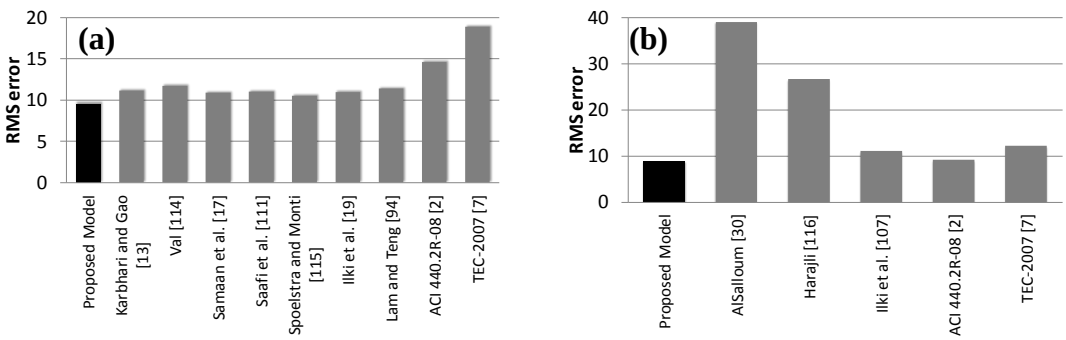


**Figure 6.16. RMS errors for the strength estimation a) Cylindrical specimens b) Prismatic specimens**

### *6.3.3.2. Ultimate axial strain estimation*

Good strain estimation is known to be necessary to have a reliable axial stress-strain relationship. For the strain estimation in order to simplify the problem, same procedure is applied; i.e., general equation for strength formulation is used for strain estimation also. In this case, $f_{cc}$ is replaced by $\varepsilon_{cc}$, $f_{co}$ is replaced by $\varepsilon_{co}$. The equation is also multiplied by a factor, which takes into account the sustained stress level, environmental exposure and temperature cycles.

$$\varepsilon_{cc} = \varepsilon_{co}\left[1 + k_2\left(\frac{2r}{D}\frac{f_l}{(f_{co})^{1.3}}\right)^{0.74}\right]CT \tag{6.12}$$

$$C = \left(1 - 0.80\frac{SL}{100}\right) \tag{6.13}$$

$$T = 0.90 \tag{6.14}$$

In Eqn. 6.12, $k_2$ is the strain factor and is equal to 40 for cylindrical and 50 for prismatic members, $\varepsilon_{cc}$ is the ultimate strain of FRP-confined concrete, $\varepsilon_{co}$ is the unconfined concrete strain at $f_{co}$ and can be taken as *0.002*.

The estimation is verified with the experimental data for cylindrical specimens (Figure 6.17) and prismatic specimens (Figure 6.18). In all data, data from literature do not contain any temperature and SL effect. Eqn. 6.12 was constructed from all data and correction factors were implemented using the data from this dissertation.

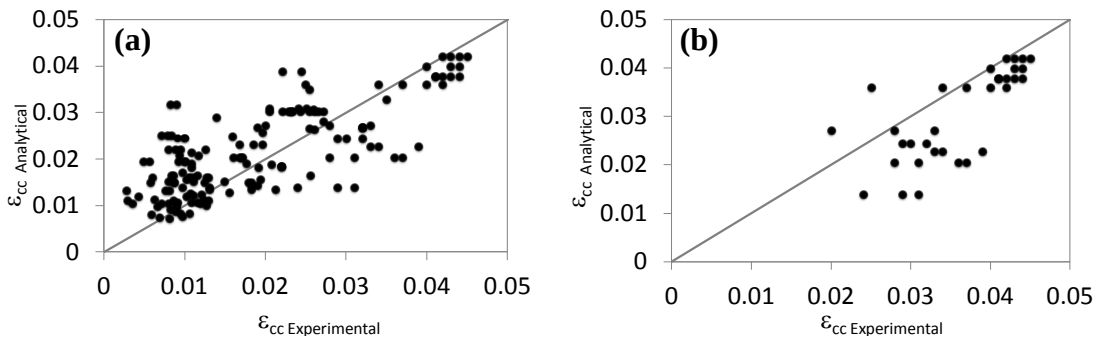


**Figure 6.17. Strain estimation of FRP-confined cylindrical specimens**
**a) All data b) Data from this dissertation**

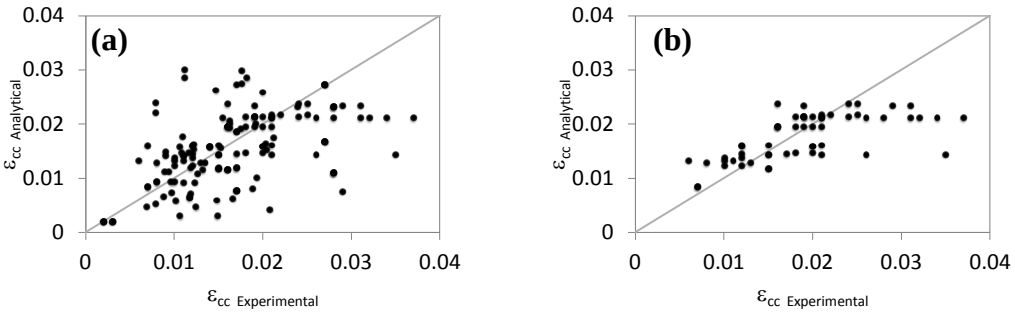


**Figure 6.18. Strain estimation of FRP-confined prismatic specimens a) All data b) Data from this dissertation**

Figure 6.19 shows the root mean square errors for the proposed equation and the available equations. Figures are given for cylindrical and prismatic specimens separately. From both figures, it can be said the proposed equations have less errors when compared to the others.

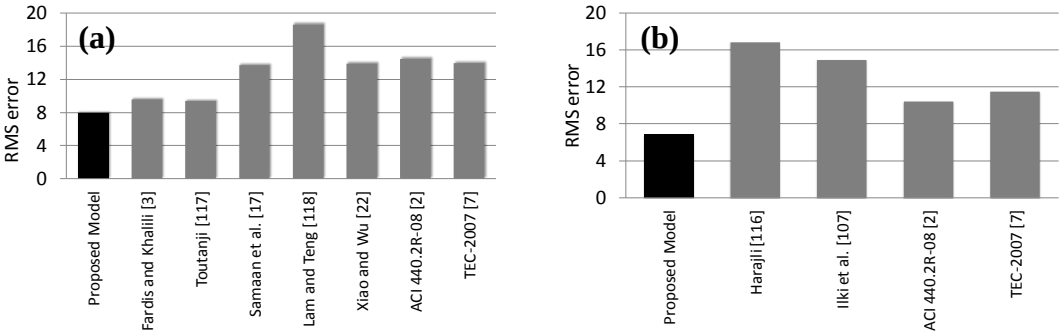


**Figure 6.19. RMS errors for the strain estimation a) Cylindrical specimens b) Prismatic specimens**

Finally, the boundary points at Point 3 are found as follows:

*Point 3 (Final BP);*

$$f_{cc} = f_{co}\left[1 + k_1\left(\frac{2r}{D}\frac{f_l}{f_{co}}\right)^{1.3}\right]CT \tag{6.6}$$

$$\varepsilon_{cc} = \varepsilon_{co}\left[1 + k_2\left(\frac{2r}{D}\frac{f_l}{(f_{co})^{1.3}}\right)^{0.74}\right]CT \tag{6.12}$$

### 6.3.4. Axial stress-strain model

In the second phase of the modeling, the axial stress-strain behavior of an FRP-confined concrete is predicted. It is assumed that the model composes of two parts as shown in Figure 6.20; the first part is controlled by concrete and the second part is controlled by FRP. In the parabolic first part, Hognestad's [113] equation (Eqn. 6.15) is used with minor modifications (Eqn. 6.16). In the equation (Eqn. 6.16), $f_{co}$ is replaced by $f_{ct}$, which takes the degree of confinement and SL level into account. With this modification high stress values can be attained for $\varepsilon_{co}=0.002$.

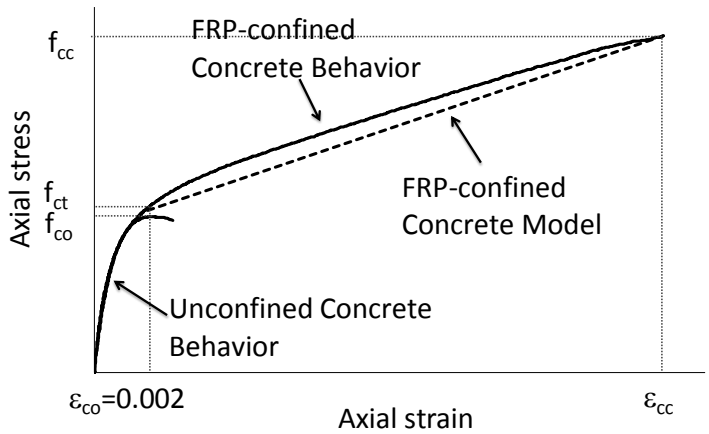


**Figure 6.20. Behavior of FRP-reinforced concrete and the assumptions for the model**

$$f_c = f_{co}\left[\frac{2\varepsilon}{\varepsilon_{co}} - \left(\frac{\varepsilon}{\varepsilon_{co}}\right)^2\right] \tag{6.15}$$

The second part of the curve is assumed to be linear (Eqn. 6.17) since FRP is the dominant material after $f_{ct}$. This assumption is acceptable because FRP behaves linear elastically until rupture. Besides, assuming a linear relationship between stress and strain simplifies the equation. The linearity starts at ($f_{ct}$, $\varepsilon_{co}$) and ends at ($f_{cc}$, $\varepsilon_{cc}$).

$0 \leq \varepsilon \leq \varepsilon_{co}$

$$f_c = f_{ct} * \left[\frac{2\varepsilon}{\varepsilon_{co}} - \left(\frac{\varepsilon}{\varepsilon_{co}}\right)^2\right] \tag{6.16}$$

$\varepsilon_{co} \leq \varepsilon \leq \varepsilon_{cc}$

$$f_c = \left[\frac{f_{cc} - f_{ct}}{\varepsilon_{cc} - \varepsilon_{co}}\right](\varepsilon - \varepsilon_{co}) + f_{ct} \tag{6.17}$$

## 6.4 MODEL VERIFICATION

Analytical model is verified with the experimental curves that were obtained from tests conducted at Middle East Technical University, Structural Engineering Lab. and Materials of Construction Lab. In the figures, continuous lines represent the analytical curves and the dashed lines are used for the experimental curves.

Figure 6.21 shows the experimental and analytical axial stress-strain diagrams of FRP-confined cylindrical specimens having 10 MPa and 20 MPa strength. In the figure, SL is the sustained load level in percent and ΔT is used to denote the temperature difference. As seen from both figures it can be said that the model can predict the behavior well. The transition points are well captured. The model estimates lower strength and corresponding strain values. The reason for having relatively low ultimate strength and strain values is that those values has been calibrated using the data available in the literature.

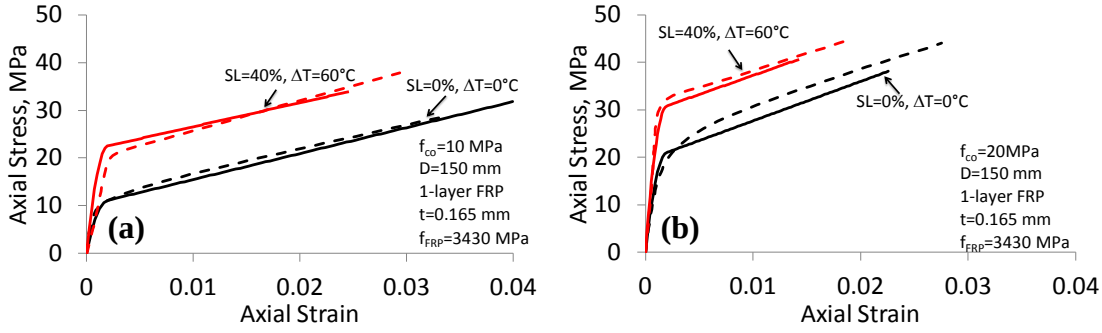


**Figure 6.21. Axial stress-strain diagrams of a) 10 MPa cylindrical specimens b) 20 MPa cylindrical specimens**

The model can also be used to predict the behavior of prismatic specimens. In the model it is assumed that the behaviors of cylindrical and prismatic specimens are the same for the first part of the axial stress-strain curve, i.e., for the part that concrete governs. Since behavior changes after reaching $f_{ct}$ the assumption is reasonable. For the second part since $f_{cc}$ and $\varepsilon_{cc}$ take corner radius into account the model can predict the behavior for prismatic specimens also.

In Figure 6.22, curves for prismatic specimens of square in section were illustrated. The figure on the left is for 11 MPa specimens having 25 mm corner radius and the one on the right is for 15 MPa specimens with 37.5 mm corner radius. Both figures have three curves with different sustained stress levels. As it is seen the transition stress increases with increasing sustained stress level. The model seems to capture the overall behavior well. Although the prediction in Figure 6.22a is not so successful, it is quite successful in Figure 6.22b.

The predictions for 16 and 28 MPa prismatic concrete specimens are shown in Figure 6.23. In Figure 6.23a, three curves are tried to be predicted. The black curves are for the control specimens, the blue curves represent the specimens having 40% of

sustained stress but not subjected to any temperature difference and the red ones are for specimens with 40% of sustained stress and exposed to 60°C temperature difference. As from the figure, the model seems to predict the overall behavior well. The figure in Figure 6.23b is for 28 MPa prismatic specimens. Similarly, the analytical model is in good agreement with the experimental data.

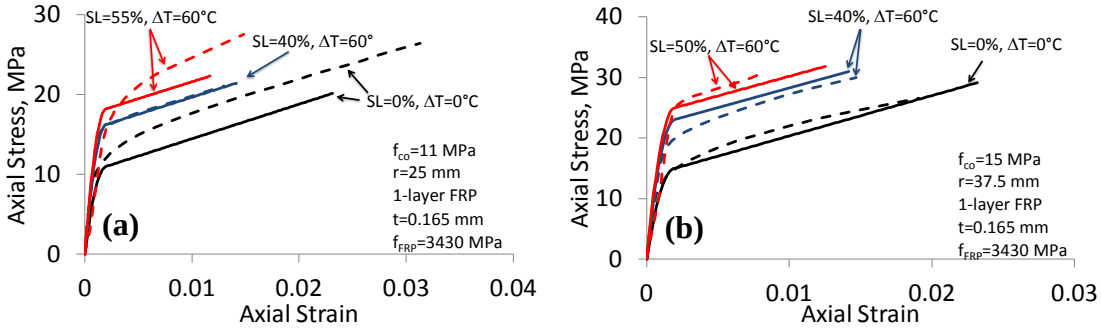


**Figure 6.22. Axial stress-strain diagram of a) 11 MPa prismatic specimens b) 15 MPa prismatic specimens**

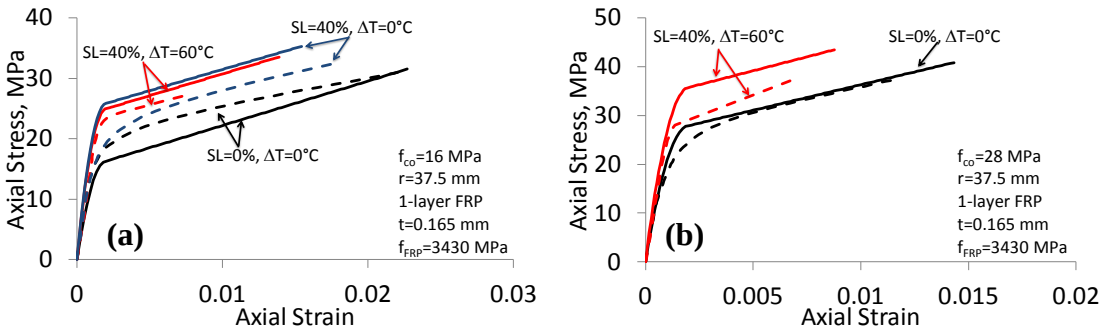


**Figure 6.23. Axial stress-strain diagram of a) 16 MPa prismatic specimens b) 28 MPa prismatic specimens**

# CHAPTER 7

# CONCLUSIONS

In this dissertation, CFRP-confined cylindrical and prismatic concrete columns were tested under various conditions such as heating-cooling cycles, sustained loading and outdoor exposures. From the experimental results and the data collected from the literature, a stress-strain model was also proposed.

The experimental tests results and analytical studies revealed that, CFRP confinement will not be effective if the adhesion between concrete and CFRP is low. Overlap length was found to be one of the key factors in confinement. Insufficient overlap would result in premature failure due to delamination. The minimum overlap length for the specimens used in this dissertation was found to be 50 mm. Besides overlap length, epoxy based adhesives should be carefully applied in order to ensure perfect bond. Therefore, it should be reminded that in CFRP confinement workmanship can directly affect the capacity of the strengthened or retrofitted members.

One-layer of CFRP was found to enhance the strength and strain capacity of cylindrical specimens with 150 mm diameter and short prismatic specimens having square sections with 150 mm side dimensions. The strength increase was 3 times in 10 MPa cylindrical specimens whereas in 20 MPa specimens the increase was only 2.3. This trend was seen in prismatic specimens also (2.5 times in 10 MPa, 1.5 times in 20 MPa prismatic specimens). Confinement effectiveness was found to be inversely proportional to the concrete strength. Strain capacity also followed the

same trend. In other words, strain capacity of 10 MPa concrete increased 14 times after confining with one-layer of CFRP whereas it was 11.7 times in 20 MPa specimens. In prismatic specimens, no apparent difference was seen in 10 and 15 MPa specimens (12 and 11.7 times, respectively) but strain increase was only 5.5 times in 20 MPa specimens.

Secant modulus of elasticity ($E_1$) of cylindrical specimens was observed to slightly increase with CFRP confinement. The increase again is higher in 10 MPa specimens than ones in 20 MPa are. Nevertheless, same conclusion cannot be drawn for prismatic specimens because although an increase was noted for some specimens, decrease also found in secant modulus of elasticity. As a conclusion, since concrete is the dominant part for the zone that $E_1$ is calculated, it will not be introduced a significant error to assume that $E_1$ is not affected by the confinement with one-layer of CFRP.

Strain distribution along the cross-section of a prismatic member is not uniform. Lateral strains at corners are lower than the strains at sides. The non-uniformity of lateral and axial strains results in a non-uniform deformation of concrete. For cylindrical specimens the place of rupture was not foreseen because it may be any place other than overlap zone. However, as for prismatic specimens failures were observed to occur at a place close to a corner. This place was observed to be the end of the curvature at the corner.

Heating-cooling cycles under 40% of relative humidity were observed to slightly affect the mechanical properties of CFRP-confined cylindrical concrete specimens. They did not experience strength reduction. The main effect was seen at the strain level, which was decreased 5%. The effect of H-C cycles on prismatic specimens was significant especially for specimens having great MCRs. The strength decrease was 24% and reduction in strain was 33% in 10 MPa specimens with 37.5 mm corner radius. As for 15 MPa specimens having 37.5 mm corner radius, the decrease in

strength was 16% and it was 17% in strain. For the specimens having low MCRs the change was not significant except 7% decrease in 10 MPa specimens with a corner radius of 25 mm.

When specimens were subjected to wet H-C cycles, further reduction in strength and strain capacities were noted. Since top and bottom faces of those specimens were not sealed and were in direct contact with water, the moisture absorbtion through the unsealed concrete faces was not avoidable. Further reduction may be attributed to the increase in moisture content, which creates problems in concrete upon freezing-thawing process.

The outdoor exposures were found to affect the mechanical properties of prismatic specimens considerably. Although strength decrease was observed in specimens having 37.5 mm corner radius, specimens with 25 mm showed strength increase about 24%. As for the change in strain capacities under outdoor exposures, it was found that CFRP-confined concrete columns exhibited 15 to 30% decrease. It should be reminded that top and bottom faces of these specimens were not sealed and moisture absorbtion through these faces was not prevented.

Simultaneous exposure of H-C cycles and sustained loading changed the shape of the axial stress-strain curve. Although there existed a smooth transition between nonlinear first part and the linear second part of the curve, the transition zone became sharp and clear with sustained loading.

The transition stress increased with increase in sustained loading. This phenomenon can be attributed to the fact that, increase in axial strains due to sustained loading increases lateral expansion due to Poisson’s effect, thus it increases the tensile forces developed in CFRP, which activates CFRP in low stress levels. The transition zone was observed to be affected by the confinement effectiveness. The more CFRP is effective, the higher and clearer the transition zone is.

CFRP-confined cylindrical concrete specimens experienced strength increase when they were subjected to simultaneous exposure of H-C cycles and sustained loading. The increase is higher for low strength concrete. Strength increase is attributed to the fact that under sustained loading, CFRP becomes active in earlier phase. However, no strength increase was observed for prismatic specimens rather they had reduction in strength under 40% of SL.

When the SL level increased to 50%, the reduction in strength was found to be recovered in a small degree for prismatic specimens. Since this level of SL creates stresses above the unconfined concrete strength, CFRP will become active upon loading. In addition to the initial state, with creep due to the stress redistribution between concrete and CFRP, tensile stresses in CFRP increases and higher levels of confinement is attained.

Strain capacities of CFRP-confined concretes reduced significantly, when they were subjected to simultaneous effects of SL and H-C cycles. The decrease was found to be in the order of 15 to 35%. Further decrease in strain capacities was found for some specimens at higher level of SL.

Proposed analytical model of strength and strain for both cylindrical and prismatic specimens confined with CFRP was found to be better than the ones available in the literature. The RMS errors of these models were lower than their counterparts. Strength and strain models consider the temperature effects and creep with factors introduced to the equations. The reliability of the model was not verified for concrete strengths above 50 MPa, specimens confined more than five plies and prismatic specimens having different sections other than square.

Considering the experimental and analytical studies conducted in this dissertation, the recommendations given below may be taken into account in the future researches:

- Overlap length of the confining materials should not be less than 50 mm.

- H-C cycles may include changes of humidity levels since wet H-C cycles resulted in a decrease in the strain. While performing these tests, direct contact of concrete with water should be eliminated.

- In this dissertation, only one layer of CFRP was used as the confinement. More layers may result in a different behavior because of the increase in confining stress.

- Only two levels of SL were examined in the experimental tests. They may be extended to various levels of SL to understand the creep limit for FRP confined concrete columns. The relationship between creep limit and the confinement level will be beneficial.

- Specimens in this dissertation were first wrapped with CFRP and then the sustained load was applied. This is different from the real-time application. Therefore, new tests may be established in which CFRP is applied on loaded specimens.

- Steel rebars were not used in this dissertation. Similar tests may be conducted with including internal steel rebars in the specimens. In this case, corrosion will be introduced as a new parameter, which directly affects the durability of the concrete.

# REFERENCES


1. Hollaway L. C., 2003. "The evolution of and the way forward for advanced polymer composites in the civil infrastructure". *Construction and Building Materials* 17, 365–378.

2. ACI440.2R-08, 2008. "Guide for the design and construction of externally bonded FRP systems for strengthening concrete structures". *ACI Committee 440,* American Concrete Institute Farmington Hills, Michigan

3. Fardis, M. N., Khalili, H., 1982. "FRP-encased concrete as a structural material". *Magazine of Concrete Research* 34(122), 191–202.

4. Homam S. M., 2000. "Durability of Fibre Reinforced Polymers (FRP) used in concrete structures", *MASc Thesis,* Department of Civil Engineering, University of Toronto.

5. Berg A. C., Bank L. C., Oliva M. G., Russell J. S., 2006. "Construction and cost analysis of an FRP reinforced concrete bridge deck". *Construction and Building Materials* 20, 515-526.

6. Qu W., Zhang X., Huang H., 2009. "Flexural behavior of concrete beams reinforced with hybrid (GFRP and Steel) bars". *Journal of Composites for Construction* ASCE, 13(5), 350-359.

7. Turkish Earthquake Code for Buildings, 2007. Ministry of Public Works and Resettlement, Ankara, Turkey.

8. Mazılıgüney L, Azılı F, Yaman İ Ö., 2008. “In-situ concrete compressive strength of residential, public and military structures”. *Proceedings of the 8th International Congress on Advances in Civil Engineering* Famagusta, Northern Cyprus, 273-280.

9. Richart F E, Brandtzaeg A, Brown R L., 1928. “A study of the failure of concrete under combined compressive stresses”. *Bulletin 185*, University of Illinois Engineering Experimental Station, Champaign.

10. Newman K., Newman J. B., 1971. “Failure theories and design criteria for plain concrete”. *Proc. Int. Civil Eng. Mat. Conf. on Struct., Solid mech. And Eng. Des.* Wiley Interscience, New York, 936-995.

11. Saadatmanesh H., Ehsani, Li M. W., 1994. “Strength and ductility of concrete columns externally reinforced with fiber composite straps”. *ACI Structural Journal* 91(4), 434-447.

12. Mander, J. B., Priestley M. J. N., Park R., 1988. “Theoretical stress-strain model for confined concrete”. *Journal of Structural Engineering* ASCE 114(8), 1804-1826.

13. Karbhari V. M., Gao Y., 1997. “Composite jacketed concrete under uniaxial compression-verification of simple design equations”. *Journal of Materials in Civil Engineering* 9(4), 185-193.

14. Rochette P., Labossiere P., 2000. “Axial testing of rectangular column models confined with composites”. *Journal of Composites for Construction* ASCE 4(3), 129-136.

15. Rochette P., 1996. “Confinement of short square and rectangular columns with composite materials”. *MASc Thesis* University of Sherbrook, Quebec, Canada.

16. Mirmiran A, Shahawy M, Samaan M, El-Echary H, Mastrapa J C, Pico O., 1998. “Effect of column parameters on FRP-confined concrete”. Journal of Composites for Construction 2(4), 175-185.

17. Samaan M, Mirmiran A, Shahawy M., 1998. “Model of concrete confined by fiber composites”. *Journal of Structural Engineering* 124(9), 1025-1031.

18. Shahawy M, Mirmiran A, Beitelman T., 2000. “Tests and modeling of carbon-wrapped concrete columns”. Composites, Part B: Engineering 31, 471-480.

19. Ilki A, Kumbasar N, Koç V., 2002. “Strength and deformability of low strength concrete confined by carbon fiber composite sheets”. *Proceedings of 15th ASCE Engineering Mechanics Conference* New York, paper no:101.

20. Li Y. F., Lin C. T., Sung Y. Y., 2003. “A constitutive model for concrete confined with carbon fiber reinforced plastics”. *Mechanics of Materials* 35, 603–619.

21. Lam L, Teng J G., 2003a. “Hoop rupture strains of FRP jackets in FRP confined concrete”. *Proceedings of FRPRCS-6* Singapore, July, 601-612.

22. Xiao Y., Wu H., 2000. “Compressive behavior of concrete confined by carbon fiber composite jackets”. *Journal of Material for Civil Engineering* 12(2), 139-46.

23. Harries K. A., Kharel G., 2003. “Experimental investigation of the behavior of variably confined concrete”. *Cement and Concrete Research* 33, 873–880.

24. Tamuzs V., Tepfers R., You C. S., Rousakis T., Repelis I., Skruls V., Vilks U., 2006. “Behavior of concrete cylinders confined by carbon-composite tapes and prestressed yarns. 1. Experimental data”. *Mechanics of Composite Materials* 42(1), 13-32.

25. Almusallam T. H., 2007. “Behavior of normal and high-strength concrete cylinders confined with E-glass/epoxy composite laminates”. *Composites: Part B* 38, 629-639.

26. Parvin A., Wang W., 2001. “Behavior of FRP Jacketed concrete columns under eccentric loading”. *Journal of Composites for Construction* ASCE 5(3), 146-152.

27. Chaallal O., Shahawy M., Hassan M., 2003. “Performance of axially loaded short rectangular columns strengthened with carbon fiber-reinforced polymer wrapping”. *Journal of Composites for Construction* ASCE 7(3), 200-208.

28. Lam L., Teng J. G., 2003b. “Design-oriented stress-strain model for FRP-confined concrete in rectangular columns”. *Journal of Reinforced Plastics and Composites* 22(13), 1149-1186.

29. Masia M. J., Gale T. N., Shrive N. G., 2004. “Size effect in axially loaded square-section concrete prisms strengthened using carbon fiber reinforced polymer wrapping”. *Canadian Journal of Civil Engineering* 31, 1-13.

30. Al-Salloum Y. A., 2007. “Influence of edge sharpness on the strength of square concrete columns confined with FRP composite laminates”. *Composites: Part B* 38, 640-650.

31. Rousakis T. C., Karabinis A. I., 2008. “Substandard reinforced concrete members subjected to compression: FRP confining effects”. *Materials and Structures* 41(9), 1595-1611.

32. Benzaid R., Chikh N., Mesbah H., 2008. “Behavior of square concrete column confined with GFRP composite Wrap”. *Journal of Civil Engineering and Management* 14(2), 115-120.

33. Wang L. M., Wu Y. F., 2008. “Effect of corner radius on the performance of CFRP-confined square concrete columns: Test”. *Engineering Structures* 30, 493-505.

34. Wu Y. F., Wei Y. Y., 2010. “Effect of cross-sectional aspect ratio on the strength of CFRP-confined rectangular concrete columns”. *Engineering Structures* 32, 32-45.

35. Ali I., Kesler C. E., 1965. “Rheology of concrete: A review of research”, *Bulletin 476*, University of Illinois Engineering Experimental Station 62(68).

36. Ersoy U., Tankut T., Özcebe G., 2004. “Reinforced Concrete”. *METU Press* Ankara, Turkey.

37. Rüsch H., 1960. “Research toward a general flexural theory for structural concrete”. *ACI Journal* 57(1), 1-28.

38. Vandewalle L., 2000. “Concrete creep and shrinkage at cyclic ambient conditions”. *Cement & Concrete Composites* 22, 201-208.

39. Raghavan J., Meshii M., 1997a. “Creep rupture of polymer composites”. *Composites Science and Technology* 57, 375-388.

40. Raghavan J., Meshii M., 1997b. “Creep of polymer composites”. *Composites Science and Technology* 57, 1673-1688.

41. Naguib W., Mirmiran A., 2002. “Time-dependent behavior of Fiber-reinforced polymer-confined concrete columns under axial loads”. *ACI Structural Journal* 99(2), 142-148.

42. Naguib W., Mirmiran A., 2003. “Creep analysis of axially loaded fiber reinforced polymer-confined concrete columns”. *Journal of Engineering Mechanics* ASCE 129(11), 1308-1319.

43. Theriault M., Pelletier M. A., Khayat K., Al-Chami G., 2003. “Creep performance of CFRP confined concrete cylinders”. Proceedings of FRPRCS-6 Singapore, 623-632.

44. Al Chami G., 2006. “Creep behavior of CFRP strengthened concrete columns and beams”. *PhD Thesis* Department of Civil Engineering, University of Sherbrooke, Canada.

45. Wang Y., Zhang D., 2009. “Creep-effect on mechanical behavior of concrete confined by FRP under axial compression”. *Journal of Engineering Mechanics* ASCE 135(11), 1315-1322.

46. Zhang D., Wang Y., Ma Y., 2010. “Compressive behavior of FRP-confined square concrete columns after creep”. *Engineering Structures*, 32, 1957-1963.

47. Erdoğan T. Y., 2003. “Beton”. *METU Press* Ankara, Turkey.

48. ACI201.2R-01, 2001. “Guide to durable concrete”. *ACI Committee 201* American Concrete Institute Farmington Hills, Michigan.

49. Powers T. C., 1945. “A working hypothesis for further studies of frost resistance of concrete”. *Bulletin No. 5,* reprinted from Journal of ACI Proceedings, 245-72.

50. Mehta P. K., Monteiro P. J., 2006. “Concrete, microstructure, properties and materials”. *McGraw-Hill*, 3rd Edition.

51. Wong A. Y. C., Anderson C. L., Hilsdorf H. K., 1973. “The effect of drying on the freeze-thaw durability of concrete”. *Bulletin 506*, University of Illinois Engineering Experimental Station, 70(66).

52. Vecchio F. J., Sato J. A., 1990. “Thermal gradient effects in reinforced concrete frame structures”. *ACI Structural Journal* 87(3), 262-275.

53. Bar Cohen Y., Meron M., Ishai O., 1979. “Nondestructive evaluation of hygrothermal effects on Fiber-reinforced plastic laminates”. *Journal of Testing and Evaluation* 7(5), 291-296.

54. Selzer R., Friedrich K., 1997. “Mechanical properties and failure behavior of carbon fibre-reinforced polymer composites under the influence of moisture”. *Composites: Part A* 28A, 595-604.

55. Al-Salehi F. A. R., Al-Hassani S. T. S., Haftchenari H., 1998. “Effect of temperature on the tensile strength and failure modes of angle ply CFRP tubes under hoop loading”. *Applied Composite Materials* 5, 319-343.

56. Rivera J., Karbhari V. M., 2002. “Cold temperature and simultaneous aqueous environment related degradation of carbon/vinylester composites”. *Composites: Part B* 33, 17-24.

57. Kobayashi S., Terada K., Takeda N., 2003. “Evaluation of long-term durability in high temperature resistant CFRP laminates under thermal fatigue loading”. *Composites: Part B* 34, 753–759.

58. Earl J. S., Shenoi R. A., 2004. “Hygrothermal ageing effects on FRP laminate and structural foam materials”. *Composites: Part A* 35, 1237–1247.

59. Hough J. A., Karad S. K., Jones F. R., 2005. “The effect of thermal spiking on moisture absorption, mechanical and viscoelastic properties of carbon fibre reinforced epoxy laminates”. *Composites Science and Technology* 65, 1299-1305.

60. Eyre, K. J., 2007. “Moisture absorption and stiffness degradation of carbon fiber reinforced polymer composite specimens exposed to accelerated environmental aging conditions”. *MASc Thesis* Department of Civil & Architectural Engineering, The University of Wyoming.

61. Labossiere P., Neale K. W., Nishizaki I., 2003. “Effect of different long-term climatic conditions on FRP durability”. *Proceedings of FRPRCS-6* Singapore, 779-784.

62. Toutanji H. A., Balaguru P., 1999. “Effects of freeze-thaw exposure on performance of concrete columns strengthened with advanced composites”. *ACI Materials Journal* 96(5), 605-610.

63. Toutanji H. A., 1998. “Durability characteristics of concrete columns confined with advanced composite materials”. *Composite Structures* 44, 155-161.

64. Karbhari V. M., Rivera J., Dutta P. K., 2000. “Effect of short-term freeze-thaw cycling on composite confined concrete”. *Journal of Composites for Construction* 4(4), 191-197.

65. Kshirsagar S., Lopez-Anido R. A., Gupta R. K., 2000. “Environmental aging of fiber reinforced polymer wrapped concrete cylinders”. *ACI Materials Journal* 97(6), 703-712.

66. Karbhari V. M., 2002. “Response of fiber reinforced polymer confined concrete exposed to freeze and freeze-thaw regimes”. *Journal of Composites for Construction* 6(1), 35-40.

67. Micelli F., De Lorenzis L., La Tegola A., 2003. “Effects of wet environment on CFRP-confined concrete cylinders”. *Proceedings of FRPRCS-6* Singapore, 795-804.

68. Bae S., 2004. “Evaluation of the effects of various environmental conditions on reinforced concrete columns wrapped with FRP sheets”. *PhD Thesis* Civil Engineering Department, University of Missouri-Rolla.

69. Belarbi A., Bae S., 2007. “An experimental study on the effect of environmental exposures and corrosion on RC columns with FRP composite jackets”. *Composites: Part B* 38, 674-684.

70. Saenz N., Pantelides C. P., 2006. “Short and medium term durability evaluation of FRP-confined circular concrete”. *Journal of Composites for Construction* 10(3), 244-253.

71. Al-Salloum Y. A., Elsanadedy H. M., Abadel A. A., 2011. “Behavior of FRP-confined concrete after high temperature exposure”. *Construction and Building Materials* 25, 838-850.

72. Kong A., Fam A., Green M. F., 2005. “Freeze-thaw behavior of FRP-confined concrete under sustained load”. *Proceedings of FRPRCS-7* Kansas City, 705-722.

73. Kong A., 2005. “Freeze-thaw behavior of circular concrete members confined by fibre reinforced polymer jackets when simultaneously subjected to sustained axial loads”. *MASc Thesis* Department of Civil Engineering Queen’s University, Canada.

74. Green M. F., Bisby L. A., Fam A. Z., Kodur V. K. R. 2006. “FRP-confined concrete columns: Behavior under extreme conditions”. *Cement and Concrete Composites* 28, 928-937.

75. Krishnaswamy R., Lopez M. M., 2006. “Time performance of concrete-CFRP bond under the effects of freeze-thaw cycles and sustained loading”. *TRB Annual Meeting*.

76. ACI440.R-07, 2007. “Report on fiber-reinforced polymer (FRP) reinforcement for concrete structures”. *ACI Committee 440* American Concrete Institute Farmington Hills, Michigan.

77. MBrace Composite Strengthening System, 2007. *BASF Construction Chemicals* UK, Version 10.

78. ASTM C 666, 1997. "Standard test method for resistance of concrete to rapid freezing and thawing". *Annual Book of ASTM Standards*.

79. Turkish State Meteorological Service, 2007. "Recorded daily maximum and minimum temperature values during 2000-2006 in each city of Turkey". *Ministry of Forest and Water Affairs Turkish State Meteorological Service*.

80. Turkish State Meteorological Service, 2011. "Recorded daily maximum and minimum humidity values during 2010-2011 in each city of Turkey", *Ministry of Forest and Water Affairs Turkish State Meteorological Service.*

81. ASTM C 469, 2002. "Standard test method for static modulus of elasticity and Poisson's ratio of concrete in compression". *Annual Book of ASTM Standards*.

82. Lam L., Teng J. G., 2004. "Ultimate condition of fiber reinforced polymer confined concrete". *Journal of Composites for Construction* ASCE 8(6), 539-548.

83. Lam L., Teng J. G., 2003c. "Design-oriented stress-strain model for FRP-confined concrete". *Construction and Building Materials* 17, 471-489.

84. ASTM C 39/C 39 M, 2001. "Standard test method for compressive strength of cylindrical concrete specimens". *Annual Book of ASTM Standards*.

85. Ronning T. F., 2001. “Freeze-thaw resistance of concrete, Effect of: curing conditions, moisture exchange and materials”. *PhD Thesis* Structural Engineering Division, The Norvegian Institute of Technology.

86. TS-500, 2000. “Building code requirements for reinforced concrete”. *Turkish Standards Institute* Ankara, Turkey.

87. Campione G., Miraglia N., 2003. “Strength and strain capacities of concrete compression members reinforced with FRP”. *Cement & Concrete Composites* 25, 31-41.

88. De Lorenzis L., Tepfers R., 2003. “Comparative study of models on confinement of concrete cylinders with fiber-reinforced polymer composites”. *Journal of Composites for Construction* ASCE 7(3), 219–237.

89. Demers M., Neale K. W., 1999. “Confinement of reinforced concrete columns with fiber-reinforced composite sheets - an experimental study”. *Canadian Journal of Civil Engineering* 26(2), 226–241.

90. Ferreira D., Barros J., 2003. “Strategies for concrete confinement with strips of CFRP sheet”. *International Conference Composites in Constructions - CCC2003* Cosenza, Italy, 483-488.

91. Jiang T., Teng J. G., 2007. “Analysis-oriented stress–strain models for FRP–confined concrete”. *Engineering Structures* 29, 2968-2986.

92. Karabinis A. I., Rousakis T. C., 2002. “Concrete confined by FRP material: a plasticity approach”. *Engineering Structures* 24, 923-932.

93. Lam L., Teng J. G., Cheung C. H., Xiao Y., 2006. “FRP-confined concrete under axial cyclic compression”. *Cement & Concrete Composites* 28, 949-958.

94. Lam L., Teng J. G., 2002. “Strength models for fiber-reinforced plastic confined concrete”. *Journal of Structural Engineering* ASCE 128(5), 612-623.

95. Lin H. J., Chen C. T., 2001. “Strength of concrete cylinder confined by composite materials”. *Journal of Reinforced Plastics and Composites* 20(18), 1577-1601.

96. Matthys S., Toutanji H., Taerwe L., 2006. “Stress–strain behavior of large-scale circular columns confined with FRP composites”. *Journal of Structural Engineering* ASCE 132 (1), 123-133.

97. Mirmiran A., Zagers K., Yuan W., 2000. “Nonlinear finite element modeling of concrete confined by fiber composites”. *Finite Elements in Analysis and Design* 35, 79–96.

98. Pessiki S., Harries K. A., Kestner J. T., Sause R., Ricles J. M., 2001. “Axial behavior of reinforced concrete columns confined with FRP Jackets”. *Journal of Composites for Construction* ASCE 5(4), 237–45.

99. Shehata I. A. E. M., Corneiro L. A. V., Shehata L. C. D., 2002. “Strength of short concrete columns confined with CFRP sheets”. *Materials and Structures* 35, 50–58.

100. Sheikh S. A., 2007. “Field and laboratory performance of bridge columns repaired with wrapped glass-fiber-reinforced-polymer sheets”. *Canadian Journal of Civil Engineering* 34, 403-413.

101. Silva M. A. G., Rodrigues C. C., 2006. “Size and relative stiffness effects on compressive failure of concrete columns wrapped with glass FRP”. *Journal of Materials in Civil Engineering* ASCE 18(3), 334-342.

102. Teng J. G., Yu T., Wong Y. L, Dong S. L., 2007. “Hybrid FRP–concrete–steel tubular columns: Concept and behavior”. *Construction and Building Materials* 21(4), 846-854.

103. Theriault M., Neale K. W. and Claude S., 2004. “Fiber-reinforced polymer-confined circular concrete columns: Investigation of size and slenderness effects”. *Journal of Composites for Construction* ASCE 8(4), 323-331.

104. Erdil B., Akyuz U., Yaman I. O., 2008. “Behavior of CFRP reinforced low strength concrete subjected to temperature changes and sustained loads”. *Proceedings of 14WCEE* Beijing, China.

105. Erdil B., Akyuz U., Yaman I. O., 2009. “Low strength concrete columns confined with CFRP: Behavior under temperature changes and loads”. *Proceedings of FRPRCS-9* Sydney, Australia.

106. Erdil B., Akyuz U., Yaman I. O., 2012. “Mechanical behavior of CFRP confined low strength concretes subjected to simultaneous heating-cooling cycles and sustained loading”. *Materials and Structures* 45(1-2), 223-233.

107. Ilki A., Peker O., Karamuk E., Demir C., Kumbasar N., 2008. “FRP retrofit of low and medium strength circular and rectangular reinforced concrete columns”. *Journal of Materials in Civil Engineering* ASCE 20 (2), 169-188.

108. Wang L. M., Wu Y. F., 2008. “Effect of corner radius on the performance of CFRP-confined square concrete columns: Test”. *Engineering Structures* 30, 493-505.

109. Feng P., Lu X. Z., Ye L. P., 2002. “Experimental research and finite element analysis of square concrete columns confined by FRP sheets under uniaxial compression”. *Proceedings of 17th Australasian Conference on the Mechanics of Structures and Materials* Gold Coast, Australia, 71-76.

110. Richart F. E., Brandtzaeg A., Brown R. L., 1929. “The failure of plain and spirally reinforced concrete in compression”. *Bulletin 190* University of Illinois Engineering Experimental Station, Champaign, Ill.

111. Saafi M., Toutanji H. A., Li Z., 1999. “Behavior of concrete columns confined with fiber reinforced polymer tubes”. *ACI Materials Journal* 96(4), 500-509.

112. Xiao Y. and Wu H., 2003. “Compressive behavior of concrete confined by various types of FRP composite jackets”. *Journal of Reinforced Plastics and Composites* 22(13), 1187-1201.

113. Hognestad E., 1951. “A study of combined bending and axial load in reinforced concrete members”. *Bulletin Series No. 399* Engineering Experiment Station, University of Illinois, Urbana, Ill..

114. Val D., 2003. “Reliability of fiber-reinforced polymer-confined reinforced concrete columns”. *Journal of Structural Engineering* ASCE 129(8), 1122-1130.

115. Spoelstra M. R., Monti G., 1999. “FRP-confined concrete model”. *Journal of Composites for Construction* ASCE 3(3), 143-150.

116. Harajli M. H., 2006. “Axial stress-strain relationship for FRP confined circular and rectangular concrete columns”. *Cement & Concrete Composites* 28, 938-948.

117. Toutanji H. A., 1999. “Stress-strain characteristics of concrete columns externally confined with advanced fiber composite sheets.” *ACI Materials Journal* 96(3), 397-404.

118. Lam, L., Teng, J. G., 2003d. “Stress–strain model for FRP-confined concrete for design applications.” *Proceedings of FRPRCS-6* Singapore, 99-110.

# CURRICULUM VITAE

## PERSONAL INFORMATION

Surname, Name: Erdil, Barış

Nationality: Turkish (TC)

Date and Place of Birth: 28 September 1979 , Bitlis

Phone: +90 543 532 42 10

email: muhberdil@yahoo.com

## EDUCATION

| Degree | Institution | Year of Graduation |
|---|---|---|
| PhD on BS | METU, Civil Engineering | 2012 |
| BS | İstanbul University, Civil Engineering | 2001 |
| High School | Bitlis Anadolu High School, Bitlis | 1997 |

## WORK EXPERIENCE

| Year | Place | Enrollment |
|---|---|---|
| 2002-2012 | METU Department of Civil Eng. | Research Assistant |
| 1999 July | KİPTAŞ | Intern Engineering Student |

## FOREIGN LANGUAGES

Advanced English

## PUBLICATIONS

1. Erdil B., Akyuz U., Yaman I. O., 2008. "Behavior of CFRP reinforced low strength concrete subjected to temperature changes and sustained loads". *Proceedings of 14WCEE* Beijing China.

2. Erdil B., Akyuz U., Yaman I. O., 2009. “Low strength concrete columns confined with CFRP: Behavior under temperature changes and loads”. *Proceedings of FRPRCS-9* Sydney Australia.
3. Aktas, Y.D., Erdil B., Akyuz U., Sahin Guchan N., Turer A., 2009. “Structural behavior of timber frame Ottoman traditional “Hımış” houses - Frame loading experiments”. *International Symposium on Historical Earthquakes and Conservation of Monuments and Sites in the Eastern Mediterranean Region for the 500th Anniversary Year of the 1509 September 10, Marmara Earthquake*, Istanbul Turkey,364-366 (poster presentation).
4. Okuyucu D., Erdil B., 2009. “Seismic performance evaluation of Emir Bayındır Cupola in Ahlat”. *Proceedings of Symposium with International Participation on Strengthening and Preserving Historical Buildings and Cultural Heritage – II* Diyarbakır Turkey.
5. Zervent A., Yılmaz C., Caner A., Erdil B., 2009. “Çelik yapıların tasarım metodlarının değerlendirilmesi: TS 648, LRFD, EUROCODE 3”. *3.Ulusal Celik Yapılar Sempozyumu* TMMOB Insaat Muhendisleri Odası, Gaziantep Türkiye.
6. Aktaş Erdem Y.D., Akyüz U., Erdil B., Türer A., Şahin Güçhan N., 2010. “Testing and Seismic Capacity Evaluation of a Typical Traditional Ottoman Timber Frame”. *Advanced Materials Research* 133-134, 629-634.
7. Aktaş Erdem Y.D., Akyüz U., Erdil B., Türer A., Şahin Güçhan N., 2010. “Assessment of seismic behavior of traditional timber frame Ottoman houses: Frame tests”. *Proceedings of Structures and Architecture* Guimaraes Portugal, 1130-1137.
8. Türer A., Aktaş Erdem Y.D., Erdil B., Akyüz U., Şahin Güçhan N., 2010. “Evaluation of the seismic resistance of traditional Ottoman timber frame “Hımış” houses: A proposal for strengthening”. *7th International Conference on Structural Analysis of Historical Constructions (SAHC2010)* Shangai China.
9. Erdil B., Akyuz U., Yaman İ. Ö., İrfanoğlu A., 2011. “A comparative study of force-deflection relationship of FRP-confined concrete columns”. *Proceedings*

*of the 3rd International Conference on Computational Methods in Structural Dynamics and Earthquake Engineering* Corfu-Greece.

10. Erdil B., Akyuz U. and Yaman İ. Ö., 2011. "Karbon takviyeli fiber polimer (CFRP) ile güçlendirilmiş silindir numunelerin sünme ve sıcaklık değişimleri altındaki davranışları". *Ulusal Yapı Mekaniği Toplantısı* Kocaeli Türkiye.
11. Okuyucu D., Erdil B., 2011. "Seismic performance evaluation of Adilcevaz Pasha (Tugrul Bey) Mosque". *Proceedings of WCCE-ECCE-TCCE Joint Conference 2; Seismic Protection of Cultural Heritage* Antalya Turkey.
12. Erdil B., Akyuz U., Yaman I. O., 2012. "Mechanical behavior of CFRP confined low strength concretes subjected to simultaneous heating-cooling cycles and sustained loading". *Materials and Structures* 45(1-2), 223-233.
13. Erdil B., Akyuz U., Yaman İ. Ö., 2012. "Behavior of CFRP confined low strength concrete columns under temperature changes". *Proceedings of FIB Symposium, Concrete Structures for Sustainable Community* Stockholm Sweden.